DYNAMICS OF HIGHLY UNSTEADY NON-DARCY FLOW THROUGH CONFINED POROUS MEDIA

by

SANGYOON HAN

Submitted
in partial fulfilment of the requirements
for the degree of

DOCTOR OF PHILOSOPHY

Major Subject: Civil Engineering

at

DALHOUSIE UNIVERSITY

Halifax, Nova Scotia April, 2007

Your file Votre référence
ISBN: 978-0-494-35794-1
Our file Notre référence
ISBN: 978-0-494-35794-1

DALHOUSIE UNIVERSITY

To comply with the Canadian Privacy Act the National Library of Canada has requested that the following pages be removed from this copy of the thesis:

Preliminary Pages
- Examiners Signature Page
- Dalhousie Library Copyright Agreement

Appendices
- Copyright Releases (if applicable)

Dynamics of Highly Unsteady Non-Darcy Flow through Confined Porous Media

TABLE OF CONTENTS

LIST OF TABLES

LIST OF FIGURES

LIST OF SYMBOLS

a	inner scaling factor for space
A	corss-scetion area of conduit
b	inner scaling factor for time
c	inner scaling factor for velocity
c_1	empirical coefficient due to Carman-Kozeny
c_2	empirical coefficient due to Burke-Plummer
c_p	celerity of pressure wave
C_1	dimensionless group number 1
C_2	dimensionless group number 2
C_3	dimensionless group number 3
C_4	dimensionless group number 4
C_5	dimensionless group number 5
C_6	dimensionless group number 6
C_7	dimensionless group number 7
C_R	Courant number
C_R'	pipe friction instability criterion number
D	diameter of the circular conduit
d	diameter of particle
D_P	diameter of sphere with volume equal to representative particle volume
E	Young's modulus of iron
e	void ratio
Eu	Euler number
f	Darcy-Weishach friction factor
F	overall pipe friction-loss coefficient
Fo	Forchheimer number
g	gravitational acceleration
h	hydraulic head
H	dimensionless head

h_a	applied head at upstream end
H_{ab}	difference between upstream head and downstream head
h_L	head loss
i	hydraulic gradient
i	imaginary unit
$_i$	(subscript) space step in FDM
$^{(i)}$	(superscript) inner expression
k_d	Darcy permeability coefficient
k_{mr}	minimum permeability ratio
K	hydraulic conductivity
KC	Keulegan-Carpenter number
K_{st}	Stephenson's friction factor
L	conduit length
m	hydraulic mean radius
Ma	Mach number
n	porosity ($volume_{voids}$/ $volume_{bulk}$)
$^{(o)}$	(superscript) outer expression
p	pressure
p_L	complex variable in Laplace transform
Pe	Peclet number
r	viscous constant
r_0	radius of the pipe
r_1	radial distance from center of well
r_e	shape factor
Re	Reynolds number
s	inertial constant
S	storativity
s_L	complex variable in Laplace transform
S_s	specific storage
t	time

T	transmissivity
t'	thickness of the conduit wall
T'	transition constant
v	bulk velocity
V	dimensionless velocity
V_∞	equilibrium velocity
v_v	void velocity
W_0	Wilkins coefficient
x	distance from the valve face
X	dimensionless distance
z	elevation head
α	compressibility of sand
β	compressibility of water
β_0	non-Darcy coefficient
γ	perturbation expansion coefficient
γ_w	weight density of fluid
δ	perturbation expansion coefficient
δ_0	|(inner expression of outer) - inner|
δ_{ij}	effective stress tensor
ε	perturbation expansion coefficient
λ	coefficient in power law
μ	absolute viscosity
ν	kinematic viscosity
ξ	perturbation expansion coefficient
ξ_1'	energy density
ρ	density of fluid
τ	Dimensionless time
τ_0	shear stress
ω	perturbation expansion coefficient
$\tilde{X}$	inner space variable

$\tilde{\tau}$	inner time variable
$\tilde{V}$	inner velocity variable

Acknowledgments

I am indebted to my supervisor, Dr. David Hansen and co-supervisor, Dr. Guy Kember. Thank you to Dr. Hansen for your smile, encouragement, support, direction, and guidance on research, squash and my life. Thank you to Dr. Kember, for your valuable advices and passion on research and training.

I would like to thank my wife, Kyungah and my daughter, Jihi for always being with me. Thank you to my parents who enabled me to be where I am. Thank you to my parents-in-law who enabled my wife and daughter to be with me.

ABSTRACT

Mathematical and numerical studies on the dynamics of highly unsteady non-Darcy flow through porous media were performed under the constraints implied by a relatively simple hypothetical experiment, i.e. the sudden introduction of a fixed head at the upstream end of a conduit filled with a saturated porous medium. A wide range of possible equilibrium pore Reynolds numbers was considered admissible. Theoretical developments then proceeded on the basis of the momentum and continuity equations. It was found that the functional dependence of the dimensional parameter was not unique, and dimensional analysis was used to reduce the complexity of the problem. Dimensionless forms of the momentum and continuity equations were obtained and seven dimensionless groups resulted. These groups gave direct indication of the relative significance or contribution of each effect, whether viscosity, inertia, local acceleration, convective acceleration or elevation.

The behaviour of the momentum-continuity model, and of sub-models having different degrees of sophistication was then compared, under different applied hydraulic gradients. The Darcy model, the Ergun-type model, the local-acceleration-included model, and the complete model showed only small differences in dimensionless head patterns for flow regimes from laminar to completely turbulent. However, the differences in dimensionless velocity for these models were not always small. The solutions obtained using various numerical methods, including the method of characteristics and certain finite-difference schemes, were also compared.

Comparison of the solutions arising from the various models did not give information about the individual effects of various terms in, or components of, the momentum and continuity equations, i.e. viscosity, inertia, local acceleration, convective acceleration, and elevation. Even though the magnitudes of most[1] of these components were found to be small, it was considered to be of interest to discover their relative magnitudes, whether some could be safely neglected, and any curious aspects of their behaviour across the time-space continuum implied by the physical problem. The regular perturbation method was used to answer these questions. The effects of each term were

[1] depending on the applied hydraulic gradient.

expressed in terms of head or velocity, depending on the choice of the dependent variable.

Even though some of the terms in the governing partial differential equations (PDE's) were multiplied by parameter-groups that were found to have very small magnitudes, application of this perturbation method revealed that these terms could not simply be neglected, because the problem was found to depend on these small parameters in a "singular" way. Matched asymptotic expansions were then used to solve these singular problems near the upstream boundary at very small times. The resulting inner and outer expansions were developed for the laminar, partially-developed turbulent (PDT), and fully-developed turbulent (FDT) flow regimes. It was found that an inner zone existed in which highly unsteady flow induced behaviours fundamentally different from those predicted by widely-accepted PDE's. The inner expansion of the complete momentum and continuity equations gave rise to an evolving-wave equation which cannot be obtained when Darcy's Law or an Ergun-like equation replace the momentum equation. It was also found that the local acceleration component, negligibly small in the outer zone, played an important role in the inner zone, near the valve face. The extent of the inner zone in time-space varied was found to strongly depend on the applied hydraulic gradient.

1. Introduction

1.1. Background

The title of this thesis makes reference to "non-Darcy flow", even though laminar flow is considered at a level of detail no less than that considered for the other two regimes. The reason for this is two-fold: (1) Laminar flow can be considered to be merely one of the two end-conditions or limiting cases of the most general condition of the flow (the other being fully-developed turbulent flow). Indeed, equations such as the Ergun equation, designed for the transitional or partially-developed turbulent zone/condition, will often give reasonable estimates of flow for either these end-conditions, especially given the considerable inaccuracies that tend to be associated with attempting to make any independent estimate of flow rates through a given porous media. (2) The desired to have a concise title that is neither complex nor too wordy.

The focus of this study was to seek a better understanding of highly unsteady non-Darcy flow phenomena, starting from Newton's second law of motion and the continuity equation. The momentum equation is founded on the former fundamental principle and explains the motion of the fluid and the resulting head loss[2]. The latter equation includes consideration of the compressibility of the fluid, the media, and the 'container' (which may be a confining geologic layer or a pipe-wall). Even though many groundwater flow problems can be solved by simply using Darcy's Law and the continuity equation, not all flow through porous media is in laminar regime, outside of which Darcy's Law is not strictly applicable. In the partially-developed turbulent (PDT) flow regime, an Ergun-type equation (Ergun 1952) can be used as an energy loss equation. In honor of Ergun (1952) who developed the first practical energy loss equation for the PDT regime, the phrase "Ergun-type equation" will hereafter be used to refer to any second-order polynomial form of energy loss equation, for semantic convenience. Forchheimer (1901) presented this form much earlier but gave little guidance as to how to estimate the two coefficients.

[2] although it is the externally applied differences in hydraulic head that cause the flow.

Porous media flow models can be used for a variety of purposes, *e.g.* they can aid in process design, permit the computation of primary quantities that may be difficult to measure, or provide insights into the causative or influencing mechanisms in the secondary effects. Over the past century, various phenomenological, theoretically, and hybrid models have been proposed. Dullien (1975) has categorized steady non-Darcy flow models into five categories:

(i) phenomenological (e.g. regression-based),

(ii) based on a conduit analogy (e.g. Ergun 1952),

(iii) based on an analogy to flow around immersed objects (e.g. Brinkman 1947),

(iv) geometric (e.g. Du Plessis 1994),

(v) Statistical (e.g. random walk model of Scheiddeger 1975).

He considered a major categorization to be based on one of two fundamentally different approaches. In one, the analogy of flow inside a conduit is used; in the other, the analogy of flow around solid objects immersed in a fluid is used. Generally, the conduit flow approach is appropriate for low to intermediate porosities, whereas the second approach is more suitable for very high porosities. In groundwater-related aspects of civil engineering, an upper limit on porosity would be about 0.45, unless the media is in a 'quick' condition (the classical example being quicksand, somewhat analogous to an expanded filter-bed undergoing backwashing). Few investigators have relied solely on a multiple regression analysis of the data that is available to them in order to obtain a purely empirical non-Darcy flow equation. Many non-Darcy flow models are based on combinations of (i) and (ii). Similarly, Hayes (1995) classified all porous media flow models into four groups.

Although numerous empirical and theoretical models have been developed, and some of them have successfully predicted unsteady non-Darcy flows through particular porous media, the physical interpretation of all of the associated phenomena has not been well established. The accuracy of the predictions seems to depend on the method used to solve the problem and/or the way to in which parameters are estimated, even though the mechanisms behind these phenomena seem to remain the same. In the context of highly unsteady flows, it appeared that in order to gain a better understanding these underlying mechanisms, it was necessary not only to analyze the solutions obtained using various

phenomenological models and various numerical methods, but to also investigate the 'inclusiveness' governing partial differential equations themselves.

In this study, one dimensional flow through porous media was investigated under various boundary conditions. The sudden opening of a gate or valve connected to a pipe filled with porous media can result in a sharp change in head and velocity in a very short time, especially near the upstream boundary. The velocity at the upstream end is infinite if a simple head diffusion model is used. This infinite velocity is unrealistic, invalidating the assumed governing mechanism in this small region of time and space. The error introduced by using a simple diffusion equation to predict the flow near the boundary can be assessed by finding the true mechanisms governing the flow. By investigating the governing equations, it will be shown that the wave propagation process is the dominant mechanism in this small region, whereas simple diffusion process is applicable to the large time and space region.

The understanding of these mechanisms of the flow obviously is of practical aid for the solutions of some of the problems connected with these processes, especially highly time-dependent processes. Wave propagation in saturated porous media can be related to geophysical, geological, and technological applications. For example, in petroleum engineering, the wave-pulse treatment technique has been applied to petroleum reservoirs in order to enhance oil recovery. This technique essentially consists of acting upon the reservoir with periodic large-amplitude pressure pulses, generated in injection wells. Another example from oil recovery is water flooding, which has become common practice. It aids nature by forcibly injecting water into the producing horizon. The sudden injection of fluid can also be found in *in-situ* groundwater treatment and filtering processes. Wave propagation through porous media problems are therefore not uncommon. This study provides a detailed framework for answering the questions of by how far and by how much these phenomena dominate flow in the laminar, PDT and FDT flow regimes.

1.2. Problem Statement

In order to study the dynamics of unsteady flow through porous media (any regime), a simple 1-D sloped pipe connected to tanks at both ends was used. A schematic of the experimental set-up is shown in Figure 1.1. The pipe packed some granular material equipped with screens at both ends in order to keep it inside of the pipe. Both are immoveable. The location of the upstream end is defined as $x = 0$ and that of downstream end as $x = L$. A head H_{ab} is the applied head difference; it drives flow and cause the discharge Q. The porous medium in question is saturated before opening the valve at $x = 0$. The valve is opened instantaneously at $t = 0$ and the length of the pipe (L) does not change after opening the valve (zero-strain condition at $x = L$). The presence of frequent axial expansion joints is also assumed. This prevents the hoop-stress shock-wave from getting ahead of, and subsequently reflecting back onto, the perturbed porous media in such a way that these phenomena are asynchronous.

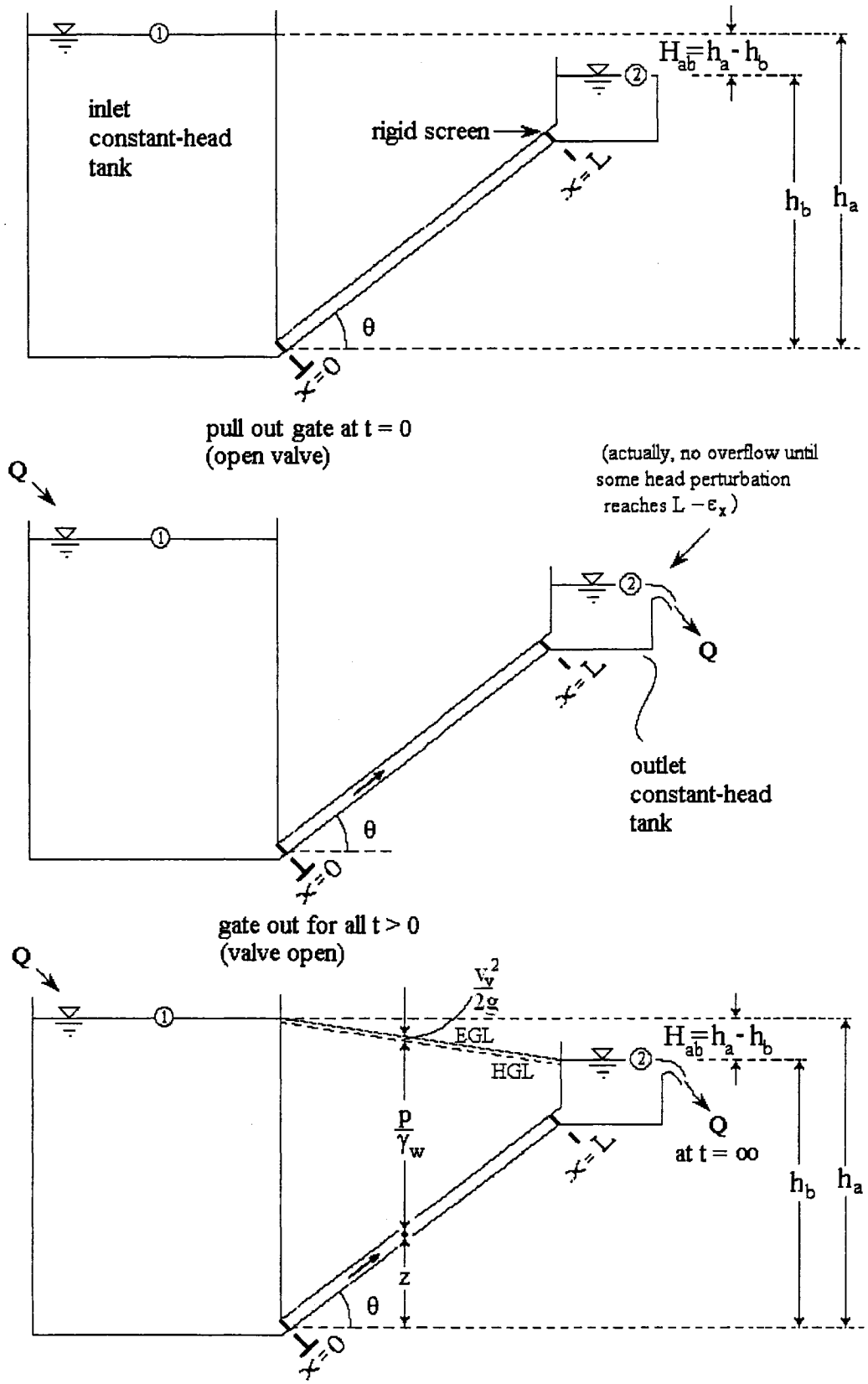

Figure 1.1 Schematic of the experimental set-up.

The head and bulk velocity of the flow were the dependent variables investigated; distance and time were the independent variables. The applied boundary conditions were temporally invariant. This meant not only that the applied head difference was fixed, but that the individual head values at either end of the sample were also fixed. Dirichlet conditions were applied by using fixed-head boundary conditions. In order to investigate the variation of head and velocity under various boundary conditions, various hydraulic gradients were applied. From Figure 1.1, a hydraulic gradient is defined by $(h_a-h_b)/L$. Even though the heads at $x = 0$ and $x = L$ are known, the velocity at the upstream boundary cannot easily be obtained. The boundary conditions of velocity can neither be accurately calculated using Darcy's Law or an Ergun-type equation, nor can they easily be measured with good accuracy. In this study, the boundary conditions of velocity were unknown. These boundary conditions can be identified by analytical and/or numerical studies.

1.3. Objectives and Expected Contributions

In order to understand highly unsteady non-Darcy flow phenomena, the governing equations were analyzed using various mathematical methods. It was desired to assess the individual effects of each term making up the governing equations and to quantify the temporal and spatial variations of each such effect. It was suspected that the dominant mechanisms in very small time and space were different from those associated with large time and space. The objectives and expected contributions of this study can be summarized as follows:

1. to develop dimensionless forms of the momentum and continuity equations, and show that the functional dependence of each dimensional parameter is not unique. It was hoped that said dimensional analysis could reduce the complexity of the problem and can produce useful dimensionless groups.
2. to obtain the solutions of various models of flow through porous media using numerical methods, and to compare the solutions using various numerical methods.

3. to obtain regular perturbation solutions of the momentum and continuity equations, and quantify the effects of the individual terms making up the equations, including the temporal and spatial variations in the magnitudes of these terms.
4. to use matched asymptotic expansions to solve the near-boundary problem, where very sharp changes in head and velocity occur. It was surmised that conventional approaches would not work very near said boundary, but that further away from it the more conventional approaches would again be valid. It was therefore surmised that the different approaches needed exploration, as to the limits of their validity.
5. Using an analogy of existing dimensionless numbers, to provide dimensionless numbers for flow through porous media, and show the applicability of the combinations of dimensionless groups as criteria to identify the changes in physical phenomena in porous media.

2. Literature Review

Highly unsteady flow through porous media phenomena can be described using the momentum and continuity equations (Wylie 1976, Nilson 1981, Blick 1988). The momentum equation can be replaced by an energy loss equation (Polubarinova-Kochina 1962, Bear 1972, Hayes *et al.* 1995). If viscous effects dominate, this energy loss equation is simply Darcy's Law. This law can be expressed as a linear relationship between a hydraulic gradient and the bulk velocity of the flow:

$$v = K i \qquad [2\text{-}1]$$

where:

K = hydraulic conductivity (L/T).

Although it is generally accepted that the range of validity of Darcy's Law cannot be definitively stated, it is widely considered to be superior to other methods for computing seepage rates (Cedergren 1997). Dake (2001) states that the application of the Darcy's Law is required to describe 90 % of petroleum reservoir engineering. An independent estimate of K can be obtained from the so-called Carman-Kozeny equation (Carman 1937, Kozeny 1927):

$$h_L = L\frac{(1-n)^2}{n^3}\frac{150\nu}{gD_p^2}v \qquad [2\text{-}2a]$$

where:

n = porosity ($volume_{voids}$/ $volume_{bulk}$, dimensionless),

D_P = diameter of sphere with volume equal to representative particle volume (L).

Chapuis and Aubertin (2003) applied the Carman-Kozeny equation to flow through porous media of terrestrial origin. It can be re-expressed as (Hansen 2004):

$$v = c_1\left[\frac{g}{\nu}n^2\right]i \qquad [2\text{-}2b]$$

or:

$$h_L = \frac{L}{c_1}\frac{\nu}{n^2}\frac{v_v}{g} \qquad [2\text{-}2c]$$

where:

$$m = \frac{e\,d}{r_e\,6} \qquad [2\text{-}2d]$$

c_1 = empirical coefficient (dimensionless),

m = hydraulic mean radius (L),

e = void ratio (= n/(1-n)), (dimensionless),

d = particle diameter (L),

v_v = V/n, void velocity (L/T),

r_e = empirical coefficient that allows for departure from surface area efficiency of a sphere (dimensionless), for which $r_e = 1$ (Sabin and Hansen 1994).

Equations [2-1] and [2-2] are applicable if

$$Re_{pore} = \frac{v\,m}{n\,\nu} \lesssim 1 \qquad [2\text{-}3]$$

where the threshold of unity is a reasonable choice (compare Ergun 1952) but has a range of in the literature. The above definition of Re_{pore} uses the most representative velocity, v/*n*, also called the average linear velocity (Freeze and Cherry 1979) and characteristic length, *m*. A measure of pore size, *m*, is much more rationale than the common use of particle diameter in *Re*. The intrinsic permeability k_I of a porous medium has dimensions L^2 and is related to hydraulic conductivity by the following definition:

$$K = \frac{g}{\nu} k_I \qquad [2\text{-}4]$$

Since the most rationale choice for the characteristic length is the hydraulic mean radius:

$$k_I = c_1\,n\,m^2 \qquad [2\text{-}5]$$

Equation [2-2d] is exactly true if the surface area of the pore volume is the same as the surface area of the particles (no surface area is lost to particle-to-particle contact). This is an approximation. How good it is depends on particle shape. It is very untrue for very oblate particles. A no-flow value of *m* must be based on a value of r_e that accounts for the area lost to inter-particle contact. With flow occurring, the existence of dead zones

near the contact areas increases in importance as v_v increases for PDT-and-above flow regimes (Wahyudi *et al.* 2002). Hansen (2004) has pointed out that replacing D_p with d and comparing the Carman-Kozeny eqn to [2-2b/c] with $r_e = 1$ yields:

$$K = \frac{36}{150}\left[\frac{g\,n}{\nu}m^2\right] = 0.24\left[\frac{g\,n}{\nu}m^2\right] \qquad [2\text{-}6]$$

which means that:

$$k_I = 0.24\,n\,m^2 \qquad [2\text{-}7]$$

Therefore, the Carman (1937, 1939) recommended c_1 value of between 0.2 and 0.5 appears to contradict the lower limit on r_e of unity. Departures from spherical shapes imply a value of c_1 that is larger than 0.24 (not smaller). This discrepancy may be due to the dynamic effects of dead zones near contact areas, and/or to the presence of artificial particles that Carman (1937) included in his research. For uni-sized media at loose-to-average porosities, m is about 10 to 12 times smaller than d. For well-graded material m can be much smaller. Laboratory methods for estimating m include gas adsorption and mercury intrusion for fine-grained media (Gregg and Sing 1967) and the use of coatings for larger particles (Garga *et al.* 1991). However, it is far better to measure K from a one-dimensional flow experiment, for which procedural standards exist (e.g. ASTM 2002a/b).

If the inertial effect is not negligible, a linear relationship between head loss and velocity cannot be used and some other (non-linear) equation needs to be considered. Examples include the Forchheimer (1901) equation, the Ergun (1952) equation, and the Burke-Plummer equation (see Sissom and Pitts 1972), all of which include 'inertial' terms in them. For flows outside the range of validity of Darcy's Law, the Brinkman equation (Brinkman 1947) is the most popular in petroleum engineering whereas the Ergun equation is probably the best-known relationships in chemical engineering. For FDT flow through porous media, there is no universally-accepted equation used to describe it. Stephenson (1979) has suggested:

$$h_L = K_{st}\left(\frac{L}{d\,n^2}\right)\frac{v^2}{g} \qquad [2\text{-}8]$$

where:

K_{st} = Stephenson's friction factor, a parameter accounting for particle angularity, ranging from 1 for polished spheres to 4 for rough and angular crushed stone (dimensionless).

The Burke-Plummer equation (Burke and Plummer 1928), used mainly by chemical engineers, is specifically intended for application to FDT flow through porous media:

$$h_L = \frac{1.75}{g}\frac{L}{D_P}\frac{1-n}{n^3}v^2 \qquad [2\text{-}9]$$

$$(Re \geq 100)$$

For PDT flow, a rather large body of similar literature built up in which revised values of the two coefficients in the zero-intercept second-order polynomial have been presented. The zero-intercept second-order polynomial form, is sometimes called the Forchheimer equation or Forchheimer form. It appears that Forchheimer (1924) actually held the following forms of non-Darcy flow expression in roughly equal regard:

$$J = \alpha_0' v + \beta_0' v^2 \qquad [2\text{-}10a]$$

$$J = \alpha_0' v^{\beta_0'} \qquad [2\text{-}10b]$$

$$J = \alpha_0' v + \beta_0' v^2 + \gamma_0' v^3 \qquad [2\text{-}10c]$$

where:

J = hydraulic gradient.

His 1924 treatise indicates clear awareness that the α_0' and β_0' coefficients should depend on particle size, and his comments on the above also harken back to his own 1901 equation for "Lechfeldes gravel":

$$J = 0.71v + 8v^2 \qquad [2\text{-}11]$$

for v from 0.12 cm/s to 1.2 cm/s.

and that of Kresnik (1906) for "pure sand", said to be in "complete harmony" with his own work:

$$1000J = \frac{u_1}{0.7 + u_1}\left(\frac{1}{d} + \frac{u_1}{0.8d + 10.5d^2} + \frac{u_1^2}{30000d^2}\right) \qquad [2\text{-}12]$$

in which u_1 was the "filter speed[3]" in m/day.

In the post-war years, interest continued in non-Darcy flow through porous media. Rose (1945) presented parallel curves on a Moody-type diagram for materials of increasing angularity. Brownell and Katz (1947) and Brownell *et al.* (1950), sought definitions of the Reynolds number that could be applied to any porous media. They stated that porosity was the most important parameter affecting resistance to flow, with particle sphericity and angularity being of secondary importance. It does not appear that any of these curves attained significant general usage, however. Dullien (1975), citing Rumpf and Gupte (1971), suggests that universal constants and a general formula for describing flow through porous media have not yet been found because of the effects of particle-size distribution and packing structure. This continued search for constants and coefficient has occurred in spite of the fact that the use of a conduit analogy with a form of friction and a form of Reynolds Number results in some spurious correlation in the regression (Hansen and George 1993). Further, such regressions are biased because they are usually done using the log's of the data (Duan 1983), and still worse, require the re-arrangement of an ordinary least-squares regression result in order to be of practical use.

The original Ergun (1952) equation, as a friction factor versus Reynolds number relationship, resulted in regression coefficients of A' = 150 and B' = 1.75:

$$f\left(\frac{n^3}{1-n}\right) = 150\left(\frac{1-n}{Re}\right) + 1.75 \qquad [2\text{-}13]$$

where:

$$f = \frac{id}{v^2/2g} \qquad [2\text{-}14]$$

and where:

$$Re = \frac{vd}{\nu} \qquad [2\text{-}15]$$

Re-arrangement gives:

$$h_L = L\left(\frac{1-n}{n^3}\right)\left[\frac{150\nu(1-n)}{gD_p^2}v + \frac{1.75}{gD_P}v^2\right] \qquad [2\text{-}16]$$

[3] Filter speed may refer to the velocity in the voids, computed as V_{bulk}/n.

Equation [2-16] is a combination of the Carman-Kozeny and Burke-Plummer equations. It has been modified by Reichelt (1972) to allow for the wall-effect. In light of eqn [2-16] Forchheimer eqn can then be expressed as:

$$i = r'v^2 + s'v^2 \qquad [2\text{-}17]$$

where:

$$r' = A'\frac{\nu}{gd^2}\frac{(1-n)^2}{n^3} \qquad [2\text{-}18]$$

and where:

$$s' = B'\frac{1}{gd}\frac{(1-n)}{n^3} \qquad [2\text{-}19]$$

The form which velocity as the dependent variable is less convenient (Hansen *et al.* 1995):

$$v = \frac{150}{2(1.75)}\frac{\nu(1-n)}{d}\left\{\sqrt{1+\frac{4(1.75)g}{150^2\nu^2}\left[\frac{nd}{(1-n)}\right]^3 i} - 1\right\} \qquad [2\text{-}20]$$

Macdonald *et al.* (1979) attempted to harmonize all existing non-Darcy flow data and arrive at a single comprehensive fit. The independent variable was a form of Darcy-Weisbach friction factor and the dependent variable was a form of Reynolds number, so that spurious correlation was built in. Their result was:

$$f\left(\frac{n^3}{1-n}\right) = C_1'\left(\frac{1-n}{Re}\right) + C_2' \qquad [2\text{-}21]$$

$$f = \frac{dp}{dx}\frac{D_{eq}}{\rho v_{bulk}^2} \qquad [2\text{-}22]$$

$$Re = \frac{\rho v_{bulk} D_{eq}}{\mu} \qquad [2\text{-}23]$$

$$C_1' = 214.25 - 151.72n \qquad [2\text{-}24]$$

where:

C_2' = 1.8 for smooth particles and 4.0 for rough particles,

D_{eq} = diameter of equivalent spherical particle (L).

Before presenting the above and various other fits, they commented that:

> "Pragmatically, the complexity of the flow pattern rules out a rigorous analytic solution of the problem and suggests that an empirical or quash-empirical correlation is the best that one can hope for."

The above equation was stated as being accurate within ± 50 %, which is certainly not an impressive outcome. As was obvious in Ergun's original plot, the uncertainty in Macdonald's equation was found to increase with increasing Reynolds number, as clearly seen by the intensity of the scatter in the versus Re plot. Du Plessis (1994) used analytical methods and a form drag considerations to argue that the coefficients of 150 and 1.75 are themselves porosity dependent, being 207 and 1.88 at n = 0.44. He also used a geometric idealization of porous media together with the Navier-Stokes equation to lend some theoretical support to eqn [2-24]. The idealization was that the particles were considered cubes, leading to a 3-D grid of pores. Du Plessis (1994) made a dubious approximation. This was that the amount of fluid-to-fluid shear stress between main-flow vectors (in the direction of the bulk flow) and side-channel flow vectors (oriented at 90°) was negligible. It is interesting that in spite of the approximation, the nominal values of C_1' and C_2' were not far from experimental values and that it was also possible to express their values in terms of the porosity (as in eqn [2-24]).

In petroleum engineering, another widely-used equation is the so-called back-pressure equation. This equation uses a power law, whereas Forchheimer and Ergun use a second order polynomial. George and Hansen (1992) have shown that the parameters in a second order polynomial can be computed from the parameters in a power law, and vice versa. Using a power law, an exponent of 3/2 on average velocity has been proposed by Chauveteau and Thirriot (1967) and by Skjetne (1999), for Re >> 1. Another dimensionally inconsistent equation based on the power law form, and which is commonly-used to describe flow through rubble mounds, is the Wilkins' equation (1956). The exponent of 1.85 in the Wilkins' expression is a clear indication that this is applicable to the upper end of the PDT regime.

Whitaker (1996) theoretically arrived at the so-called Forchheimer form by beginning with the Navier-Stokes equations. He showed that the Forchheimer correction

is quadratic in the velocity even for small values of the Reynolds number and argued that this functional dependence should not change greatly with increasing Reynolds number. In the second-order polynomial form, the square-of-velocity term is generally accepted to represent inertial effects. However, why and when this term arises has still not been completely settled. Skjetne (1999) pointed out that although Forhheimer form has been known for about 100 years, the component which has the square of the velocity is far from well understood. Many efforts have been made to find out the mechanism behind the square-of-velocity term. Happel and Brenner (1965) believed that Darcy's Law failed when the distortion that occurs in streamlines, owing to changes in direction of motion, is great enough for inertial forces to become significant (compared with viscous forces). Similarly, Foster (1967) explained that non-linear dependence of the 'pressure' gradient on the velocity should naturally appear because the steady-flow stream lines in most porous media are not parallel, but rather converge and diverge, even for steady flow. Wright (1968) has described the fluid processes taking place in a porous medium as the velocity of flow increases toward fully-developed turbulence. He proposed the existence of "steady inertial" and "turbulent transition" regimes. For the "steady inertial" regime, the convective accelerations are thought to be are important and cause the relationship between hydraulic gradient and velocity to begin to be non-linear. These convective accelerations, caused by the tortuosity of the flow paths, suppress full turbulence in this regime. At higher velocities, a "turbulent transition" regime begins, in which random micro-velocity fluctuations occur. These fluctuations cannot be measured directly without sophisticated equipment. In this regime, the hydraulic gradient is proportional to nearly the square of the velocity.

Hassanizadeh and Gray (1987) suggested Re = 10 as a critical value for non-Darcy flow on-set and believed that it is due to an increase in microscopic viscous forces at high velocities. A weak inertial law has been investigated by correcting Darcy's Law with a cubic term in velocity (Mei and Auriault 1991). They found that this weak inertia law is valid when Re = O(1)[4]. The non-linear term has been modelled by Du Plessis (1994) and was attributed (*op. cit.*) to a form drag resulting from the pressure difference between a stagnation point and the wake. Hayes *et al.* (1995) stated that the non-linearity

[4] O(x) in this thesis indicates "of order x".

is due to bends in the flow path and tried to include a pressure drop due to solely the change in flow direction around corners, using an energy-loss equation for bends. They applied a model based on square channels with sharp (90°) bends, which does not seem to be very suitable as a physical model of porous media composed of spherical particles. Andrade *et al.* (1999) explained the deviation associated with non-linearity as due to localized "channeling effects". They characterized the flow transition from laminar to PDT in terms of a partition in the spatial distribution of the kinetic energy in the system; namely, that the flow at low Re values is more localized due to channeling effects than the flow at high Re conditions. Skjetne (1999) felt that the rationale for the non-linearity due to form drag and bends is rather weak. He proposed that the transition in the flow is caused by the development of strong, localized dissipation zones around flow separations.

One of the more recent and noticeable works to describe the relationship between gradient for porous media flow and the velocity over the entire range of Reynolds number has been achieved by Barree *et al.* (2004, 2005). They developed a new equation which can predict the velocity at high gradients (so called trans-Forchheimer flow), and which can be simplified to either the Forchhiemer or the Darcy equation under their governing assumptions. Their so-called complete equation can be expressed as:

$$\frac{\partial p}{\partial x} = \frac{\mu v}{k_d\left(k_{mr} + \frac{(1-k_{mr})}{(1+\rho v/\mu T')}\right)} \qquad [2\text{-}25]$$

where:

p = pressure (atm),

v = velocity of fluid (cm/sec),

μ = absolute viscosity (g/100 cm-sec),

k_d = Darcy permeability coefficient (darcies or cm-g/100-atm-sec^2),

k_{mr} = minimum permeability ratio (dimensionless),

T' = transition constant which can be determined by non-linear regression of actual laboratory apparent permeability data (100/cm if inertial flow parameter β has units of atm-sec^2/g).

Their results show that the so-called trans-Forchheimer flow can occur at values of Re in the range of 10-100. They explained the deviation from the Forchheimer equation as due to either streamlining or flow diversion. The associated trans-Forchheimer (*op. cit.*) equation implies that the inertial effect (V^2 term) may not be the sole factor causing deviation from Darcy's Law, or perhaps that the physical explanation for the V^2 term is something other than an inertial effect caused by local (convective) acceleration. Zeng and Crigg (2006) suggested that the term 'non-Darcy' be used in place of 'inertial effect' and explained non-Darcy effects as being due to liquid-solid interactions. They pointed out that in most porous media the pore diameter is very small, so that the spatial change in velocity across and through pore throats must be negligible.

Even though high-velocity mechanisms within porous media are still not completely understood (Golan and Whitson, 1991), and existing equations do not quantitatively explain and account for all the mechanisms that induce deviations from linear flow behaviour, a pragmatic approach was taken in this study. The research described herein was not intended to unequivically resolve such questions and point to the 'best' non-Darcy flow equation. In this study, a very widely used non-Darcy flow equation was used, namely, the Ergun-type equation. It can be readily re-arranged to a quadratic form and describes flow resistance over quite a wide range of Re numbers. By incorporating such a (well-known) energy loss relationship in the momentum equation, it was nonetheless possible to investigate the effects of the various individual terms found in the governing partial differential equations. The contribution of each term was compared, and the spatial and temporal variations of each term were investigated. It was expected that, if desired, the approach used in this study could be applied to 'more accurate' and/or more general energy-loss equations, so as to obtain more information about the various solutions to the governing partial differential equations.

Various criteria have been suggested to indicate the on-set of the deviation from Darcy's Law. The Reynolds number has been very widely used as the criteria for regime change and many researchers have reported various 'critical' Re values for the transition from Darcy to non-Darcy flow (Fancher and Lewis 1933, Ergun 1952, Bear 1972, Scheidegger 1974, Hassanizadeh and Gray 1987, Blick and Civan 1988, Du Plessis and Masliyah 1988, Ma and Ruth 1993, Andrade *et al.* 1998, Thauvin and Mohanty 1998).

Although the value of the threshold Reynolds number associated with transition from laminar to turbulent flow is well-accepted for flow in conduits (Re =2000), said threshold is difficult to define for flow through porous media. This is partly because investigators have tended to define the Reynolds number for flow through porous media inconsistently. Based on many researchers' investigations, Bear (1972) presented a classification of flow through porous media[5]. In Figure 2.1, three regimes of flow are identified: laminar flow, transition flow (also called the non-linear laminar flow regime), and turbulent flow. Herein these three regimes are referred as the laminar, partially developed turbulent (PDT) flow, fully developed turbulent (FDT) flow regimes.

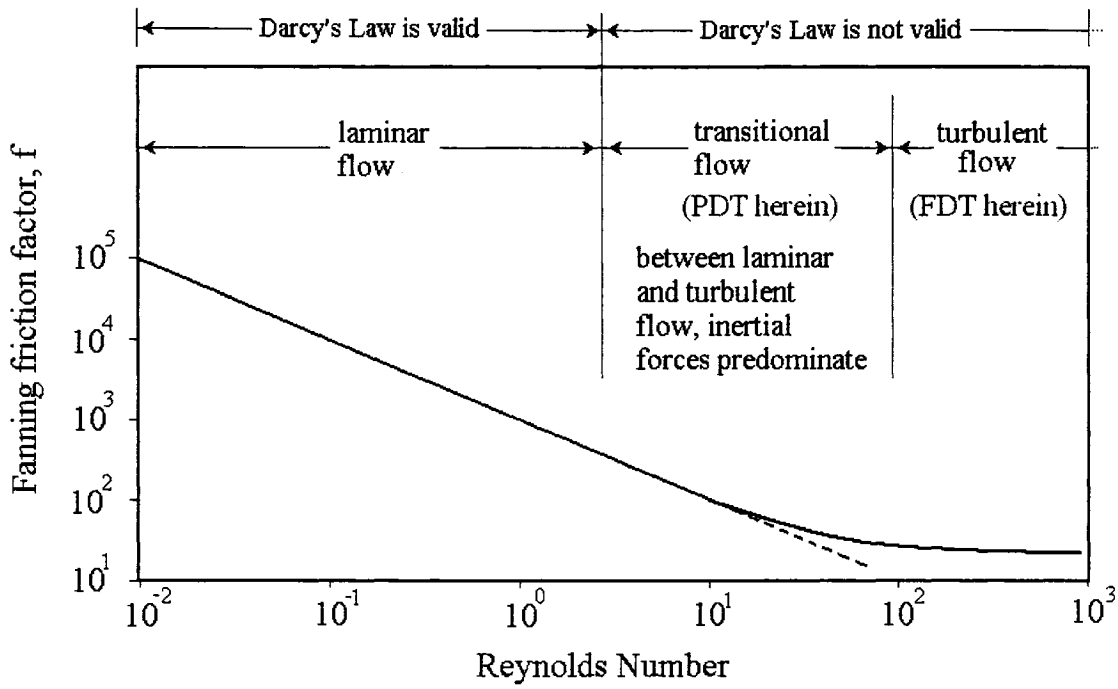

Figure 2.1 Classification of flow through porous media of Bear (1972).

The three Re_{pore} 'thresholds' shown in Table 1 are approximate. These thresholds of Re = 1 and Re = 100 were however used in this study to identify the two transitions in flow regime, partly for pragmatic reasons. The difficulty in selecting such regime-change thresholds for flow through porous media can be readily appreciated in the presentation

[5] others exist: McCorquodale *et al.* (1978), Arbhabhirama and Dinoy (1973).

of the friction-factor Reynolds-number diagram found in such widely-used monographs as Sissom and Pitts (1972). Beyond the fact that there is significant vertical scatter in the data at any given Reynolds number, the best-fit through the three regimes is a smooth curve with no 'kinks' in it.

Table 2.1 Flow regimes and parameters for conduit and porous media flow.

	Laminar (LAM) flow	Partially-developed turbulent (PDT) flow	Fully-developed turbulent (FDT) flow
$Re_{conduit}$	$Re_{cond} < 2000$	$4000 < Re_{cond} < 3500/(\varepsilon_1/D_h)$	$Re_{cond} > 3500/(\varepsilon_1/D_h)^*$
Re_{porous}	Re_{pore} < about 1	$1 < Re_{pore} < 100$	Re_{pore} > about 100

* Pigott (1944).

Venkataraman (1998) derived an empirical equation to better identify the transitions from laminar to PDT, and from PDT to FDT. The Reynolds number at which Darcy's Law deviates from the linear range was obtained as:

$$Re = \frac{0.17}{(C_w)^{1.1}} \qquad [2\text{-}26a]$$

where:

$$C_w = \frac{d}{\sqrt{k_I}} \qquad [2\text{-}26b]$$

d = a particle diameter,

k_I = an intrinsic permeability.

The Reynolds number above which the flow becomes turbulent was expressed as:

$$Re = \frac{10}{C_w} \qquad [2\text{-}27]$$

More detailed divisions of flow regime associated with Re are possible. For example, Fand (1987) showed five regimes, including four regimes identified by Dybbs and

Edwards (1975) and one regime pointed out by Bear (1972). These five regimes are the pre-Darcy flow regime, the Darcy regime, the inertial flow regime, an unsteady laminar flow regime, and a highly unsteady and chaotic regime that qualitatively resembles turbulent flow. Using the range of Re reported in other studies, Zeng and Crigg (2006) summarized critical Re values for "non-Darcy flow" from 1 to 100. They also suggested the use of a Forchheimer number (*Fo*), which was first introduced by Ma and Ruth (1993). *Fo* is the ratio of pressure drop caused by liquid-solid interactions to that by viscous resistance. This number can be used as a criteria to indicate the on-set of non-Darcy flow. *Fo* can be defined as:

$$\mathrm{Fo} = \frac{k\beta_0 \rho v}{\mu} \qquad [2\text{-}28]$$

where:

β_0 = the non-Darcy coefficient,

μ = the absolute viscosity of fluid.

Using dimensional analysis, many other dimensionless numbers can be used to describe various aspects of the conditions of flow through porous media. In this study, analogies to the Mach, Euler and Peclet numbers were used to find relationships between existing dimensionless numbers and various dimensionless groups developed herein, and to discover criteria for identifying changes in the relative importance of various physical phenomena in fluid mechanics that are particular to flow through porous media.

Dimensional analysis can be used to reduce the complexity of a problem. Flow through porous media studies tend to have many variables and parameters, and this increases the complexity of the analysis and the challenges of interpretating the data. Even though important dimensional parameters can be clearly identified, few (if any) reasonable inferences about functional dependence can be made. By using dimensional analysis, the number and complexity of variables which affect a given physical phenomenon can be significantly reduced. Ward (1964) carried out a dimensional analysis in order to obtain expressions for 'a'' and 'b'' in a Forchheimer type equation:

$$\frac{dp}{dx} = a'v + b'v^2 \qquad [2\text{-}29]$$

By assuming the 'pressure' gradient to be a function of the velocity of the flow, the permeability (k) of the porous medium, the density (ρ) of the fluid, and the absolute viscosity (μ) of the fluid, Ward (1964) obtained 'a'' and 'b'' as:

$$a' = \frac{\mu}{k} \qquad [2\text{-}30]$$

and

$$b' = \frac{c'\rho}{\sqrt{k}} \qquad [2\text{-}31]$$

where c' is a dimensionless constant of proportionality.

Ward (1964) also showed that the Reynolds number for porous media can be derived from the ratio of the second term to the first term in eqn [2-29]. Greenkorn (1964) used dimensional analysis to scale down the flows which takes place in a large petroleum reservoir over a period of many years to flows which can be simulated within a smaller time-space continuum. Barree *et al.* (2004) showed that the laboratory data obtained using various porous-media types at various stresses collapse to a single line, using dimensional analysis.

Mathematical models of various degrees of sophistication have long been used to predict flow behavior in porous media. The traditional unsteady groundwater flow equation is precisely analogous to one known as the heat equation (Freeze and Cherry 1979). It is derived from Darcy's Law and the continuity equation, and is a form of diffusion equation, with hydraulic head as the scalar potential (Freeze and Cherry 1979, Fetter 2001):

$$\frac{\partial^2 h}{\partial x^2} = \frac{S_S}{K}\frac{\partial h}{\partial t} \qquad [2\text{-}32]$$

where:

S_S = specific storage (dimensionless),

K = hydraulic conductivity (L/T).

Wylie (1976) included a local acceleration term in the momentum equation to apply the method of characteristics to radially-symmetric transient aquifer flows. Wylie (1976) expressed this momentum equation for unsteady radial flow towards a well as:

$$\frac{1}{gn}\frac{\partial v}{\partial t} + \frac{v}{K} = \frac{\partial h}{\partial r_l} \qquad [2\text{-}33]$$

where:

r_l = radial distance from center of well (L),

v = Darcy velocity (L/T),

h = hydraulic head (L).

Biot (1955) represented the link between the flow field and the stress field in three dimensions, which necessarily accompanies the fluid movement in an elastic porous medium. He showed that the deformation is determined by both strain tensors in both the solid and the fluid, and suggested using the velocity of the fluid relative to the grains in Darcy's Law. However, a general groundwater flow equation (diffusion eqn) without Biot's correction terms can give satisfactory results in the vast majority of applications. Gambolati (1973) showed that the diffusion equation is good when the formation (aquifer) compacts less than 5 % of the initial thickness. Gambolati (1974) also showed that the so-called 'three-dimensional effect' causes the deviation from the diffusion equation. This effect is due to the pore pressure changes in the rest of the system surrounding a given point of interest in a three-dimensional elastic system. He pointed out that if this effect is negligible, the equation of flow reduces to the usual diffusion equation and in one-dimensional problems, the effect is identically zero. Brinkman (1947) modified Darcy's Law by introducing Laplacian term to account for the friction at the solid-fluid interface and the momentum transfer inside the fluid caused by a velocity gradient. The Brinkman expression can be expressed as:

$$\nabla p = -\frac{\mu}{k_I} v + \tilde{\mu}\nabla^2 v \qquad [2\text{-}34]$$

where:

p = fluid pressure (F/L^2),

μ = fluid viscosity (M/L/T),

k_I = intrinsic permeability (L^2),

v = velocity of fluid (L/T),

$\tilde{\mu}$ = effective viscosity[6] (M/L/T).

Even though the use of the Brinkman equation is used for relatively large porosity i.e. the fraction of void to total volume of the body is close to unity (Yamamoto 1973, Kolodziej 1988, Belhaj 2004), this expression can be used to generalize the Darcy's Law by the matching of velocities and stresses at the boundary between the fluid and the porous medium (Yamamoto 1973). Yamamoto (1973) investigated the asymptotic behavior of the flow near the surface of the porous medium.

These models can be used to predict the general behaviour of groundwater flow but may not be used to predict the behaviour of high-Re flows because they do not include a term to account for inertial effects. An Ergun or Forchheimer-like equation that retains the local acceleration term in addition to the viscous and inertial terms, can be used to account for the non-linear behavior of the flow. Many numerical and laboratory studies have proven that flow through porous media can be predicted very well using a simple model that has no local acceleration term and/or convective acceleration term (Wiest 1962, Blick 1987 and 1988, Wylie 1976, Nield 1991). However, these studies were limited to large space and time scales. In order to investigate dynamics of the flow under various boundary conditions and within a more complete space and time region, a local (temporal) acceleration term and/or convective acceleration term may need to be included in the model. Polubarinova-Kochina (1952) suggested an extended form of the Forchheimer equation that included a local acceleration term for cases of unsteady flow in porous media:

$$i = a_3 v + b_3 \mid v \mid v + c_3 \frac{\partial v}{\partial t} \qquad [2\text{-}35]$$

Burcharth (1995) pointed out that a possible convective acceleration term ($v(\partial v / \partial x)$) can not be treated in the same way as a temporal (local) acceleration term ($\partial v / \partial t$), so the

[6] usually taken to be the same as the nominal absolute viscosity. If $n \approx 1$ under expanded-bed conditions, Brinkman (1947) suggested using Einstein's eqn (1906) to evaluate $\tilde{\mu}$.

coefficient 'c_3' cannot also be applied to a convective acceleration term. Therefore, $(\partial v / \partial t)$ cannot be substituted by the total derivative (dv/dt). However, it can be verified using dimensional analysis that the total derivative in Newton's second law can account for the fact that the quadratic term dominates over the local acceleration term, which in turn dominates over the convective acceleration term. Therefore, the total derivative can often substitute for the partial derivative in eqn [2-35]. Blick (1987) proposed the so-called capillary-orifice model to better approximate high-speed flows through porous media. This model included a convective acceleration term beyond the extended Forchheimer model proposed by Polubarinova-Kochina (1952). This capillary-orifice model uses a form of momentum equation very similar to that derived from the Newton's second law equipped with the Ergun equation. It exhibits a form similar to one arising from the Navier-Stokes equation, which will be presented later. Macedo *et al.* (2001) used the κ-ε model for turbulence to investigate the influence of certain turbulent effects on a fluid flow through porous media by numerically solving the Reynolds-averaged Navier-Stokes equations.

Analytical solutions to the classical groundwater flow equation using Darcy's Law and continuity are available for various boundary conditions (Carslaw and Jaeger 1959). Various analytical methods for solving groundwater flow equation were summarized by Bear (1972). However, relatively few analytical solutions and numerical schemes are available in the literature for PDT flow through porous media, even though there is practical and theoretical interest in such solutions (Moutsopoulos and Tsihrintzis 2005). Existing analytical solutions to the so-called Forchheimer equation include those of Volker (1975), Lacher (1976) and Bear (1979). Approximate analytical solutions have been obtained by Wu (2002) and Moutsopoulos and Tsihrintzis (2005) for certain practical applications. The approximate solution of Moutsopoulos and Tsihrintzis (2005), could be used to check the accuracy of the numerical solutions in this study. For boundary conditions a Δh of 1 m and head of 0 m at $L = \infty$ were used. The head of 0 m at the downstream end ($L = \infty$) ensured that the disturbance at the upstream end never arrived at the downstream end. Their approximate analytical solution was presented as:

$$h_0^* = 1 - \frac{2}{\pi}\left[\frac{\theta^*}{\left(1+\theta^*\right)^2} + \operatorname{arctg}\left(\theta^*\right)\right] \qquad [2\text{-}36a]$$

where

$$h_0^* = \frac{h_0'}{\Delta h} \qquad [2\text{-}36b]$$

$$\theta^* = \frac{xt^{-2/3}}{\gamma_0'} \qquad [2\text{-}36c]$$

$$\gamma_0' = \sqrt[3]{\frac{\pi}{\Delta h \Lambda^2}} \qquad [2\text{-}36d]$$

$$\Lambda = \frac{2}{3} S_0 \sqrt{b_0} \qquad [2\text{-}36e]$$

$$S_0 = \frac{S}{B_2} \qquad [2\text{-}36f]$$

where h_0' = hydraulic head,

B_2 = aquifer thickness,

S = storage coefficient,

b_0 = empirical coefficient in Forchheimer-Dupuit eqn.

Falade (1979) used a generalized Green's function approach to the problem of unsteady fluid flow and indicated how this could be used for some of the systems frequently encountered in oil and water reservoir problems. Furman and Neuman (2003) solved a particular transient flow through porous media problem using a Laplace-transform analytic element method (LT-AEM). They performed a Laplace transform of the original flow problem and solved the equation using the analytic element method. The solution was inverted numerically back into the time domain. The governing equation used was, however, the two-dimensional linear diffusion equation. Auriault *et al.* (1985) applied a 'homogenization process', in which a macroscopic description of the problem was constructed from the microscopic one.

When the problem includes complicated geometric configurations and variable aquifer characteristics, analytical methods have very limited application. However, numerical methods have reached a level of sophistication that efficient solutions to many practical complex problems can now be obtained. Mahdaviani (1967) solved steady and unsteady flow towards gravity wells using the method of characteristics (MoC).

Mahdaviani (1967) demonstrated the power, simplicity, and practical uses of this numerical solution for unconfined aquifers and also pointed out that the Theis solution for confined aquifers is not very accurate for unconfined aquifers. The perceived advantages of using MoC for solving transient flow problems included:

(i) the explicit nature of the solutions, both at interior positions and at interactive boundaries,

(ii) the inherent stability of this method.

The method of characteristics has often been used to solve so-called water-hammer problems. Even though the governing equations describe pipe-flow transients and not unsteady flow in porous media, the mathematical methods used in the former can be adapted to solve the latter because the partial differential equations governing these two classes of problems have similar forms. The water-hammer equation describes the propagation of a pressure wave, which can be accompanied by sharp changes in head and velocity. In general, if explicit finite-difference methods are applied to solve this problem, stability problems normally arise; these can be resolved using MoC. An alternative way to solve this sharp-change problem using finite difference methods is to use a technique to make the solution smooth, such as successive over relaxation (Smith 1978).

Wylie (1976) used the method of characteristics to solve the problem of transient radial leaky aquifer flows. He transformed the governing partial differential equations to a set of ordinary differential equations that can be integrated. The result was a set of algebraic equations that could be solved using the method of characteristics. Wylie (1976) used an inertia multiplier to modify the acceleration term. By introducing this multiplier, unequal time and space steps could be used between computational sections. Outcomes obtained using MoC compared well with the analytical solution for the case of a single pumped well. Streeter and Wylie (1968) used the MoC to solve two and three-dimensional transient flow problems using the one-dimensional water-hammer equations arranged in a latticework. The latticework technique can be applied directly to problems of 2-D and 3-D flows in porous media. The method of characteristics can also be applied to the study of the seismic response of reservoir-dam systems (Wylie 1975). The

response of a reservoir to seismic shocks was simulated and the numerical solutions were shown to be compared well with analytical ones. Wiggert and Wylie (1976) solved a two-dimensional transient groundwater flow problem using the method of characteristics in the horizontal plane. They replaced the two-dimensional space domain with a latticework of line elements which intersected at nodal points. They suggested that the MoC could be adapted to other two-dimensional and even three-dimensional diffusive problems.

Ghidaoui and Karney (1995) showed how the continuity and momentum equations are interrelated by solving the so-called water-hammer equation using the method of characteristics. Ghidaoui *et al.* (1998) subsequently developed an integrated energy approach for transient problems in pipelines using the MoC, and estimated discretization errors. Arfaie *et al.* (1993) studied the stability and accuracy of pipe friction approximations within MoC solutions to water-hammer problems. They sought to identify the physical and numerical conditions which effect both numerical stability and accuracy, for various discrete models of the non-linear friction term. In addition to the Courant-Friedrichs-Lewy (CFL) criterion, the pipe friction instability criterion number of Wylie (1983) was used as a second criterion for numerical stability. Wylie (1983) had presented the theoretical stability limit for large numbers of nodes (n') as:

$$C_R' < \frac{1}{2} \qquad [2\text{-}37]$$

Arfaie *et al.* (1983) rearranged this number into the following form:

$$C_R' = \frac{1}{4}(MaF)\left[\frac{C_R}{(n'-1)}\right] \qquad [2\text{-}38]$$

where:

n' = number of solution nodes,

C_R = Courant number,

Ma = Mach number,

F = overall pipe friction-loss coefficient.

Relatively recent interest in energy-related approaches has provided new impetus for the study of flow through porous media. Nilson (1981) studied highly unsteady cases and showed that the 'early' flows are inertia-dominated, in accordance with the Ergun equation, but that 'late' flows are viscous-dominated, in accordance with Darcy's Law. These results are relevant to the solutions in which the regular perturbation method was applied, to be described herein.

Pruess and Narasimhan (1985) applied a multiple-interacting-continua method (MINC) for modelling fluid and heat flow in fractured porous media. They lumped appropriate portions of the flow region (e.g., certain groups of well-connected fractures or portions of porous blocks) into distinct continua that interact with each other. Mass flux and energy flux were then used to model the thermodynamic conditions of the system.

Pedras and Lemos (2000) studied the turbulent kinetic energy in flow through porous media using a double-decomposition (time and volume) methodology. For the interpretation of unsteady flow through porous media, Karney (1989) has suggested using an energy concept. He applied this concept not only to unsteady Darcy flow through porous media but also to unsteady closed-conduit flow (McInnis and Karney 1990). This energy concept or balance can be derived from the first law of thermodynamics:

$$\underbrace{\Delta U}_{\substack{\text{change in}\\ \text{interal energy}}} = \underbrace{W}_{\substack{\text{heat added}\\ \text{to the system}}} - \underbrace{V}_{\substack{\text{work done}\\ \text{by the system}}} \qquad [2\text{-}39]$$

The work done at the boundaries is partly used to increase the internal energy of the system and partly to overcome the resistance to flow. The increase in internal energy is further partitioned into the strain energy stored in the elastic soil matrix and the strain energy stored in the pore water, due to fluid compression. An 'energy-density' concept has been further suggested by Karney (1989):

$$\frac{\Delta W}{\Delta t} = \frac{\xi'_{1\text{soil}}}{dt} + \frac{\xi'_{1\text{waterl}}}{dt} + \frac{\Delta_{\text{dissipation}}}{\Delta t} \qquad [2\text{-}40]$$

where:

ξ'_1 = energy density ($FL/T/L^3$, F/TL^2).

For non-Darcy flow, the energy dissipation can be further partitioned into viscous dissipation and inertial dissipation. This interpretation, using energy concepts, is similar to the approach used in this study, i.e. the perturbation expansions associated with H and V. However, the perturbation method (as applied herein) uses dimensionless head and velocity to show the contribution of each term. It is therefore not necessary to convert each term into an energy density form. Further, because dimensionless forms of the governing equations were used in this study, the relative importance of each term can (in general) be readily shown using an order-of-magnitude investigation of the dimensionless groups, which become the coefficients of the individual terms in the governing PDE's.

The momentum equation consists of viscous, inertial, local acceleration, and convective acceleration terms. In the laminar regime, the viscous effect is dominant and the magnitudes of the other terms are very small compared to the viscous term. Even though the magnitudes of these terms are very small, it is of interest to know whether these terms can be safely neglected, how small they are, and to better understand their variations in time and space. It is also of interest to see how these various effects may change in relative importance as the regime of the flow changes. In order to answer these questions, information is needed about the nature of the solutions of the governing equations. This information may not be obtained from the exact analytical solutions because they are sometimes useless for making such physico-mathematical interpretations. The only way to get this information is through the use of approximations, numerical solutions, or combinations thereof.

Foremost among the so-called approximate methods are perturbation methods (Nayfeh 1973). The terms in perturbation expansions are often governed by simpler equations, for which exact solution techniques are available. Even though the exact solutions of the perturbation expansions cannot be obtained, the numerical methods used to solve the perturbation equations (even approximately) are often easier to construct than the numerical approximations of the original governing equations (Bush 1993). In this study, numerical solutions of the perturbation equations were obtained using explicit finite-difference schemes. Perturbation methods have been widely used in the study of flow through porous media. However, most of these studies have focused on the investigation of the concentration of contaminants or thermal convection in saturated

porous media (Nield *et al.* 2003a and 2003b, Hooman and Ranjbar-Kani 2004). Water-hammer problem can also be solved using perturbation methods (Jayasinghe and Leutheusser 1972, Walker 1975). Walker (1975) applied perturbation methods to fluid transients using the steady-state form of a planar water-hammer wave equation.

Using the regular perturbation method, even though some of the terms are multiplied by parameters having very small magnitudes, the presence of these terms often cannot be simply neglected. This is because the problem can depend on these small parameters in a 'singular' way. Matched asymptotic expansions can be used to solve such singular problems. The method used by Ludwig Prandtl in 1904 to analyse viscous boundary layers spread to other fields and has been generalized to the "method of matched asymptotic expansions." Blasius (1908) used it in boundary-layer theory to arrive at an analytical expression of the velocity distribution in the laminar layer. The theory was later generalized to cover the transition from laminar to turbulent flow, and then to turbulent flow (Schlichting 1951). Kaplun (1954) introduced the formal inner-limit and outer-limit processes for boundary-layer theory and presented the corresponding inner and outer expansions. The application of this method to various fields has been described by van Dyke (1975, 1994), O'Malley (1994), Cole (1994), Eckhaus (1994), and Veldman (2001). Dyke (1994) presented applications of matched asymptotic expansions in hydrostatics, hydrodynamics, elasticity, electrostatics, and acoustics. Benilov (2004) compared the method of matched asymptotic expansions with intuitive approaches, and presented some of its advantages. Similarly, Wang *et al.* (2003) used a two-scale homogenized method to solve the Navier-Stokes equation at low Reynolds number. This homogenization method adopted an asymptotic expansion of velocity and pressure through the micro-structures of porous media. In the local problem (micro-scale), the momentum component was derived from a version of the Navier-Stokes equation without an acceleration term $(\partial v / \partial t)$.

Asymptotic methods has also been applied for research on the dynamics of waves in saturated porous media. Edelman (1997, 1999) used two-scale asymptotic methods to solve the generalized Biot model (1955). The Biot model has a correction term to account for deviations from the Darcy's Law. This Biot correction term, included in the momentum equation with a differential operator η, may be written:

$$\eta = 1 - a_0 \frac{\partial}{\partial t} + b_0 \frac{\partial^2}{\partial t^2} \qquad [2\text{-}41]$$

In the momentum equation, this η operator applies to the velocity as:

$$n\rho_l \left[\frac{\partial}{\partial t} + \left(v_{lj} \frac{\partial}{\partial x_j} \right) \right] v_{li} + n \frac{\partial}{\partial x_j} p\delta_{ij} + n^2 \eta (v_{li} - v_{si}) = 0 \qquad [2\text{-}42]$$

where:

n = the porosity,

v = the velocity vector,

p = the pressure,

δ_{ij} = the effective stress tensor,

and where the subscripts l and s indicate liquid and solid, respectively.

The above momentum equation does not retain the inertial term (v^2). The Biot correction therefore only has local acceleration and the second order derivative of velocity with respect to time. Levy *et al.* (1996) added an inertial term to Euler's equation to investigate wave propagation in a saturated rigid porous media. The momentum equation associated with pressure and velocity was expressed as:

$$\frac{\partial v}{\partial t} + v \frac{\partial v}{\partial x} + \frac{1}{\rho} T_f \frac{\partial p}{\partial x} = -F' v^2 \qquad [2\text{-}43]$$

where:

F' = coefficient which depends on porous material structure and associated with v^2 term (1/L),

T_f = tortuosity coefficient (dimensionless).

The above momentum equation does not account for the viscous effect. In this study, the viscous term, inertial term, and local acceleration terms were included in the momentum equation and the effects of these terms on the development of head and velocity were investigated, and under a range of boundary conditions.

Even though the matched asymptotic method has seen numerous applications in various areas, it is difficult to find examples where the interest has been in the hydraulic

head and/or velocity of flow through porous media. Dagan (1968) developed a Dupuit solution of steady flow toward wells using matched asymptotic expansions. He investigated the steady-state free surface-flow of an incompressible liquid through a homogeneous and non-deformable porous medium, toward a well. In his matched asymptotic expansions, the inner expansion was only valid in the vicinity of the well and the outer expansion only at large distances from it. The Dupuit approximation coincides with the zero-order term of the potential outer expansion. The derivation of a second-order outer term makes possible the discussion of the validity of the Dupuit approximation, which tends asymptotically toward the exact solution. Carrier (1970) applied matched asymptotic methods to geophysical problems to do with the dynamics of oceans and atmospheres. Nayfeh (1971) used the method of multiple scales to describe non-linear dispersive waves occurring at the interface between two fluids. The physical systems of dispersive waves were divided into three sub-systems:

(i) waves on the interface between a liquid layer and a subsonic gas flowing parallel to the undisturbed interface,

(ii) waves on the surface of a circular jet of liquid,

(iii) waves in a hot electron plasma.

Nayfeh (1971) found that the partial differential equations governing the temporal and spatial variations of the wave-numbers, amplitudes, and phases have the same form for all these systems. Many other mathematical methods have been applied to solve wave propagation problems in saturated porous media. Boer *et al.* (1993) derived a one-dimensional analytical solution for transient wave propagation in fluid-saturated incompressible porous media using Laplace transforms. Levin (1996) investigated the propagation of pressure waves in saturated porous media for wave-pulses in petroleum reservoir by solving the classical heat conduction equation (with a non-linear term) using the method of quasi-characteristics. Zhang (2005) used a numerical method known as the transmission matrix method to describe wave propagation in saturated visco-elastic porous media. This was achieved by taking the Laplace transform for time and the Fourier transform for space.

If the matched asymptotic method is applied to the momentum and continuity equations, the inner expansion can represent the wave propagation phenomena and the outer expansion can represent diffusion. The diffusion part can be related with a so-called porous medium equation (PME), which is well known in applied mathematics and physics. In spite of the simplicity of the equation and of its applications, and due perhaps to its non-linear and degenerate character, a mathematical theory for the PME has only very recently been developed. Vazquez (1992) has remarked that although these techniques depart strongly from the linear methods used to treat the classical heat equation, and that some of the basic techniques are neither difficult nor require 'heavy machinery'. They can also be applied in, or adapted to, the study of many other non-linear PDE's of the parabolic type. The PME was first derived by Boussinesq in 1903, in the study of gas flows through porous media. As discussed by Aronson (1985), the porous medium equation can show non-linear diffusion mechanisms. It can be expressed as:

$$u_t = \Delta\left(u^{m_0}\right) \qquad [2\text{-}44a]$$

or

$$u_t = \nabla \cdot \left(m_0 u^{m_0 - 1} \nabla u\right) = \nabla \cdot \left(\frac{\nabla u}{u^{p_0}}\right) \qquad [2\text{-}44b]$$

where Δ is a Laplacian operator.

The quantity u can present any physical property in eqn [2-44] and is referred to as a scalar potential. It can be the density or concentration in a diffusion process, the hydraulic head in flow through porous media, or the temperature in a hot medium. Depending on the exponent, m, equation [2-44] can be categorized into three mechanisms. If $m_0 > 1$, the governing mechanism is a slow diffusion. If $m_0 < 1$, the governing mechanism is a fast diffusion. When $m_0 = 1$, the equation reverts to the classical heat conduction equation and the governing mechanism is simple diffusion. One of the applications of slow diffusion can be found in the theory of ionized gases at high temperature. Vazquez (1983) studied the asymptotic behaviour and propagation properties of one-dimensional flow gases in porous media when $m_0 > 1$. In that study, u was the density of a gas which itself was a function of time and space. When $m_0 = 2$, the

PME can be applied to Prandtl's boundary layer theory (Schlichting, 1960) and to the Dupuit approximation for groundwater flow. Boussinesq was the first person to present an exact solution of eqn [2-44], for $m_0 = 2$. Bear (1972) showed that Boussinesq's equation can be used to solve the Dupuit approximation. Using the Dupuit assumptions, the total discharge through any vertical surface of thickness b can be expressed as:

$$Q = -KB_2 h(x)\frac{dh}{dx} \qquad [2\text{-}45]$$

where:

Q = discharge (L^3/T),

B_2 = the thickness of confined aquifer (L).

The total discharge for a given vertical surface at specific location (given by x) is constant. The Dupuit approximation, eqn [2-45], shows the form of the PME for a steady-state case with $m_0 = 2$. In most engineering fields, the study of the PME has been focused on the slow diffusion equation. Applications of PME in the fast diffusion case can be found in physics. When $m_0 = 0$, PME arises in the study of the expansion of a thermalised electron cloud (Lonngren and Hirose 1976), in gas kinetics as the central dynamical limit of Carleman's model of the Boltzman equation (Kaper *et al.* 1980), and in ion exchange kinetics in the cross-field convective diffusion of plasma (Hellfferich and Plesset 1958). Peletier and Zhang (1994) used a non-linear eignevalue to obtain solutions to a fast-diffusion equation that do not conserve mass. Rosenau (1995) investigated fast and superfast diffusion processes in which a subclass of superfast diffusions was discovered where in the whole process terminates within a finite time. PME was applied by King (1988) to the diffusion of impurities in silicon, where the values of m_0 were between 0 and 1. Even though the PEM was derived from flows through porous media, not many applications have been found in the fields of hydrogeology or petroleum engineering. The main difficulty of applying the PME in these fields is that the forms of the equations used in hydrogeology and petroleum engineering cannot be easily converted to the form of the PME except the classic heat conduction equation ($m_0 = 1$). As a result, even though numerous solutions and mathematical interpretations are available for the porous medium equation, it is difficult to find the connections between

the porous media equations based on the momentum and continuity equations, and the porous medium equation. In this study, it will be shown the former equations for flow through porous media (for a given regime) can be converted to the form of the PME, and which mechanisms dominant under the defined boundary conditions. Aronson (1985) has stated that

> "the most striking manifestation of this nonlinear degeneracy is that in porous medium flow there is a finite speed of propagation of disturbances from rest. This is in stark contrast to the linear heat equation ($m_0 = 1$) where there is an infinite speed of propagation."

This study analytically arrives at this finite speed of propagation using matched asymptotic expansions and suggests an equation to estimate this speed. Foster (1967) had confirmed the existence of this finite speed of propagation. Using an analytical solution known as the telegrapher's equation, he showed that the pressure pulse through the pores of the medium have a finite speed and that a time lag exists between initiation of a disturbance and its arrival at same down-stream point. Matched asymptotic expansions have been applied to the PEM with $m_0 > 1$ to show asymptotic behavior of the solutions when $t \rightarrow \infty$ (Peletier 1971 and 1977, Vazquez 1981 and 2003, Aronson 1985).

3. Theoretical Development

3.1. Fundamental Equations

Energy loss equations have been presented for all three relevant regimes i.e. laminar, PDT and FDT regime e.g. (eqns 3-3, 3-8, and 3-10). These equations were presented in a form of a general power function and a zero-intercept second-order polynomial. Energy loss equations accounted resistance of flow in the momentum equation which could be derived from Newton's second law whereas the continuity equation from mass conservation. Head and velocity of the flow were the dependent variables and time and space were the independent variables. Even though this study was limited to 1-D in space, in order to present the effect of elevation head, the momentum and continuity equations were developed for the conduit being not horizontal ($\theta \neq 0$).

3.1.1. Energy Loss Equations

Flow through conduits and through porous media can both be described by either a power function:

$$i = a_1 v^N \qquad [3\text{-}1]$$

or by a zero-intercept second-order polynomial:

$$i = r' v + s' v^2 \qquad [3\text{-}2]$$

where:

i = slope of the energy grade line, = h_L/L (dimensionless),

a_1, r', and s' = empirical coefficients,

v = velocity, definable as Q/A,

N = exponent whose value is bounded by 1 and 2 (inclusive).

The parameter a_1 is governed by the geometric characteristics of the porous medium in question, as well as by the type of fluid moving through it. The parameter N is mainly governed by the prevailing flow regime; i.e. by the intensity of the turbulence (if any).

The values of some of the parameters are known *a priori*. Table 3.1 summarizes how the turbulent regime and the values of a_1, N, r', and s' are related (certain terms to be defined presently). It should be noted that while the transition from laminar to turbulent flow is sudden for conduits, it is gradual for flow through porous media. Parameters for three regimes were shown in Table 3.1.

Table 3.1 Flow regimes and parameters.

	Laminar (LAM) flow	Partially-developed turbulent (PDT) flow	Fully-developed turbulent (FDT) flow
r'	$\frac{1}{K}$ or $\frac{32\nu}{gD_h^2}$	*v.e.r.a.*	0
s'	0	*v.e.r.a.*	✓
a_1	$\frac{1}{K}$ or $\frac{32\nu}{gD_h^2}$	*v.e.r.a.*	✓
N	1	$1 < N < 2$	2

v.e.r.a. = various empirical relations available (and/or the subject of on-going research).

✓ = well understood for conduit flow.

(i) Laminar (LAM) Flow Regime

If laminar flow is in effect, the hydraulic gradient will be directly proportional to the velocity of flow through a porous medium. For laminar flow in a cylinder that contains a porous medium, a re-arrangement of Darcy's Law ($v = K\,i$) gives:

$$h_L = \frac{L}{K} v \qquad [3\text{-}3]$$

where:

K = hydraulic conductivity (L/T),

L = conduit length, i.e. of the fracture (L),

v = average velocity (L/T).

In light of eqn [3-3] it can be seen that the head loss associated with laminar flow through a porous medium can be expressed as:

$$h_L = \lambda v \qquad [3\text{-}4a]$$

where:

$$\lambda = \frac{L}{K} \qquad [3\text{-}4b]$$

Hydraulic conductivity depends on the intrinsic permeability and the fluid moving through the sample. An independent estimate of K can be obtained from the Carman-Kozeny equation:

$$h_L = L\frac{(1-n)^2}{n^3}\frac{150\nu}{g D_p^2}v \qquad [3\text{-}5]$$

where:

n = porosity ($volume_{voids}$/ $volume_{bulk}$, dimensionless),

D_P = diameter of sphere with volume equal to representative particle volume (L).

The velocity at equilibrium, associated with the passage of an infinite amount of time, can be found by using the instantaneously applied H instead of h_L in a re-arrangement of eqn [3-4a]:

$$v_{t=\infty} = \frac{1}{\lambda}H \qquad [3\text{-}6]$$

However, the above equation must also show that the applied head will not result in a regime change, a transition that would make the underlying linear flow law invalid. This is, in fact, the main use of said law when applying the flow establishment equation; it provides the upper bound for the problem.

(ii) Fully Developed Turbulent (FDT) Flow Regime

Although this class of flow will be uncommon for the typical settings considered herein, it does represent the maximum possible turbulent intensity. It is therefore a useful

upper limiting condition (laminar flow representing the lower limit). If FDT flow is in effect, the gradient will be proportional to the square of velocity. Fully-developed turbulent flow through porous media is an even less common occurrence than FDT flow in conduits. It may occur in flow through very coarse porous media (Hansen and Bari 2002) or in situations where the applied hydraulic gradient is very high (Anandakrishnan and Varadalajulu 1963), or in combinations thereof. The Burke-Plummer equation can be used to describe FDT flow through porous media. If $r_e = 1$:

$$h_L = 0.583 \frac{L}{m n^2} \frac{v^2}{2g} \qquad [3\text{-}7]$$

Or, since v_v is more representative of the kinetic head than v and the preference for porous media flow has always been to think in terms of conductance rather than resistance:

$$h_L = \frac{1}{c_2} \left(\frac{L}{m} \right) \frac{v_v^2}{2g} \qquad [3\text{-}8]$$

Equations [3-7] and [3-8] show a form of:

$$h_L = \lambda v^N \qquad [3\text{-}1]$$

with N = 2.

(iii) Partially Developed Turbulent (PDT) Flow Regime

Partially-developed turbulent flow through porous media has been studied by many researchers. As with FDT flow, PDT may occur if the medium is made up of coarse particles or if the applied gradient applied to it is high (or both). There is no universally-accepted equation for describing PDT flow through porous media. Equations of the form of [3-1] and [3-2] are both available. One of the commonly used equations using the power law is due to Wilkins (1956):

$$h_L = \frac{1}{W_0} \left(\frac{L}{m^{0.93}} \right) \frac{v^{1.85}}{n} \qquad [3\text{-}9]$$

where:

$W_0 = 5.243$ for m-sec units.

The Ergun (1952) equation can be re-stated as:

$$h_L = \frac{L}{m}\left(\frac{\nu}{c_1 m}\frac{v_V}{g} + \frac{1}{c_2}\frac{v_V^2}{2g}\right) \qquad [3\text{-}10a]$$

or:

$$i = \frac{\nu}{c_1 m^2}\frac{v_V}{g} + \frac{1}{c_2 m}\frac{v_V^2}{2g} \qquad [3\text{-}10b]$$

where:

$c_1 = 0.240$ (due to Carman-Kozeny),

$c_2 = 1.714$ (= 3/1.75, 1.75 being due to Burke-Plummer).

In this study, eqn [3-10b] was used to describe PDT flow instead of Forchheimer equation. The main disadvantage of using Forchheimer equation is that the constants cannot adequately account for the combined effects of geometry and viscosity and hence the empirical constants contained therein must be re-determined for each specific porous medium (Fand 1987, 1990). Equation [3-10b] is a simple expression. Engelund (1953) synthesized a substantial body of data on PDT flow in porous media, including packings of spheres. It is interesting that a c_1 of 0.20 and a c_2 of 1.67 can be inferred using the lower limits on Engelund's recommended range of values for these parameters and by assuming n = 0.375 (an average value), d = 1 mm, and $r_e = 1$. Table 3.2 summarized parameters associated with the energy loss equation using a power law for three flow regime cases.

Table 3.2 Summary of parameters for three flow regimes associated with $h_L = \lambda v^N$.

	LAM	PDT	FDT
λ	$\frac{L}{K}$ or $\frac{1}{C}\left(\frac{L\nu}{m^2 n}\right)\frac{1}{g}$	$\frac{1}{W_0}\left(\frac{L}{m^{0.93}n}\right)$ *	$h_L = \frac{1}{C_2}\left(\frac{L}{mn^2}\right)\frac{1}{2g}$
N	1	$1 < N < 2$ **	2

* Eqn [3-9] is dimensionally inconsistent. N = 1.85 according to both the Hazen-Williams and the Wilkins' eqns.

** use N = 2 but **only** if f is independently estimated; f under PDT flow is a function of the Reynolds number. Use Swamee-Jain equation or Moody diagram to evaluate f.

Table 3.3 presented parameters associated with the equation using the zero intercept second order polynomial for three flow regimes.

Table 3.3 Summary of parameters for three regimes associated with $h_L = r\,V + s\,V^2$.

	LAM	PDT	FDT
r	$\frac{L}{K}$ or $\frac{1}{c}\left(\frac{L\nu}{m^2 n}\right)\frac{1}{g}$	$\frac{1}{c_1}\left(\frac{L\nu}{m^2 n}\right)\frac{1}{g}$	0
s	0	$\frac{1}{c_2}\left(\frac{L}{mn^2}\right)\frac{1}{2g}$	$\frac{1}{c_2}\left(\frac{L}{mn^2}\right)\frac{1}{2g}$

It must be emphasized that for flow through porous media, only the expression L/K is universally accepted (even if the use of the hydraulic conductivity K raises the difficult question of how to obtain an accurate K without performing a packed column experiment). For PDT and FDT flow through porous media, other expressions for λ and values of N can be found in the literature.

3.1.2. Momentum Equation

Schematic of the experimental set-up was shown in Figure 3.1. The pipe was packed with sand. The variables h_a, h_b and L are constants, whereas v is time and space-

dependent. The energy loss h_L depends on v, and is therefore also time and space-dependent. The 'driving force' of flow, H_{ab}, is constant.

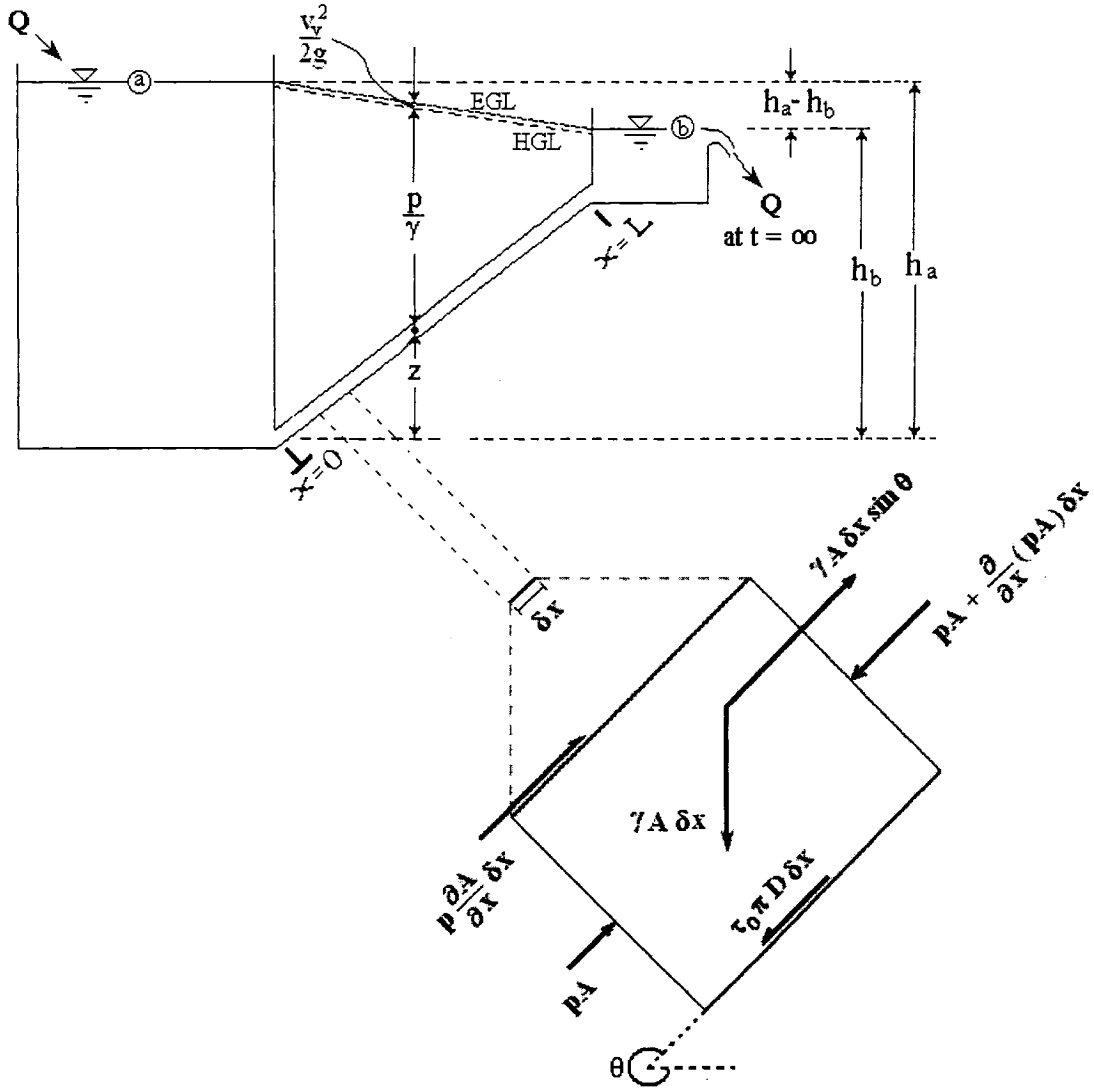

Figure 3.1 Schematic of experimental set-up and the force valance inside of the pipe.

The momentum equation for pipe flow can be described as:

$$pA - \left[pA + \frac{\partial}{\partial x}(pA)\delta x\right] + p\frac{\partial A}{\partial x}\delta x + \gamma A \delta x \sin\theta - \tau_0(2\pi r_0)\delta x = \rho A \delta x \frac{dv}{dt} \qquad [3\text{-}11]$$

By computing the total time derivative of the velocity vector, acceleration vector field for Newton's second law can be obtained. Dividing both sides by $\rho A \delta x$ gives:

$$-\frac{1}{\rho}\frac{\partial p}{\partial x}+g\sin\theta-\frac{4\tau_0}{2r\rho}=\frac{dv_v}{dt} \qquad [3\text{-}12]$$

where:

r_0 = radius of the pipe (L),

v_v = pore velocity, v/n (L/T).

For pipe flow, the head loss can be expressed as:

$$h_L=\frac{\tau_0(2\pi r_0)\delta x}{\rho g A}=\frac{2\tau_0\delta x}{\rho g r_0} \qquad [3\text{-}13]$$

Because $p = \rho g(h-z)$, $\frac{\partial p}{\partial x}\approx\rho g\left(\frac{\partial h}{\partial x}-\frac{\partial z}{\partial x}\right)$ where h is hydraulic head and z is an elevation head. Using $\frac{\partial z}{\partial x}=-\sin\theta$:

$$\frac{\partial p}{\partial x}\approx\rho g\left(\frac{\partial h}{\partial x}+\sin\theta\right) \qquad [3\text{-}14]$$

Substituting τ_0 and $\partial p/\partial x$ into eqn [3-12] gives:

$$g\frac{\partial h}{\partial x}+\frac{g}{\delta x}h_L+\frac{dv_v}{dt}=0 \qquad [3\text{-}15]$$

For porous media the head loss can be expressed using $h_L = rv + sv^2$ (viscous and so-called inertial effects). If the whole length of pipe is considered and the bulk velocity v is used instead of v_v eqn [3-15] becomes:

$$gn\frac{\partial h}{\partial x}+v\frac{\partial v}{\partial x}+\frac{\partial v}{\partial t}+\frac{gn}{L}(rv+sv^2)=0 \qquad [3\text{-}16]$$

Using r and s of the Ergun equation (1952), the laminar case (s = 0) becomes:

$$gn\frac{\partial h}{\partial x}+v\frac{\partial v}{\partial x}+\frac{\partial v}{\partial t}+\frac{gn}{L}\frac{1}{c_1}\left(\frac{\nu L}{m^2 n}\right)\frac{1}{g}v=gn\frac{\partial h}{\partial x}+v\frac{\partial v}{\partial x}+\frac{\partial v}{\partial t}+\frac{1}{c_1}\left(\frac{\nu}{m^2}\right)v=0 \qquad [3\text{-}17]$$

or using Darcy's Law,

$$gn\frac{\partial h}{\partial x}+v\frac{\partial v}{\partial x}+\frac{\partial v}{\partial t}+\frac{gn}{K}v=0 \qquad [3\text{-}18]$$

For PDT,

$$gn\frac{\partial h}{\partial x}+v\frac{\partial v}{\partial x}+\frac{\partial v}{\partial t}+\frac{n}{c_1}\left(\frac{\nu}{m^2n}\right)v+\frac{n}{2c_2}\left(\frac{1}{mn^2}\right)v^2=0 \qquad [3\text{-}19]$$

For FDT,

$$gn\frac{\partial h}{\partial x}+v\frac{\partial v}{\partial x}+\frac{\partial v}{\partial t}+\frac{n}{2c_2}\left(\frac{1}{mn^2}\right)v^2=0 \qquad [3\text{-}20]$$

(i) Darcy's Law and the Ergun-type equation

Darcy's Law and the Ergun equation can be considered to be reduced forms of the momentum equation. If we are considering ordinary groundwater flow, the acceleration of the flow can be ignored because the velocity of groundwater is normally very small. From eqn [3-16], if the acceleration terms are neglected, the momentum equation becomes:

$$\frac{\partial h}{\partial x}+\frac{(rv+sv^2)}{L}=0 \qquad [3\text{-}21]$$

Equation [3-21] is a form of the Ergun equation and has the so-called inertial term. By setting $r=\frac{L}{K}$ and neglecting the inertial term, eqn [3-21] reduces to Darcy's Law:

$$\frac{\partial h}{\partial x}+\frac{1}{K}v=0 \qquad [3\text{-}22]$$

(ii) Navier-Stokes equation

Navier and Stokes added newtonian viscous terms to the equation of motion (White 1999). The equation of motion can be expressed as:

$$\rho g_x-\frac{\partial p}{\partial x}+\frac{\partial \tau}{\partial x}=\rho\left(\frac{\partial v}{\partial t}+v\frac{\partial v}{\partial x}\right) \qquad [3\text{-}23]$$

If the flow is incompressible and newtonian, and if the viscous stresses are proportional to the element strain-rates and to the absolute viscosity, the 1-D Navier-Stokes equation becomes:

$$\rho g_x - \frac{\partial p}{\partial x} + \mu \frac{\partial^2 v}{\partial x^2} = \rho\left(\frac{\partial v}{\partial t} + v\frac{\partial v}{\partial x}\right) \qquad [3\text{-}24]$$

By multiplying ρ to the momentum equation (eqn [3-12]):

$$-\frac{\partial p}{\partial x} + \rho g \sin\theta - \frac{2\tau_0}{r} = \rho\frac{dv_v}{dt} \qquad [3\text{-}25]$$

Re-arrangement gives:

$$\rho g \sin\theta - \frac{\partial p}{\partial x} - \frac{\rho g}{L}(rv + sv^2) = \rho\left(\frac{\partial v_v}{\partial t} + v\frac{\partial v_v}{\partial x}\right) \qquad [3\text{-}26]$$

If we compare eqn [3-26] and [3-24], it can be shown that the only the only difference between these two equations is the resistance of flow. The Navier-Stokes equation explains it with viscous stresses which are proportional to the element strain-rates and the viscosity coefficient. In the momentum equation (eqn [3-26]), the resistance force is explained using viscous resistance (rv) and inertial resistance (sv^2).

3.1.3. Continuity Equation

The continuity equation for typical groundwater flow can be expressed as:

$$-\frac{\partial(\rho v)}{\partial x} = \frac{\partial(\rho n)}{\partial t} \qquad [3\text{-}27]$$

v is the bulk velocity of the flow. If pore velocity is used instead of bulk velocity and the cross-section area of the pipe is considered variable in time and space, the continuity equation can be expressed as:

$$-\frac{\partial(\rho n v_v A \sigma x)}{\partial x} = \frac{\partial(\rho n A)\sigma x}{\partial t} \qquad [3\text{-}28]$$

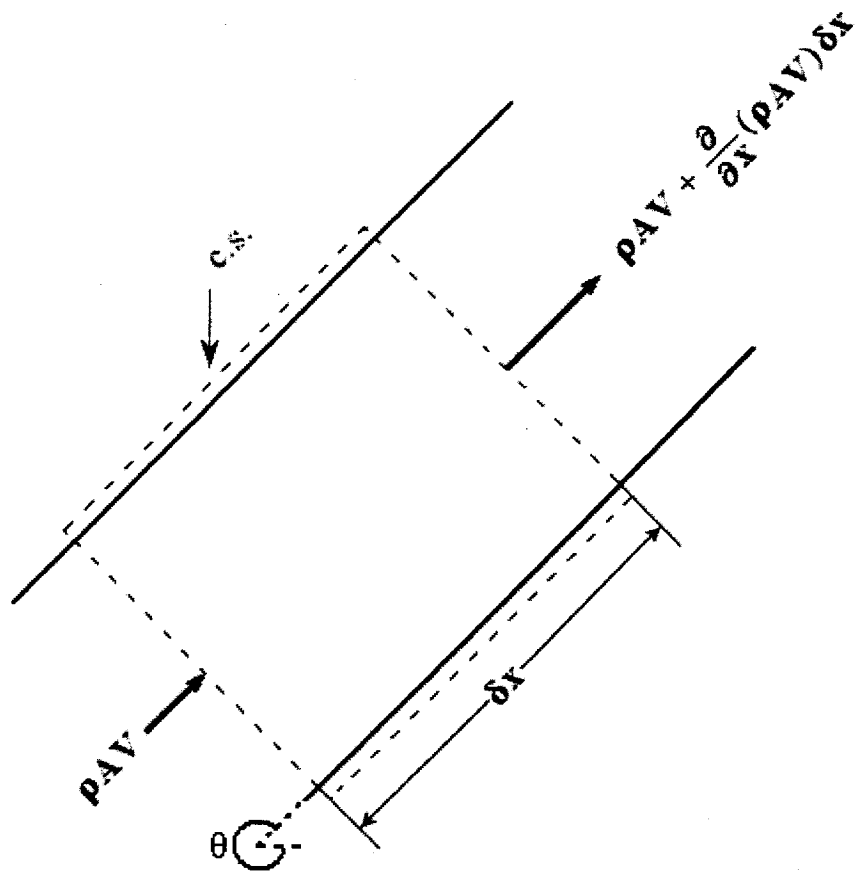

Figure 3.2 Control volume relevant to derivation of continuity equation.

Expanding and dividing eqn [3-28] by σx gives:

$$nv_v A\frac{\partial \rho}{\partial x} + \rho v_v A\frac{\partial n}{\partial x} + \rho n v_v \frac{\partial A}{\partial x} + \rho nA\frac{\partial v_v}{\partial x} + \rho n\frac{\partial A}{\partial t} + nA\frac{\partial \rho}{\partial t} + \rho A\frac{\partial n}{\partial t} = 0 \quad [3\text{-}29]$$

Dividing by ρnA gives:

$$\frac{v_v}{n}\frac{\partial n}{\partial x} + \frac{1}{n}\frac{\partial n}{\partial t} + \frac{v_v}{\rho}\frac{\partial \rho}{\partial x} + \frac{1}{\rho}\frac{\partial \rho}{\partial t} + \frac{v_v}{A}\frac{\partial A}{\partial x} + \frac{1}{A}\frac{\partial A}{\partial t} + \frac{\partial v_v}{\partial x} = 0 \quad [3\text{-}30]$$

If the partial derivatives are converted to total differentials:

$$\frac{1}{n}\frac{dn}{dt}+\frac{1}{\rho}\frac{d\rho}{dt}+\frac{1}{A}\frac{dA}{dt}+\frac{\partial v_v}{\partial x}=0 \qquad [3\text{-}31]$$

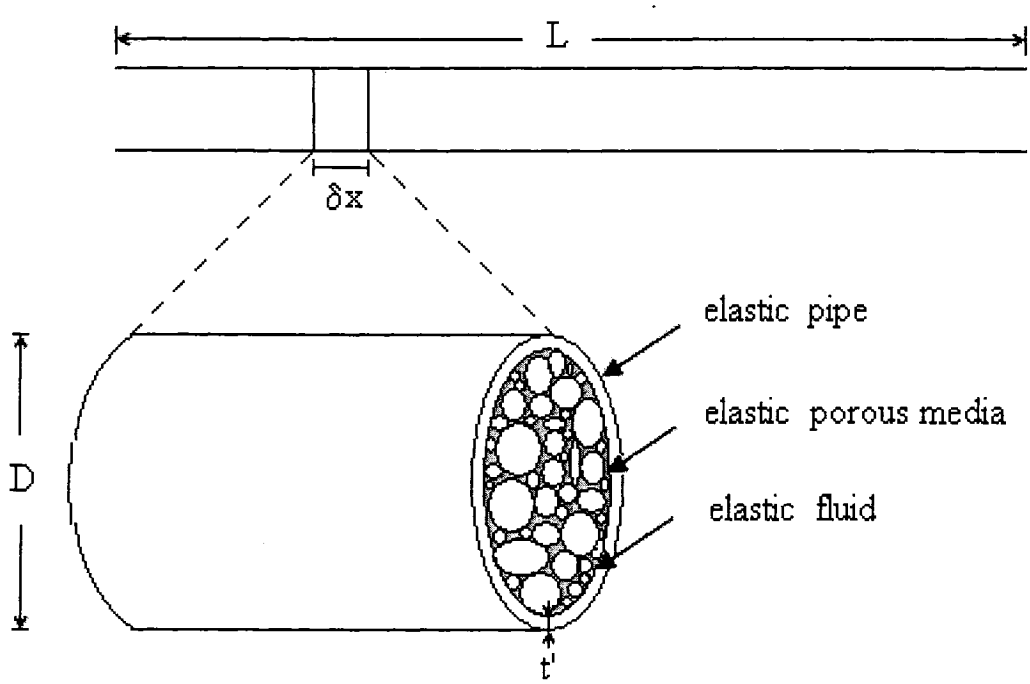

Figure 3.3 Schematic of Porous media in pipe.

The first term is related to the compressibility of the porous media. The associated porosity change can be expressed in terms of the pressure change (Fetter, 2001):

$$\frac{1}{n}\frac{dn}{dt}=\frac{1-n}{n}\alpha\frac{dp}{dt} \qquad [3\text{-}32]$$

The second term accounts for the elasticity of fluid. The associated density change can be expressed in terms of the pressure change (Freeze and Cherry, 1979):

$$\frac{1}{\rho}\frac{d\rho}{dt}=\beta\frac{dp}{dt} \qquad [3\text{-}33]$$

The third term accounts for the elasticity of the pipe itself. The associated cross-sectional area change can be expressed in terms of the pressure change (Streeter and Wylie, 1975):

$$\frac{1}{A}\frac{dA}{dt} = \frac{D}{t'E}\frac{dp}{dt} \qquad [3\text{-}34]$$

Using these three definitions in eqn [3-30], we obtain:

$$\beta\frac{dp}{dt}\left(1+\frac{1-n}{n}\frac{\alpha}{\beta}+\frac{D}{t'E}\frac{1}{\beta}\right)+\frac{\partial v_v}{\partial x}=0 \qquad [3\text{-}35]$$

For convenience and using an analogy to the celerity of a pressure perturbation in a pipeline[7], the constants in eqn [3-35] are re-defined as follows:

$$\beta\left(1+\frac{1-n}{n}\frac{\alpha}{\beta}+\frac{D}{t'E}\frac{1}{\beta}\right)=\frac{1}{\rho}\frac{1}{c_p^{\,2}} \qquad [3\text{-}36]$$

Re-arranging for c_p gives:

$$c_P^2=\frac{1}{\beta\rho}\frac{1}{\left(1+\frac{1-n}{n}\frac{\alpha}{\beta}+\frac{D}{t'E}\frac{1}{\beta}\right)} \qquad [3\text{-}37]$$

Equation [3-35] then becomes:

$$\frac{1}{\rho}\frac{dp}{dt}+c_p^{\,2}\frac{\partial v_p}{\partial x}=0 \qquad [3\text{-}38]$$

If v_v is transformed to v_{bulk} (v):

$$\frac{1}{\rho}\frac{dp}{dt}+\frac{c_p^{\,2}}{n}\frac{\partial v}{\partial x}=0 \qquad [3\text{-}39]$$

Using p = ρg(h-z):

$$\frac{dp}{dt}=v\frac{\partial p}{\partial x}+\frac{\partial p}{\partial t}=v\rho g\left(\frac{\partial h}{\partial x}-\frac{\partial z}{\partial x}\right)+\rho g\left(\frac{\partial h}{\partial t}-\frac{\partial z}{\partial t}\right) \qquad [3\text{-}40]$$

[7] $c_p^{\,2}=\gamma_w K$ celerity of a hydraulic transient ('water hammer') in a water main, where K is a composite elasticity of water and pipeline material.

The pipe is not moving so $\frac{\partial z}{\partial t} = 0$. Using $\frac{\partial z}{\partial x} = -\sin\theta$:

$$\frac{1}{\rho}\frac{dp}{dt} = vg\left(\frac{\partial h}{\partial x} + \sin\theta\right) + g\frac{\partial h}{\partial t} \qquad [3\text{-}41]$$

Equation [3-39] then becomes:

$$\frac{c_p^{\,2}}{gn}\frac{\partial v}{\partial x} + v\frac{\partial h}{\partial x} + \frac{\partial h}{\partial t} + v\sin\theta = 0 \qquad [3\text{-}42]$$

Equation [3-42] is a continuity equation for an elastic fluid in a elastic pipe that is filled with elastic porous media. If the pipe is horizontal then $v\sin\theta = 0$.

3.2. Dimensional Analysis

3.2.1. The Buckingham Pi Theorem

The Buckingham Pi theorem is a rule to decide how many dimensionless groups can be derived or are implied by a problem. The momentum equation and the continuity equation were expressed with eqn [3-16] and [3-42] respectively. These two equations contain $n_0 = 9$ dimensional terms (h, v, x, t, g, r, s, L, c_p) which can be divided into variables and parameters. The variables are h, v, x, t and the parameters are g, r, s, L, c_p. In order to nondimensionalize the equations, the number of dimensions contained amongst the variables and parameters must be found. From Table 3.4 it can be seen that two dimensions exist, length {L} and time {T}.

Table 3.4 List of dimensions of variables and parameters

h	v	x	t	g	r	S	L	c_p
{L}	$\{LT^{-1}\}$	{L}	{T}	$\{LT^{-2}\}$	{T}	$\{T^2L^{-1}\}$	{L}	$\{LT^{-1}\}$

The number of dimensionless variables can be calculated by subtracting a number j_0 from the number of dimensional terms:

$$k = n_0 - j_0 \qquad [3\text{-}43]$$

where j_0 is the maximum number of variables which do not form a pi group among themselves. This j_0 is always less than or equal to the number of dimensions describing the variables. It can be shown that there are combinations of two terms which do not form a pi among themselves, i.e. r and L. Therefore $j_0 = 2$ and from eqn [3-43], 7 dimensionless groups are expected. Head can be expressed as a function of 8 dimensional terms:

$$h = f(v, x, t, g, r, s, L, c_p) \qquad [3\text{-}44]$$

If r and L are selected as repeating parameters in pi:

(removing length)
$$\frac{h}{L} = f\left(\frac{v}{L}, \frac{x}{L}, t, \frac{g}{L}, r, sL, \frac{c_p}{L}\right) \qquad [3\text{-}45]$$

(removing time)
$$\frac{h}{L} = f\left(\frac{vs}{L}, \frac{x}{L}, ts, \frac{g}{L}r^2, \frac{sL}{r^2}, \frac{c_p r}{L}\right) \qquad [3\text{-}46]$$

As expected from eqn [3-43], the number of dimensionless groups is 7. There can be other options depending on which parameters are selected as repeating parameters. The Buckingham pi theorem only indicates that there must be at least a certain number of dimensionless groups involved. It gives little assurance that all the dimensionless groups have been found (Ipsen, 1960). In this study, a more general approach is used. This involves the use of the boundary conditions as scaling factors.

3.2.2. Development of Dimensionless Form

Dimensional variables in the equations are scaled by known values. Defining:

$$H = \frac{h}{h_a} \qquad [3\text{-}47a]$$

$$V = \frac{v}{V_\infty} \qquad [3\text{-}47b]$$

$$X = \frac{x}{L} \qquad [3\text{-}47c]$$

$$q = \frac{t}{b_0'} \qquad [3\text{-}47d]$$

where h_a is the applied head at the upstream end, V_∞ is the steady state velocity at the downstream end when $t = \infty$. L is the total length of pipe and b_0' is the time-scaling factor. Scaling factors for H, V and X can be readily obtained using knowledge of the boundary conditions. However, the time-scaling factor should be given a reasonable value in order to make further study possible. The value of b_0' can be estimated from the simplest form of momentum and continuity equation which is the typical groundwater flow equation. The standard 1-D groundwater flow equation (Laminar regime) is a simple diffusion equation, and includes storativity (S) and transmissivity (T).

$$h_{XX} = \frac{S}{T} h_t \qquad [3\text{-}48]$$

By introducing the relevant scaling factors:

$$\frac{h_a}{L^2} H_{XX} = \frac{S}{T} \frac{h_a}{b_0'} H_q \qquad [3\text{-}49]$$

A dimensionless form of eqn [3-48] is then:

$$H_{XX} = \frac{S}{T} \frac{L^2}{b_0'} H_q \qquad [3\text{-}50]$$

For further numerical and analytical study it is beneficial to give b_0' a value that makes the time scale order 1. It will therefore be approximated using:

$$b_0' = \frac{SL^2}{T} \qquad [3\text{-}51]$$

If all these scaling factors are applied to the momentum equation:

$$gn \frac{h_a}{L} H_x + \frac{V_\infty^2}{L} V V_x + \frac{T V_\infty}{SL^2} V_q + \frac{gnr}{L} V_\infty V + \frac{gns}{L} V_\infty^2 V^2 = 0 \qquad [3\text{-}52]$$

A dimensionless form of the momentum equation is then:

$$H_x + \frac{V_\infty^2}{gnh_a} VV_x + \frac{V_\infty T}{gnh_a SL} V_q + \frac{r}{h_a} V_\infty V + \frac{s}{h_a} V_\infty^2 V^2 = 0 \qquad [3\text{-}53]$$

Equation. [3-53] can be re-arranged to the following equation, for convenient formulation of the numerical method.

$$V_q = -\underbrace{\frac{gnh_a SL}{V_\infty T}}_{C_1} H_x - \underbrace{\frac{V_\infty SL}{T}}_{C_2} VV_X - \underbrace{\frac{gnSLr}{T}}_{C_3} V - \underbrace{\frac{gnSLsV_\infty}{T}}_{C_4} V^2 \qquad [3\text{-}54]$$

Similarly, if the stated scaling factors are applied to the continuity equation:

$$\frac{c_p^{\,2}}{gn}\frac{V_\infty}{L} V_x + \frac{V_\infty h_a}{L} VH_x + V_\infty \sin\theta V + \frac{h_a T}{SL^2} H_q = 0 \qquad [3\text{-}55]$$

A dimensionless form of the continuity equation is then:

$$V_x + \frac{gnh_a}{c_p^{\,2}} VH_x + \frac{gnL\sin\theta}{c_p^{\,2}} V + \frac{gnh_a T}{c_p^{\,2} V_\infty SL} H_q = 0 \qquad [3\text{-}56]$$

Re-arrangement gives:

$$H_q = -\underbrace{\frac{V_\infty SL}{T}}_{C_5} VH_x - \underbrace{\frac{c_p^{\,2} V_\infty SL}{gnh_a T}}_{C_6} V_X - \underbrace{\frac{V_\infty SL^2 \sin\theta}{h_a T}}_{C_7} V \qquad [3\text{-}57]$$

C_2 and C_5 become identical. An additional time-scaling will make the momentum and continuity equations simpler for subsequent manipulations and calculation:

$$C_6 q = \tau \qquad [3\text{-}58]$$

The scaling from dimensional time is then:

$$\tau = \frac{t}{\frac{b_0}{C_6}} = \frac{t}{\frac{gnh_a L}{c_p^{\,2} V_\infty}} \qquad [3\text{-}59]$$

If the above scaling is applied, the momentum equation becomes:

$$C_6 V_\tau = -C_1 H_x - C_2 V V_X - C_3 V - C_4 V^2 \qquad [3\text{-}60]$$

Similarly, the continuity equation becomes:

$$C_6 H_\tau = -C_5 V H_x - C_7 V - C_6 V_X \qquad [3\text{-}61]$$

3.2.3. Definition of Problem Scope

The dimensionless groups retain dimensional parameters which define the scope of the problem. Although one set of physical parameters was used in the numerical experiments, the effects of the various magnitudes of dimensional parameters on the various dimensionless groups will be presented section 4.4.3. Table 3.5 shows the values of the dimensional parameters used in the numerical experiments.

Table 3.5 Values of physical parameters used in numerical experiments.
(a) assumed parameter values.

No.	Symbols	Parameters/constants	Typical units	Value	Notes
1	d	diameter of particle	m	0.001	size of sand
2	D	diameter of the pipe	m	0.1	-
3	L	total length	m	10	-
4	t'	thickness of pipe	m	0.0005	-
5	r_e	shape factor	-	1.0	-
6	n	Porosity (sand)	-	0.375	-
7	α	compressibility of sand[1]	1/Pa	1.0E-08	-
8	β	compressibility of water	1/Pa	4.4E-10	-
9	E	Young's modulus of iron	Pa	2.0E+11	-
10	c_1	empirical coefficient	-	0.24	due to Carman-Kozeny
11	c_2	empirical coefficient	-	1.714	due to Burke-Plummer
12	g	gravitational acceleration	m/sec^2	9.806	-

No.	Symbols	Parameters/constants	Typical units	Value	Notes
13	ρ	density of water	kg/m^3	1000	-
14	γ	weight density of water	$kg/m^2/sec^2$	9806	-
15	ν	kinematic viscosity	m^2/s	1E-06	-

[1] of the matrix or skeleton of the media, not of the individual grains.

(b) values of parameters computed using assumed parameters from (a), via 'accepted' equations.

No.	Symbols	Parameters/constants	Typical units	Value	Notes
1	e	void ratio	-	0.6	$e = \frac{n}{1-n}$
2	m	hydraulic mean radius	m	0.0001	eqn [2-2d]
3	K	hydraulic conductivity	m/s	8.83E-03	eqn [2-6]
4	S_s	specific storage	1/m	9.97E-05	$S_s = \gamma(\alpha + n\beta)$
5	T	transmissivity	m^2/s	8.83E-04	T = KD
6	S	storativity	-	9.97E-06	$S = S_sD$
7	r	viscous constant	sec	1133.1	Table 3.3
8	s	inertial constant	sec^2/m	21154.6	Table 3.3
9	c_p	celerity of pressure wave	m/s	235.01	eqn [3-37]

With respect to the values that were simply assumed for the physical parameters and quantities stated in Table 3.5 (a), the intention was to conceive of a problem which, in some sense, was 'typical' or representative of a 1-D unsteady permeability test, i.e. a typical porous media in which LAM, PDT, or FDT regimes would be physically possible (true of a coarse sand), packed to a typical or average porosity, having a typical matrix compressibility (α), and placed in a relatively rigid but still elastic conduit (a steel pipe).

3.2.4. Magnitude of Dimensionless Groups

Table 3.6 shows the magnitudes of dimensionless groups in the momentum and continuity equation. These dimensionless groups were obtained at various applied

hydraulic gradients. It can be seen that for all the cases, C_2, C_5, C_6 and C_7 are very small compared to C_1, C_3 and C_4.

Table 3.6 Magnitudes of dimensionless groups.

i	0.01	0.1	0.4249	1	10	100	340	400
C_1	470.55	470.55	470.55	538.33	883.50	2159.80	3522	3820.1
C_2	1.0E-05	1.0E-04	4.2E-04	8.7E-04	5.3E-03	2.2E-02	0.045	0.049
C_3	470.55	470.55	470.55	470.55	470.55	470.55	470.55	470.55
C_4	0.78	7.75	32.94	67.77	412.94	1689.20	3522	3820.1
C_5	1.0E-05	1.0E-04	4.2E-04	8.7E-04	5.3E-03	2.2E-02	0.045	0.049
C_6	1.50	1.50	1.50	1.31	0.80	0.33	0.20	0.18
C_7 *	-1.0E-03	-1.0E-03	-1.0E-03	-8.7E-04	-5.3E-04	-2.2E-04	-1.3E-04	-1.2E-04

* 45 degree up-slope applied

Table 3.6 shows how the ratios of various pairs of dimensionless groups change with applied hydraulic gradient. By investigating these ratios, the effects of each term in the PDE's can be investigated and compared with traditional groundwater flow equations. The magnitude of the ratio of dimensionless groups for traditional groundwater flow equation C_3 / C_1 is unity for laminar regime. If the regime changes to PDT and then FDT, the inertial effect C_4 / C_1 becomes significant. If the magnitude of the ratio of interest is much smaller than unity, we may expect that the effect of that term is negligible.

Table 3.7 Ratio of dimensionless groups.

i	0.01	0.1	0.4249	1	10	100	340	400
C_2/C_1	2.1E-08	2.1E-07	9.0E-07	1.6E-06	6.0E-06	1.0E-05	1.3E-05	1.3E-05
C_3/C_1	1	1	1	0.87	0.53	0.22	0.13	0.12
C_4/C_1	1.6E-03	1.6E-02	7.0E-02	0.13	0.47	0.78	1	1
C_6/C_1	3.2E-03	3.2E-03	3.2E-03	2.4E-03	9.0E-04	1.5E-04	5.7E-05	4.8E-05
C_5/C_6	6.7E-06	6.7E-05	2.8E-04	6.7E-04	6.7E-03	6.7E-02	0.226	0.266
C_7/C_6	-6.7E-04	-6.7E-04	-6.7E-04	-6.7E-04	-6.7E-04	-6.7E-04	-6.7E-04	-6.7E-04

3.3. Models of Flow through Porous Media

The complete momentum equation consists of viscous term, inertial term, local acceleration term, and convective acceleration term. Figure 3.4 shows the terms in the complete momentum and continuity equation. Starting from the simplest law for flow through porous media, Darcy's Law, additional terms can be successively included to show the effects of each term.

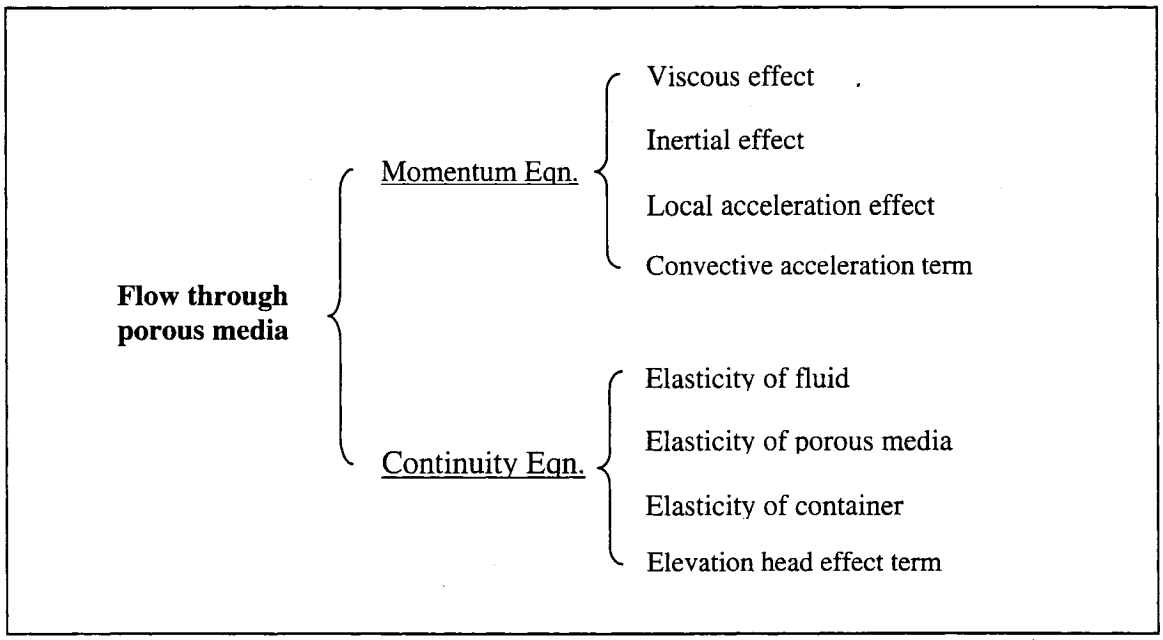

Figure 3.4 Terms included in fundamental equations.

3.3.1. Model Classification

The momentum equation can be re-arranged to help show the effects of each term, starting from Darcy's Law:

$$H_x + \underbrace{\frac{C_3}{C_1}V}_{\text{viscous term}} + \underbrace{\frac{C_4}{C_1}V^2}_{\text{inertial term}} + \underbrace{\frac{C_6}{C_1}V_\tau}_{\text{local acceleration term}} + \underbrace{\frac{C_2}{C_1}VV_X}_{\text{convective acceleration term}} = 0 \qquad [3\text{-}62]$$

The continuity equation can be re-arranged to help show the effects of each term:

$$H_\tau + \underbrace{V_X}_{\substack{\text{elasticity}\\ \text{term}}} + \underbrace{\frac{C_7}{C_6} V H_x}_{\substack{\text{elevation head}\\ \text{term}}} + \underbrace{\frac{C_5}{C_6} V H_x}_{\substack{\text{advection}\\ \text{term}}} = 0 \qquad [3\text{-}63]$$

It can be seen from eqn [3-62] that various forms of momentum equation can be stated by adding the relevant terms to the one based on the simplest model:

$$\underbrace{\underbrace{\underbrace{\underbrace{H_x}_{\text{Darcy's law}} + \frac{C_3}{C_1} V}_{\text{Ergun or Forchheimer equation}} + \frac{C_4}{C_1} V^2}_{\text{Unsteady acceleration model}} + \frac{C_6}{C_1} V_\tau}_{\text{Complete equation of motion}} + \frac{C_2}{C_1} V V_X = 0 \qquad [3\text{-}62]$$

In light of eqn [3-63], two forms of continuity equation can be stated; again, by adding a term to the simplest model (that based on Darcy's Law):

$$\underbrace{\underbrace{\underbrace{H_\tau + V_X}_{\substack{\text{General}\\ \text{groundwater}\\ \text{continuity equation}}} + \frac{C_7}{C_6} V}_{\substack{\text{Continuity equation}\\ \text{with elevation head effect}}} + \frac{C_5}{C_6} V H_x}_{\text{Complete continuity equation}} = 0 \qquad [3\text{-}63]$$

3.3.2. Models for 1-D Flow through Porous Media

The generally-accepted model for laminar flow of naturally-occurring groundwater consists of Darcy's Law and the continuity equation. From Figure 3.4, this model has a viscous term with respect to momentum equation and has three elasticity terms with respect to continuity (for the porous media, the fluid, and the container). The elasticity of the container (or confined layer) is not included in the usual statement of the continuity equation for groundwater flow, but for the consistent use of dimensionless groups in this study, it will be included in all the models, unless otherwise specified. If

we neglect inertial, local acceleration, and convective acceleration terms from momentum equation, eqn [3-60], we obtain:

$$H_x = -\frac{C_3}{C_1} V \qquad [3\text{-}64]$$

Equation [3-64] is simply a dimensionless form of Darcy's Law and V can be readily calculated from the hydraulic gradient. Also, V_X can be obtained from the second derivative of H by differentiating eqn [3-64]:

$$V_X = -\frac{C_1}{C_3} H_{XX} \qquad [3\text{-}65]$$

If we neglect the advection term in the continuity equation (eqn [3-63]), it becomes:

$$H_\tau + V_X = 0 \qquad [3\text{-}66]$$

Substitution of V_X in eqn [3-65] into eqn [3-66] results in:

$$H_\tau = \frac{C_1}{C_3} H_{XX} \qquad [3\text{-}67]$$

3.3.2.1. Darcy's Law Combined with Complete Continuity

This model incorporates viscous effects into the complete statement of the continuity equation. This is the same as saying that the momentum equation will only be represented by Darcy's Law. If V in eqn [3-64], and V_X in eqn [3-65] were substituted into the complete continuity equation (eqn [3-63]) the following expression is obtained:

$$H_\tau = \frac{C_5}{C_6}\frac{C_1}{C_3}(H_X)^2 + \frac{C_1}{C_3} H_{XX} + \frac{C_7}{C_6}\frac{C_1}{C_3} H_X \qquad [3\text{-}68]$$

3.3.2.2. Ergun-type Model

This model consists of viscous term, inertial term and continuity equation. If the local and convective acceleration terms in eqn [3-62] are neglected, the following equation is obtained:

$$H_x = -\frac{C_3}{C_1}V - \frac{C_4}{C_1}V^2 \qquad [3\text{-}69]$$

After re-arranging for V:

$$V^2 + \frac{C_3}{C_4}V + \frac{C_1}{C_4}H_x = 0 \qquad [3\text{-}70]$$

So V as a function of H_x is:

$$V = \frac{-\frac{C_3}{C_4} \pm \sqrt{\left(\frac{C_3}{C_4}\right)^2 - 4\frac{C_1}{C_4}H_X}}{2} \qquad [3\text{-}71]$$

If the negative V is neglected, then by re-arrangement:

$$V = \frac{-C_3 + \sqrt{C_3{}^2 - 4C_1C_4H_x}}{2C_4} \qquad [3\text{-}72]$$

Differentiating eqn [3-70] by X yields:

$$\frac{\partial V^2}{\partial X} + \frac{C_3}{C_4}\frac{\partial V}{\partial X} + \frac{C_1}{C_4}\frac{\partial^2 H}{\partial X^2} = 0 \qquad [3\text{-}73]$$

or:

$$V_X\left(2V + \frac{C_3}{C_4}\right) + \frac{C_1}{C_4}H_{XX} = 0 \qquad [3\text{-}74]$$

or:

$$V_X = -\frac{C_1}{2C_4V + C_3}H_{XX} \qquad [3\text{-}75]$$

Substitution of eqn [3-72] into eqn [3-75] results in:

$$V_X = -\frac{C_1}{\sqrt{C_3^{\,2} - 4C_1C_4H_x}} H_{XX} \qquad [3\text{-}76]$$

Substitution of $\partial V / \partial X$ (eqn [3-76]) and V (eqn [3-72]) into the continuity equation (eqn [3-63]) gives:

$$H_\tau - \frac{C_1}{\sqrt{C_3^{\,2} - 4C_1C_4H_X}} H_{XX} + \frac{C_5}{C_6} \frac{-C_3 + \sqrt{C_3^{\,2} - 4C_1C_4H_X}}{2C_4} H_X + \frac{C_7}{C_6} \frac{-C_3 + \sqrt{C_3^{\,2} - 4C_1C_4H_X}}{2C_4} = 0 \qquad [3\text{-}77]$$

3.3.2.3. Model which retains Local Acceleration Term

This model retains the viscous term, the inertial term, and the acceleration term in the momentum equation. It uses the statement of the complete continuity equation. The momentum equations for the previous models were essentially steady-state equations; in other words, there was no temporal (local) acceleration term. As a result, the momentum equation and continuity equation could be combined into one equation with relative ease. However, if the temporal acceleration term is included in the momentum equation, this becomes difficult. It becomes necessary to calculate H from the continuity equation and V from the momentum equation, and to do so separately (but in a coupled model or system). In order to get H at a given time, the H and the V from the previous time step must be used. Similarly, to calculate V at a given time, both H and V from the previous time step must be used. The momentum equation can be expressed as:

$$H_x = -\frac{C_3}{C_1} V - \frac{C_4}{C_1} V^2 - \frac{C_6}{C_1} V_\tau \qquad [3\text{-}78]$$

3.3.2.4. Complete Model

This model consists of the complete momentum equation and the complete continuity equation. Because of the complexity of this model, the momentum and

continuity equation cannot be combined to describe equation of H and V. Instead, these equations are solved separately. The momentum equation is used to obtain V and the continuity equation is applied to get H.

3.4. Regular Perturbation Method

Comparison of the solutions arising from the various models may not give information about the individual effects of various terms in, or components of, the momentum and continuity equations, i.e. viscosity, inertia, local acceleration, convective acceleration, and elevation. In the laminar regime, the viscous effect is dominant and the magnitudes of the other terms are very small compared with the viscous term. Even though the magnitudes of these terms are very small, it is of interest to know whether these terms can be safely neglected, how small these terms are, and their variations in time and space. It is also interesting to see how these effects can change in relative importance as the regime of the flow changes. In order to answer these questions, we need to obtain information about the nature of the solutions of the governing equations. This information may not be obtained from the exact analytical solutions because they can be useless for such physico-mathematical interpretations. The only way to get this information is through the use of approximations, numerical solutions, or combinations thereof. Foremost among the so-called approximation methods are perturbation methods (Nayfeh 1973). By defining the coefficients of each term as coefficients of regular perturbation expansions, the effects of viscous, inertial, acceleration and convective terms could be investigated separately. The effects of each term could be expressed in terms of head or velocity, depending on the choice of dependent variable.

The regular perturbation method was applied to two cases, one with the coefficient of the inertial term included as one of the regular perturbation expansions, and one with without it. The first case considered was the laminar regime. For this regime the inertial effect is small and can be included as one of the regular perturbation expansion terms. The second case considered was the PDT and FDT regimes, in which inertial effects are relatively large or even dominant, and cannot be considered as RP expansion terms.

3.4.1. Perturbation Expansions for Laminar Case

The standard and simplest groundwater flow model, based on Darcy's Law and the continuity equation was the obvious starting point for investigating the separate effects of the additional terms and their associated physical meanings. To facilitate this, the momentum equation can be re-arranged so that the coefficient on H_X becomes unity:

$$H_x + \frac{C_3}{C_1}V + \frac{C_4}{C_1}V^2 + \frac{C_6}{C_1}V_\tau + \frac{C_2}{C_1}VV_x = 0 \qquad [3\text{-}79]$$

If we define C_4/C_1 as ε, C_6/C_1 as δ, and C_2/C_1 as γ:

$$H_x + \frac{C_3}{C_1}V + \varepsilon V^2 + \delta V_\tau + \gamma VV_X = 0 \qquad [3\text{-}80]$$

In the continuity equation, the coefficient on VH_X can be re-written C_2 because $C_5 = C_2$:

$$H_\tau + V_X + \frac{C_2}{C_6}VH_x + \frac{C_7}{C_6}V = 0 \qquad [3\text{-}81]$$

If we define C_2/C_6 as ξ, and C_7/C_6 as ω:

$$H_\tau + V_x + \xi VH_X + \omega V = 0 \qquad [3\text{-}82]$$

Using a perturbation expansion, the quantity H can be expressed as:

$$H = H_0 + \varepsilon H_1 + \delta H_2 + \gamma H_3 + \xi H_4 + \omega H_5 + O(\varepsilon^2) \qquad [3\text{-}83]$$

Using a perturbation expansion, the quantity V can be expressed as:

$$V = V_0 + \varepsilon V_1 + \delta V_2 + \gamma V_3 + \xi V_4 + \omega V_5 + O(\varepsilon^2) \qquad [3\text{-}84]$$

From eqn [3-83], we can expect that the effects of each term on H could be found using H_0, H_1, H_2, H_3, H_4 and H_5. Similarly, from eqn [3-84], we can find the effects on V using V_0, V_1, V_2, V_3, V_4 and V_5. Table 3.7 summarizes the expansion coefficients with the

order-of-magnitude and relevant H and V for each. The value of the order of magnitude was obtained with an applied hydraulic gradient of 0.1.

Table 3.8 Expansion coefficient and relevant H and V.

	expansion coefficient	expression	order of magnitude	relevant H and V
viscous effect	-	C_3/C_1	O(1)	H_0 and V_0
inertial effect	ε	C_4/C_1	$O(10^{-2})$	H_1 and V_1
local acceleration	δ	C_6/C_1	$O(10^{-3})$	H_2 and V_2
convective acceleration	γ	C_2/C_1	$O(10^{-6})$	H_3 and V_3
advective acceleration	ξ	C_2/C_6	$O(10^{-4})$	H_4 and V_4
elevation head	ω	C_7/C_6	$O(10^{-3})$	H_5 and V_5

If we differentiate H with respect to τ:

$$H_\tau = H_{0\tau} + \varepsilon H_{1\tau} + \delta H_{2\tau} + \gamma H_{3\tau} + \xi H_{4\tau} + \omega H_{5\tau} + O(\varepsilon^2) \qquad [3\text{-}85]$$

If we differentiate H with respect to X:

$$H_X = H_{0_X} + \varepsilon H_{1_X} + \delta H_{2_X} + \gamma H_{3_X} + \xi H_{4_X} + \omega H_{5_X} + O(\varepsilon^2) \qquad [3\text{-}86]$$

If we differentiate V with respect to τ:

$$V_\tau = V_{0\tau} + \varepsilon V_{1\tau} + \delta V_{2\tau} + \gamma V_{3\tau} + \xi V_{4\tau} + \omega V_{5\tau} + O(\varepsilon^2) \qquad [3\text{-}87]$$

If we differentiate V with respect to X:

$$V_X = V_{0_X} + \varepsilon V_{1_X} + \delta V_{2_X} + \gamma V_{3_X} + \xi V_{4_X} + \omega V_{5_X} + O(\varepsilon^2) \qquad [3\text{-}88]$$

VV_X and VH_X can be expressed as:

$$\begin{aligned} VV_X = {} & V_0 V_{0_X} + \varepsilon V_0 V_{1_X} + \delta V_0 V_{2_X} + \gamma V_0 V_{3_X} + \xi V_0 V_{4_X} + \omega V_0 V_{5_X} \\ & + \varepsilon V_1 V_{0_X} + \delta V_2 V_{0_X} + \gamma V_3 V_{0_X} + \xi V_4 V_{0_X} + \omega V_5 V_{0_X} + O(\varepsilon^2) \end{aligned} \qquad [3\text{-}89]$$

VV_X and VH_X can be expressed as:

$$VH_X = V_0H_{0_x} + \varepsilon V_0H_{1_x} + \delta V_0H_{2_x} + \gamma V_0H_{3_x} + \xi V_0H_{4_x} + \omega V_0H_{5_x}$$
$$+ \varepsilon V_1H_{0_x} + \delta V_2H_{0_x} + \gamma V_3H_{0_x} + \xi V_4H_{0_x} + \omega V_5H_{0_x} + O(\varepsilon^2) \quad [3\text{-}90]$$

If the V^2 term is expressed with first-order accuracy:

$$V^2 = V_0^2 + 2\varepsilon V_0V_1 + 2\delta V_0V_2 + 2\gamma V_0V_3 + 2\xi V_0V_4 + 2\omega V_0V_5 + O(\varepsilon^2) \quad [3\text{-}91]$$

Substitution of H_X, V_τ, VV_X, and V^2 into eqn [3-80] gives:

$$H_{0_x} + \varepsilon H_{1_x} + \delta H_{2_x} + \gamma H_{3_x} + \xi H_{4_x} + \omega H_{5_x} + \frac{C_3}{C_1}(V_0 + \varepsilon V_1 + \delta V_2 + \gamma V_3 + \xi V_4 + \omega V_5)$$
$$+ \varepsilon V_0^2 + \delta V_{0_\tau} + \gamma V_0V_{0_x} + O(\varepsilon^2) = 0 \quad [3\text{-}92]$$

Substitution of H_τ, V_X, and VH_X into eqn [3-82] yields:

$$H_{0\tau} + \varepsilon H_{1\tau} + \delta H_{2\tau} + \gamma H_{3\tau} + \xi H_{4\tau} + \omega H_{5\tau} + V_{0_x} + \varepsilon V_{1_x} + \delta V_{2_x} + \gamma V_{3_x} + \xi V_{4_x} + \omega V_{5_x}$$
$$+ \xi V_0H_{0_x} + \omega V_0 + O(\varepsilon^2) = 0 \quad [3\text{-}93]$$

From eqn [3-92], equating coefficients of ε^0 gives:

$$(\varepsilon)^0: \qquad H_{0_x} = -\frac{C_3}{C_1}V_0 \quad [3\text{-}94a]$$

where $(\varepsilon)^0$ represents order of ε^0.

From eqn [3-93], equating coefficients of ε^0 yields:

$$(\varepsilon)^0: \qquad V_{0_x} = -H_{0_\tau} \quad [3\text{-}94b]$$

After differentiating eqn [3-94a] with respect to X, substitution of eqn [3-94b] for V_{0_x} gives:

$$H_{0_{xx}} = \frac{C_3}{C_1}H_{0_\tau} \quad [3\text{-}94c]$$

From eqn [3-92], equating coefficients of ε^1 gives:

$$(\varepsilon)^1: \qquad H_{1_X} = -\frac{C_3}{C_1} V_1 - V_0^2 \qquad [3\text{-}95a]$$

where $(\varepsilon)^1$ represents order of ε^1.

From eqn [3-93], equating coefficients of ε^1 yields:

$$(\varepsilon)^1: \qquad V_{1_X} = -H_{1_\tau} \qquad [3\text{-}95b]$$

After differentiating eqn [3-95a] with respect to X, substitution of eqn [3-95b] for V_{1_X} gives:

$$H_{1_{XX}} = \frac{C_3}{C_1} H_{1_\tau} - 2V_0 V_{0_X} \qquad [3\text{-}95c]$$

From eqn [3-92], equating coefficients of δ^1 gives:

$$(\delta)^1: \qquad H_{2_X} = -\frac{C_3}{C_1} V_2 - V_{0\tau} \qquad [3\text{-}96a]$$

where $(\delta)^1$ represents order of δ^1.

From eqn [3-93], equating coefficients of δ^1 yields:

$$(\delta)^1: \qquad V_{2_X} = -H_{2_\tau} \qquad [3\text{-}96b]$$

After differentiating eqn [3-96a] with respect to X, substitution of eqn [3-96b] for V_{2_X} gives:

$$H_{2_{XX}} = \frac{C_3}{C_1} H_{2_\tau} - V_{0_{\tau X}} \qquad [3\text{-}96c]$$

From eqn [3-92], equating coefficients of γ^1 gives:

$$(\gamma)^1: \qquad H_{3_X} = -\frac{C_3}{C_1} V_3 - V_0 V_{0_X} \qquad [3\text{-}97a]$$

where $(\gamma)^1$ represents order of γ^1.

From eqn [3-93], equating coefficients of γ^1 yields:

$$(\gamma)^1: \qquad V_{3_x} = -H_{3_\tau} \qquad [3\text{-}97b]$$

After differentiating eqn [3-97a] with respect to X, substitution of eqn [3-97b] for V_{3_x} gives:

$$H_{3_{xx}} = \frac{C_3}{C_1} H_{3_\tau} - \left(V_{0_x}\right)^2 - V_0 V_{0_{xx}} \qquad [3\text{-}97c]$$

From eqn [3-92], equating coefficients of ξ^1 gives:

$$(\xi)^1: \qquad H_{4_x} = -\frac{C_3}{C_1} V_4 \qquad [3\text{-}98a]$$

where $(\xi)^1$ represents order of ξ^1.

From eqn [3-93], equating coefficients of ξ^1 yields:

$$(\xi)^1: \qquad V_{4_x} = -H_{4_\tau} - V_0 H_{0_x} \qquad [3\text{-}98b]$$

After differentiating eqn [3-98a] with respect to X, substitution of eqn [3-98b] for V_{4_x} gives:

$$H_{4_{xx}} = \frac{C_3}{C_1}\left(H_{4_\tau} + V_0 H_{0_x}\right) \qquad [3\text{-}98c]$$

From eqn [3-92], equating coefficients of ω^1 gives:

$$(\omega)^1: \qquad H_{5_x} = -\frac{C_3}{C_1} V_5 \qquad [3\text{-}99a]$$

where $(\omega)^1$ represents order of ω^1.

From eqn [3-93], equating coefficients of ω^1 yields:

$$(\omega)^1: \qquad V_{5_X} = -H_{5_\tau} - V_0 \qquad [3\text{-}99b]$$

After differentiating eqn [3-99a] with respect to X, substitution of eqn [3-99b] for V_{5_X} gives:

$$H_{5_{XX}} = \frac{C_3}{C_1}\left(H_{5_\tau} + V_0\right) \qquad [3\text{-}99c]$$

3.4.2. Perturbation Expansions for PDT and FDT Cases

If the regular perturbation expansion coefficient becomes large, the regular perturbation method can fail. If the applied hydraulic gradient is increased, the inertial effect becomes significant and the regime of the flow can change from laminar to PDT, and from PDT to FDT. In the PDT and FDT regimes we may exclude the inertial term from expansion. However, the inertial term can be investigated by subtracting H obtained using the Darcy's Law model from the H obtained using the Ergun model. Ergun equation and continuity equation can be a starting point to investigate separate effects of the each additional term. From eqn [3-79] and [3-81], if we define $C_6/C_1 = \varepsilon$, $C_2/C_1 = \delta$, $C_2/C_6 = \gamma$, and $C_7/C_6 = \xi$, the momentum equation becomes:

$$H_x + \frac{C_3}{C_1}V + \frac{C_4}{C_1}V^2 + \varepsilon V_\tau + \delta V V_X = 0 \qquad [3\text{-}100]$$

The continuity equation becomes:

$$H_\tau + V_x + \gamma V H_X + \xi V = 0 \qquad [3\text{-}101]$$

The inertial effects can still be investigated by comparing the Darcy's Law model with the Ergun model. If we define H_D and V_D as H and V of Darcy's Law, the momentum and continuity equations are:

$$H_{Dx} + \frac{C_3}{C_1}V_D = 0 \qquad [3\text{-}102]$$

$$H_{D\tau} + V_{Dx} = 0 \qquad [3\text{-}103]$$

If we define H_E and V_E as the H and V associated with the Ergun model, the momentum and continuity equations may be stated as:

$$H_{Ex} + \frac{C_3}{C_1} V_E + \frac{C_4}{C_1} V_E^{\,2} = 0 \qquad [3\text{-}104]$$

$$H_{E\tau} + V_{Ex} = 0 \qquad [3\text{-}105]$$

The only difference between these two models is the inertial term. Eqns [3-104] and [3-105] may be used to express H_E using H_D and $H_{inertial}$:

$$H_E = H_D + \frac{C_4}{C_1} H_{inertial} \qquad [3\text{-}106]$$

The inertial effect can be separated by re-arranging eqn [3-106] for $H_{inertial}$:

$$H_{inertial} = (H_E - H_D)\frac{C_1}{C_4} \qquad [3\text{-}107]$$

In the PDT and FDT regimes the inertial effect can be investigated using eqn [3-107]. In order to show the effects of the other terms, regular perturbation method was used. Using a regular perturbation expansion on H yields:

$$H = H_0 + \varepsilon H_1 + \delta H_2 + \gamma H_3 + \xi H_4 + O(\varepsilon^2) \qquad [3\text{-}108]$$

Similarly, V can be expressed as:

$$V = V_0 + \varepsilon V_1 + \delta V_2 + \gamma V_3 + \xi V_4 + O(\varepsilon^2) \qquad [3\text{-}109]$$

Equation [3-108] could be used to investigate the effects of each term (H_0, H_1, H_2, H_3 and H_4) on H. Similarly, eqn [3-09] could be used to investigate the effects of V_0, V_1, V_2, V_3 and V_4 on V. Table 3.8 summarizes expansion coefficients along with their orders of magnitude and relevant H and V terms. The stated values of the order of magnitude were obtained using an applied hydraulic gradient of 10.

Table 3.9 Expansion coefficient and relevant H and V.

	expansion coefficient	expression	order of magnitude	relevant H and V
viscous and inertial effect	-	C_3/C_1 and C_4/C_1	$O(1)$	H_0 and V_0
local acceleration	ε	C_6/C_1	$O(10^{-3})$	H_1 and V_1
convective acceleration	δ	C_2/C_1	$O(10^{-5})$	H_2 and V_2
advective acceleration	γ	C_2/C_6	$O(10^{-2})$	H_3 and V_3
elevation head	ξ	C_7/C_6	$O(10^{-3})$	H_4 and V_4

Differentiating H with respect to τ yields:

$$H_\tau = H_{0_\tau} + \varepsilon H_{1_\tau} + \delta H_{2_\tau} + \gamma H_{3_\tau} + \xi H_{4_\tau} + O(\varepsilon^2) \qquad [3\text{-}110]$$

Differentiating H with respect to X yields:

$$H_x = H_{0_x} + \varepsilon H_{1_x} + \delta H_{2_x} + \gamma H_{3_x} + \xi H_{4_x} + O(\varepsilon^2) \qquad [3\text{-}111]$$

Differentiating V with respect to τ yields:

$$V_\tau = V_{0_\tau} + \varepsilon V_{1_\tau} + \delta V_{2_\tau} + \gamma V_{3_\tau} + \xi V_{4_\tau} + O(\varepsilon^2) \qquad [3\text{-}112]$$

Differentiating V with respect to X yields:

$$V_x = V_{0_x} + \varepsilon V_{1_x} + \delta V_{2_x} + \gamma V_{3_x} + \xi V_{4_x} + O(\varepsilon^2) \qquad [3\text{-}113]$$

VV_X can be expressed as:

$$VV_x = V_0 V_{0_x} + \varepsilon V_0 V_{1_x} + \delta V_0 V_{2_x} + \gamma V_0 V_{3_x} + \xi V_0 V_{4_x} + \varepsilon V_1 V_{0_x} + \delta V_2 V_{0_x} + \gamma V_3 V_{0_x} + \xi V_4 V_{0_x} + O(\varepsilon^2) \qquad [3\text{-}114]$$

VH_X can be expressed as:

$$VH_x = V_0 H_{0_x} + \varepsilon V_0 H_{1_x} + \delta V_0 H_{2_x} + \gamma V_0 H_{3_x} + \xi V_0 H_{4_x} + \varepsilon V_1 H_{0_x} + \delta V_2 H_{0_x} + \gamma V_3 H_{0_x} + \xi V_4 H_{0_x} + O(\varepsilon^2) \qquad [3\text{-}115]$$

If the V^2 term is expressed to first-order accuracy:

$$V^2 = V_0^2 + 2\varepsilon V_0 V_1 + 2\delta V_0 V_2 + 2\gamma V_0 V_3 + 2\xi V_0 V_4 + O(\varepsilon^2) \qquad [3\text{-}116]$$

then substitution of H_X, V_τ, VV_X, and V^2 into eqn [3-100] gives:

$$H_{0_X} + \varepsilon H_{1_X} + \delta H_{2_X} + \gamma H_{3_X} + \xi H_{4_X} + \frac{C_3}{C_1}\left(V_0 + \varepsilon V_1 + \delta V_2 + \gamma V_3 + \xi V_4\right) + \frac{C_4}{C_1}\left(V_0^2 + \right.$$

$$\left. + 2\varepsilon V_0 V_1 + 2\delta V_0 V_2 + 2\gamma V_0 V_3 + 2\xi V_0 V_4\right) + \varepsilon V_{0_\tau} + \delta V_0 V_{0_X} + O(\varepsilon^2) = 0 \qquad [3\text{-}117]$$

Substitution of H_τ, V_X, and VH_X into eqn [3-101] yields:

$$H_{0_\tau} + \varepsilon H_{1_\tau} + \delta H_{2_\tau} + \gamma H_{3_\tau} + \xi H_{4_\tau} + V_{0_X} + \varepsilon V_{1_X} + \delta V_{2_X} + \gamma V_{3_X} + \xi V_{4_X}$$

$$+ \gamma V_0 H_{0_X} + \xi V_0 + O(\varepsilon^2) = 0 \qquad [3\text{-}118]$$

Using eqn [3-117], equating coefficients of ε^0 gives:

$$(\varepsilon)^0: \qquad H_{0_X} = -\frac{C_3}{C_1} V_0 - \frac{C_4}{C_1} V_0^2 \qquad [3\text{-}119a]$$

where $(\varepsilon)^0$ represents order of ε^0.

Using eqn [3-118], equating coefficients of ε^0 yields:

$$(\varepsilon)^0: \qquad V_{0_X} = -H_{0_\tau} \qquad [3\text{-}119b]$$

Similar arguments can be used to get the Ergun model solution. Differentiating eqn [3-119a] with respect to X yields:

$$V_{0_X} = -\frac{C_1}{\sqrt{C_3^2 - 4C_1C_4H_{0_X}}} H_{0_{XX}} \qquad [3\text{-}119c]$$

Substitution of V_{0X} into eqn [3-119c] gives:

$$H_{0_{XX}} = -\frac{\sqrt{C_3^2 - 4C_1C_4H_{0_X}}}{C_1} H_{0_\tau} \qquad [3\text{-}119d]$$

Using eqn [3-117], equating coefficients of ε^1 gives:

$$(\varepsilon)^1: \qquad H_{1_X} = -\frac{C_3}{C_1} V_1 - 2\frac{C_4}{C_1} V_0 V_1 - V_{0_\tau} \qquad [3\text{-}120a]$$

where $(\varepsilon)^1$ represents order of ε^1.

Using eqn [3-118], equating coefficients of ε^1 yields:

$$(\varepsilon)^1: \qquad V_{1_X} = -H_{1_\tau} \qquad [3\text{-}120b]$$

Re-arrangement gives:

$$\left(\frac{C_3}{C_1} + 2\frac{C_4}{C_1} V_0\right) V_1 = -H_{1_X} - V_{0_\tau} \qquad [3\text{-}120c]$$

or

$$V_1 = \frac{C_1}{C_3 + 2C_4 V_0}\left(-H_{1_X} - V_{0_\tau}\right) \qquad [3\text{-}120d]$$

Differentiating eqn [3-120a] with respect to X:

$$H_{1_{XX}} = -\frac{C_3}{C_1} V_{1_X} - 2\frac{C_4}{C_1}\left(V_1 V_{0_X} + V_{1_X} V_0\right) - V_{0_\tau} \qquad [3\text{-}120e]$$

Substituting V_1 and V_{1X} yields:

$$H_{1_{XX}} = \frac{C_3}{C_1} H_{1_\tau} + 2\frac{C_4}{C_1}\left(\frac{C_1}{C_3 + 2C_4 V_0}\left(H_{1_X} + V_{0_\tau}\right) V_{0_X} + H_{1_\tau} V_0\right) - V_{0_{\tau X}} \qquad [3\text{-}121]$$

Using eqn [3-117], equating coefficients of δ^1 gives:

$$(\delta)^1: \qquad H_{2_X} = -\frac{C_3}{C_1} V_2 - 2\frac{C_4}{C_1} V_0 V_2 - V_{0_X} \qquad [3\text{-}122a]$$

where $(\delta)^1$ represents order of δ^1.

Using eqn [3-118], equating coefficients of δ^1 yields:

$$(\delta)^1: \qquad V_{2_X} = -H_{2_\tau} \qquad [3\text{-}122b]$$

Re-arrangement of eqn [3-122a] gives:

$$\left(\frac{C_3}{C_1} + 2\frac{C_4}{C_1}V_0\right)V_2 = -H_{2_X} - V_0 V_{0_X} \qquad [3\text{-}122c]$$

or

$$V_2 = \frac{C_1}{C_3 + 2C_4 V_0}\left(-H_{2_X} - V_0 V_{0_X}\right) \qquad [3\text{-}122d]$$

Differentiating eqn [3-122a] with respect to X:

$$H_{2_{XX}} = -\frac{C_3}{C_1}V_{2_X} - 2\frac{C_4}{C_1}\left(V_2 V_{0_X} + V_{2_X} V_0\right) - \left({V_{0_X}}^2 + V_0 V_{0_{XX}}\right) \qquad [3\text{-}122e]$$

Substituting V_2 and V_{2X} yields:

$$H_{2_{XX}} = \frac{C_3}{C_1}H_{2_\tau} + 2\frac{C_4}{C_1}\left(\frac{C_1}{C_3 + 2C_4 V_0}\left(H_{2_X} + V_0 V_{0_X}\right)V_{0_X}\right) + 2\frac{C_4}{C_1}\left(H_{2_\tau} V_0\right) - \left({V_{0_X}}^2 + V_0 V_{0_{XX}}\right) \qquad [3\text{-}122f]$$

Using eqn [3-117], equating coefficients of γ^1 gives:

$$(\gamma)^1: \qquad H_{3_X} = -\frac{C_3}{C_1}V_3 - 2\frac{C_4}{C_1}V_0 V_3 \qquad [3\text{-}123a]$$

where $(\gamma)^1$ represents order of γ^1.

Using eqn [3-118], equating coefficients of γ^1 yields:

$$(\gamma)^1: \qquad V_{3_X} = -H_{3_\tau} - V_0 H_{0_X} \qquad [3\text{-}123b]$$

Re-arrangement of eqn [3-123a] gives:

$$\left(\frac{C_3}{C_1}+2\frac{C_4}{C_1}V_0\right)V_3=-H_{3_x} \qquad [3\text{-}123c]$$

or

$$V_3=\frac{-C_1}{C_3+2C_4V_0}H_{3_x} \qquad [3\text{-}123d]$$

Differentiating eqn [3-123a] with respect to X gives:

$$H_{3_{xx}}=-\frac{C_3}{C_1}V_{3_x}-2\frac{C_4}{C_1}\left(V_3V_{0_x}+V_{3_x}V_0\right) \qquad [3\text{-}123e]$$

Substituting V_3 and V_{3X} yields:

$$H_{3_{xx}}=\frac{C_3}{C_1}\left(H_{3_\tau}+V_0H_{0_x}\right)+2\frac{C_4}{C_1}\left(\frac{C_1}{C_3+2C_4V_0}H_{3_x}V_{0_x}\right)+2\frac{C_4}{C_1}\left(H_{3_\tau}+V_0H_{0_x}\right)V_0 \qquad [3\text{-}123f]$$

Using eqn [3-117], equating coefficients of ξ^1 gives:

$$(\xi)^1: \qquad H_{4_x}=-\frac{C_3}{C_1}V_4-2\frac{C_4}{C_1}V_0V_4 \qquad [3\text{-}124a]$$

where $(\xi)^1$ represents order of ξ^1.

Using eqn [3-118], equating coefficients of ξ^1 yields:

$$(\xi)^1: \qquad V_{4_x}=-H_{4_\tau}-V_0 \qquad [3\text{-}124b]$$

Re-arrangement of eqn [3-124a] gives:

$$V_4=\frac{-C_1}{C_3+2C_4V_0}H_{4_x} \qquad [3\text{-}124c]$$

Differentiating eqn [3-124a] with respect to X:

$$H_{4_{xx}}=-\frac{C_3}{C_1}V_{4_x}-2\frac{C_4}{C_1}\left(V_4V_{0_x}+V_{4_x}V_0\right) \qquad [3\text{-}124d]$$

Substituting V_4 and V_{4X} then yields:

$$H_{4_{xx}} = \frac{C_3}{C_1}\left(H_{4_\tau} + V_0\right) + 2\frac{C_4}{C_1}\left(\frac{C_1}{C_3 + 2C_4V_0}H_{4_x}V_{0_x} + \left(H_{4_\tau} + V_0\right)V_0\right) \quad [3\text{-}124e]$$

3.5. Matched Asymptotic Expansions

3.5.1. Introduction

Using the regular perturbation method, even though some of the terms are multiplied by parameters having very small magnitudes, the presence of these terms often cannot be simply neglected because the problem can depend on these small parameters in a "singular" way. Matched asymptotic expansions can be used to solve such singular problems. The method of matched asymptotic expansions has been devised as an efficient means to treat problems which have the different phenomenologies in different regions of space and/or time. For example, the sudden opening of a gate which is connected to a pipe packed with porous media can result in a sharp change in head and velocity in very small space/time. This flow through porous media problem near such a boundary cannot be properly solved using Darcy's Law and an Ergun-type model. Even though the resulting near-boundary wave propagation disappears quickly, it can cause noticeable differences in head and velocity near the boundary, as compared to the solutions to such 'naïve' models. Figure 3.5 shows the inner, intermediate, and outer region in space-time.

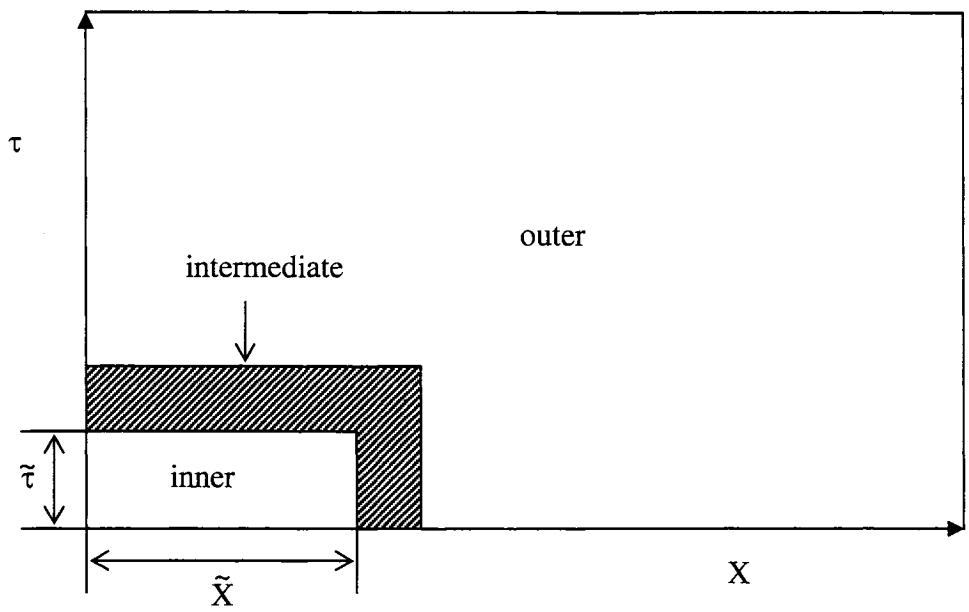

Figure 3.5 Inner, intermediate, and outer zones in time and space.

In order to obtain asymptotic expansions that have an appropriately broad range of validity, the fact that the sharp changes are characterized by a magnified scale which is different from the scale characterizing the behaviour of the dependent variables outside the sharp-change regions must be utilized (Nayfeh, 1973). Some important features of singular perturbations (Naidu, 2002) can be summarized as follows:

(1) If the order of the problem becomes lower for $\varepsilon = 0$ than for $\varepsilon \neq 0$, then the problem becomes a singular perturbation problem where ε is the small parameter used as a perturbation coefficient.

(2) There exists a thin and/or short layer and/or zone where the solution changes rapidly.

(3) The degenerate problem, also called the unperturbed problem, is of reduced order and cannot satisfy all the boundary conditions of the original fully perturbed problem.

(4) The singularly perturbed problem has two widely separated characteristic roots, giving rise to slow and fast components in time and/or small and large components in space. Thus, the singularly perturbed problem possesses a multi-scale property. The simultaneous presence of multi-

scale phenomena makes the problem stiff from a numerical solution point of view because the numerical method should simultaneously satisfy restrictions in each scale.

3.5.2. Template Problem

Using the regular perturbation method, the incremental effects of the each term in the full problem were presented. Even though some of the terms were multiplied by parameters having very small magnitudes, it was found that we may not simply ignore the presence of these terms because the problem can depend on these small parameters in a "singular" way. In this chapter, by solving one template problem using matched asymptotic expansions:

(1) the singularity of the problem will be shown,
(2) the selection of inner variables will be presented ,
(3) the inner expansion becomes an evolving-wave form which has both wave and diffusion aspects to it,
(4) which boundary condition can be dropped in the inner and outer zones is analytically proved,
(5) that a matching between the inner and outer zones can be achieved,
(6) that a composite solution can be obtained using superposition,
(7) that the numerical solutions are valid; this is proved by comparing the analytical and numerical solutions.

The template problem, which has a similar form to that of the laminar case, will be solved with matched asymptotic expansion under the same boundary and initial conditions as were used for the original problem. The template problem may be stated as:

$$H_x + V + \varepsilon_0 V_\tau = 0 \qquad [3\text{-}125]$$

$$H_\tau + V_x = 0 \qquad [3\text{-}126]$$

where ε_0 can be the ratio C_6/C_1 in the problem statement.

Boundary and initial conditions for H are therefore those stated in the original problem, but it will be possible to derive boundary conditions on V using the special characteristics of the delta function and the relationship between H and V in the continuity equation. These additional conditions on V make it possible to solve for V regardless of the behavior of H.

The boundary and initial conditions can be presented separately. The boundary conditions for H are:

$$H = 1 \text{ at } X = 0 \qquad [3\text{-}127a]$$

$$H = 0 \text{ at } X = 1 \qquad [3\text{-}127b]$$

The initial conditions for H are:

$$H = 0 \text{ when } \tau = 0 \qquad [3\text{-}127c]$$

$$H_\tau = 0 \text{ when } \tau = 0 \qquad [3\text{-}127d]$$

Similarly, the boundary conditions for V are:

$$V_X = -\delta(\tau) \text{ at } X = 0 \qquad [3\text{-}128a]$$

$$V_X = 0 \text{ at } X = 1 \qquad [3\text{-}128b]$$

The initial conditions for V are:

$$V = 0 \text{ when } \tau = 0 \qquad [3\text{-}128c]$$

$$V_\tau = 0 \text{ when } \tau = 0 \qquad [3\text{-}128d]$$

The condition given by [3-127d] is derived from the fact that as X and τ go to zero, the equation for H becomes the wave equation:

$$H \rightarrow u(\tau - \sqrt{\varepsilon_0} X) \qquad \text{as } (X, \tau) \rightarrow 0 \qquad [3\text{-}129]$$

The conditions given by [3-128a] and [3-128d] are derived from the fact that as X and τ approach to zero, the equation of V becomes the wave equation:

$$V \rightarrow \frac{1}{\sqrt{\varepsilon_0}} u(\tau - \sqrt{\varepsilon_0} X) \qquad \text{as } (X, \tau) \rightarrow 0 \qquad [3\text{-}130]$$

The condition given by [3-128b] is derived from the fact that H is constant at X = 1. From the continuity equation at $X = 1$, $H_\tau = 0$ so $V_x = 0$.

3.5.3. Outer Expansions

If we combine eqn [3-125] and [3-126], we can get an equation in H:

$$H_{XX} = H_\tau + \varepsilon_0 H_{\tau\tau} \qquad [3\text{-}131]$$

The above equation in H was solved using Laplace transformations with conditions of [6-3a] through [6-3d]. The three-step method of Kuhfitting (1978) was used:

(a) The Laplace transform of both sides of the differential equation was found.

(b) The resulting equation was solved algebraically.

(c) The inverse transform was applied.

In general, a Laplace transform is defined by:

$$L\{f(t)\} = F(p_L) = \int_0^\infty e^{-p_L t} f(t)dt \qquad [3\text{-}132]$$

where p_L is a complex variable. If we use $H(\tau)$ instead of $f(t)$:

$$L\{H(\tau)\} = \overline{H}(p_L) \qquad [3\text{-}133]$$

The Laplace transform of the LHS of eqn [3-131] is:

$$L\{H_{XX}\} = \overline{H}_{XX} \qquad [3\text{-}134]$$

The Laplace transform of the RHS includes a second-order derivative with respect to time. The Laplace transform of second order derivative is:

$$L\{H_{\tau\tau}\} = p_L{}^2 L\{H(\tau)\} - p_L H(0) - H_\tau(0) \qquad [3\text{-}135]$$

From the initial conditions, $H(0) = 0$ and $H_\tau(0) = 0$. Therefore:

$$L\{H_{\tau\tau}\} = p_L^2 \overline{H} \qquad [3\text{-}136]$$

The Laplace transform of first-order derivative is:

$$L\{H_\tau\} = p_L L\{H(\tau)\} - H(0) \qquad [3\text{-}137]$$

From the initial condition H(0) = 0. Therefore:

$$L\{H_\tau\} = p_L \overline{H} \qquad [3\text{-}138]$$

The Laplace transform of eqn [3-131] is:

$$\overline{H}_{XX} = \tilde{p}^2 \overline{H} \qquad [3\text{-}139]$$

where $\tilde{p}^2 = p_L + \varepsilon_0 p_L^2$.

The boundary conditions become:

$$\overline{H} = \int_0^\infty e^{-p_L \tau} d\tau = \frac{1}{p_L} \qquad \text{at } X = 0 \qquad [3\text{-}140]$$

$$\overline{H} = 0 \qquad \text{at } X = 1 \qquad [3\text{-}141]$$

The general solution of eqn [3-139] can be expressed as:

$$\overline{H} = A_1' e^{a_2 X} + B_1' e^{b_2 X} \qquad [3\text{-}142]$$

Combining eqn [3-142] and [3-139]:

$$A_1' a_2^2 e^{a_2 X} + B_1' b_2^2 e^{b_2 X} = \tilde{p}^2 \left(A_1' e^{a_2 X} + B_1' e^{b_2 X} \right) \qquad [3\text{-}143]$$

It can be readily shown that $a_2 = \tilde{p}$ and $b_2 = -\tilde{p}$. Using the boundary condition given by [3-140], if we substitute X = 0 in eqn [3-143]:

$$A_1' + B_1' = \frac{1}{p_L} \qquad [3\text{-}144]$$

From the boundary condition given by [3-141]:

$$A_1' e^{\tilde{p}} + B_1' e^{-\tilde{p}} = 0 \qquad [3\text{-}145]$$

Substituting A from eqn [3-144] into eqn [3-145] and multiplying both sides by $e^{-\sqrt{\tilde{s}}}$ gives:

$$\frac{1}{p_L} - B_1' + B_1' e^{-2\tilde{p}} = 0 \qquad [3\text{-}146]$$

or

$$B_1' = \frac{1}{p_L\left(1 - e^{-2\tilde{p}}\right)} \qquad [3\text{-}147]$$

Using eqn [3-147], A_1' can be expressed as:

$$A_1' = \frac{1}{p_L} - 1 = \frac{-e^{-2\tilde{p}}}{p_L\left(1 - e^{-2\tilde{p}}\right)} \qquad [3\text{-}148]$$

Using A_1' and B_1', $\overline{H}$ becomes:

$$\overline{H} = \frac{-e^{-2\tilde{p}}e^{\tilde{p}X} + e^{-\tilde{p}}}{p_L\left(1 - e^{-2\tilde{p}}\right)} \qquad [3\text{-}149]$$

By re-arrangement of eqn [3-149], the exact solution for $\overline{H}$ is then:

$$\overline{H} = \frac{e^{\tilde{p}X} - e^{(2-X)\tilde{p}}}{p_L\left(1 - e^{2\tilde{p}}\right)} \qquad [3\text{-}150]$$

The first-order outer expansion of eqn [3-150] can be obtained by applying the limit $\varepsilon_0 \to 0$:

$$\overline{H}^{(o)} \sim \frac{e^{\sqrt{p_L}X} - e^{(2-X)\sqrt{p_L}}}{p_L\left(1 - e^{2\sqrt{p_L}}\right)} + O(\varepsilon_0) \qquad [3\text{-}151]$$

where superscript (o) denotes outer.

Because the outer expansion follows a first-order approximation of the exact solution, the governing equation for the outer zone can be expressed as:

$$H_{XX} = H_{\tau} \qquad [3\text{-}152]$$

for which the boundary conditions are given by [3-127a] and [3-127b], and the initial condition by [3-127c]. One initial condition given by [3-127d] was dropped because as $\varepsilon_0 \to 0$, the $H_{\tau\tau}$ term in eqn [3-131] becomes negligible.

At this juncture it might seem natural to obtain the inverse Laplace transform of eqn [3-151], but the solution of Laplace transform will instead be used to compare the inner and outer solutions and to find a matching condition between them, a condition which will exist within the overlap or intermediate zone. The expression for $\overline{V}$ will be obtained via procedure similar to that used to obtain the one for $\overline{H}$.

If we combine eqns [3-125] and [3-1276], we get:

$$V_{XX} = V_{\tau} + \varepsilon_0 V_{\tau\tau} \qquad [3\text{-}153]$$

Laplace transform of eqn [3-153] is:

$$\overline{V}_{XX} = \tilde{p}^2 \overline{V} \qquad [3\text{-}154]$$

where $\tilde{p}^2 = p_L + \varepsilon_0 p_L^2$.

The boundary conditions become:

$$\overline{V}_X = -1 \qquad \text{at } X = 0 \qquad [3\text{-}155]$$

$$\overline{V}_X = 0 \qquad \text{at } X = 1 \qquad [3\text{-}156]$$

Using these boundary conditions, the exact solution for $\overline{V}$ can be found as:

$$\overline{V} = -\frac{e^{\tilde{p}X} + e^{(2-X)\tilde{p}}}{\tilde{p}\left(1 - e^{2\tilde{p}}\right)} \qquad [3\text{-}157]$$

The first-order outer expansion of eqn [3-157] can be obtained by taking the limit $\varepsilon_0 \to 0$:

$$\overline{V}^{(o)} \sim -\frac{e^{\sqrt{p_L}X} + e^{(2-X)\sqrt{p_L}}}{\sqrt{p_L}\left(1 - e^{2\sqrt{p_L}}\right)} + O(\varepsilon_0) \qquad [3\text{-}158]$$

Because the outer expansion follows a first-order approximation of the exact solution, it can be expressed as:

$$V_{XX} = V_{\tau} \qquad [3\text{-}159]$$

The associated boundary conditions are given by [3-128a] and [3-128b], and the initial condition given by [3-128c]. One initial condition (that of eqn [3-128d]) was dropped because as $\varepsilon_0 \to 0$, the $V_{\tau\tau}$ term in eqn [3-153] becomes negligible.

3.5.4. Inner Expansion

(i) Selection of Inner Variables

In order to investigate the sharp-change region very near the upstream valve immediately after it has been opened, it will necessary to magnify this small region. Both independent variables, X and τ, will be rescaled so as to stretch the time and space scales. For the dependent variables, H and V, only V needs to be rescaled because the H at the upstream and the downstream ends of the conduit are both constant, and the variation in H will be within the range of 0 to 1. However, the boundary conditions on V were not completely defined by the problem. The quantity V at the upstream end can be expected to be much higher than V at the downstream end because the wave equation will dominate the flow at the upstream boundary.

To begin, X, τ and V are rescaled:

$$\tilde{X} = \frac{X}{a} \qquad [3\text{-}160a]$$

$$\tilde{\tau} = \frac{\tau}{b} \qquad [3\text{-}160b]$$

$$\tilde{V} = \frac{V}{c} \qquad [3\text{-}160c]$$

where a<<1, b<<1, and c>>1.

If we substitute $\tilde{X}$, $\tilde{\tau}$ and $\tilde{V}$ into eqn [3-126] we obtain:

$$\frac{1}{b} H_{\tilde{\tau}} + \frac{c}{a} \tilde{V}_{\tilde{X}} = 0 \qquad [3\text{-}161]$$

If we assume that the continuity equation is geometrically invariant in the inner zone, we can get the identical form of continuity equation for the outer zone by defining:

$$\frac{1}{b} = \frac{c}{a} \qquad [3\text{-}162]$$

Using eqn [3-162], eqn [3-161] becomes:

$$H_{\tilde{\tau}} + \tilde{V}_{\tilde{X}} + = 0 \qquad [3\text{-}163]$$

If we substitute $\tilde{X}$, $\tilde{\tau}$ and $\tilde{V}$ into eqn [3-125] we obtain:

$$\frac{1}{a} H_{\tilde{X}} + c\tilde{V} + \varepsilon_0 \frac{c}{b} \tilde{V}_{\tilde{\tau}} = 0 \qquad [3\text{-}164]$$

In order to investigate the sharp-change region, the unsteady acceleration component can be enhanced by defining:

$$\frac{1}{a} = \varepsilon_0 \frac{c^2}{a} \qquad [3\text{-}165]$$

which results in:

$$c = \frac{1}{\sqrt{\varepsilon_0}} \qquad [3\text{-}166]$$

where c>>1.

In order to better investigate the role of diffusion, defining:

$$\frac{1}{a} = c \qquad [3\text{-}167]$$

and using eqn [3-162] and [3-166], simple expressions for a and b are obtained:

$$a = \sqrt{\varepsilon_0} \qquad [3\text{-}168]$$

$$b = \varepsilon_0 \qquad [3\text{-}169]$$

Using the above new expressions for a, b and c (all in terms of ε_0), the inner variables can be redefined:

$$\tilde{X} = \frac{X}{\sqrt{\varepsilon_0}} \qquad [3\text{-}170a]$$

$$\tilde{\tau} = \frac{\tau}{\varepsilon_0} \qquad [3\text{-}170b]$$

$$\tilde{V} = \sqrt{\varepsilon_0} V \qquad [3\text{-}170c]$$

(ii) Inner Expansion

The conditions dropped in the outer expansion can be rectified by developing an inner expansion. The conditions given by [3-127d] and [3-128d] were lost in the outer expansion. An inner expansion would recover these conditions as $\varepsilon_0 \to 0$. If we substitute the inner variables in eqns [3-125] and [3-126]:

$$H_{\tilde{x}} + \tilde{V} + \tilde{V}_{\tilde{\tau}} = 0 \qquad [3\text{-}171]$$

$$H_{\tilde{\tau}} + \tilde{V}_{\tilde{x}} = 0 \qquad [3\text{-}172]$$

The boundary conditions for H can be presented in inner coordinates using inner variables:

$$H = 1 \text{ at } \tilde{X} = 0 \qquad [3\text{-}173a]$$

$$H = 0 \text{ at } \tilde{X} = \frac{1}{\sqrt{\varepsilon_0}} \qquad [3\text{-}173b]$$

The initial conditions for H are:

$$H = 0 \text{ when } \tilde{\tau} = 0 \qquad [3\text{-}173c]$$

$$H_{\tilde{\tau}} = 0 \text{ when } \tilde{\tau} = 0 \qquad [3\text{-}173d]$$

Similarly, the boundary conditions for $\tilde{V}$ are:

$$\tilde{V}_{\tilde{X}} = -\delta(\tilde{\tau}) \text{ at } \tilde{X} = 0 \qquad [3\text{-}174a]$$

$$\tilde{V}_{\tilde{X}} = 0 \text{ at } \tilde{X} = \frac{1}{\sqrt{\varepsilon_0}} \qquad [3\text{-}174b]$$

The initial conditions for $\tilde{V}$ are:

$$\tilde{V} = 0 \text{ when } \tilde{\tau} = 0 \qquad [3\text{-}174c]$$

$$\tilde{V}_{\tilde{\tau}} = 0 \text{ when } \tilde{\tau} = 0 \qquad [3\text{-}174d]$$

In the momentum equation, as $\varepsilon_0 \to 0$, the $\tilde{V}_{\tilde{\tau}}$ term becomes non-negligible. As a result, we can satisfy the conditions given by [3-173d] and [3-174d] as $\varepsilon_0 \to 0$. If we combine eqns [3-171] and [3-172], an equation for H is obtained:

$$H_{\tilde{X}\tilde{X}} = H_{\tilde{\tau}} + H_{\tilde{\tau}\tilde{\tau}} \qquad [3\text{-}175]$$

For the Laplace transform, the outer Laplace transform variable is rescaled as:

$$s_L = \varepsilon_0 p_L \qquad [3\text{-}176]$$

The Laplace transform of eqn [3-175] is:

$$\overline{H}_{\tilde{X}\tilde{X}} = \tilde{s}^2 \overline{H} \qquad [3\text{-}177]$$

where $\tilde{s}^2 = s_L + s_L^2$.

The exact solution of $\overline{H}$ becomes:

$$\overline{H} = \frac{e^{\tilde{s}X} - e^{(2-\sqrt{\varepsilon_0}\tilde{X})\tilde{s}/\sqrt{\varepsilon_0}}}{s_L\left(1 - e^{2\tilde{s}/\sqrt{\varepsilon_0}}\right)} \qquad [3\text{-}178]$$

The first-order inner expansion of eqn [3-178] can be obtained by taking the limit $\varepsilon_0 \to 0$:

$$\overline{H}^{(i)} = \frac{e^{-\sqrt{s_L^2 + s_L}\tilde{X}}}{s_L} + O(\varepsilon_0) \qquad [3\text{-}179]$$

This first-order expansion will satisfy:

$$H_{\tilde{X}\tilde{X}} = H_{\tilde{\tau}} \qquad [3\text{-}180]$$

The boundary condition is given by [3-173a] and the initial conditions by [3-173c] and [3-173d]. One boundary condition, [3-173b], was dropped because as $\varepsilon_0 \to 0$, $\tilde{X} \to \infty$. This condition can be replaced by:

$$H \to 0 \text{ at } \tilde{X} = \infty \qquad [3\text{-}181]$$

If we combine eqn [3-171] and [3-172] for $\tilde{V}$, we can get an equation of $\tilde{V}$:

$$\tilde{V}_{\tilde{X}\tilde{X}} = \tilde{V}_{\tilde{\tau}} + \tilde{V}_{\tilde{\tau}\tilde{\tau}} \qquad [3\text{-}182]$$

The Laplace transform of eqn [3-182] is:

$$\overline{\tilde{V}}_{\tilde{X}\tilde{X}} = \tilde{s}^2 \overline{\tilde{V}} \qquad [3\text{-}183]$$

where $\tilde{s}^2 = s_L + s_L^2$.

The exact solution for $\tilde{V}$ is:

$$\overline{\tilde{V}} = -\frac{e^{\tilde{s}X} + e^{(2-\sqrt{\varepsilon_0}\tilde{X})\tilde{s}/\sqrt{\varepsilon_0}}}{\tilde{s}\left(1 - e^{2\tilde{s}/\sqrt{\varepsilon_0}}\right)} \qquad [3\text{-}184]$$

The first-order inner expansion of eqn [3-184] can be obtained by taking the limit $\varepsilon_0 \to 0$:

$$\overline{\tilde{V}}^{(i)} = \frac{e^{-\sqrt{s_L^2 + s_L}\tilde{X}}}{\sqrt{s_L^2 + s_L}} + O(\varepsilon_0) \qquad [3\text{-}185]$$

A first-order expansion will satisfy eqn [3-182]. The boundary condition is given by [3-174a], and the initial conditions by [3-174c] and [3-174d] are valid. However, one boundary condition [3-174b] was dropped because as $\varepsilon_0 \to 0$, $\tilde{X} \to \infty$. This condition can be replaced by:

$$\tilde{V}_{\tilde{X}} \to 0 \text{ at } \tilde{X} = \infty \qquad [3\text{-}186]$$

3.5.5. Matching of Inner and Outer Expansions

The existence of an overlapping domain implies that the inner expansion of the outer expansion should, to appropriate orders, agree with the outer expansion of the inner expansion (Lagerstrom 1957). One of the principles of matching is:

"inner representation of the outer representation
= outer representation of the inner representation"

Through such a matching procedure it can be confirmed that conditions were properly dropped in the inner and outer expansions. The solution of overlap region can then be used to construct composite expansion.

3.5.5.1. Matching via Laplace Transform

(i) Conversion Factor

When matching is performed with Laplace transform it should be remembered that there is a conversion factor between the inner and outer coordinates. This conversion factor can be obtained using the simple example of a Laplace transform. If we define the outer function as:

$$f^{(o)} = e^{-\tau} \qquad [3\text{-}187]$$

The Laplace transform of this is:

$$\bar{f}^{(o)} = \frac{1}{p_L + 1} \qquad [3\text{-}188]$$

If we define the inner variables to be the same for the template problem, $\tilde{\tau} = \frac{\tau}{\varepsilon_0}$ and $s_L = \varepsilon_0 p_L$, and the inner representation of (outer representation) for $\bar{f}$ is then:

$$\left(\bar{f}^{(o)}\right)^{(i)} = \frac{1}{1 + \frac{s_L}{\varepsilon_0}} \approx \frac{\varepsilon_0}{s_L} \qquad [3\text{-}189]$$

To compare this to in the outer coordinate, converting eqn [3-189] back to outer coordinate gives:

$$\left(\left(\bar{f}^{(o)}\right)^{(i)}\right)^{(o)} = \frac{1}{p_L} \qquad [3\text{-}190]$$

Substituting the inner variables in the outer expansion gives:

$$f^{(i)} = e^{-\varepsilon_0 \tilde{\tau}} \sim 1 \qquad [3\text{-}191]$$

The Laplace transform of eqn [3-187] is:

$$\bar{f}^{(i)} = \frac{1}{s_L} \qquad [3\text{-}192]$$

The outer representation of the inner representation is then:

$$\left(\bar{f}^{(i)}\right)^{(o)} = \frac{1}{\varepsilon_0 p_L} \qquad [3\text{-}193]$$

If we compare eqns [3-190] and [3-193], the conversion factor is seen to be $\frac{1}{\varepsilon_0}$. Thus, in order to compare and match the Laplace transform in outer coordinate form, this conversion factor must be incorporated.

$$\left(\left(\bar{f}^{(o)}\right)^{(i)}\right)^{(o)} = \varepsilon_0 \left(\bar{f}^{(i)}\right)^{(o)} \qquad [3\text{-}194]$$

This inversion factor is due to the fact that we have an integral formulation in the Laplace transform.

$$L\{f\} = \int_0^\infty e^{-p_L \tau} f dt \qquad [3\text{-}195]$$

The inversion factor will disappear when the inverse Laplace transform is taken.

(ii) Matching using Laplace Transform

Following the previously described matching principle, the inner representation of the outer representation for $\bar{H}$ can be found using $\left(\bar{H}^{(o)}\right)^{(i)}$, and the outer representation

of the inner representation can be found using $\left(\overline{H}^{(i)}\right)^{(o)}$. The inner representation of the outer representation for $\overline{H}$ is obtained by applying the inner variables to eqn [3-151]:

$$\left(\overline{H}^{(o)}\right)^{(i)} \sim \frac{e^{\sqrt{s_L}\tilde{X}} - e^{(2-\sqrt{\varepsilon_0}\tilde{X})\sqrt{s_L}/\sqrt{\varepsilon_0}}}{\frac{s_L}{\varepsilon_0}\left(1 - e^{2\sqrt{s_L}/\sqrt{\varepsilon_0}}\right)} \qquad [3\text{-}196]$$

When $\varepsilon_0 << 1$, this can be approximated by:

$$\left(\overline{H}^{(o)}\right)^{(i)} \sim \frac{e^{-\sqrt{s_L}\tilde{X}}}{\frac{s_L}{\varepsilon_0}} \qquad [3\text{-}197]$$

In order to compare and match the Laplace transform in outer coordinate form, converting eqn [3-197] back to outer coordinate form gives:

$$\left(\left(\overline{H}^{(o)}\right)^{(i)}\right)^{(o)} \sim \frac{e^{-\sqrt{p_L}X}}{p_L} \qquad [3\text{-}198]$$

The outer representation of the inner representation is obtained by applying the outer variables to eqn [3-179]:

$$\left(\overline{H}^{(i)}\right)^{(o)} \sim \frac{e^{-\sqrt{\varepsilon_0^2 p_L^2 + \varepsilon_0 p_L}X/\sqrt{\varepsilon_0}}}{\varepsilon_0 p_L} \qquad [3\text{-}199]$$

After re-arrangement:

$$\left(\overline{H}^{(i)}\right)^{(o)} \sim \frac{e^{-\sqrt{p_L}X}}{\varepsilon_0 p_L} \qquad [3\text{-}200]$$

Matching is obtained from eqn [3-198] and [3-200] by applying the conversion factor $1/\varepsilon_0$ in eqn [3-198]. Similarly, the inner representation of the outer representation for $\overline{V}$ is obtained by applying the inner variables to eqn [3-158]:

$$\left(\overline{V}^{(o)}\right)^{(i)} \sim -\frac{e^{\sqrt{s_L}\tilde{X}} + e^{(2-\sqrt{\varepsilon_0}\tilde{X})\sqrt{s_L}/\sqrt{\varepsilon_0}}}{\sqrt{\frac{s_L}{\varepsilon_0}}\left(1 - e^{2\sqrt{s_L}/\sqrt{\varepsilon_0}}\right)} \qquad [3\text{-}201]$$

When $\varepsilon_0 << 1$, eqn [3-201] can be approximated by:

$$\left(\overline{V}^{(o)}\right)^{(i)} \sim -\frac{e^{-\sqrt{s_L}\tilde{X}}}{\sqrt{\frac{s_L}{\varepsilon_0}}} \qquad [3\text{-}202]$$

In order to compare and match the Laplace transform in outer coordinate form, converting eqn [3-202] back to outer coordinate form gives:

$$\left(\left(\overline{V}^{(o)}\right)^{(i)}\right)^{(o)} \sim \frac{e^{-\sqrt{p_L}X}}{\sqrt{p_L}} \qquad [3\text{-}203]$$

The outer representation of the inner representation is obtained by applying the outer variables to eqn [3-185]:

$$\left(\overline{\tilde{V}}^{(i)}\right)^{(o)} \sim \frac{e^{-\sqrt{\varepsilon_0^2 p_L^2 + \varepsilon_0 p_L}X/\sqrt{\varepsilon_0}}}{\sqrt{\varepsilon_0^2 p_L^2 + \varepsilon_0 p_L}} \qquad [3\text{-}204]$$

When $\varepsilon_0 << 1$, eqn [3-204] can be approximated by:

$$\left(\overline{\tilde{V}}^{(i)}\right)^{(o)} \sim \frac{e^{-\sqrt{p_L}X}}{\sqrt{\varepsilon_0 p_L}} \qquad [3\text{-}205]$$

In order to compare eqn [3-203] and [3-205], we need to use the conversion of V between inner and outer systems:

$$\left(\overline{\tilde{V}}^{(i)}\right)^{(o)} = \sqrt{\varepsilon_0}\left(\overline{V}^{(i)}\right)^{(o)} \qquad [3\text{-}206]$$

Using eqn [3-206], eqn [3-205] becomes:

$$\left(\overline{V}^{(i)}\right)^{(o)} \sim \frac{e^{-\sqrt{p_L}X}}{\varepsilon_0\sqrt{p_L}} \qquad [3\text{-}207]$$

Therefore, matching between eqns [3-203] and [3-207] can be obtained by applying the conversion factor $1/\varepsilon_0$ to eqn [3-203].

3.5.5.2. Matching without Exact Solution

The outer expansion for H can be expressed as:

$$H^{(o)} = H_0 + \varepsilon_0 H_1 + \varepsilon_0^2 H_2 + \cdots \qquad [3\text{-}208]$$

Substitution of eqn [3-208] in the outer equation for H gives a first-order approximation when $\varepsilon_0 \to 0$:

$$H_{0_{xx}} = H_{0_\tau} \qquad [3\text{-}209]$$

The boundary conditions for H_0 are:

$$H_0 = 1 \text{ at } X = 0 \qquad [3\text{-}210a]$$

$$H_0 = 0 \text{ at } X = 1 \qquad [3\text{-}210b]$$

The initial conditions for H_0 are:

$$H_0 = 0 \text{ when } \tau = 0 \qquad [3\text{-}210c]$$

$$H_{0\tau} = 0 \text{ when } \tau = 0 \qquad [3\text{-}210d]$$

The condition [3-210d] will be dropped because as $\varepsilon_0 \to 0$, no freedom in the definition of $H_0^{(o)}$ arises. The solution of eqn [3-209] becomes identical to that of eqn [3-151]. Outer expansion for V can be expressed as:

$$V^{(o)} = V_0 + \varepsilon_0 V_1 + \varepsilon_0^2 V_2 + \cdots \qquad [3\text{-}211]$$

Substitution of eqn [3-211] in the outer equation for V gives the following first-order approximation when $\varepsilon_0 \to 0$:

$$V_{0_{xx}} = V_{0_{\tau}} \qquad [3\text{-}212]$$

The solution to eqn [3-212] then becomes identical to that of eqn [3-158]. $H^{(o)}$ is invalid near $\tau = 0$ because the condition [3-210d] was dropped. The inner expansion for H can be expressed as:

$$H^{(i)} = H_0 + \varepsilon_0 H_1 + \varepsilon_0^2 H_2 + \cdots \qquad [3\text{-}213]$$

Substitution of eqn [3-213] in the inner equation for H gives a first-order approximation when $\varepsilon_0 \to 0$:

$$H_{0_{\tilde{X}\tilde{X}}} = H_{0_{\tilde{\tau}}} + H_{0_{\tilde{\tau}\tilde{\tau}}} \qquad [3\text{-}214]$$

The boundary conditions for H_0 are:

$$H_0 = 1 \text{ at } \tilde{X} = 0 \qquad [3\text{-}215a]$$

$$H_0 = 0 \text{ at } \tilde{X} = \frac{1}{\sqrt{\varepsilon_0}} \qquad [3\text{-}215b]$$

The initial conditions for H_0 are:

$$H_0 = 0 \text{ when } \tilde{\tau} = 0 \qquad [3\text{-}215c]$$

$$H_{0_{\tilde{\tau}}} = 0 \text{ when } \tilde{\tau} = 0 \qquad [3\text{-}215d]$$

The condition [3-215b] will be dropped because as $\varepsilon_0 \to 0$, $\tilde{X} \to \infty$. The solution is identical to that of eqn [3-179]. The inner expansion for V is:

$$\tilde{V}^{(i)} = \tilde{V}_0 + \varepsilon_0 \tilde{V}_1 + \varepsilon_0^2 \tilde{V}_2 + \cdots \qquad [3\text{-}216]$$

Substitution of eqn [3-211] into the inner equation for V gives the following first-order approximation when $\varepsilon_0 \to 0$:

$$\tilde{V}_{0_{\tilde{X}\tilde{X}}} = \tilde{V}_{0_{\tilde{\tau}}} + \tilde{V}_{0_{\tilde{\tau}\tilde{\tau}}} \qquad [3\text{-}217]$$

The resulting solution is identical to that of eqn [3-185]. The matching results are same the as those obtained using the Laplace transform method

3.5.5.3. Implications of Matching

First, in the outer expansion, as $\varepsilon_0 \to 0$, the $H_{\tau\tau}$ term and the $V_{\tau\tau}$ term were seen to become lost. As a result, the conditions of $H_\tau = 0$ and $V_\tau = 0$ at $\tau = 0$ could be safely dropped. Therefore $H^{(o)}$ and $V^{(o)}$ do not have the freedom to keep these conditions in the definition of the outer problem. Second, in the inner expansion, as $\varepsilon_0 \to 0$, $\tilde{X} = 1/\sqrt{\varepsilon_0} \to \infty$. As a result, the conditions $H = 0$ and $\tilde{V}_{\tilde{X}} = 0$ at $\tilde{X} = \dfrac{1}{\sqrt{\varepsilon_0}}$ also became negligible. Therefore the quantities $H^{(i)}$ and $V^{(i)}$ do not have the freedom to keep these conditions within the definition of the inner problem. The outer expansion in the inner coordinate and the inner expansion in the outer coordinate were same. Therefore, the solutions should be functionally identical in the overlap zone.

3.5.6. Composite Expansion

The inner and outer expansions complement each other. One is valid in the region where the other fails. Using this complementary feature, a single uniformly valid expansion can be constructed. A composite expansion was constructed using an additive composition. This composition is the sum of the inner and outer expansions corrected by subtracting the overlapping part. Thus, the overlapping part will not be counted twice. The overlapping part can be calculated as the inner expansion of the outer expansion, or vice versa. The composite expansion for H can be expressed by:

$$\underbrace{\left(\overline{H}_c\right)^{(o)}}_{\text{composite}} = \underbrace{\overline{H}^{(o)}}_{\text{outer}} + \underbrace{\left(\overline{H}^{(i)}\right)^{(o)}}_{\text{inner}} - \underbrace{\left(\left(\overline{H}^{(o)}\right)^{(i)}\right)^{(o)}}_{\text{overlap}} \qquad [3\text{-}218]$$

The composite expansion for Laplace transform of H can be obtained using eqns [3-151], [3-179], and [3-198]:

$$\left(\overline{H}_c\right)^{(o)} = \frac{e^{\sqrt{p_L}X} - e^{(2-X)\sqrt{p_L}}}{p_L\left(1 - e^{2\sqrt{p_L}}\right)} + \frac{e^{-\sqrt{\varepsilon_0^2 p_L^2 + \varepsilon_0 p_L}X/\sqrt{\varepsilon_0}}}{p_L} - \frac{e^{-\sqrt{p_L}X}}{p_L} \qquad [3\text{-}219]$$

Instead of getting the inverse Laplace transform, the outer and inner expansions can be solved for H using numerical methods. For the overlapping region, the inverse Laplace transform can be expressed with a complimentary error function. The inverse Laplace transform was found as (see tables of Erdelyi, 1954):

$$H_{overlap} = \text{erfc}\left[\frac{X}{2\sqrt{\tau}}\right] \qquad [3\text{-}220]$$

3.5.7. Results of Template Problem

In the outer zone, the composite solution was compared with the outer solution. Figure 3.6 is a contour plot of the difference in H between the solutions of composite expansion, and outer expansion in outer coordinates, when $\varepsilon_0 = 0.01$. This difference can be considered as an error which has an order of ε_0 over the whole region except the inner and the overlap region. The inner region can be predicted using compound scaling factors[8]. From this compound scaling, the maximum X and τ in the inner region are $X = \sqrt{\varepsilon_0}$ and $\tau = \varepsilon_0$. It can be seen from Figure 3.7 that $X = 0.1$ and $\tau = 0.01$ define the inner region. The overlap region can be roughly defined as the zone having an order-of-error larger than 0.01.

Figure 3.8 shows the spatial variation in H using the outer and composite expansions, at various times. The solutions associated with these two expansions for $\tau = 0.01$ were compared to show the differences in H in the inner zone. Similarly, the solutions for $\tau = 0.05$ were compared for the intermediate zone, and those for $\tau = 0.2$ were compared for the outer zone. Large differences are evident in the inner and intermediate zones. However, these differences are not as large as those found in the inner zone. In the outer zone, it is evident that small differences are evenly distributed across the whole region.

Figure 3.9 presents the temporal variation in H using the outer and composite expansions, at various locations. The largest differences between the two expansion solutions are evident for $X = 0.1$ and at very small times. As X increases, the differences decrease.

[8] i.e. factors which represent the second of two scale adjustments, so that a scaled quantity is scaled again.

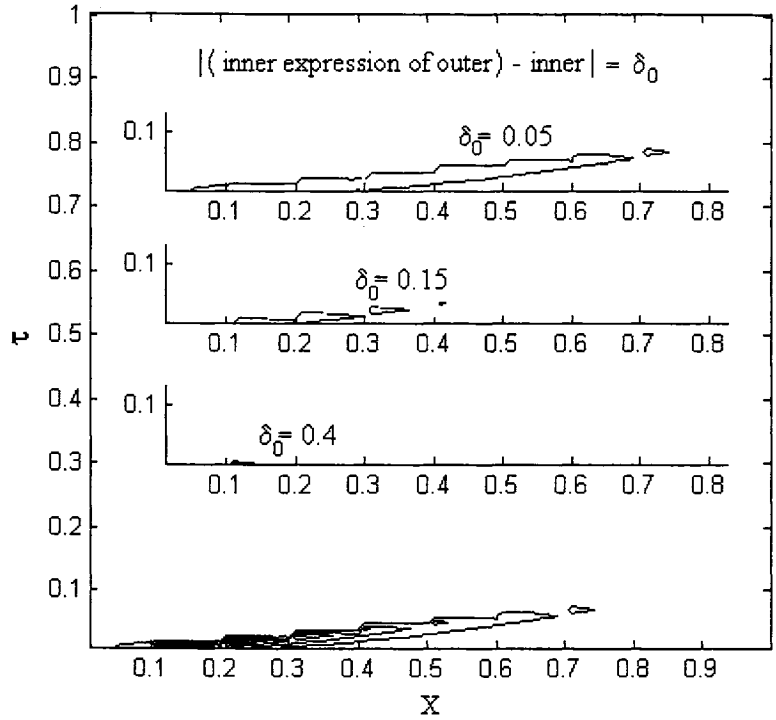

Figure 3.6 Contour plot for difference inf H between composite solution and outer in outer coordinate when $\varepsilon_0 = 0.01$.

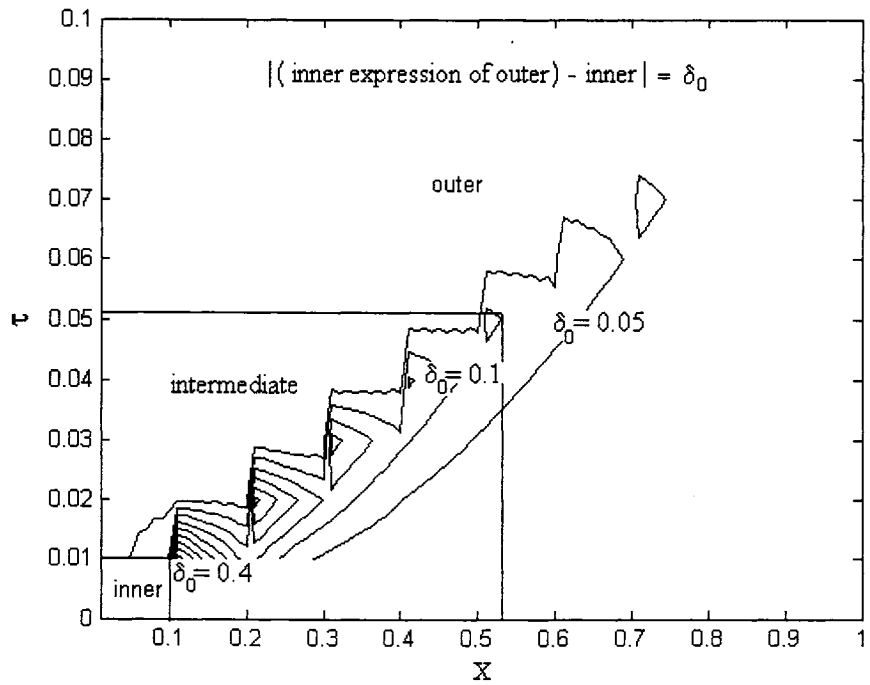

Figure 3.7 Inner, intermediate and outer division from the difference in H using outer expansion and composite expansion.

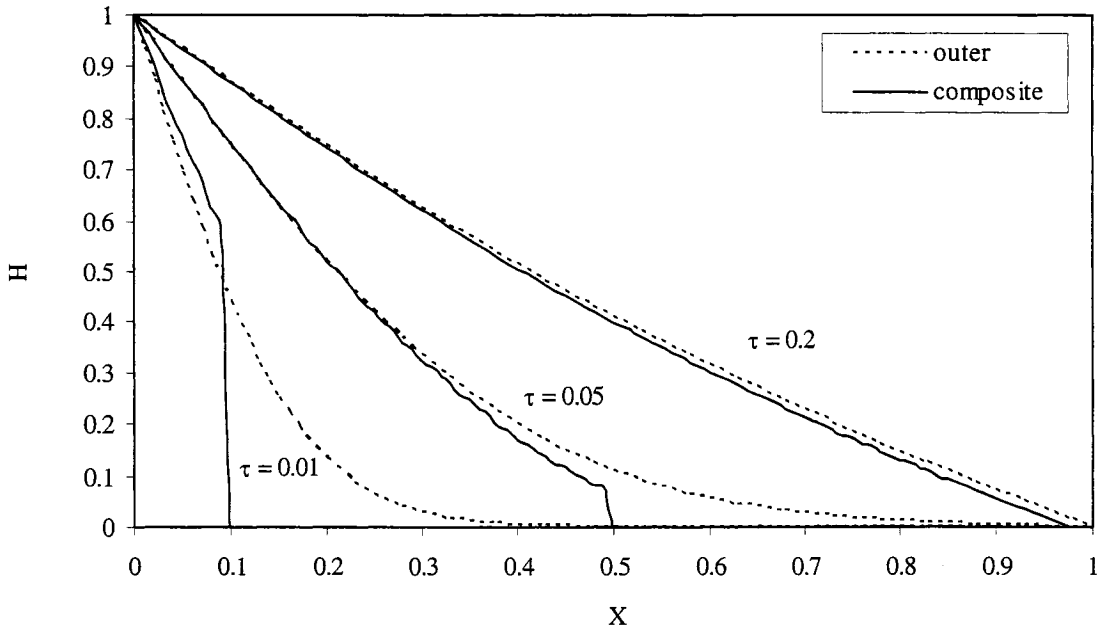

Figure 3.8 Spatial variation in H at various τ's.

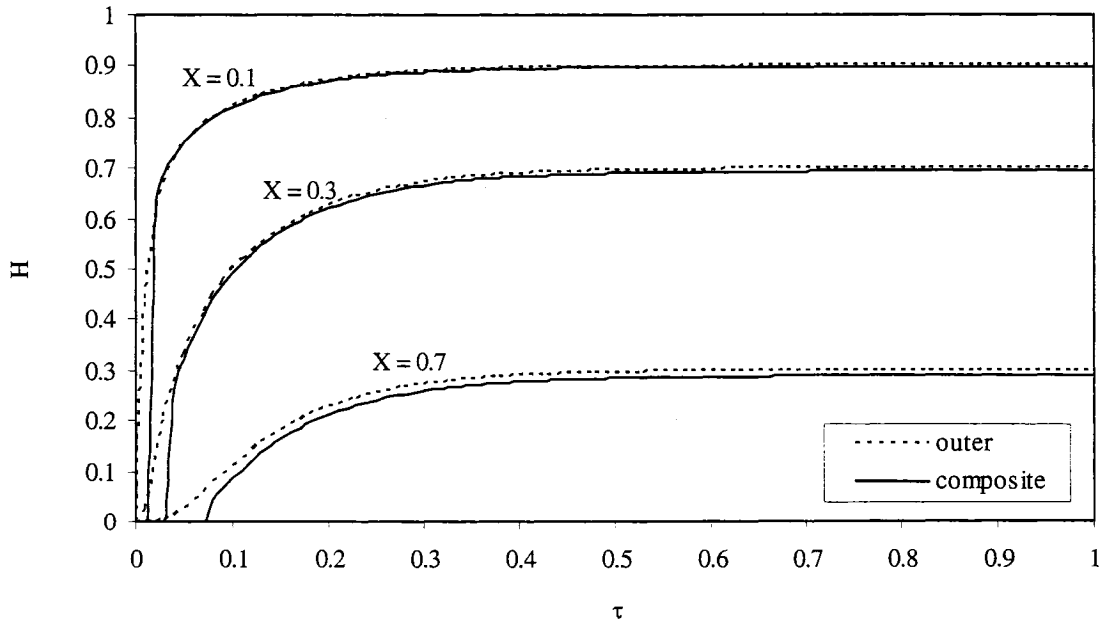

Figure 3.9 Temporal variation in H at various locations.

The composite expansion for V can be expressed by:

$$\underbrace{\left(\overline{V}_c\right)^{(o)}}_{\text{composite}} = \underbrace{\overline{V}^{(o)}}_{\text{outer}} + \underbrace{\left(\overline{V}^{(i)}\right)^{(o)}}_{\text{inner}} - \underbrace{\left(\left(\overline{V}^{(o)}\right)^{(i)}\right)^{(o)}}_{\text{overlap}} \qquad [3\text{-}221]$$

Substitution of the inner, overlap, and outer solutions gives:

$$\left(\overline{V}_c\right)^{(o)} = -\frac{e^{\sqrt{p_L}X} + e^{(2-X)\sqrt{p_L}}}{\sqrt{p_L}\left(1-e^{2\sqrt{p_L}}\right)} + \frac{e^{-\sqrt{\varepsilon_0^2 p_L^2 + \varepsilon_0 p_L}X/\sqrt{\varepsilon_0}}}{\sqrt{p_L}} - \frac{e^{-\sqrt{p_L}X}}{\sqrt{p_L}} \qquad [3\text{-}222]$$

Instead of obtaining the inverse Laplace transform, the inner and outer expansions were solved for V using numerical methods with the stated boundary conditions. For the overlapping region, the inverse Laplace transform was found as (see tables of Erdelyi 1954):

$$V_{overlap} = \frac{e^{-\frac{X^2}{4\tau}}}{\sqrt{\pi}\sqrt{\tau}} \qquad [3\text{-}223]$$

Figure 3.10 is a contour plot of the differences in V between the solutions arising from the composite expansion and outer-expansion solutions, in the outer zone, and when $\varepsilon_0 = 0.01$. Large differences are evident in the inner and the overlap zones. In the outer zone, the error is small and distributed in a relatively uniform manner.

Figure 3.11 shows the division of the inner, outer, and overlap zones for V. The large difference along $\tau = \sqrt{\varepsilon_0}X$ is due to the fact that it falls on the characteristic line of the evolving-wave equation. The properties of evolving-wave can be seen in Figure 3.12 and 3.13.

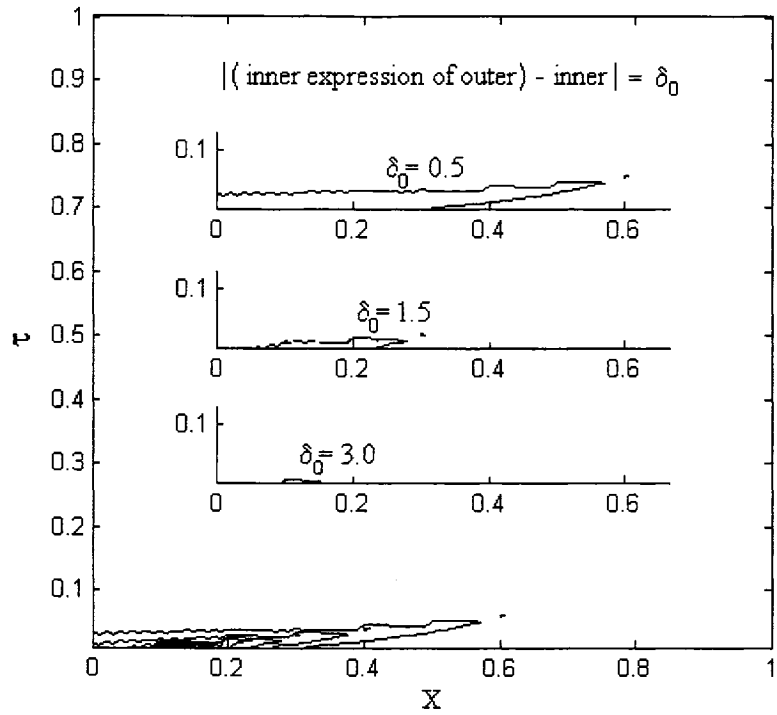

Figure 3.10 Contour plot for difference in V between composite solution and outer in outer coordinate when $\varepsilon_0 = 0.01$.

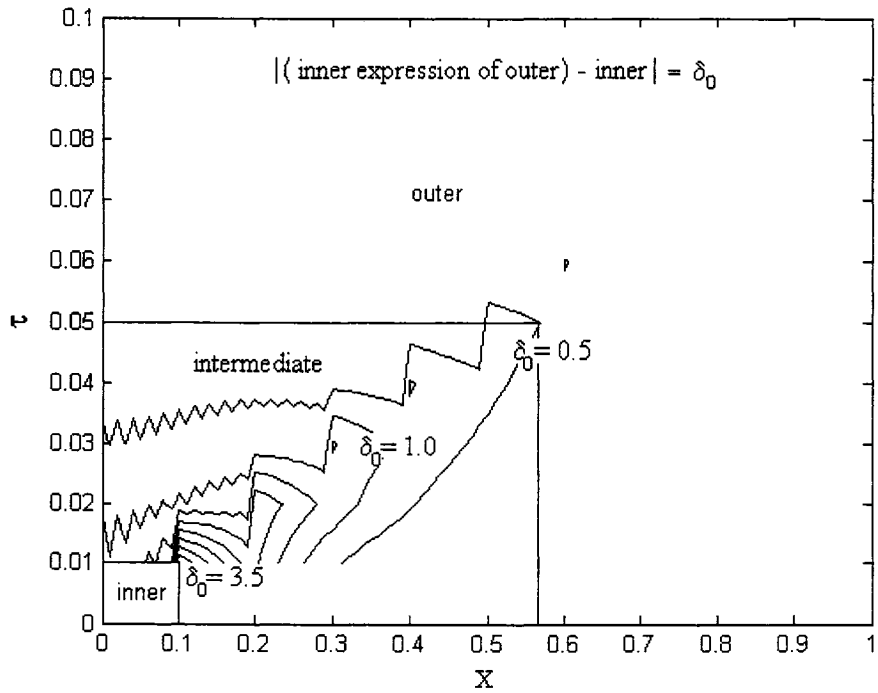

Figure 3.11 Inner, intermediate and outer division from the difference in V using outer expansion and composite expansion.

Figure 3.12 shows the spatial variation in V using the solutions arising from the outer and composite expansions, at various times. They show behaviours for V that are similar to those found for H. The expansion solutions for $\tau = 0.01$ in Figure 3.12 bring out the differences in V in the inner zone. Similarly, the solutions for $\tau = 0.05$ in Figure 3.12 bring out the differences in the intermediate zone, and for $\tau = 0.2$ in the outer zone. Large differences are evident in the inner and intermediate zones again. However, the differences in the intermediate zone are not as large as those found in the inner zone. In the outer zone, small differences are evenly distributed across the whole region.

Figure 3.13 presents the temporal variation in H using the outer and composite expansions, at various locations. The largest differences are evident between the expansion solutions for $X = 0.1$, at very small times. As X increases, the differences decrease. Further, it is evident that the outer expansion overestimates V's, compared to those obtained using the composite expansion up to the temporal position $\tau = \sqrt{\varepsilon_0}X$. Beyond this 'position' the outer expansion underestimates V.

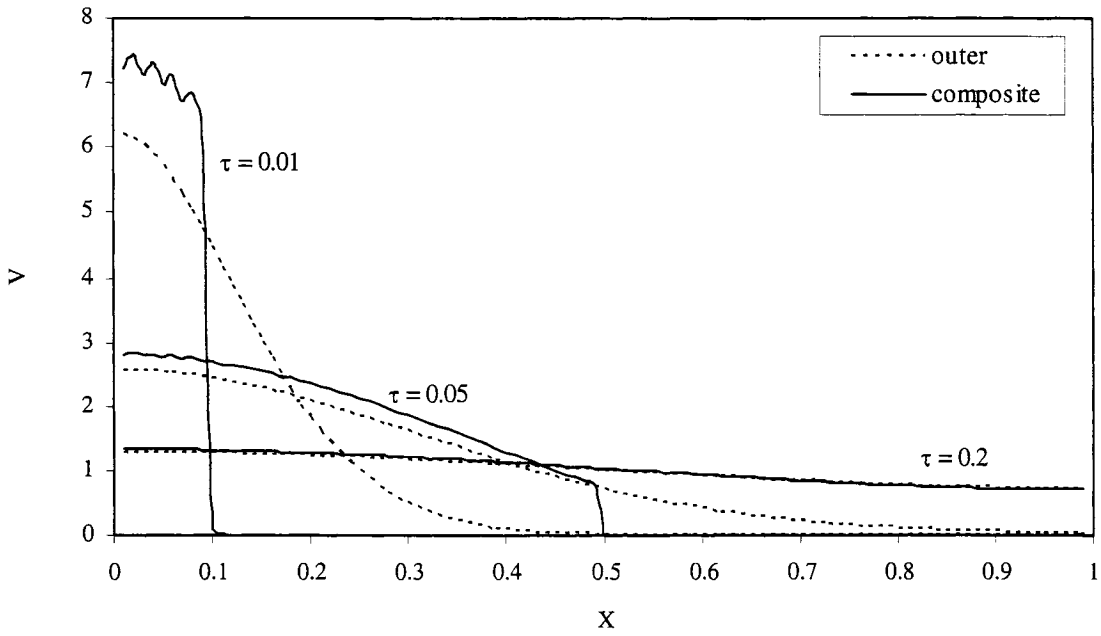

Figure 3.12 Spatial variation of V at various τ's.

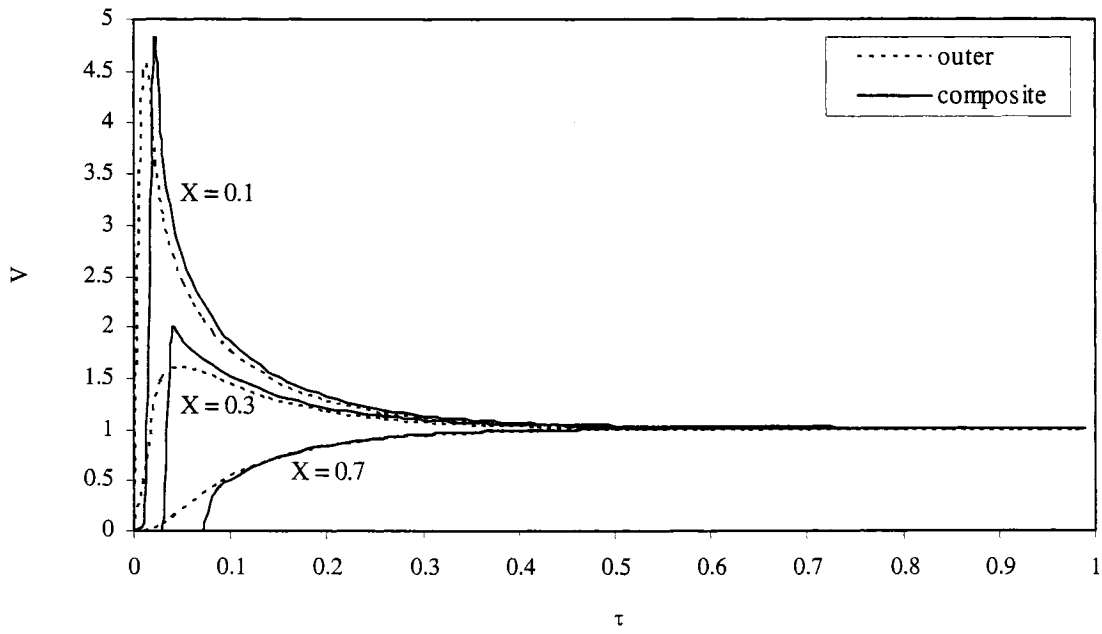

Figure 3.13 Temporal variation of V at various locations.

3.5.8. Evolving Wave Equation

In the original problem, the boundary and initial conditions were clearly defined for H. However, these conditions were not well defined for V. These conditions were determined by using matched asymptotic methods. In this section, the validity of these conditions is considered by comparing analytical solutions to numerical solutions. The evolving wave equation for V can be expressed as:

$$V_{XX} = V_{\tau} + V_{\tau\tau} \qquad [3\text{-}224]$$

The boundary conditions for V are:

$$V_X = -\delta(\tau) \text{ at } X = 0 \qquad [3\text{-}225a]$$

$$V_X = 0 \text{ at } X = 1 \qquad [3\text{-}225b]$$

The initial conditions for V are:

$$V = 0 \text{ when } \tau = 0 \qquad [3\text{-}225c]$$

$$V_{\tau} = 0 \text{ when } \tau = 0 \qquad [3\text{-}225d]$$

3.5.8.1. Solution using Laplace Transform

Laplace transforms were used to solve the evolving wave equation. In order to obtain the inverse Laplace transform, a residue theorem (Dettman 1965, Rahman 1992) was applied. Contour integrals were used in the residue theorem. Within these contour integrals, all the integrals other than the residues from the poles became zero. Therefore, the inverse Laplace transform was obtained using the sum of the residues of the two sets of poles. The details of the derivation of the solution are provided in Appendix IV. The solution of V can be expressed as:

$$V(X,\tau) = \left[\left\{\sum_{n=1}^{\infty} 2\cos(n'\pi X)\sin\left(\sqrt{n'^2\pi^2 - \frac{1}{4}}\tau\right)\right\} + 2\sinh\left(\frac{\tau}{2}\right)\right]e^{-\frac{\tau}{2}} \qquad [3\text{-}226]$$

3.5.8.2. Solution using MoC

The boundary conditions for H can be used to obtain boundary values of V without defining boundary conditions for V. The applied boundary conditions were:

$$H = 1 \text{ at } X = 0 \qquad [3\text{-}227a]$$

$$H = 0 \text{ at } X = 1 \qquad [3\text{-}227b]$$

The initial conditions were:

$$H = 0 \text{ when } \tau = 0 \qquad [3\text{-}227c]$$

$$V = 0 \text{ when } \tau = 0 \qquad [3\text{-}227d]$$

The procedure to get H and V is similar to the method used to obtain numerical solutions for the complete model (Appendix III). The dimensionless head H_{P_i} can be expressed as:

$$H_{P_i} = 0.5\left[H_{i-1} + H_{i+1} + (V_{i-1} - V_{i+1}) - \Delta X(V_{i-1} - V_{i+1})\right] \qquad [3\text{-}228]$$

The dimensionless velocity V_{P_i} can be found using the above-calculated H_{P_i} as:

$$V_{P_i} = \left[-H_{P_i} + H_{i-1} - \Delta X V_{i-1}\right] + V_{i-1} \qquad [3\text{-}229]$$

or:

$$V_{P_i} = \left[H_{P_i} - H_{i+1} + \Delta X V_{i+1}\right] + V_{i+1} \qquad [3\text{-}230]$$

The V at the upstream end can be calculated using eqn [3-230] and V at the downstream end can be calculated using eqn [3-229].

3.5.8.3. Stability of Explicit FDM

Various magnitudes and ratios of ΔX and $\Delta\tau$ were used to obtain the FD solutions of the evolving-wave equation. An explicit finite-difference form of eqn [3-224] can be written:

$$\frac{V_{w+1,y} - 2V_{w,y} + V_{w-1,y}}{h_0^2} = \frac{V_{w,y} - V_{w,y-1}}{k_0} + \frac{V_{w,y+1} - 2V_{w,y} + V_{w,y-1}}{k_0^2} \qquad [3\text{-}231]$$

where:

$h_0 = \Delta X$,

$k_0 = \Delta\tau$,

(both dimensionless).

After many trials with various time and space steps, it was found that stable solutions could not be obtained using this finite-difference scheme. The instability of this method can be shown using von Neumann's method. The errors at the points along $\tau = 0$, between $X = 0$ and $N'*h_0$ can be defined as $E(wh) = E_w$. Using the complex exponential form, E_w can be expressed as:

$$E_w = \sum_{n'=0}^{N'} A_{n'} e^{i\beta_{n'}' wh_0}, \qquad w = 0, 1, \ldots, N' \qquad [3\text{-}232]$$

where:

$\beta_{n'}' = n'\pi / N'h_0$,

N' = total number of spatial nodes,

w = number of spatial steps.

The coefficient $A_{n'}$ is a constant and can thus be neglected. In order to present the propagation of the error as time increases, an error function $E_{w,y}$ was investigated. This function can be expressed as:

$$E_{w,y} = e^{i\beta' X} e^{\alpha'\tau} \qquad [3\text{-}234]$$

where α' is a complex constant.

Using $X = ph_0$ and $\tau = yk_0$:

$$E_{w,y} = e^{i\beta' wh_0} \xi_0^{\,y} \qquad [3\text{-}235]$$

where:

$\xi_0 = e^{\alpha' k_0}$,

y = number of time steps.

The error function given by eqn [3-235] shows that the error can be reduced to $e^{i\beta' wh_0}$ when y = 0 and that it will not increase as time increases if:

$$\xi_0 \leq 1 \qquad [3\text{-}236]$$

Because the error function satisfies the same finite-difference equations, $E_{w,y}$ can replace $V_{w,y}$ in eqn [3-231]:

$$r_2^2\left(e^{i\beta'(w+1)h_0}\xi_0^y - 2e^{i\beta' wh_0}\xi_0^y + e^{i\beta'(w-1)h_0}\xi_0^y\right)$$
$$= k_0\left(e^{i\beta' wh_0}\xi_0^y - e^{i\beta' wh_0}\xi_0^{(y-1)}\right) + e^{i\beta' wh_0}\xi^{(y+1)} - 2e^{i\beta' wh_0}\xi_0^y + e^{i\beta' wh_0}\xi_0^{(y-1)} \qquad [3\text{-}237]$$

where $r_2^2 = k_0^2 / h_0^2$.

Division by $e^{i\beta' wh_0}$ gives:

$$r_2^2\left(e^{i\beta' wh_0} - 2 + e^{-i\beta' wh_0}\right) = k\left(1 - \xi_0^{-1}\right) + \xi_0 - 2 + \xi_0^{-1} \qquad [3\text{-}238]$$

Using $e^{i\beta' wh_0} + e^{-i\beta' wh_0} = 2\cos(\beta' h_0)$:

$$-4r_2^2 \sin^2\left(\frac{\beta' h_0}{2}\right) = k\left(1 - \xi_0^{-1}\right) + \xi_0 - 2 + \xi_0^{-1} \qquad [3\text{-}239]$$

Multiplying by ξ_0 gives:

$$\xi_0^2 + A_0^{'}\xi_0 + (1 - k_0) = 0 \qquad [3\text{-}240]$$

where $A_0^{'} = 4r_2^2 \sin^2\left(\frac{\beta' h_0}{2}\right) + k_0 - 2$.

The term ξ_0 can be obtained from eqn [3-240]:

$$\xi_0 = \frac{-A_0^{'} \pm \sqrt{A_0^{'2} - 4(1 - k_0)}}{2} \qquad [3\text{-}241]$$

When $A_0^{'2} + 4k_0 \geq 4$ the roots are real; the values of ξ_1 and ξ_2 that result were presented in Figure 3.14. If $A_0^{'} \geq k_0 - 2$:

$$|\xi_1| = \left| \frac{-A_0' + \sqrt{A_0'^2 - 4(1-k_0)}}{2} \right| \qquad [3\text{-}242]$$

If $|\xi_1| \leq 1$ the solutions are stable. However, ξ_2 induces instability if $|\xi_2| > 1$ where:

$$|\xi_2| = \left| \frac{-A_0' - \sqrt{A_0'^2 - 4(1-k_0)}}{2} \right| \qquad [3\text{-}243]$$

On the other hand, if $A_0' \leq k_0\text{-}2$, it is ξ_1 that induces the instability.

Stability only exists at two points in Figure 3-14; $A_0' = k_0 - 2$ and $A_0' = 2 - k_0$. If $A_0' = k_0 - 2$, the following relationship can be obtained:

$$4r_2^2 \sin^2\left(\frac{\beta' h_0}{2}\right) + k_0 - 2 = k_0 - 2 \qquad [3\text{-}244]$$

The above relationship is only true when n' = 0. This condition can therefore not ensure numeric stability along the whole length, L, of the problem.

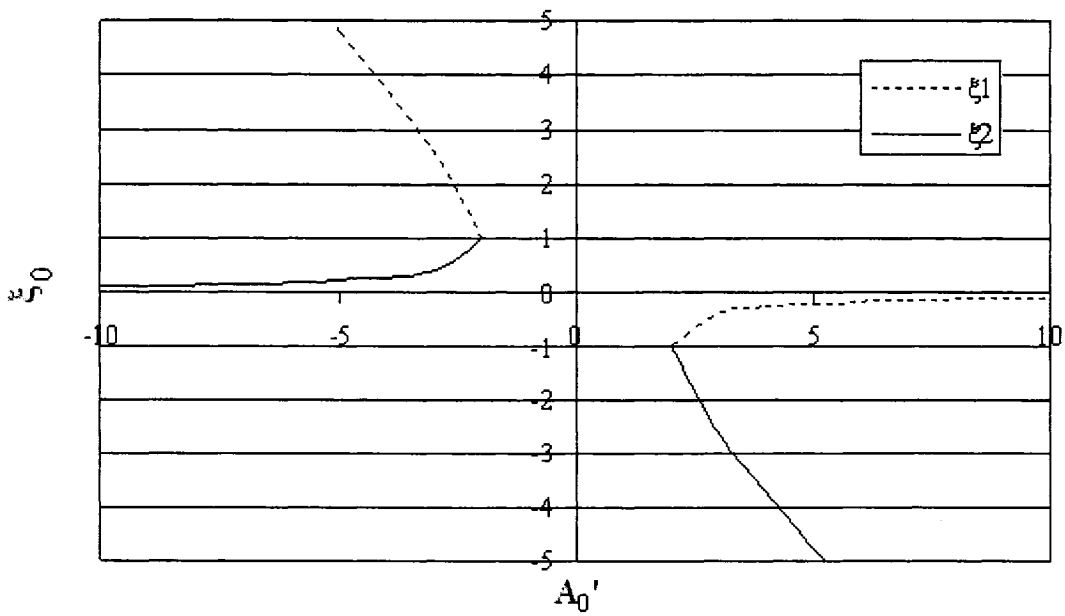

Figure 3.14 Stability using von Neumann's method for $k_0 << 1$.

Similarly, if $A_0' = 2 - k_0$, the relationship can be true only for a specific n', one which cannot ensure the stability along the entire length L.

When $A_0'^2 + 4k_0 < 4$, using $A_0' = 4r_2^2 \sin^2\left(\frac{\beta' h_0}{2}\right) + k_0 - 2$ the following relationship results:

$$\left(k_0 + 2r_2 \sin\left(\frac{\beta' h_0}{2}\right)\right)^2 \left(k_0 - 2r_2 \sin\left(\frac{\beta' h_0}{2}\right)\right)^2 < 0 \qquad [3\text{-}245]$$

Equation [3-245] can never be true because all of the terms in the parentheses are real numbers. Therefore, stability cannot be obtained using an explicit finite-difference method.

3.5.8.4. Comparison of Results

Spatial and temporal variations in V are compared in Figures 3.15 and 3.16, respectively. Figure 3.15 shows a very good match between the solutions obtained using MoC vs the method of Laplace transforms including the values of V at X = 0. It can be seen in Figure 3.16, that the V's approach the equilibrium velocity, at all three locations. Figure 3.17 shows the temporal development of V at the upstream end of the problem. In order to obtain the boundary V's using MoC, it was necessary to obtain the solutions for H and V for the entire time-space continuum of the rest of the problem. The method of Laplace transforms, on the other hand, can be used to calculate the values of V at the upstream end without the need to obtain the solution to the rest of the problem *a priori*. The requisite values of V can be readily obtained using eqn [3-226] with X = 0:

$$V(0,\tau) = \left[\left\{\sum_{n'=1}^{\infty} 2\sin\left(\sqrt{n'^2\pi^2 - \frac{1}{4}}\tau\right)\right\} + 2\sinh\left(\frac{\tau}{2}\right)\right] e^{-\frac{\tau}{2}} \qquad [3\text{-}231]$$

Similarly, if we substitute X = 1 into eqn [3-226], the expression of V at the downstream end becomes:

$$V(1,\tau)=\left[\left\{\sum_{n'=1}^{\infty}2\cos(n'\pi)\sin\left(\sqrt{n'^2\pi^2-\frac{1}{4}}\tau\right)\right\}+2\sinh\left(\frac{\tau}{2}\right)\right]e^{-\frac{\tau}{2}} \qquad [3\text{-}232]$$

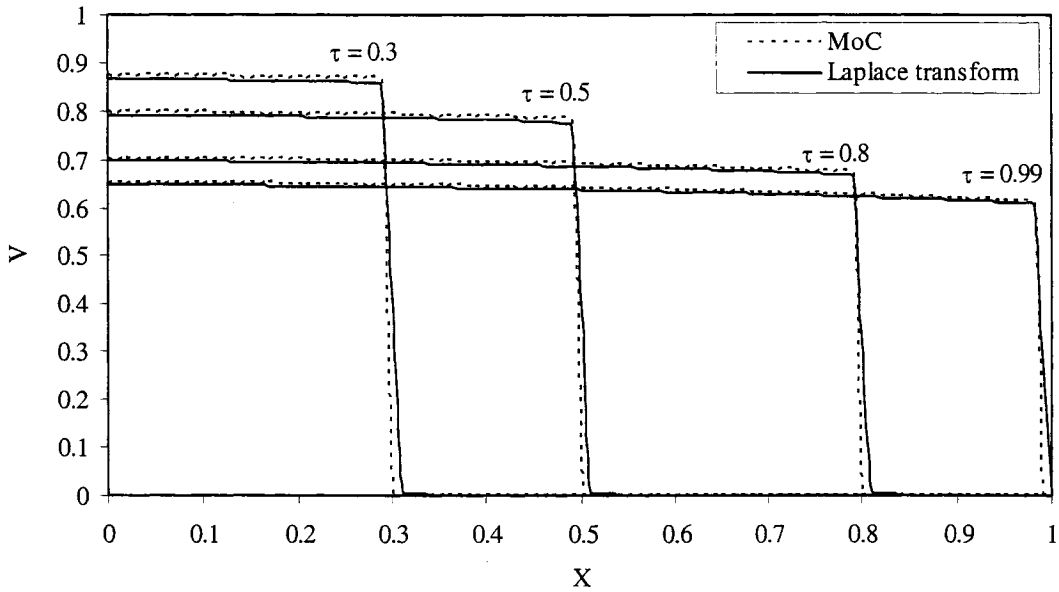

Figure 3.15 Spatial variation of V for various times.

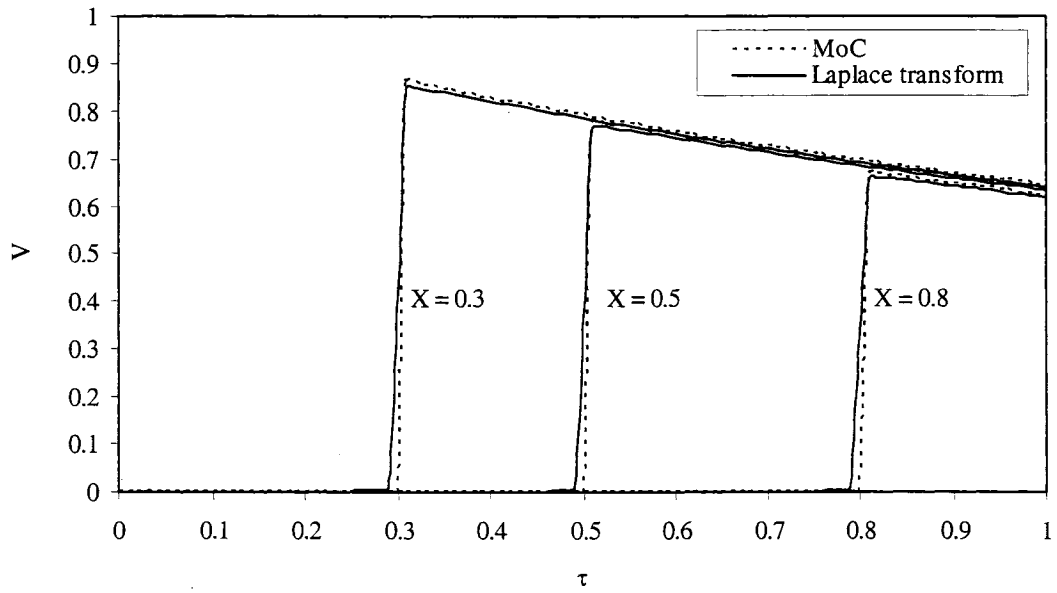

Figure 3.16 Temporal variation of V at various locations.

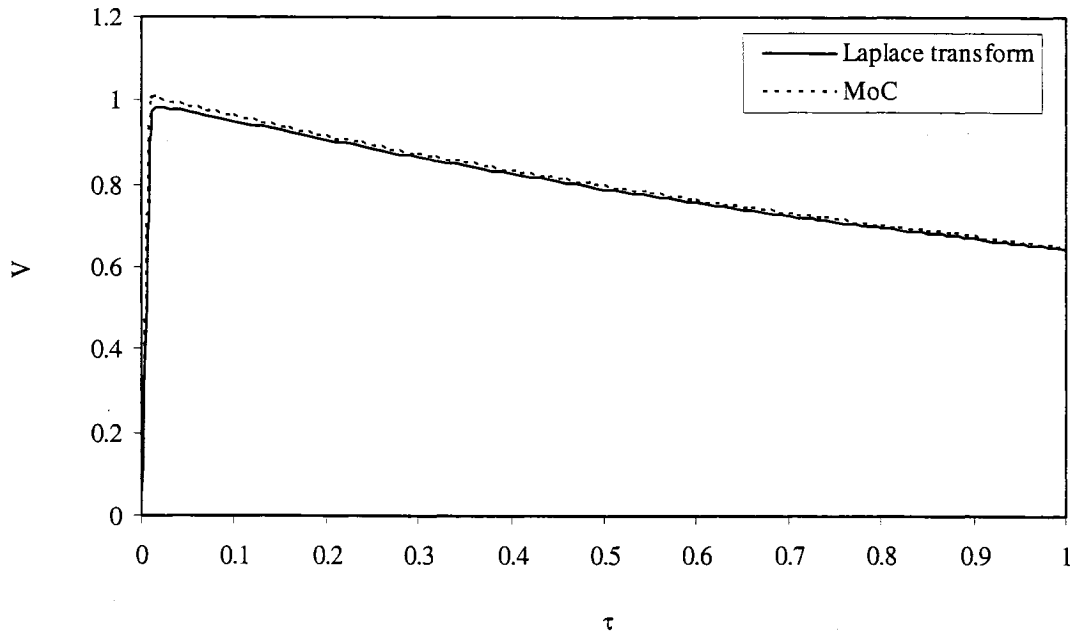

Figure 3.17 Velocity development at X = 0.

4. Application and Results

4.1. Solutions of Models

An explicit finite-difference method was applied for the solutions of each model. The results were compared for each regime, i.e. laminar, PDT, and FDT flow regime. In order to show the accuracy of an explicit finite difference method using backward difference in time and central difference in space under given boundary and initial conditions, the results were compared with those obtained using analytical solution for laminar case and also compared with those obtained using the Lax-Wendroff centered half-mesh scheme and the method of characteristics.

4.1.1. Groundwater Flow Equation

(i) Explicit FDM Solution

The general groundwater flow equation was:

$$H_\tau = \frac{C_1}{C_3} H_{XX} \qquad [3\text{-}67]$$

An explicit finite-difference form, using a backward difference in time, is:

$$-\frac{C_1}{C_3}\frac{H_{i+1}^{k-1} - 2H_i^{k-1} + H_{i-1}^{k-1}}{\Delta X^2} + \frac{H_i^k - H_i^{k-1}}{\Delta\tau} = 0 \qquad [4\text{-}1]$$

where subscript, i, denotes a space step and superscript, k, denotes a time step.

By re-arrangement:

$$H_i^k = \frac{C_1}{C_3}\Delta\tau\left(\frac{H_{i+1}^{k-1} - 2H_i^{k-1} + H_{i-1}^{k-1}}{\Delta X^2}\right) + H_i^{k-1} \qquad [4\text{-}2]$$

The dimensionless velocity, V_i^k, can readily be obtained from Darcy's Law. An explicit finite-difference expression, using a central difference scheme in space, is:

$$V_i^k = -\frac{C_1}{C_3}\frac{H_{i+1}^k - H_{i-1}^k}{2\Delta X} \qquad [4\text{-}3]$$

(ii) Analytical Solution

Equation [3-67] can be re-written as:

$$H_\tau = JH_{XX} \qquad [4\text{-}4]$$

where $J = \frac{C_1}{C_3}$.

The analytical solution can be obtained by separating the problem into a problem of steady head with the stated boundary conditions and a problem of unsteady diffusion with fixed zero boundary head. The unsteady diffusion problem with fixed boundary head can be solved using separation of variables. The analytical solution of eqn [4-4] is:

$$H = 1 - X - \frac{2}{\pi}\sum_{n=1}^{\infty} e^{-Jn^2\pi^2\tau}\frac{\sin(n\pi X)}{n} = 0 \qquad [4\text{-}5]$$

The step-by step derivation of the solution, [4-5], was provided in Appendix I.

4.1.2. Model of Darcy's Law with Complete Continuity Equation

This model incorporating viscous effects into the complete statement of the continuity equation was expressed as:

$$H_\tau = \frac{C_5}{C_6}\frac{C_1}{C_3}(H_X)^2 + \frac{C_1}{C_3}H_{XX} + \frac{C_7}{C_6}\frac{C_1}{C_3}H_X \qquad [3\text{-}68]$$

An explicit finite-difference form, using a backward difference in time and a central difference in space, can be expressed as:

$$\frac{H_i^k - H_i^{k-1}}{\Delta\tau} = \frac{C_5}{C_6}\frac{C_1}{C_3}\left(\frac{H_{i+1}^{k-1} - H_{i-1}^{k-1}}{2\Delta X}\right)^2 + \frac{C_1}{C_3}\frac{H_{i+1}^{k-1} - 2H_i^{k-1} + H_{i-1}^{k-1}}{\Delta X^2}$$

$$+\frac{C_7}{C_6}\frac{C_1}{C_3}\left(\frac{H_{i+1}^{k-1}-H_{i-1}^{k-1}}{2\Delta X}\right)=0 \qquad [4\text{-}6]$$

By re-arrangement:

$$H_i^k=\Delta\tau\frac{C_5}{C_6}\frac{C_1}{C_3}\left(\frac{H_{i+1}^{k-1}-H_{i-1}^{k-1}}{2\Delta X}\right)^2+\Delta\tau\frac{C_1}{C_3}\frac{H_{i+1}^{k-1}-2H_i^{k-1}+H_{i-1}^{k-1}}{\Delta X^2}$$

$$+\Delta\tau\frac{C_7}{C_6}\frac{C_1}{C_3}\left(\frac{H_{i+1}^{k-1}-H_{i-1}^{k-1}}{2\Delta X}\right)+H_i^{k-1} \qquad [4\text{-}7]$$

Because Darcy's Law is used as a momentum equation, the dimensionless velocity, V_i^k, can be obtained using eqn [4-3].

4.1.3. Ergun-type Model

Ergun-type model was expressed as:

$$H_\tau-\frac{C_1}{\sqrt{C_3{}^2-4C_1C_4H_X}}H_{XX}+\frac{C_5}{C_6}\frac{-C_3+\sqrt{C_3{}^2-4C_1C_4H_X}}{2C_4}H_X$$

$$+\frac{C_7}{C_6}\frac{-C_3+\sqrt{C_3{}^2-4C_1C_4H_X}}{2C_4}=0 \qquad [3\text{-}77]$$

An explicit finite-difference form of eqn [3-77], using a backward difference in time and a central difference in space, is:

$$\frac{H_i^k-H_i^{k-1}}{\Delta\tau}-\frac{C_1}{\sqrt{C_3{}^2-4C_1C_4\dfrac{H_{i+1}^{k-1}-H_{i-1}^{k-1}}{2\Delta X}}}\frac{H_{i+1}^{k-1}-2H_i^{k-1}+H_{i-1}^{k-1}}{\Delta X^2}$$

$$+\frac{C_5}{C_6}\frac{-C_3+\sqrt{C_3{}^2-4C_1C_4\dfrac{H_{i+1}^{k-1}-H_{i-1}^{k-1}}{2\Delta X}}}{2C_4}\frac{H_{i+1}^{k-1}-H_{i-1}^{k-1}}{2\Delta X}$$

$$+\frac{C_7}{C_6}\frac{-C_3+\sqrt{C_3^{\,2}-4C_1C_4\dfrac{H_{i+1}^{k-1}-H_{i-1}^{k-1}}{2\Delta X}}}{2C_4}=0 \qquad [4\text{-}8]$$

By re-arrangement:

$$H_i^k=\frac{C_1}{\sqrt{C_3^{\,2}-4C_1C_4\dfrac{H_{i+1}^{k-1}-H_{i-1}^{k-1}}{2\Delta X}}}\Delta\tau\frac{H_{i+1}^{k-1}-2H_i^{k-1}+H_{i-1}^{k-1}}{\Delta X^2}$$

$$-\frac{C_5}{C_6}\Delta\tau\frac{-C_3+\sqrt{C_3^{\,2}-4C_1C_4\dfrac{H_{i+1}^{k-1}-H_{i-1}^{k-1}}{2\Delta X}}}{2C_4}\frac{H_{i+1}^{k-1}-H_{i-1}^{k-1}}{2\Delta X}$$

$$-\frac{C_7}{C_6}\Delta\tau\frac{-C_3+\sqrt{C_3^{\,2}-4C_1C_4\dfrac{H_{i+1}^{k-1}-H_{i-1}^{k-1}}{2\Delta X}}}{2C_4}+H_i^{k-1} \qquad [4\text{-}9]$$

An explicit finite-difference form of Ergun-type equation, eqn [3-72], using a central-difference scheme for space, is:

$$V_i^k=\frac{-C_3+\sqrt{C_3^{\,2}-4C_1C_4\dfrac{H_{i+1}^{k}-H_{i-1}^{k}}{2\Delta X}}}{2C_4} \qquad [4\text{-}10]$$

4.1.4. Model which retains Local Acceleration Term

For this model, the momentum and continuity equations practically cannot be easily combined into one equation associated with H or V. However, two equations can be separately solved. The momentum equation which has a time derivative of V can be used to obtain V and the continuity equation which has a time derivative of H can be used to calculate H. Even though these two equations were not solved simultaneously, the values of H and V obtained from each equation can interact to update V and H of next time step. The momentum equation was expressed as:

$$H_x=-\frac{C_3}{C_1}V-\frac{C_4}{C_1}V^2-\frac{C_6}{C_1}V_\tau \qquad [3\text{-}78]$$

An explicit finite-difference form of eqn [3-78], using a backward difference in time and a central difference in space, is:

$$\frac{H_{i+1}^{k-1} - H_{i-1}^{k-1}}{2\Delta X} = -\frac{C_3}{C_1} V_i^{k-1} - \frac{C_4}{C_1}\left(V_i^{k-1}\right)^2 - \frac{C_6}{C_1}\frac{V_i^{k} - V_i^{k-1}}{\Delta\tau} \qquad [4\text{-}11]$$

By re-arrangement:

$$V_i^{k} = -\frac{C_1}{C_6}\Delta\tau\left(\frac{H_{i+1}^{k-1} - H_{i-1}^{k-1}}{2\Delta X}\right) - \frac{C_3}{C_6}\Delta\tau V_i^{k-1} - \frac{C_4}{C_6}\Delta\tau\left(V_i^{k-1}\right)^2 + V_i^{k-1} \qquad [4\text{-}12]$$

An explicit finite-difference form of the continuity equation, using a backward difference in time and a central difference in space, is:

$$\frac{H_i^{k} - H_i^{k-1}}{\Delta\tau} + \left(\frac{V_{i+1}^{k-1} - V_{i-1}^{k-1}}{2\Delta X}\right) + \frac{C_5}{C_6} V_i^{k-1}\left(\frac{H_{i+1}^{k-1} - H_{i-1}^{k-1}}{2\Delta X}\right) + \frac{C_7}{C_6} V_i^{k-1} = 0 \qquad [4\text{-}13]$$

By re-arrangement:

$$H_i^{k} = -\Delta\tau\left(\frac{V_{i+1}^{k-1} - V_{i-1}^{k-1}}{2\Delta X}\right) - \frac{C_5}{C_6}\Delta\tau V_i^{k-1}\left(\frac{H_{i+1}^{k-1} - H_{i-1}^{k-1}}{2\Delta X}\right) - \frac{C_7}{C_6}\Delta\tau V_i^{k-1} + H_i^{k-1} \qquad [4\text{-}14]$$

Figure 4.1 shows the staggered mesh and the associated nodes used to get H_i^k. In order to get H_i^k, the values of H and V in the previous time step were used.

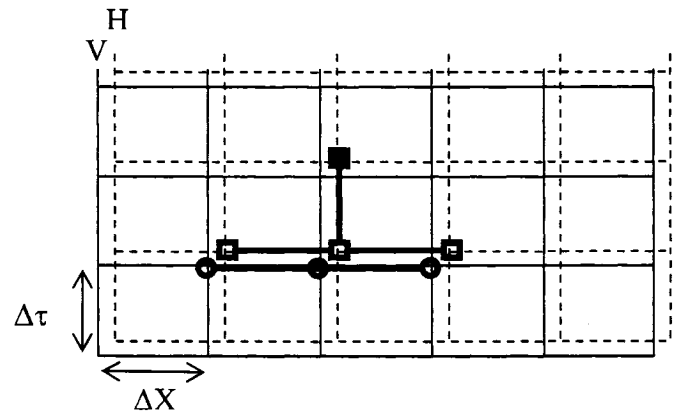

Figure 4.1 Staggered mesh and node stencil for H in explicit finite difference scheme.

At the boundaries, V is not available which is required to calculate H of the nodes beside the boundary at the next time step. This invokes a forward difference for the upstream end and a backward difference for the downstream end. Figure 4.2 shows the staggered mesh for H at the boundaries.

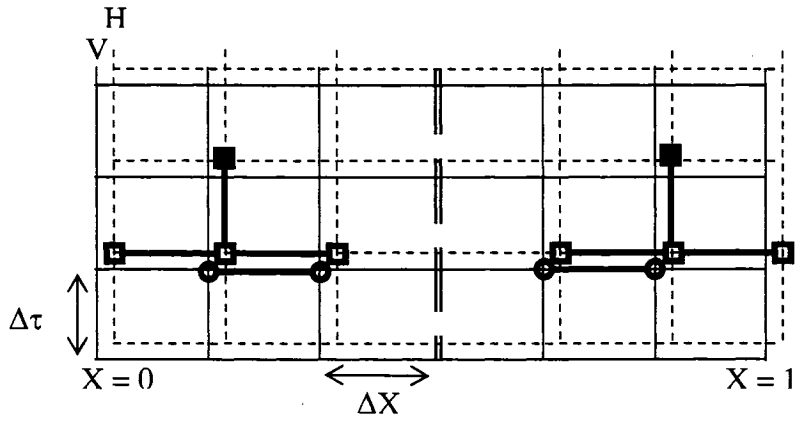

Figure 4.2 Staggered mesh for H at the upstream and downstream boundaries.

4.1.5. Complete Model

(i) Explicit FDM Solution

Explicit finite difference method was used to solve complete statement of the momentum equation and continuity equations. If backward differences in time and space are taken for V, and central differences in space and backward difference in time are taken for H, a finite-difference form of the momentum equation can be stated as:

$$\frac{H_{i+1}^{k-1}-H_{i-1}^{k-1}}{2\Delta X}=-\frac{C_3}{C_1}V_i^{k-1}-\frac{C_4}{C_1}\left(V_i^{k-1}\right)^2-\frac{C_6}{C_1}\frac{V_i^{k}-V_i^{k-1}}{\Delta\tau}-\frac{C_2}{C_1}V_i^{k-1}\frac{V_{i+1}^{k-1}-V_{i-1}^{k-1}}{2\Delta X} \quad [4\text{-}15]$$

By re-arrangement:

$$V_i^{k}=-\frac{C_1}{C_6}\Delta\tau\left(\frac{H_{i+1}^{k-1}-H_{i-1}^{k-1}}{2\Delta X}\right)-\frac{C_3}{C_6}\Delta\tau V_i^{k-1}-\frac{C_4}{C_6}\Delta\tau\left(V_i^{k-1}\right)^2$$
$$-\frac{C_2}{C_6}\Delta\tau V_i^{k-1}\left(\frac{V_{i+1}^{k-1}-V_{i-1}^{k-1}}{2\Delta X}\right)+V_i^{k-1} \quad [4\text{-}16]$$

Figure 4.3 shows the staggered mesh and the nodal definitions used to get V_i^k :

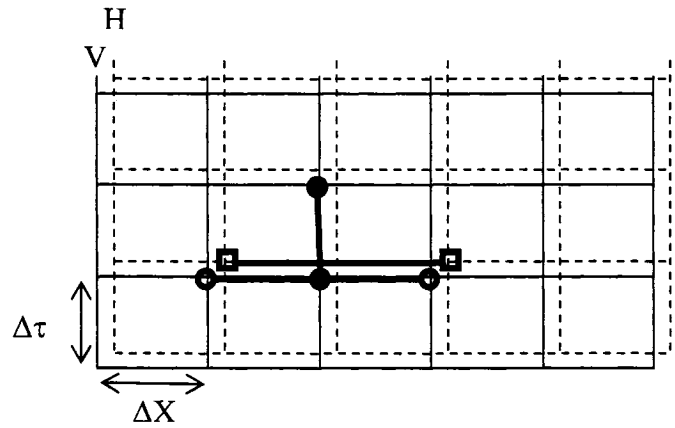

Figure 4.3 Mesh grid for V in explicit finite difference scheme .

H_i^k can be calculated using eqn [4-14] which was used for the model retaining local acceleration term. Table 4.1 summarizes the finite-difference strategies to be involved.

Table 4.1 Finite difference schemes of V and H

	upstream		interior nodes		downstream	
	time (τ)	space (X)	time (τ)	space (X)	time (τ)	space (X)
V	backward difference	forward difference	backward difference	central difference	backward difference	backward difference
H	backward difference	central difference	backward difference	central difference	backward difference	central difference

(ii) FDM Solution using Lax-Wendroff Scheme

The FDM solution of the continuity and momentum equation can be obtained using Lax-Wendroff scheme:

$$V_i^{k+1} = V_i^k - \frac{C_1}{C_6}\Delta\tau\frac{\left(H_{i+\frac{1}{2}}^{k+\frac{1}{2}} - H_{i-\frac{1}{2}}^{k+\frac{1}{2}}\right)}{\Delta X} - \frac{C_2}{C_6}\Delta\tau\frac{\left(\frac{V_{i+\frac{1}{2}}^{k+\frac{1}{2}} + V_{i-\frac{1}{2}}^{k+\frac{1}{2}}}{2}\right)\left(V_{i+\frac{1}{2}}^{k+\frac{1}{2}} - V_{i-\frac{1}{2}}^{k+\frac{1}{2}}\right)}{\Delta X}$$

$$-\frac{C_3}{C_6}\Delta\tau\frac{\left(V_{i+\frac{1}{2}}^{k+\frac{1}{2}}+V_{i-\frac{1}{2}}^{k+\frac{1}{2}}\right)}{2}-\frac{C_4}{C_6}\Delta\tau\frac{\left(V_{i+\frac{1}{2}}^{k+\frac{1}{2}}+V_{i-\frac{1}{2}}^{k+\frac{1}{2}}\right)^2}{4} \qquad [4\text{-}17]$$

$$H_i^{k+1}=H_i^k-\frac{C_5}{C_6}\Delta\tau\frac{\left(V_{i+\frac{1}{2}}^{k+\frac{1}{2}}+V_{i-\frac{1}{2}}^{k+\frac{1}{2}}\right)}{2}\frac{\left(H_{i+\frac{1}{2}}^{k+\frac{1}{2}}-H_{i-\frac{1}{2}}^{k+\frac{1}{2}}\right)}{\Delta X}-\Delta\tau\frac{\left(V_{i+\frac{1}{2}}^{k+\frac{1}{2}}-V_{i-\frac{1}{2}}^{k+\frac{1}{2}}\right)}{\Delta X}$$

$$-\frac{C_7}{C_6}\Delta\tau\frac{\left(V_{i+\frac{1}{2}}^{k+\frac{1}{2}}+V_{i-\frac{1}{2}}^{k+\frac{1}{2}}\right)}{2} \qquad [4\text{-}18]$$

Step-by-step derivation of the solutions was provided in Appendix II.

(iii) Method of Characteristics

Using method of characteristics, H_{Pi} can be expressed as:

$$H_{P_i}=0.5\left[H_{i-1}+H_{i+1}+\sqrt{\frac{C_6}{C_1}}(V_{i-1}-V_{i+1})-\frac{C_3}{C_1}\Delta X(V_{i-1}-V_{i+1})\right.$$

$$\left.-\frac{C_7}{\sqrt{C_1C_6}}\Delta X(V_{i-1}+V_{i+1})-\frac{C_4}{C_1}\Delta X\left(V_{i-1}|V_{i-1}|-V_{i+1}|V_{i+1}|\right)\right] \qquad [4\text{-}19]$$

After obtaining H_{Pi}, V_{Pi} can be calculated using:

$$V_{P_i}=\sqrt{\frac{C_1}{C_6}}\left[-H_{P_i}+H_{i-1}-\left(\frac{C_3}{C_1}+\frac{C_7}{\sqrt{C_1C_6}}\right)\Delta XV_{i-1}-\frac{C_4}{C_1}\Delta XV_{i-1}|V_{i-1}|\right]+V_{i-1} \qquad [4\text{-}20]$$

or

$$V_{P_i}=\sqrt{\frac{C_1}{C_6}}\left[H_{P_i}-H_{i+1}+\left(-\frac{C_3}{C_1}+\frac{C_7}{\sqrt{C_1C_6}}\right)\Delta XV_{i+1}-\frac{C_4}{C_1}\Delta XV_{i+1}|V_{i+1}|\right]+V_{i+1} \qquad [4\text{-}21]$$

Step-by-step derivation of the solutions was provided in Appendix III.

4.1.6. Boundary Conditions

Figure 4.4 shows boundary conditions for the numerical simulations of a horizontal case. Even though the sloped pipe ($\theta \neq 0$) can represent elevation head effect, this effect is neglected in the model comparisons because the equation can be much more simplified by neglecting elevation-head term and it was found that the elevation head term was negligible in most cases based on the order-of-magnitude study. The effects of elevation head can still be of interest and will be investigated using the regular perturbation methods.

Dirichlet conditions are used by applying various hydraulic gradients. From Figure 4.4, a hydraulic gradient is defined by $(h_a-h_b)/L$. For any given hydraulic gradient, if h_b and L are known, h_a can be obtained and used as a fixed-head boundary. Table 4.2 shows dimensional and dimensionless applied boundary conditions. Dimensionless boundary values for L and H_a are not changing but the magnitudes of dimensionless groups will be changed.

Table 4.2 Boundary conditions for horizontal pipe

Hydraulic Gradient, $i = (h_a-h_b)/L$	Total length (L) [m]	h_a [m]	Dimensionless total length [dimensionless]	H_a [dimensionless]
0.1	10	1	1	1
10	10	100	1	1
400	10	4000	1	1

Various hydraulic gradients were applied to compare the solutions of the models under various regimes. The smallest applied hydraulic gradient is for laminar regime, the applied hydraulic gradient of 10 for PDT flow and the largest one is for FDT flow.

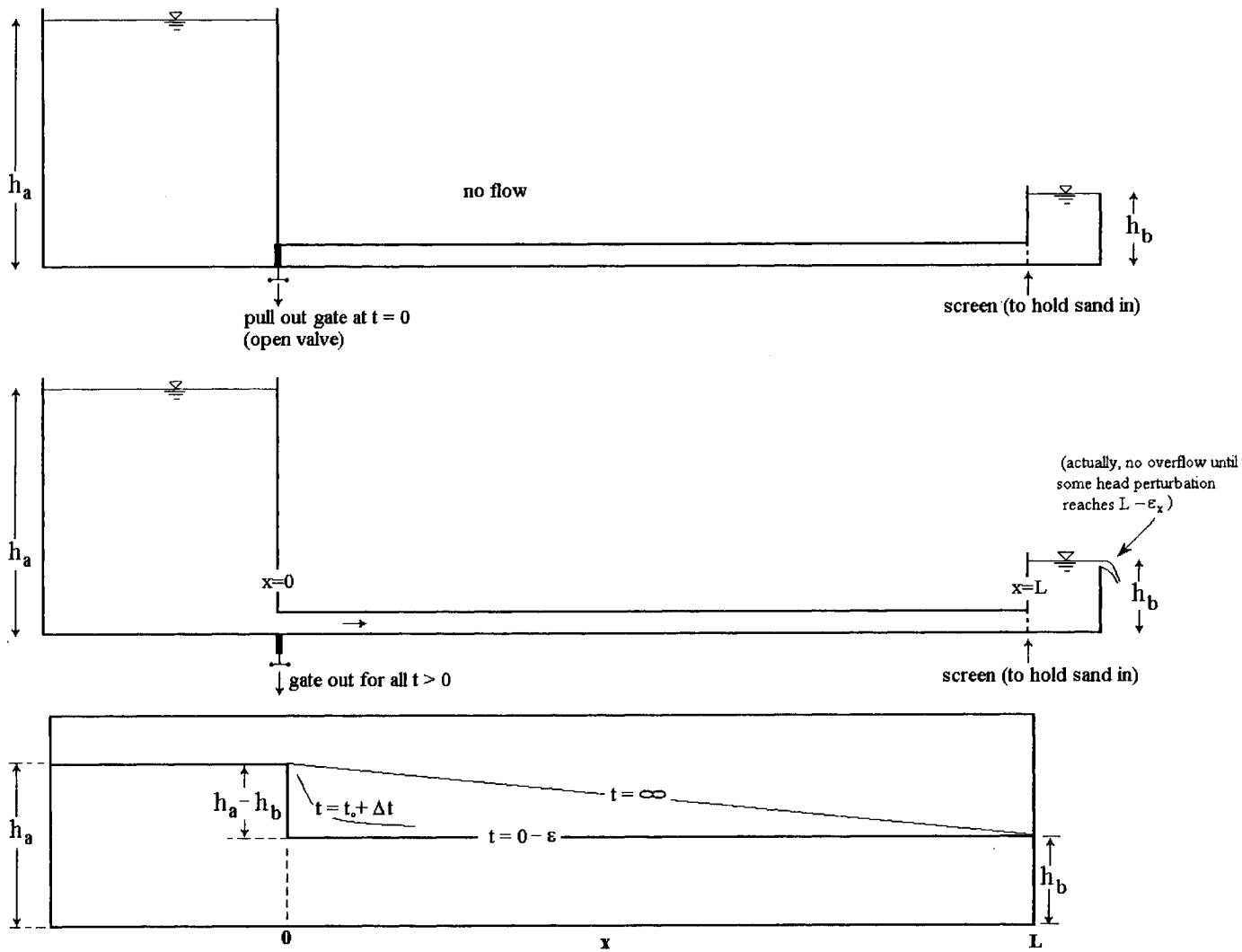

Figure 4.4 Schematic to show physical set-up and boundary conditions for horizontal case.

4.1.7. Various Models and Numerical Methods

In the studies of the various models having different levels of sophistication, only the horizontal case was dealt with because the governing equations could be greatly simplified by neglecting the elevation head term. Further, it was found that the effect of elevation head was negligible in all cases (see Table 3.6), based on the order-of-magnitude study. However, as a matter of interest, the effects of elevation head were still investigated using the regular perturbation method. This elevation head term was included in the model by considering a sloped pipe ($\theta \neq 0$).

In Figures 4.5 and 4.6, various models were compared in terms of H with the applied hydraulic gradient of 0.1. Figure 4.5 shows spatial variation of H at various times. In the laminar flow regime, the viscous effect is dominant and the inertial effect is negligible. It can be shown that the results of Darcy's Law model matches very well with the Ergun-type model at all three stated times. Similarly, the acceleration-included model matches very well with the complete model which tells that the convective acceleration effect is negligible. At very small time ($\tau = 0.03$), the acceleration-included model shows some discrepancies with the Darcy's Law model and the Ergun-type model. These discrepancies are due to the local acceleration term. It was found that the local acceleration term may not be negligible at very small times. Figure 4.6 shows temporal variation of H at various locations. All the models show good match at three stated locations. H approaches steady-state value of H before τ becomes 1. In Figures 4.7 and 4.8, V using various models was compared under the applied hydraulic gradient of 0.1. Figure 4.7 shows spatial variation of the V at various times. The comparison of models shows similar results found in H. The V using the Darcy's Law model and the Ergun-type model matches very well, and the V using the acceleration-included model and the complete model matches very well. The discrepancy in V using the Ergun-type model and the acceleration-included model is large at small time ($\tau = 0.03$) and it becomes small as time increases ($\tau = 0.1$ and $\tau = 0.3$). Compared with the magnitude of the discrepancy appeared in H, it is relatively large. These discrepancies indicate that the local acceleration term may not be neglected at small times. Figure 4.8 shows temporal variation of the V at various locations. It can be shown that the difference between the V

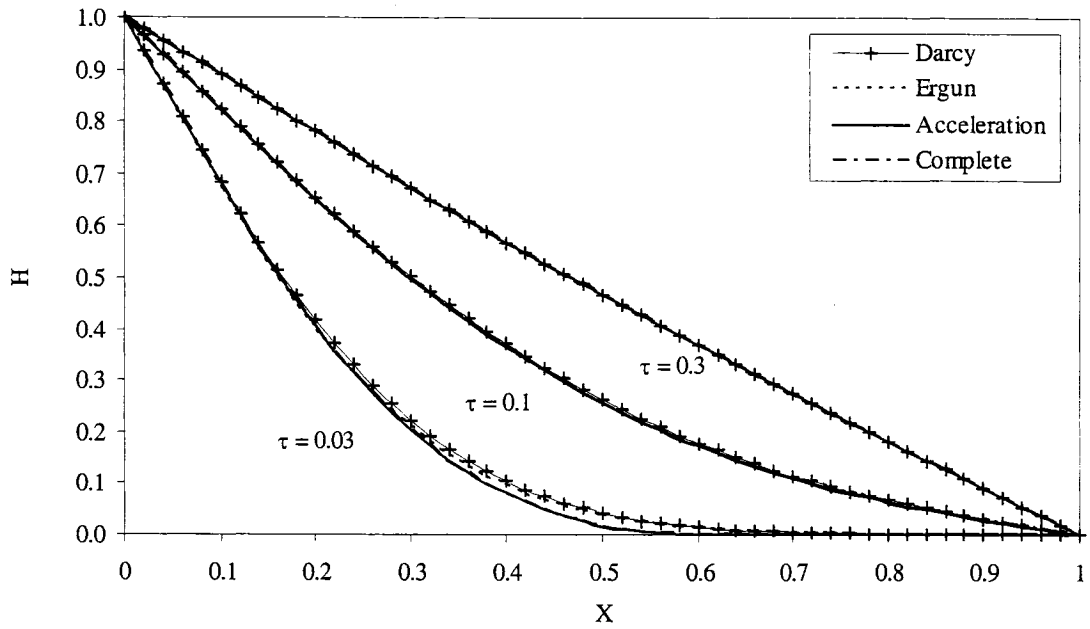

Figure 4.5 Spatial variation of H at various dimensionless times using Darcy's Law, the Ergun eqn, an acceleration-included model, and the complete model (i = 0.1).

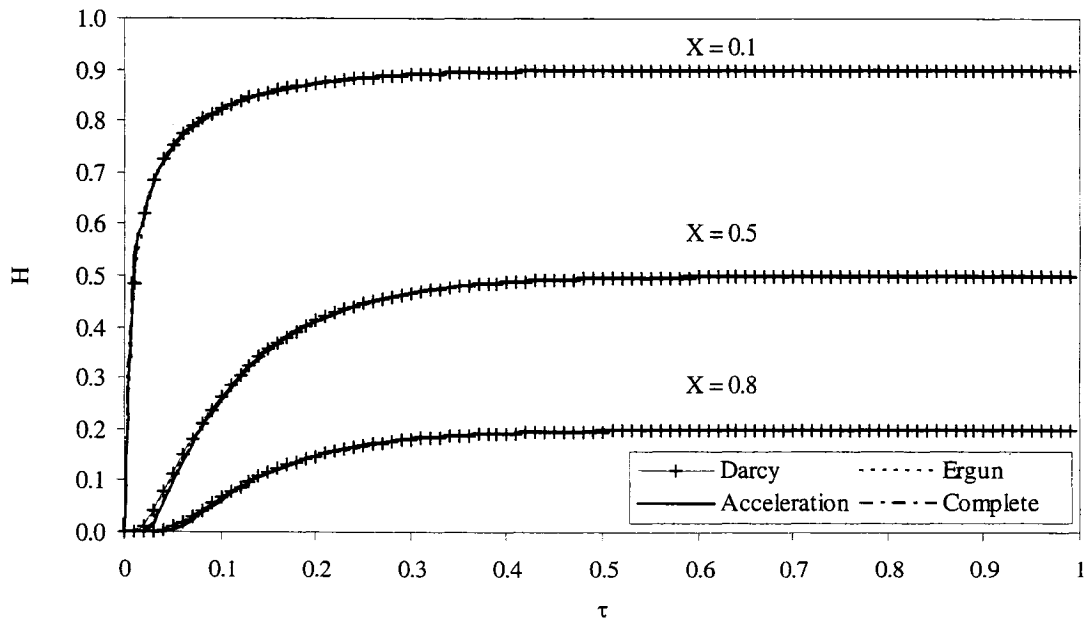

Figure 4.6 Temporal variation of H at various locations using Darcy's Law, the Ergun eqn, an acceleration-included model, and the complete model (i = 0.1).

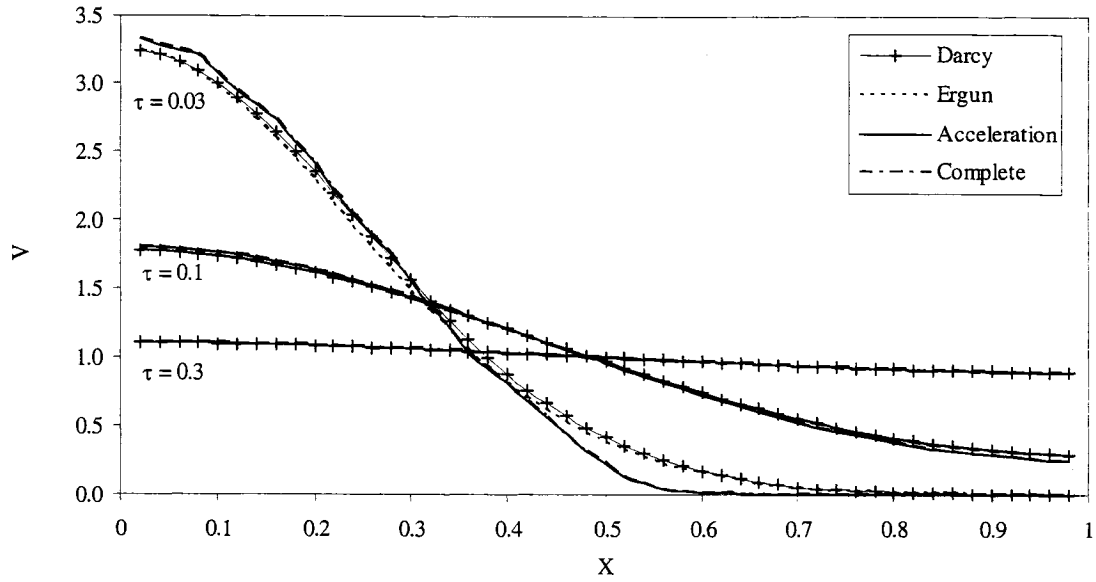

Figure 4.7 Spatial variation of V at various dimensionless times using Darcy's Law, the Ergun eqn, an acceleration-included model, and the complete model (i = 0.1).

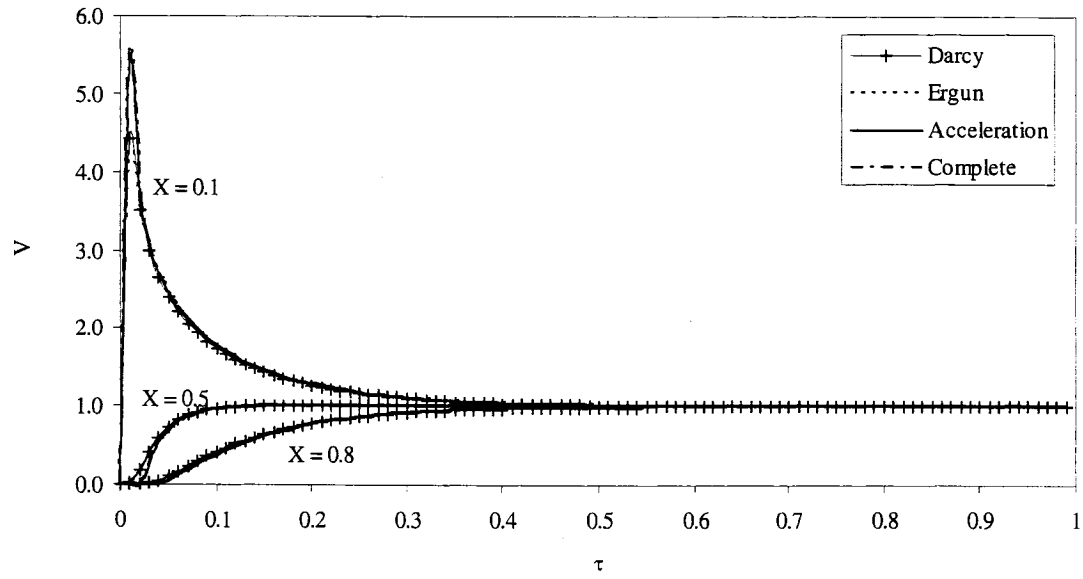

Figure 4.8 Temporal variation of V at various locations using Darcy's Law, the Ergun eqn, an acceleration-included model, and the complete model (i = 0.1).

using Ergun model and acceleration-included model is large at small X (X = 0.1) and τ. The V at three stated locations approaches to the one value of equilibrium/steady-state V.

In Figures 4.9 and 4.10, various models were compared in terms of H with the applied hydraulic gradient of 10 (PDT flow). Figure 4.9 shows spatial variation of H at various times. In the PDT flow regime, the inertial effect is not negligible. It can be shown that the results of all the models match well except the Darcy's Law model. As can be expected, Darcy's Law model could not predict the flow well. At three stated times, the differences between the Ergun-type model and the local acceleration-included model are negligible which shows that the local acceleration effect is not important. However, in the matched asymptotic expansion studies, it can be shown that the local acceleration can not be neglected in smaller time and space scale compared with those of laminar flow regime. Figure 4.10 shows temporal variation of H at various locations. All the models show good match at three stated locations except the Darcy's Law model. H approaches steady-state value of H before τ becomes 1. In Figures 4.11 and 4.12, the V using various models was compared under the applied hydraulic gradient of 10. Figure 4.11 shows spatial variation of the V at various times. The comparison of models shows similar results found in H. The V using a model other than the Darcy's Law model matches well. It can be shown that the difference between the V using the Darcy's Law model and the other models is large at small τ. Figure 4.12 shows temporal variation of the V at various locations. The V at three stated locations approaches to the one value of equilibrium/steady-state V.

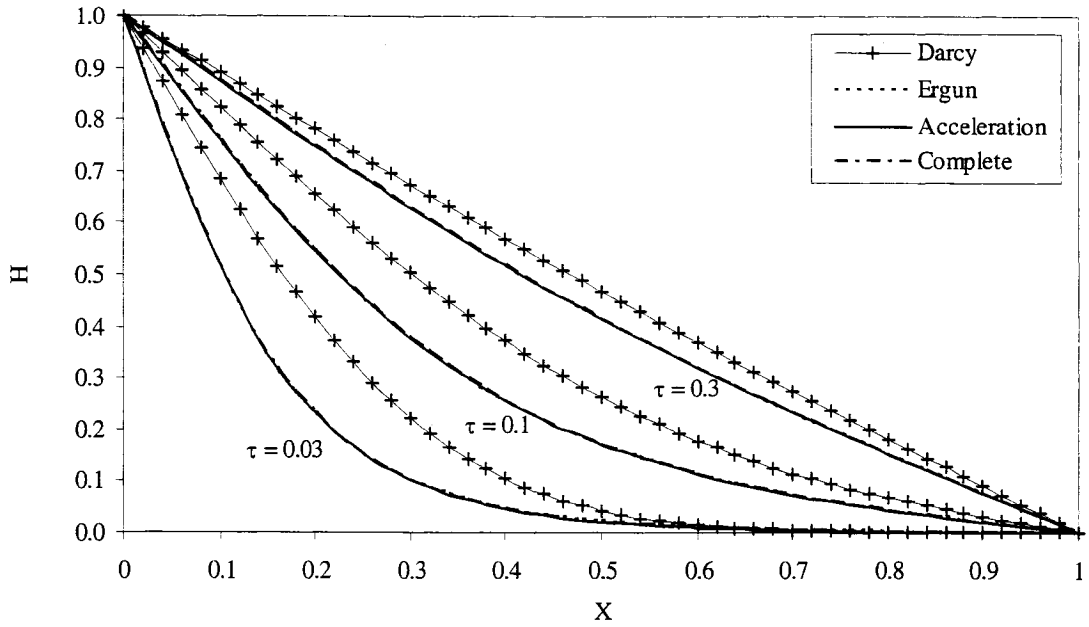

Figure 4.9 Spatial variation of H at various dimensionless times using Darcy's Law, the Ergun eqn, an acceleration-included model, and the complete model (i = 10).

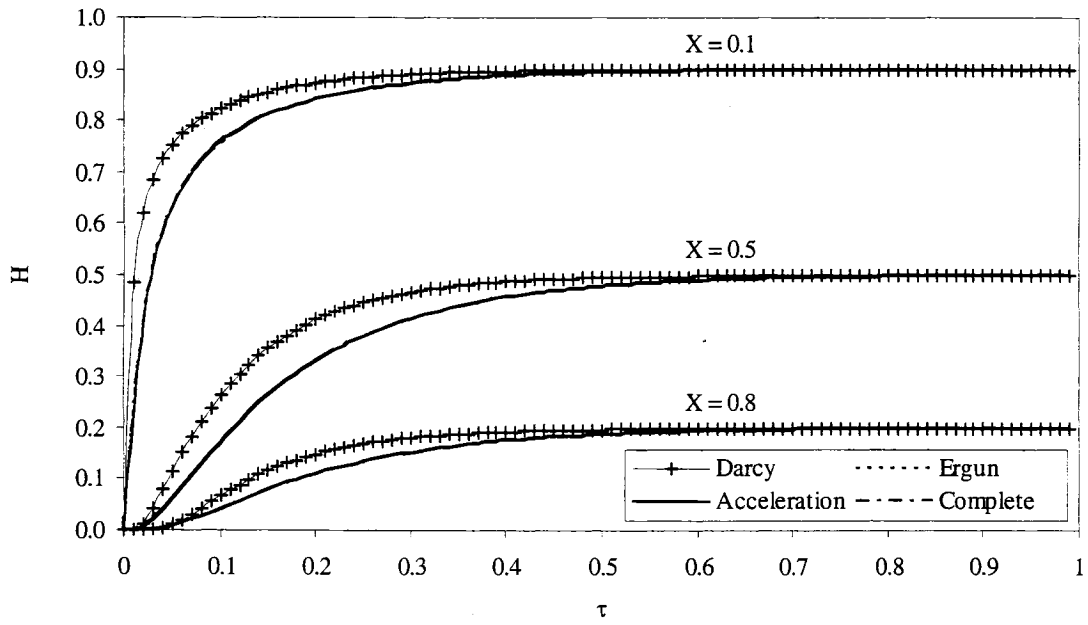

Figure 4.10 Temporal variation of H at various locations using Darcy's Law, the Ergun eqn, an acceleration included-model, and the complete model (i = 10).

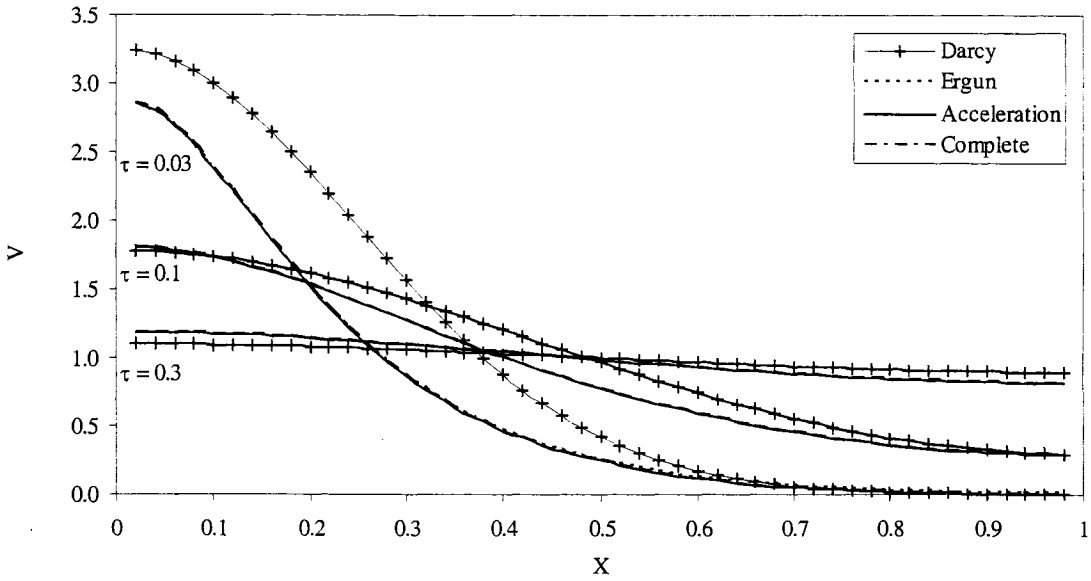

Figure 4.11 Spatial variation of V at various dimensionless times using Darcy's Law, the Ergun eqn, an acceleration-included model, and the complete model (i = 10).

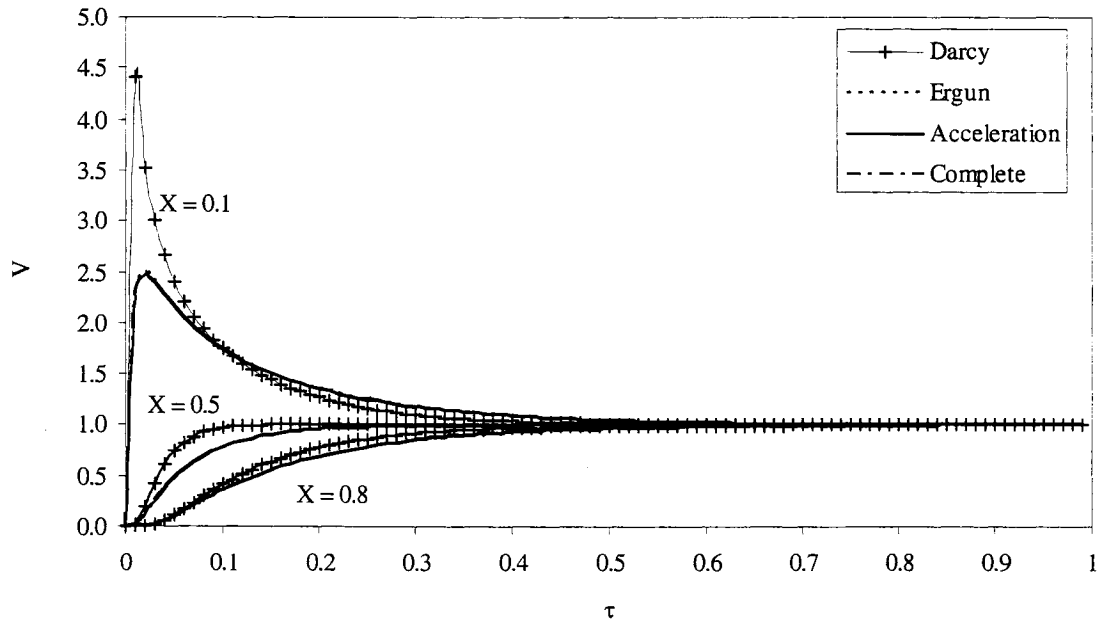

Figure 4.12 Temporal variation of V at various locations using Darcy's Law, the Ergun eqn, an acceleration-included model, and the complete model (i = 10).

In Figures 4.13 and 4.14, various models were compared in terms of H with the applied hydraulic gradient of 400 (FDT flow). The results for FDT flow case are very close to those of PDT flow case. Figure 4.13 shows spatial variation of H at various times. In the FDT flow regime, the inertial effect is dominant. It can be shown that the results of all the models match well except the Darcy's Law model. As can be expected, Darcy's Law model could not predict the flow well in the FDT flow regime. At three stated times, the differences between the Ergun-type model and the local acceleration-included model are negligible. Figure 4.14 shows temporal variation of H at various locations. All the models show good match at three stated locations except the Darcy's Law model. In Figures 4.15 and 4.16, the V using various models was compared under the applied hydraulic gradient of 400. Figure 4.15 shows spatial variation of the V at various times. The comparison of models shows similar results found in H. The V using a model other than the Darcy's Law model is close to each other. It can be shown that the difference between the V using the Darcy's Law model and the other models is large at small τ. Figure 4.16 shows temporal variation of the V at various locations. The V at three stated locations approaches to the one value of equilibrium/steady-state V. In Figure 4.17 and 4.18, various schemes of finite difference method were compared. The solutions were obtained by solving the complete momentum and continuity equation under the applied hydraulic gradient of 1 (PDT flow). Figure 4.17 shows spatial variation of H at various times using the explicit finite difference method (FDM) with backward difference in time and central difference in space, FDM with Lax-Wendroff scheme, and method of characteristics. The results show excellent match at all three stated times. It was found that the accuracy of explicit FDM can be considered good to predict H and V at stated time and space scales. Figure 4.18 shows spatial variation of V at various times using the methods applied for Figure 4.17.

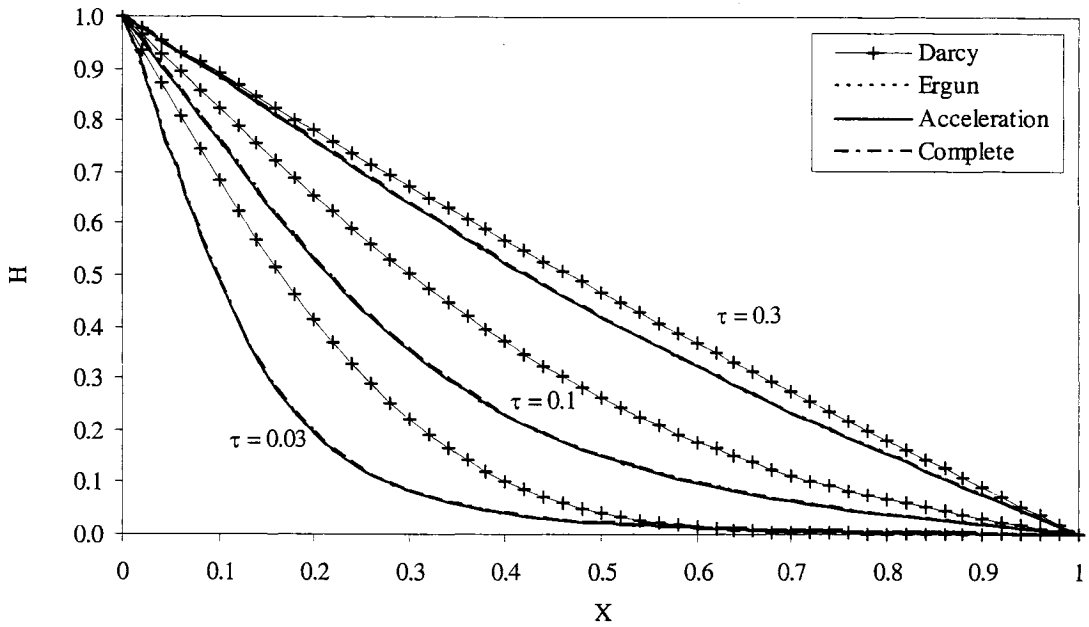

Figure 4.13 Spatial variation of H at various dimensionless times using Darcy's Law, the Ergun eqn, an acceleration-included model, and the complete model (i = 400).

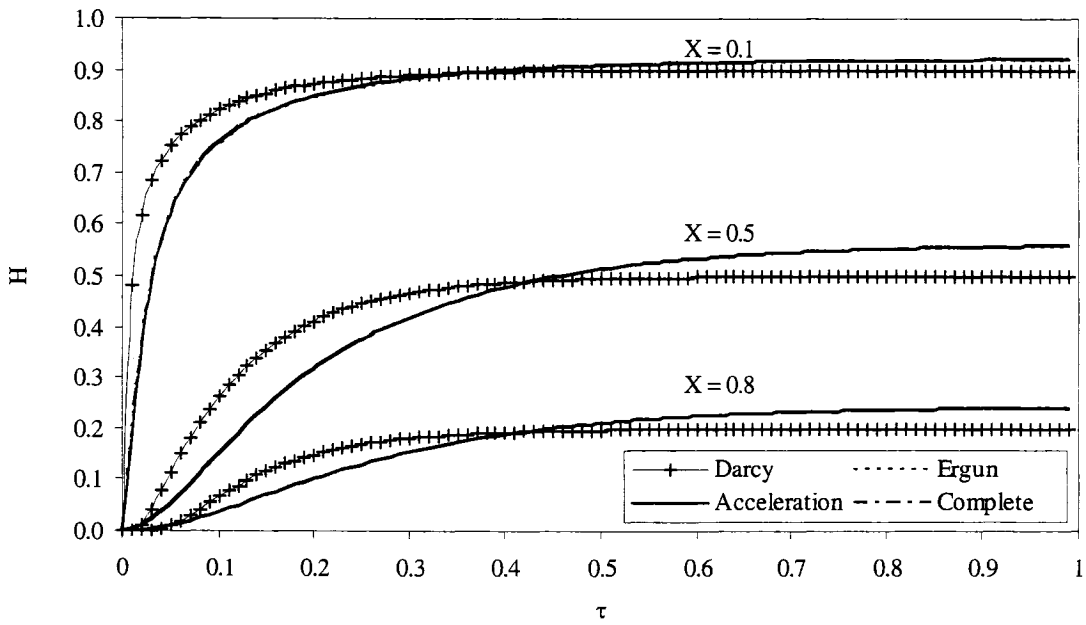

Figure 4.14 Temporal variation of H at various locations using Darcy's Law, the Ergun eqn, an acceleration-included model, and the complete model (i = 400).

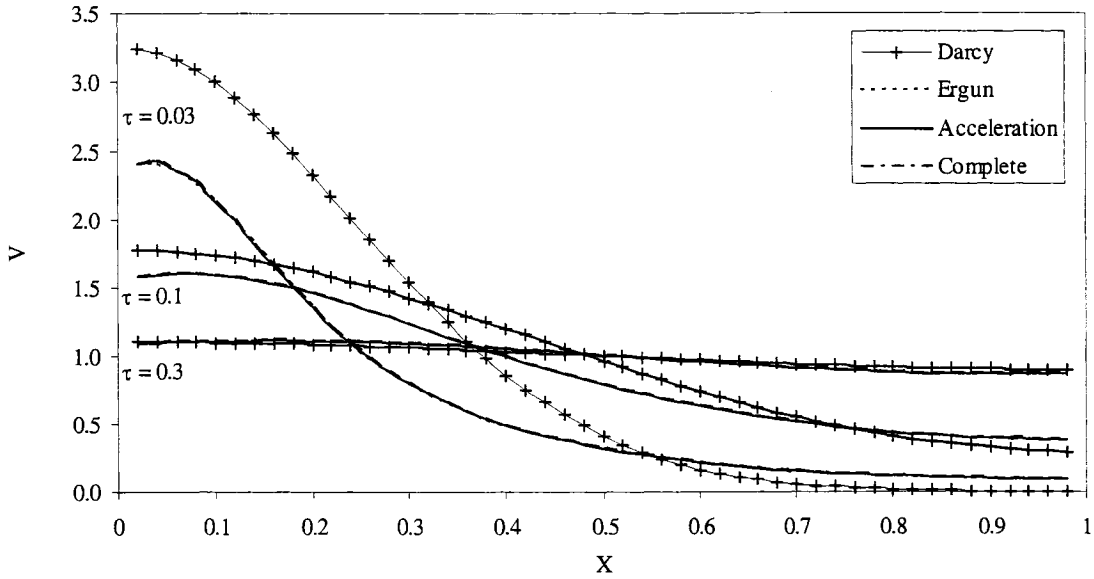

Figure 4.15 Spatial variation of V at various dimensionless times using Darcy's Law, the Ergun eqn, an acceleration-included model, and the complete model (i = 400).

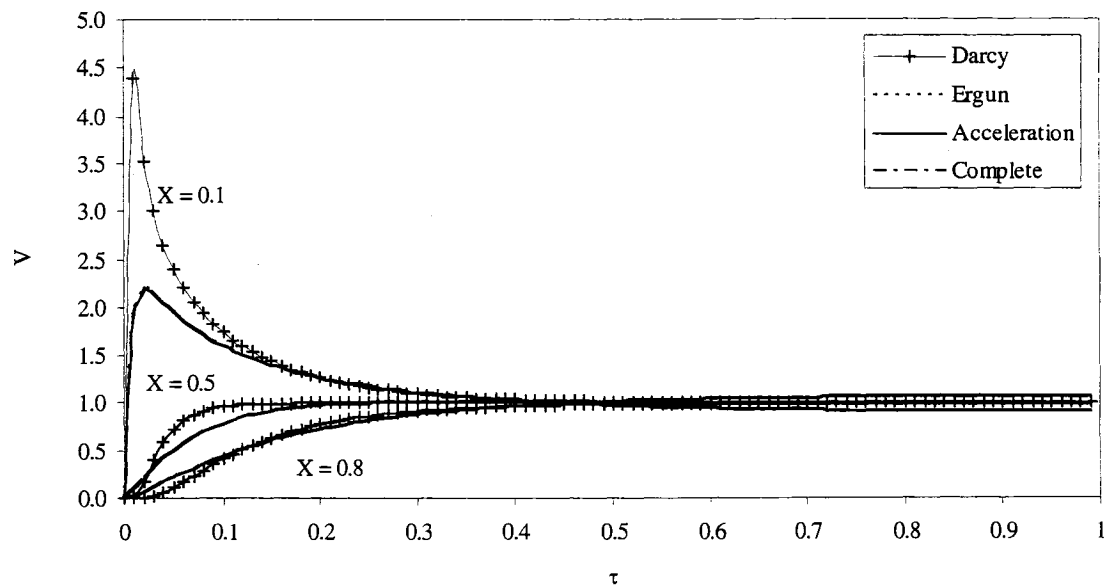

Figure 4.16 Temporal variation of V at various locations using Darcy's Law, the Ergun eqn, an acceleration-included model, and the complete model (i = 400).

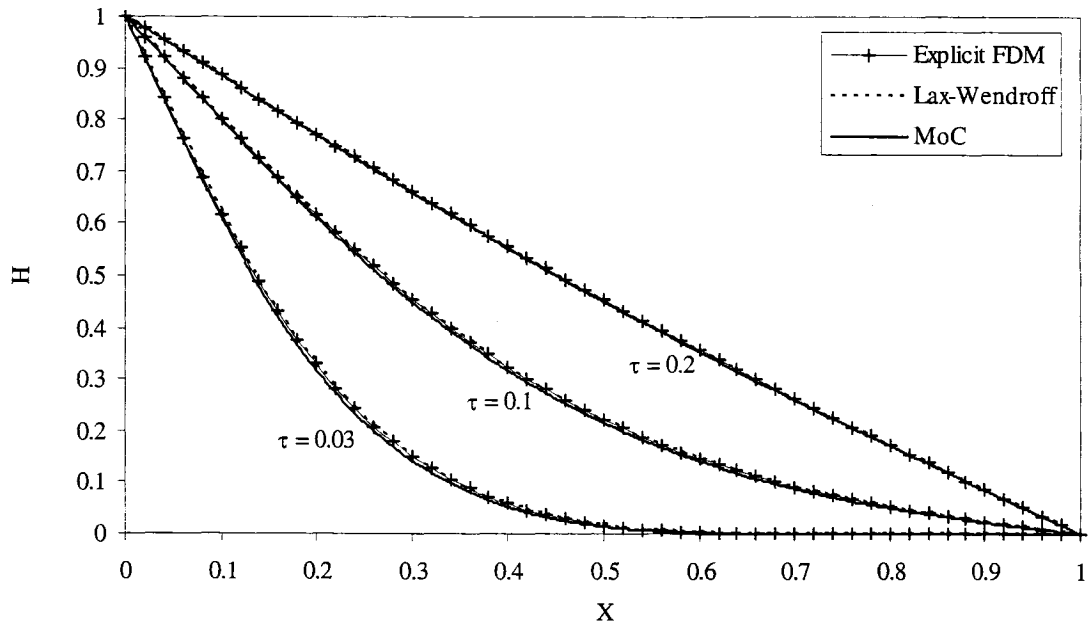

Figure 4.17 Spatial variation of H at various dimensionless times using an explicit FDM, Lax-Wendroff scheme, and MoC (i = 1).

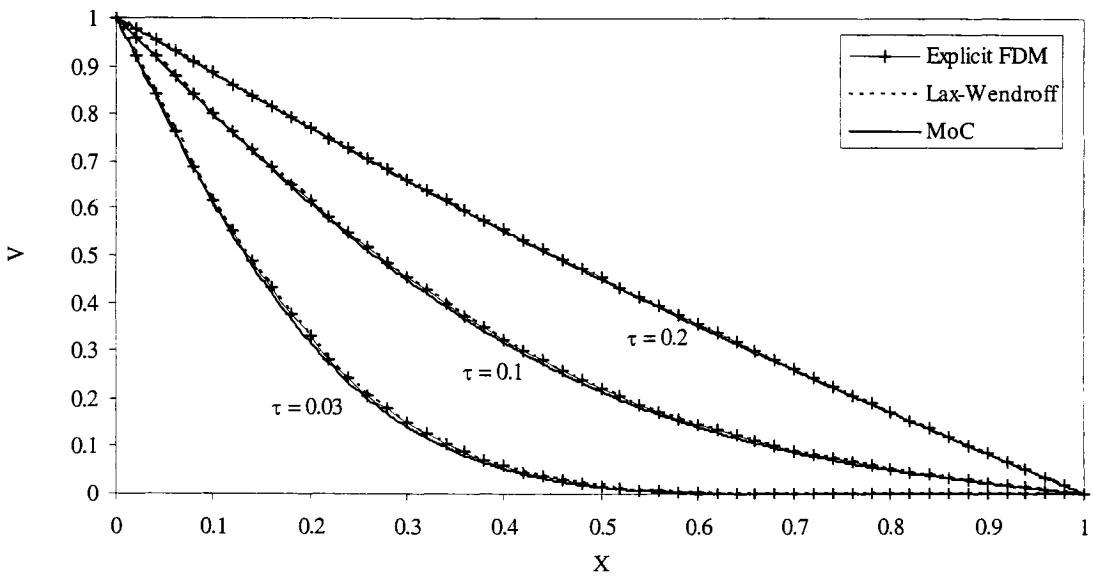

Figure 4.18 Spatial variation of V at various dimensionless times using an explicit FDM, Lax-Wendroff scheme, and MoC (i = 1).

4.2. Regular Perturbation Solutions

Explicit finite difference method was used to obtain solutions of H_0, H_1, H_2, H_3, H_4, and H_5 separately. Similarly, V_0, V_1, V_2, V_3, V_4 and V_5 were obtained using explicit FDM. For laminar regime, hydraulic gradient of 0.1 was applied, and for PDT and FDT case hydraulic gradient of 10 was applied.

4.2.1. Solutions in Laminar Regime

The boundary and initial conditions of H_0, H_1, H_2, H_3, H_4, and H_5 can be obtained using those of H. The boundary and initial conditions of H are:

$$H = 1 \text{ at } X = 0 \qquad [4\text{-}22a]$$

$$H = 0 \text{ at } X = 1 \qquad [4\text{-}23a]$$

$$H = 0 \text{ at } \tau = 0 \qquad [4\text{-}24a]$$

Using the expansion on H, eqn [3-83], the boundary and initial conditions can then be written:

$$H_0(0,\tau) + \varepsilon H_1(0,\tau) + \delta H_2(0,\tau) + \gamma H_3(0,\tau) + \xi H_4(0,\tau) + \omega H_5(0,\tau) = 1 \qquad [4\text{-}22b]$$

$$H_0(1,\tau) + \varepsilon H_1(1,\tau) + \delta H_2(1,\tau) + \gamma H_3(1,\tau) + \xi H_4(1,\tau) + \omega H_5(1,\tau) = 0 \qquad [4\text{-}23b]$$

$$H_0(X,0) + \varepsilon H_1(X,0) + \delta H_2(X,0) + \gamma H_3(X,0) + \xi H_4(X,0) + \omega H_5(X,0) = 0 \qquad [4\text{-}24b]$$

(i) Solutions of H_0 and V_0

The boundary and initial conditions for H_0 can be obtained from eqn [4-22b], [4-23b] and [4-24b] and they are:

$$H_0 = 1 \text{ at } X = 0 \qquad [4\text{-}22c]$$

$$H_0 = 0 \text{ at } X = 1 \qquad [4\text{-}23c]$$

$$H_0 = 0 \text{ at } \tau = 0 \qquad [4\text{-}24c]$$

If we recall equation of H_0:

$$H_{0_{xx}} = \frac{C_3}{C_1} H_{0_\tau} \qquad [3\text{-}94c]$$

An explicit finite-difference form of eqn [3-94c], using a backward difference in time and a central difference in space, is:

$$\frac{\left(H_{0i+1}^{k-1} - 2H_{0i}^{k-1} + H_{0i-1}^{k-1}\right)}{\Delta X^2} = \frac{C_3}{C_1}\frac{H_{0i}^{k} - H_{0i}^{k-1}}{\Delta\tau} \qquad [4\text{-}25]$$

which may be re-arranged:

$$H_{0i}^{k} = \frac{\Delta\tau}{\Delta X^2}\frac{C_1}{C_3}\left(H_{0i+1}^{k-1} - 2H_{0i}^{k-1} + H_{0i-1}^{k-1}\right) + H_{0i}^{k-1} \qquad [4\text{-}26]$$

Dimensionless V may then be obtained simply using Darcy's Law:

$$V_{0i}^{k} = -\frac{C_1}{C_3}\frac{H_{0i+1}^{k} - H_{0i-1}^{k}}{2\Delta X} \qquad [4\text{-}27]$$

(ii) Solutions of H_1 and V_1

The boundary and initial conditions for H_1 can be obtained from eqn [4-22b], [4-23b] and [4-24b] and they are:

$$H_1 = 0 \text{ at } X = 0 \qquad [4\text{-}22d]$$

$$H_1 = 0 \text{ at } X = 1 \qquad [4\text{-}23d]$$

$$H_1 = 0 \text{ at } \tau = 0 \qquad [4\text{-}24d]$$

An explicit finite-difference form of eqn [3-95c], using a backward difference in time and a central difference in space, is:

$$\frac{\left(H_{1i+1}^{k-1} - 2H_{1i}^{k-1} + H_{1i-1}^{k-1}\right)}{\Delta X^2} = \frac{C_3}{C_1}\frac{H_{1i}^{k} - H_{1i}^{k-1}}{\Delta\tau} - 2V_{0i}^{k}\frac{V_{0i+1}^{k} - V_{0i-1}^{k}}{2\Delta X} \qquad [4\text{-}28]$$

Because V_0 is not defined at either X = 0 or X = 1, $-H_{0\tau}$ is used instead of V_{0X} from eqn [3-94b].

$$\frac{\left(H_{1i+1}^{k-1} - 2H_{1i}^{k-1} + H_{1i-1}^{k-1}\right)}{\Delta X^2} = \frac{C_3}{C_1}\frac{H_{1i}^{k} - H_{1i}^{k-1}}{\Delta\tau} + 2V_{0i}^{k}\frac{H_{0i}^{k} - H_{0i}^{k-1}}{\Delta\tau} \qquad [4\text{-}29]$$

which may be re-arranged:

$$H_{1i}^{k} = \frac{\Delta\tau}{\Delta X^2}\frac{C_1}{C_3}\left(H_{1i+1}^{k-1} - 2H_{1i}^{k-1} + H_{1i-1}^{k-1}\right) - 2\Delta\tau\frac{C_1}{C_3}V_{0i}^{k}\frac{H_{0i}^{k} - H_{0i}^{k-1}}{\Delta\tau} + H_{1i}^{k-1} \qquad [4\text{-}30]$$

Using eqn [3-95a], the dimensionless velocity, V_{1i}^{k}, becomes:

$$V_{1i}^{k} = -\frac{C_1}{C_3}\frac{H_{1i+1}^{k} - H_{1i-1}^{k}}{2\Delta X} - \frac{C_1}{C_3}\left(V_{0i}^{k}\right)^2 \qquad [4\text{-}31]$$

(iii) Solutions of H_2 and V_2

The boundary and initial conditions for H_2 can be obtained from eqn [4-22b], [4-23b] and [4-24b] and they are:

$$H_2 = 0 \text{ at } X = 0 \qquad [4\text{-}22e]$$

$$H_2 = 0 \text{ at } X = 1 \qquad [4\text{-}23e]$$

$$H_2 = 0 \text{ at } \tau = 0 \qquad [4\text{-}24e]$$

An explicit finite-difference form of eqn [3-96c], using a backward difference in time and a central difference in space, is:

$$\frac{\left(H_{2i+1}^{k-1} - 2H_{2i}^{k-1} + H_{2i-1}^{k-1}\right)}{\Delta X^2} = \frac{C_3}{C_1}\frac{H_{2i}^{k} - H_{2i}^{k-1}}{\Delta\tau} - \frac{\left(\frac{V_{0i+1}^{k} - V_{0i+1}^{k-1}}{\Delta\tau} - \frac{V_{0i-1}^{k} - V_{0i-1}^{k-1}}{\Delta\tau}\right)}{2\Delta X} \qquad [4\text{-}32]$$

which may be re-arranged:

$$H_{2i}^{k} = \frac{\Delta\tau}{\Delta X^2}\frac{C_1}{C_3}\left(H_{2i+1}^{k-1} - 2H_{2i}^{k-1} + H_{2i-1}^{k-1}\right) + \frac{C_1}{C_3}\frac{\left(V_{0i+1}^{k} - V_{0i+1}^{k-1} - V_{0i-1}^{k} + V_{0i-1}^{k-1}\right)}{2\Delta X} + H_{2i}^{k-1} \qquad [4\text{-}33]$$

Using eqn [3-96a], the dimensionless velocity, V_{2i}^{k}, is then:

$$V_{2i}^{k} = -\frac{C_1}{C_3}\frac{H_{2i+1}^{k} - H_{2i-1}^{k}}{2\Delta X} - \frac{C_1}{C_3}\frac{V_{0i}^{k} - V_{0i}^{k-1}}{\Delta\tau} \qquad [4\text{-}34]$$

(iv) Solutions of H_3 and V_3

The boundary and initial conditions for H_3 can be obtained from eqn [4-22b], [4-23b] and [4-24b] and they are:

$$H_3 = 0 \text{ at } X = 0 \qquad [4\text{-}22f]$$

$$H_3 = 0 \text{ at } X = 1 \qquad [4\text{-}23f]$$

$$H_3 = 0 \text{ at } \tau = 0 \qquad [4\text{-}24f]$$

An explicit finite-difference form of eqn [3-97c], using a backward difference in time and a central difference in space, is:

$$\frac{\left(H_{3i+1}^{k-1} - 2H_{3i}^{k-1} + H_{3i-1}^{k-1}\right)}{\Delta X^2} = \frac{C_3}{C_1}\frac{\left(H_{3i}^{k} - H_{3i}^{k-1}\right)}{\Delta\tau} - \left(\frac{V_{0i+1}^{k} - V_{0i-1}^{k}}{2\Delta X}\right)^2 - V_{0i}^{k}\left(\frac{V_{0i+1}^{k} - 2V_{0i}^{k} + V_{0i-1}^{k}}{\Delta X^2}\right) \qquad [4\text{-}35]$$

V_0 is not defined at either X = 0 or X = 1. However, using the relationships $V_{0_x} = -H_{0_\tau}$ and $V_{0_{xx}} = -H_{0_{\tau x}}$, eqn [4-35] can be re-stated as:

$$\frac{\left(H_{3i+1}^{k-1} - 2H_{3i}^{k-1} + H_{3i-1}^{k-1}\right)}{\Delta X^2} = \frac{C_3}{C_1}\frac{\left(H_{3i}^{k} - H_{3i}^{k-1}\right)}{\Delta\tau} - \left(\frac{H_{0i}^{k} - H_{0i}^{k-1}}{\Delta\tau}\right)^2 + V_{0i}^{k}\frac{\left(\frac{H_{0i+1}^{k} - H_{0i+1}^{k-1}}{\Delta\tau} - \frac{H_{0i-1}^{k} - H_{0i-1}^{k-1}}{\Delta\tau}\right)}{2\Delta X} \qquad [4\text{-}36]$$

By re-arrangement:

$$H_{3i}^{k} = \Delta\tau\frac{C_1}{C_3}\frac{\left(H_{3i+1}^{k-1} - 2H_{3i}^{k-1} + H_{3i-1}^{k-1}\right)}{\Delta X^2} + \Delta\tau\frac{C_1}{C_3}\left(\frac{H_{0i}^{k} - H_{0i}^{k-1}}{\Delta\tau}\right)^2 - \frac{C_1}{C_3}V_{0i}^{k}\left(\frac{H_{0i+1}^{k} - H_{0i+1}^{k-1} - H_{0i-1}^{k} + H_{0i-1}^{k-1}}{2\Delta X}\right) + H_{3i}^{k-1} \qquad [4\text{-}37]$$

Similarly, the dimensionless velocity, V_{3i}^{k}, can be obtained using eqn [3-97a] and the fact that $V_{0_x} = -H_{0_\tau}$:

$$V_{3i}^{k} = -\frac{C_1}{C_3}\left[\frac{\left(H_{3i+1}^{k} - H_{3i-1}^{k}\right)}{2\Delta X} - V_{0i}^{k}\left(\frac{H_{0i}^{k} - H_{0i}^{k-1}}{\Delta\tau}\right)\right] \qquad [4\text{-}38]$$

(v) Solutions of H_4 and V_4

The boundary and initial conditions for H_4 can be obtained from eqn [4-22b], [4-23b] and [4-24b] and they are:

$$H_4 = 0 \text{ at } X = 0 \qquad [4\text{-}22g]$$

$$H_4 = 0 \text{ at } X = 1 \qquad [4\text{-}23g]$$

$$H_4 = 0 \text{ at } \tau = 0 \qquad [4\text{-}24g]$$

An explicit finite-difference form of eqn [3-98c], using a backward difference in time and a central difference in space, is:

$$\frac{\left(H_{4i+1}^{k-1} - 2H_{4i}^{k-1} + H_{4i-1}^{k-1}\right)}{\Delta X^2} = \frac{C_3}{C_1}\left[\frac{\left(H_{4i}^{k} - H_{4i}^{k-1}\right)}{\Delta\tau} + V_{0i}^{k}\left(\frac{H_{0i+1}^{k} - V_{0i-1}^{k}}{2\Delta X}\right)\right] \qquad [4\text{-}39]$$

By re-arrangement:

$$H_{4i}^{k} = \Delta\tau\frac{C_1}{C_3}\frac{\left(H_{4i+1}^{k-1} - 2H_{4i}^{k-1} + H_{4i-1}^{k-1}\right)}{\Delta X^2} - \Delta\tau V_{0i}^{k}\left(\frac{H_{0i+1}^{k} - V_{0i-1}^{k}}{2\Delta X}\right) + H_{4i}^{k-1} \qquad [4\text{-}40]$$

The quantity V_{4i}^{k} can be expressed as:

$$V_{4i}^{k} = -\frac{C_1}{C_3}\frac{H_{4i+1}^{k} - H_{4i-1}^{k}}{2\Delta X} \qquad [4\text{-}41]$$

(vi) Solutions of H_5 and V_5

The boundary and initial conditions for H_5 can be obtained from eqn [4-22b], [4-23b] and [4-24b] and they are:

$$H_5 = 0 \text{ at } X = 0 \qquad [4\text{-}42c]$$

$$H_5 = 0 \text{ at } X = 1 \qquad [4\text{-}23c]$$

$$H_5 = 0 \text{ at } \tau = 0 \qquad [4\text{-}24c]$$

An explicit finite-difference form of eqn [3-99c], using a backward difference in time and a central difference in space, is:

$$\frac{\left(H_{5i+1}^{k-1} - 2H_{5i}^{k-1} + H_{5i-1}^{k-1}\right)}{\Delta X^2} = \frac{C_3}{C_1}\left[\frac{\left(H_{5i}^{k} - H_{5i}^{k-1}\right)}{\Delta\tau} + V_{0i}^{k}\right] \qquad [4\text{-}42]$$

By re-arrangement:

$$H_{5i}^{k} = \Delta\tau\frac{C_1}{C_3}\frac{\left(H_{5i+1}^{k-1} - 2H_{5i}^{k-1} + H_{5i-1}^{k-1}\right)}{\Delta X^2} - \Delta\tau V_{0i}^{k} + H_{5i}^{k-1} \qquad [4\text{-}43]$$

The quantity V_{5i}^{k} can be found using:

$$V_{5i}^{k} = -\frac{C_1}{C_3}\frac{H_{5i+1}^{k} - H_{5i-1}^{k}}{2\Delta X} \qquad [4\text{-}44]$$

4.2.2. Effects of Each Term in Laminar Case

Spatial and temporal variations of each effect were presented in terms of H and V. The RP solutions were compared with the solutions obtained from the relevant models.

(i) Viscous Effect

The magnitude of viscous effects was computed using the RP expression for H_0 given by eqn [4-36] together with the previously stated boundary conditions for H_0 and V_0. It can be seen that the behaviour of H_0 obtained using the RP expansion method is virtually identical to the behaviour of H obtained from the FDM solution to the traditional groundwater flow equation.

(ii) Inertial Effect

The Spatial variation in H obtained by solving eqn [4-9] of Ergun-type model and that obtained by RP expansion (eqn [4-30]) is shown in Figure 4.19, for an applied hydraulic

gradient of 0.1. The solution of RP expansion can be obtained from $H = H_0 + \varepsilon H_1$. As can be seen in said Figure, the outcomes from these two numerical simulations are nearly identical. However, some differences between the Darcy's Law and Ergun equation outcomes. These differences are due to the inertial effect (εH_1). The largest differences occurred around mid-length of the conduit (see Figure 4.20). The difference is also relatively even in this zone. Figures 4.21 and 4.22 show spatial and temporal variation in H_1. H_1 is negative for all observed times and locations. In Figure 4.21, the minimum H_1 is found at the smallest observed time ($\tau = 0.1$). This result can be related to the 'early' flows which are inertia-dominated in accordance with the Ergun equation, and the 'late' flows which are viscous-dominated in accordance with Darcy's Law suggested by Nilson (1981). It can also be seen that the minimum H_1 for each snapshot in time is located near the mid-length for all three such times, and that the location of minimum H_1 moves downstream as time increases. Figure 4.22 shows that the minimum H_1 occurred near the upstream end of the conduit. The time required to reach the minimum H_1 at a given location increased in the downstream direction. From Figures 4.21 and 4.22 we may conclude that the largest inertial effect occurs at expected at the beginning of the experiment and nearer the upstream end of the conduit for the case of purely laminar flow. The overall effect on H can be obtained by multiplying ε and H_1. Figures 4.23 and 4.24 show the spatial and temporal variation in V_1, respectively. V_1 also shows negative values at all tree observed times and locations. The results show trends that are similar to those of H_1. However, near the boundary V_1 behaves quite differently. For example, near the upstream end, inertial effect increases and reduces the velocity of the flow, as time passes.

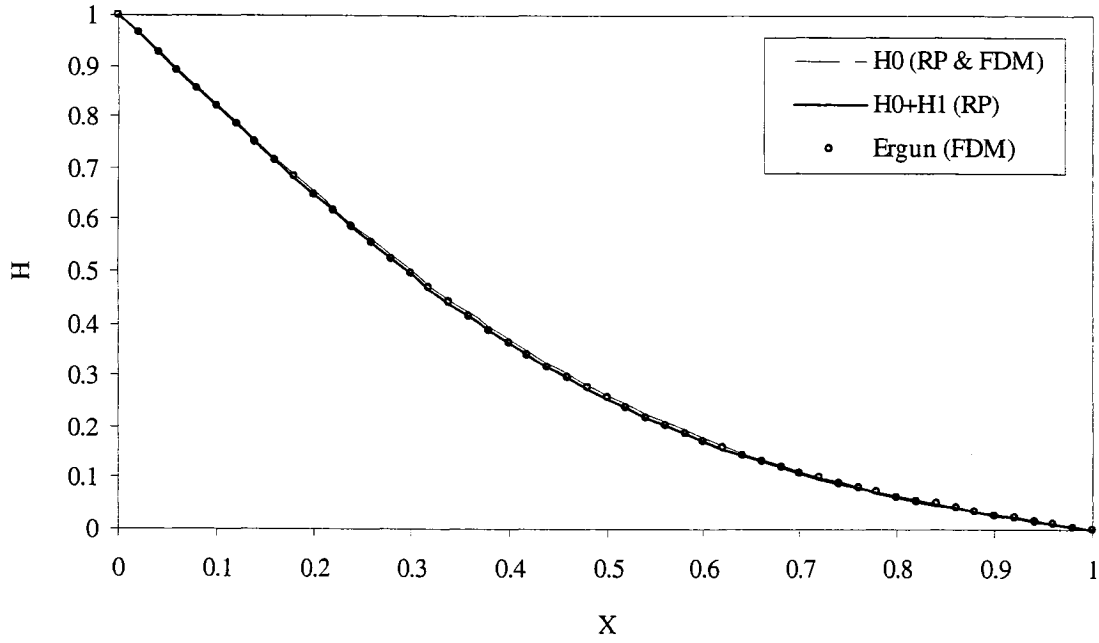

Figure 4.19 Spatial variation of H using explicit FDM and RP (i = 0.1 and τ = 0.1).

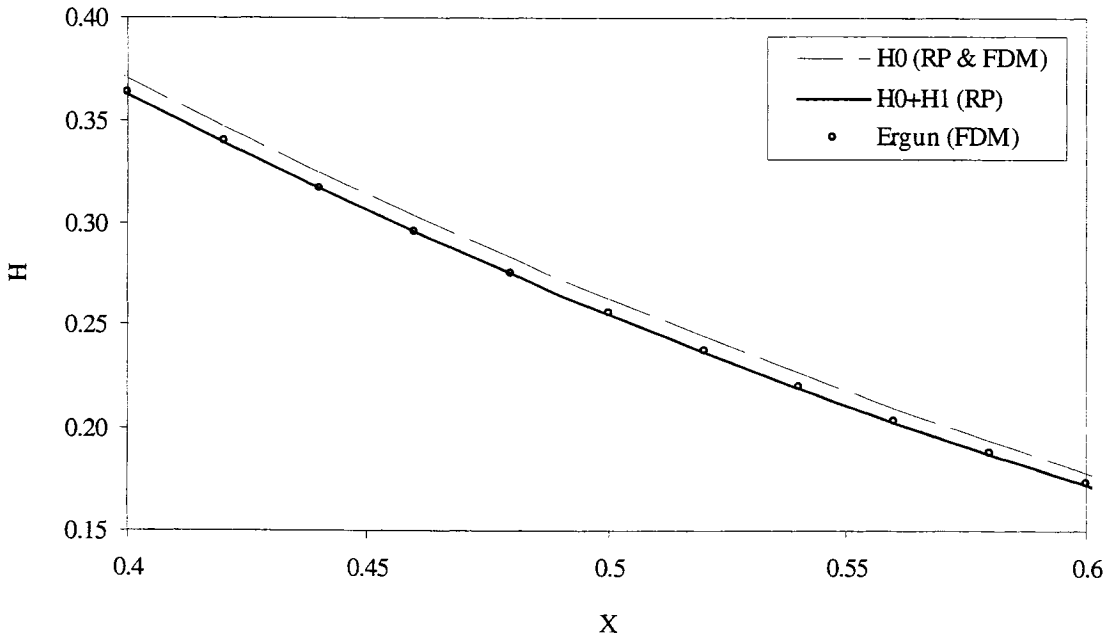

Figure 4.20 Close-up of spatial range, 0.4 ≤ X ≤ 0.6.

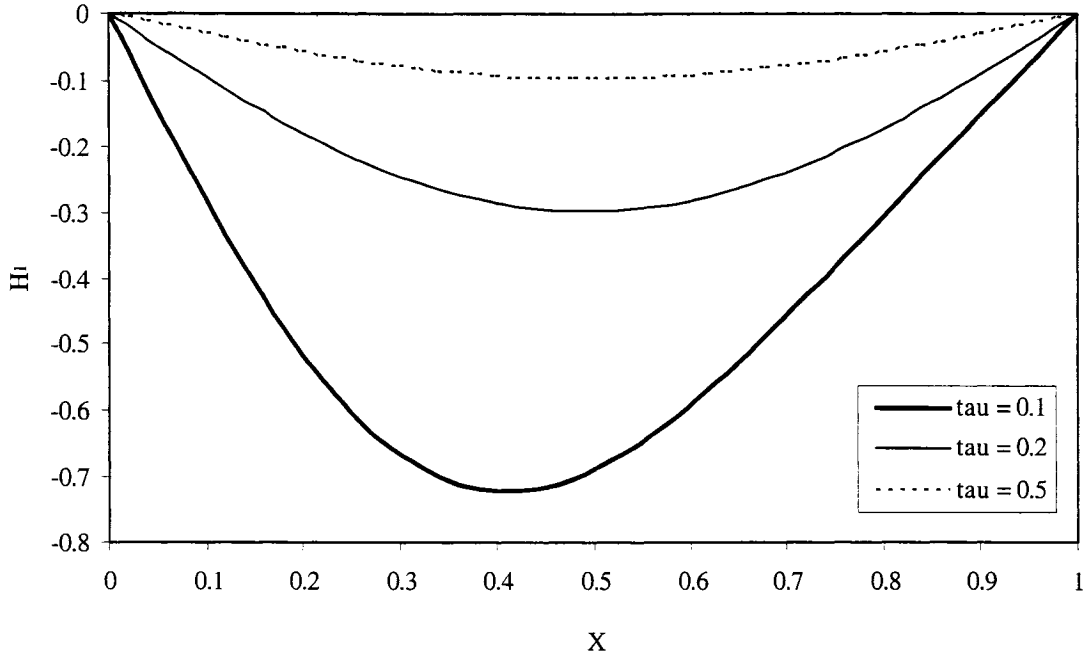

Figure 4.21 Spatial variation of H_1 (inertial effect, i = 0.1).

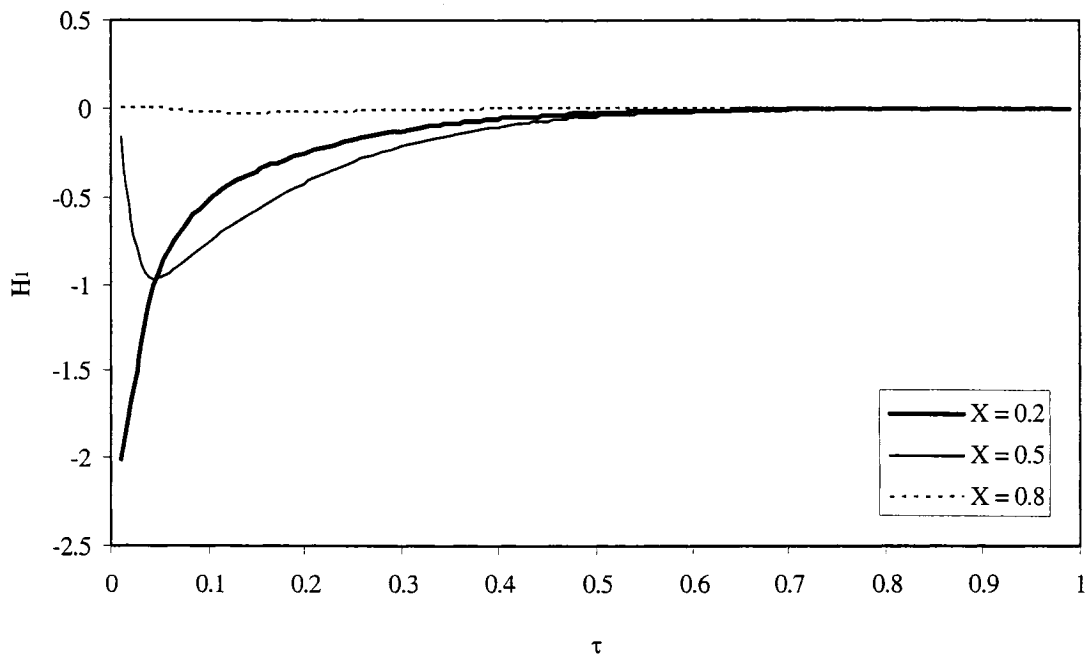

Figure 4.22 Temporal variation of H_1 (inertial effect, i = 0.1).

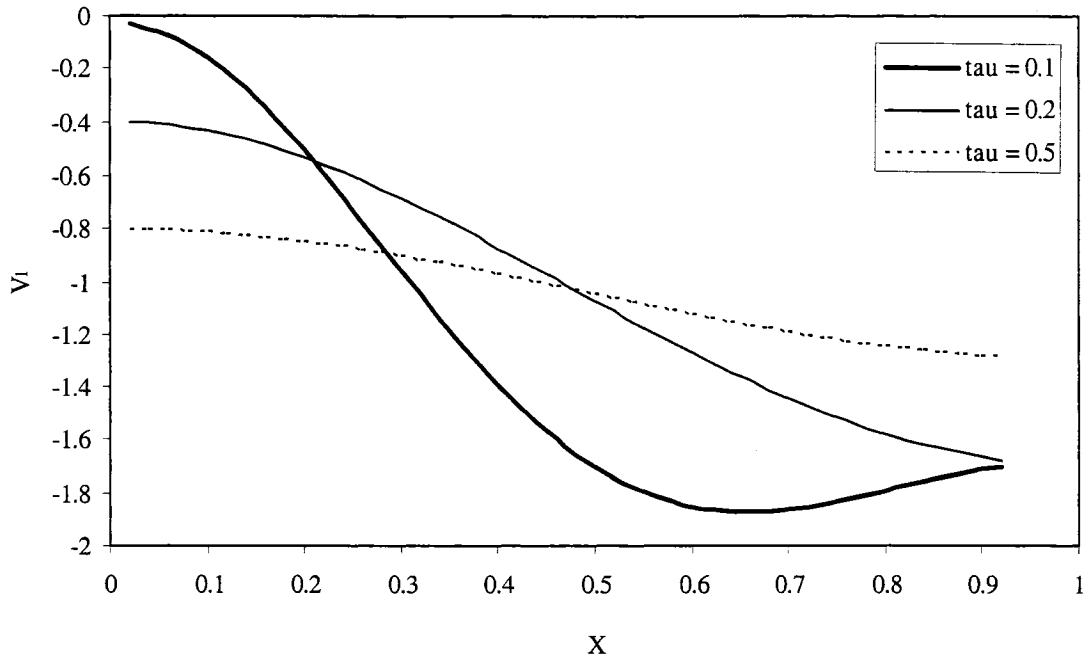

Figure 4.23 Spatial variation of V_1 (inertial effect, i = 0.1).

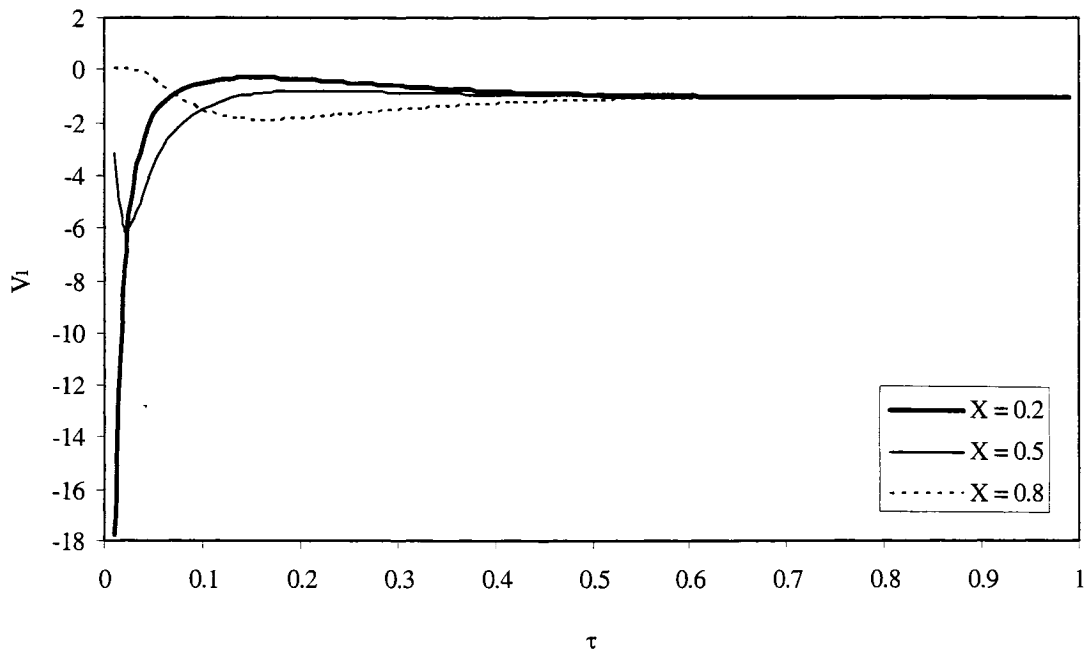

Figure 4.24 Temporal variation of V_1 (inertial effect, i = 0.1).

(iii) Local Acceleration Effect

The local acceleration effect was investigated using H_2 and V_2 (eqn [4-33] and eqn [4-34]). The regular perturbation solutions for H and V including viscous, inertial and local acceleration term were obtained using $H = H_0 + \varepsilon H_1 + \delta H_2$ and $V = V_0 + \varepsilon V_1 + \delta V_2$. In Figure 4.25, the results of applying the regular perturbation method are compared. These include presentation of the effects of local acceleration, inertial effects, and viscosity effects only (traditional groundwater flow model). Solutions obtained using RP expansion with local accelerative effects included in the model show a near-perfect match with the model described in the previous section. Only small differences are evident between it and the H variation obtained using the Ergun (inertial) model. These differences are evidently due to the local acceleration term δH_2. Figure 4.26 highlights near the mid-length discrepancy. It can be seen that the difference between this three-part model (laminar plus inertial plus local acceleration) and the previous two-part model is spatially inconsistent. This implies that the local acceleration term H_2 can be positive or negative with time and space. Figures 4.27 and 4.28 show the spatial and temporal variation in H_2. Figure 4.27 shows negative values of H_2 at small values of τ. The profile at $\tau = 0.1$ shows that the local acceleration term increases the H at the upstream end but decreases it at the downstream end. Figure 4.28 shows that H_2 becomes close to zero as time increases at all locations. The absolute value of minimum is larger than that of maximum at any given location. The overall effect of H_2 on the propagation of H can be obtained by multiplying δ and H_2. Figures 4.29 and 4.30 show the spatial and temporal variation in V_2. V_2 shows some positive and some negative values at all three stated times and locations. It can be seen that V_2 shows patterns that are similar to V_1 (and H_1) at the upstream and downstream ends. Figure 4.30 shows that the effect of V_2 becomes close to zero as time increases. The value of V_2 at $X = 0.2$ is always positive. This can be related to the characteristics of the evolving-wave equation. This will be explained later using matched asymptotic expansions. Positive values of H_2 are expected at very small τ and X from the same characteristics of evolving-wave equation. We may

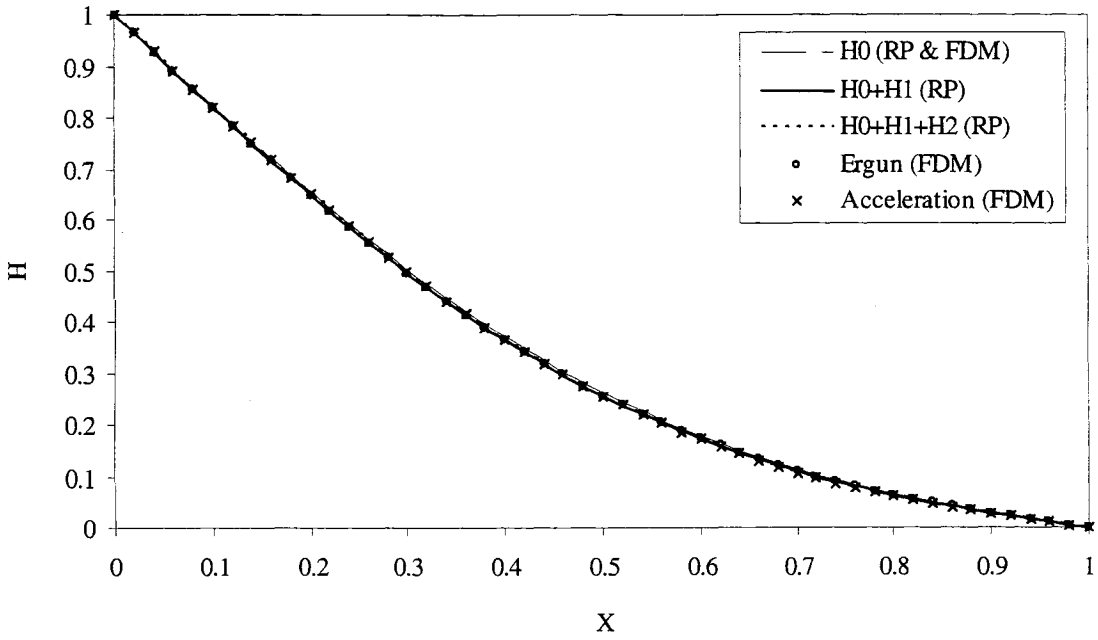

Figure 4.25 Spatial variation of H using explicit FDM and RP (i = 0.1 and τ = 0.1).

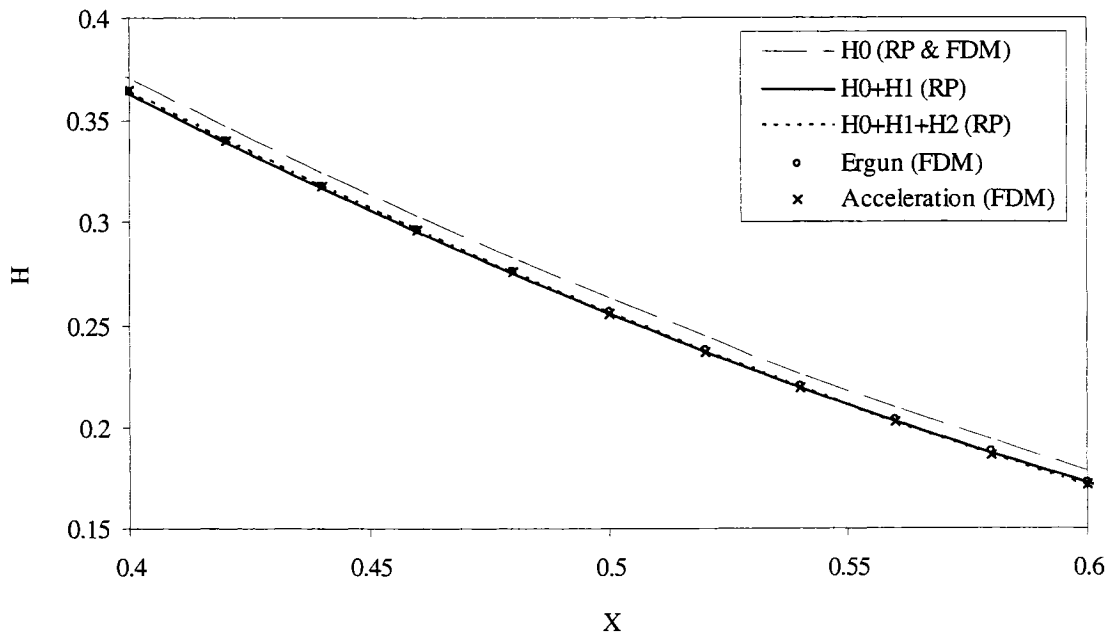

Figure 4.26 Close-up of spatial range, $0.4 \leq X \leq 0.6$.

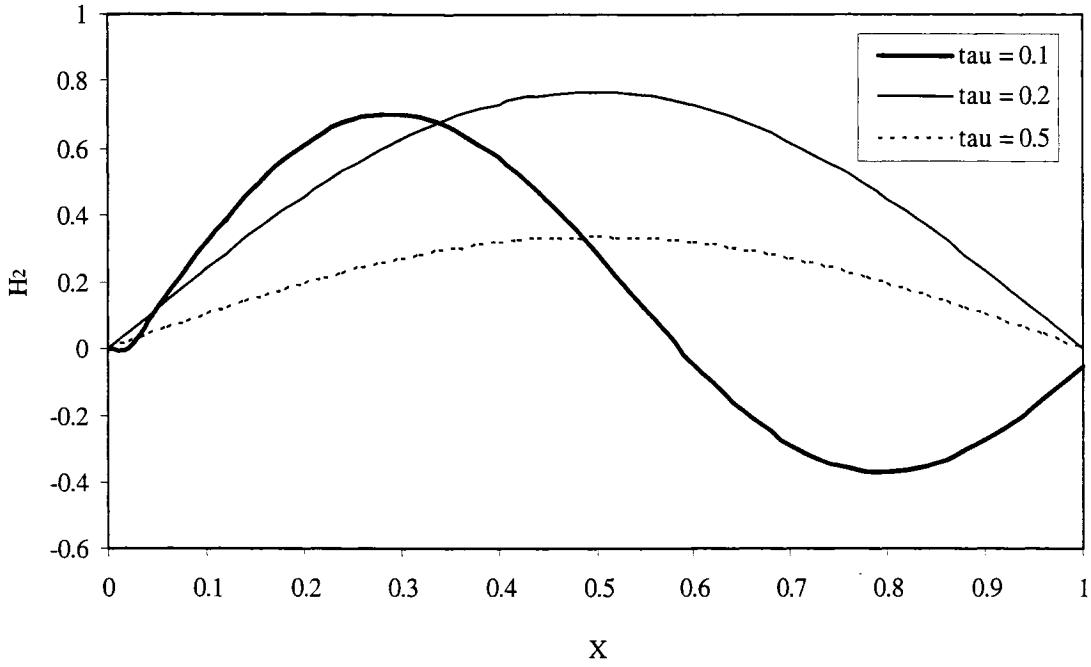

Figure 4.27 Spatial variation of H_2 (local acceleration effect, i = 0.1).

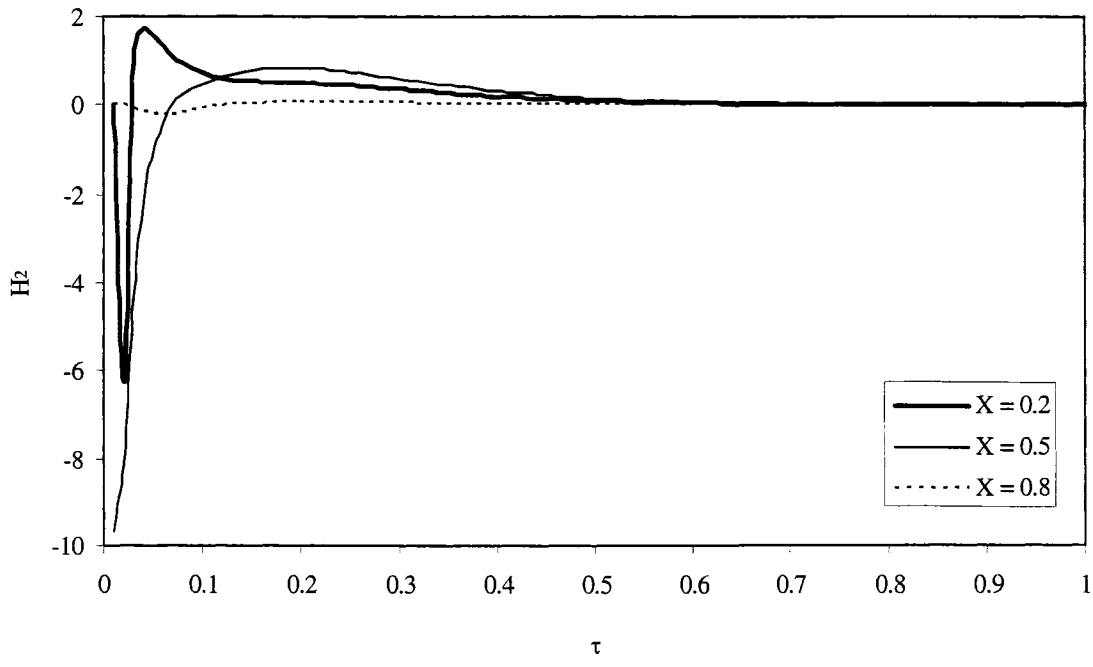

Figure 4.28 Temporal variation of H_2 (local acceleration effect, i = 0.1).

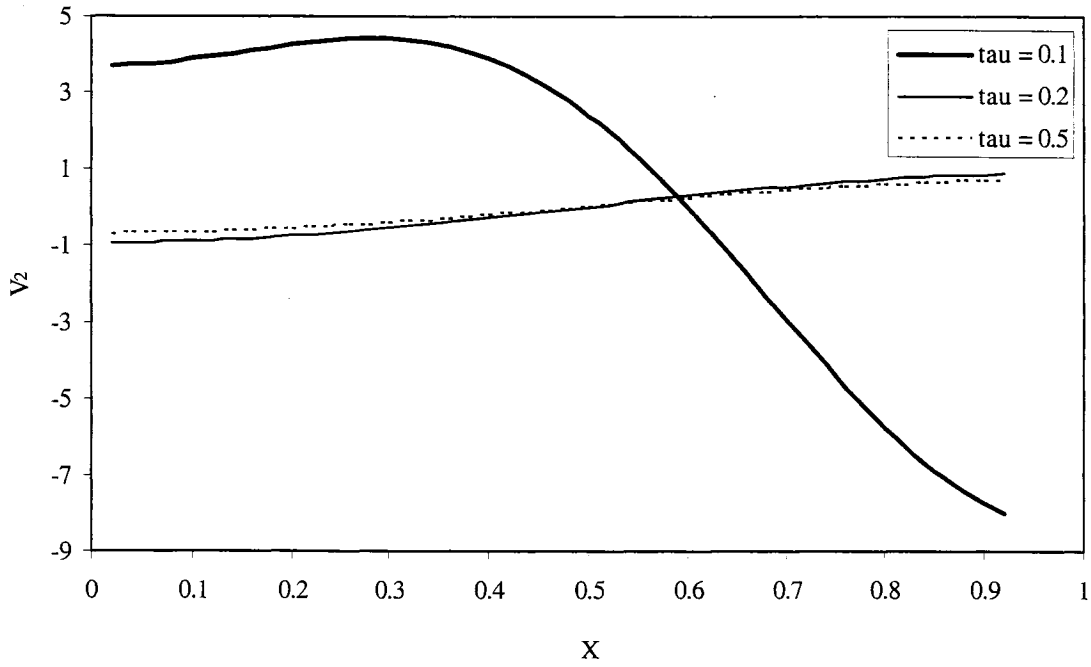

Figure 4.29 Spatial variation of V_2 (local acceleration effect, i = 0.1).

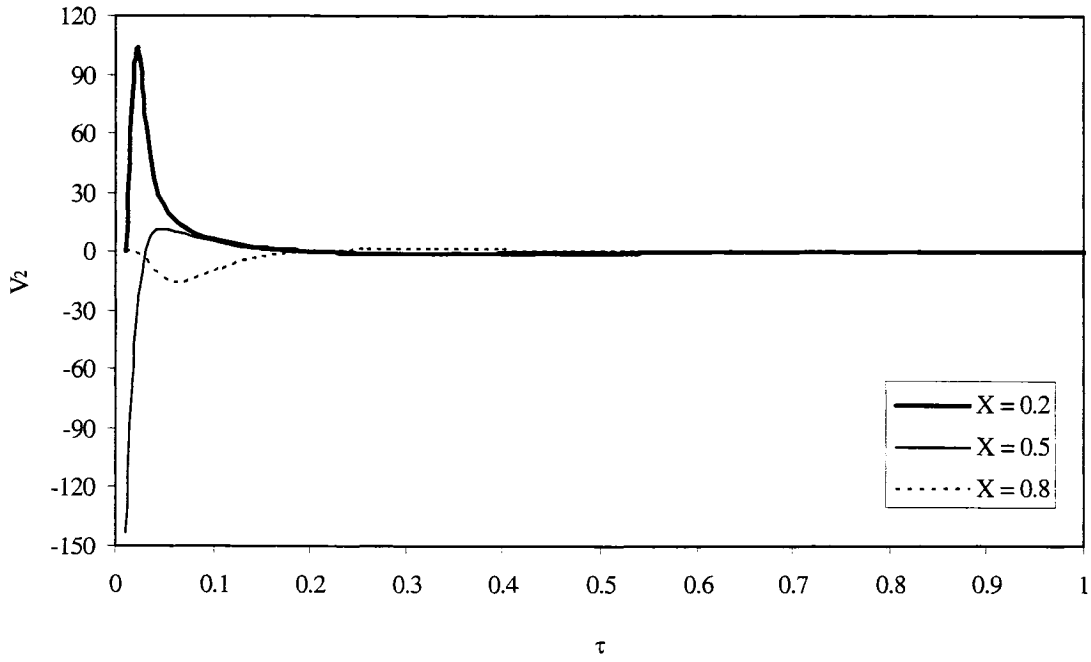

Figure 4.30 Temporal variation of V_2 (local acceleration effect, i = 0.1).

summarize the effect of H_2 on the propagation of head as follows:

(1) as time increases, H_2 (and therefore V_2) approach to zero. The local acceleration term can increase or decrease H (and V) depending on time and location.

(2) as time increases, H_2 and V_2 approach to zero.

(3) H_2 obviously has fixed boundary values as set by the boundary conditions, but V_2 has variable boundary values.

(4) positive V_2 in small τ and X can be explained by the concept of an evolving wave.

(iv) Convective Acceleration Effect

The convective acceleration effect was investigated using H_3 and V_3 (eqn [4-37] and eqn [4-38]). The regular perturbation solutions for H and V including viscous, inertial, local acceleration, and convective acceleration term, were obtained using $H = H_0 + \varepsilon H_1 + \delta H_2 + \gamma H_3$ and $V = V_0 + \varepsilon V_1 + \delta V_2 + \gamma V_3$. Figures 4.31and 4.32 show the spatial and temporal variation in H_3. Figure 4.31 shows all positive values of H_3 at all three stated times thus the convective acceleration term always increases head at any given location and time. Figure 4.32 shows that H_3 is large at small time and space and it becomes close to zero as time increases. The overall effect of H_3 on the propagation of H can be obtained by multiplying γ and H_3. Figures 4.33 and 4.34 show the spatial and temporal variation in V_3. V_3 shows some positive and some negative values at all three stated times. Figure 4.34 shows that V_3 can be maximized at small values of τ and become close to zero as time increases. We may summarize the effect of H_3 on the propagation of head as follows:

(1) convective acceleration term increases H for all given times and locations.

(2) convective acceleration term can increase or decrease V depending on the time and location.

(3) as time increases H_2 and V_2 approach to zero.

(v) Advective Acceleration Effect

The advective acceleration effect was investigated using H_4 and V_4 (eqns [4-40] and [4-51]). The regular perturbation solutions of H and V including viscous,

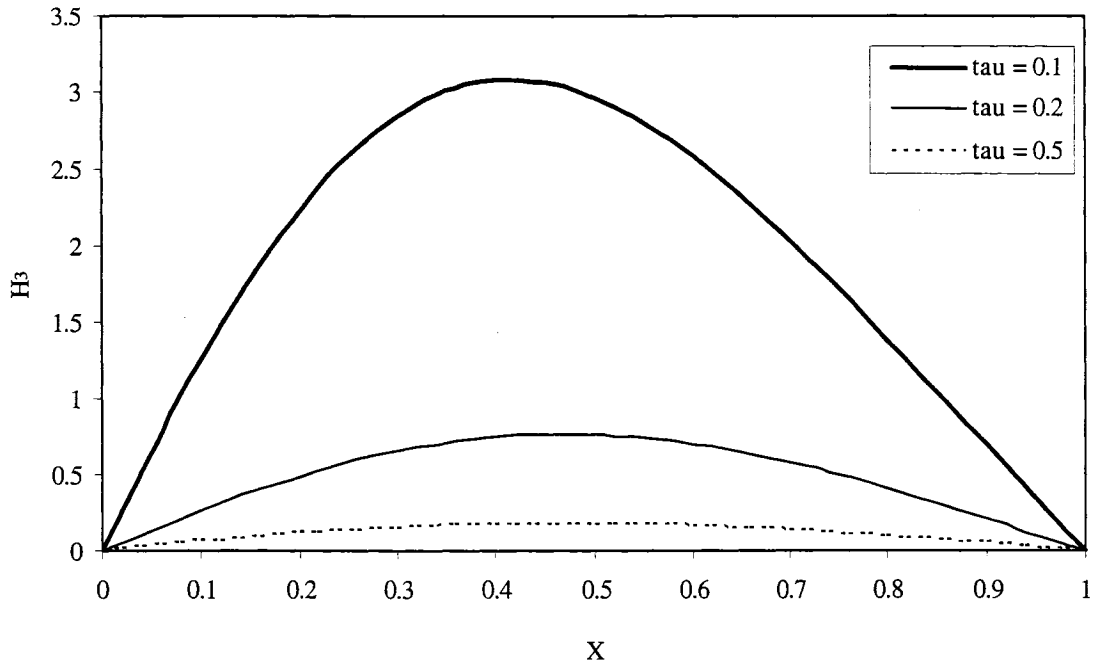

Figure 4.31 Spatial variation of H_3 (convective acceleration effect, i = 0.1).

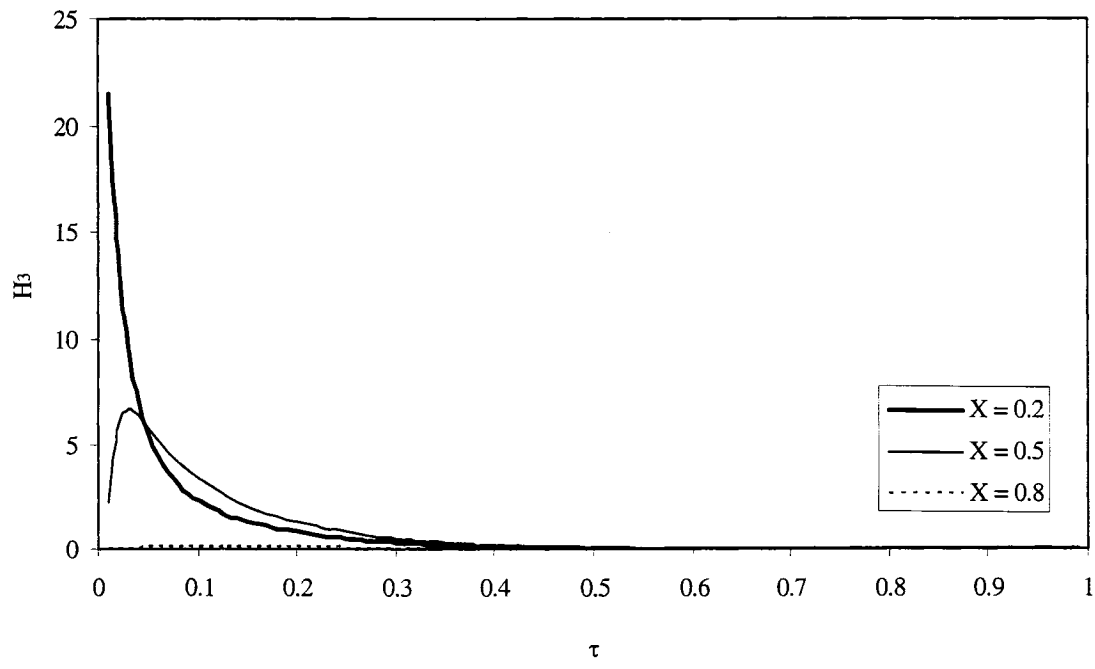

Figure 4.32 Temporal variation of H_3 (convective acceleration effect, i = 0.1).

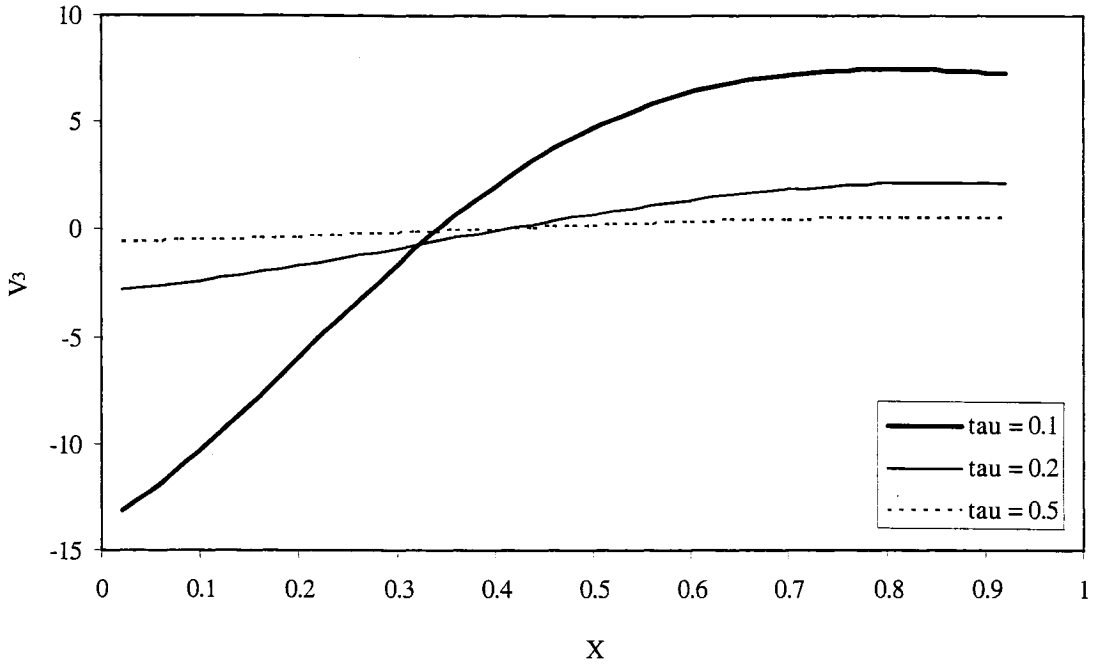

Figure 4.33 Spatial variation of V_3 (convective acceleration effect, i = 0.1).

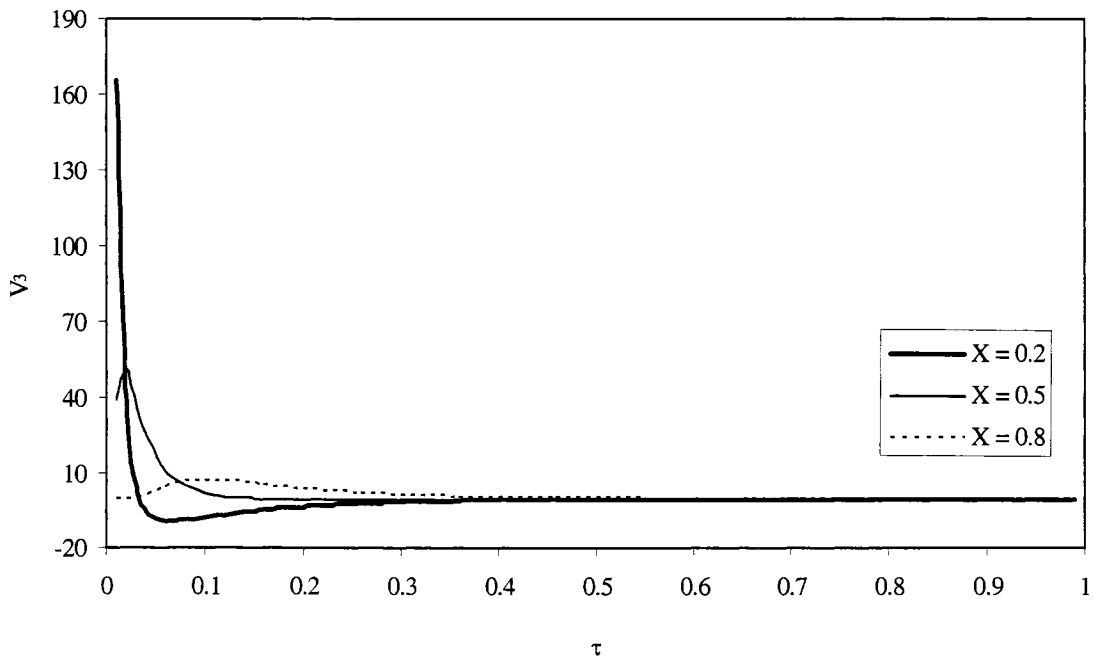

Figure 4.34 Temporal variation of V_3 (convective acceleration effect, i = 0.1).

inertial, local acceleration, convective acceleration and advective acceleration term, were obtained using $H = H_0 + \varepsilon H_1 + \delta H_2 + \gamma H_3 + \xi H_4$ and $V = V_0 + \varepsilon V_1 + \delta V_2 + \gamma V_3 + \xi V_4$. Figures 4.35 and 4.36 show the spatial and temporal variation in H_4. Figure 4.35 shows all positive values of H_4 at all three stated times thus the advective acceleration term always increases head at any location and time. Figure 4.36 shows that H_4 does not become close to zero as time increases. The overall effect of H_4 on the propagation of H can be obtained by multiplying ξ and H_4. Figures 4.37 and 4.38 show the spatial and temporal variation in V_4. V_4 shows some positive and some negative values at all three stated times. V_4 almost linearly increases as X increases when $\tau = 0.2$ and 0.5. Figure 4.38 shows that V_4 decreases as time increases at small X ($X = 0.2$); however, it increases as time increases at large X ($X = 0.8$). We may summarize the effect of H_3 on the propagation of H as follows:

(1) the advective acceleration term increases H at all stated times and locations.

(2) the advective acceleration term can increase or decrease V depending on time and location.

(3) H_4 does not approach to zero as time increases.

(4) the magnitude of H_4 is relatively small compared with H_1, H_2 and H_3, and V_4 also shows small magnitude compared with V_1, V_2, and V_3.

(vi) Elevation Head Effect

The elevation head effect was investigated using H_5 and V_5 (eqn [4-43] and eqn [4-44]). The regular perturbation solutions of H and V including viscous, inertial, local acceleration, convective acceleration, advective acceleration and elevation head term, were obtained using $H = H_0 + \varepsilon H_1 + \delta H_2 + \gamma H_3 + \xi H_4 + \omega H_5$ and $V = V_0 + \varepsilon V_1 + \delta V_2 + \gamma V_3 + \xi V_4 + \omega V_5$. Figures 4.39 and 4.40 show the spatial and temporal variation in H_5. Figure 4.39 shows that H_5 is negative at all three stated times. The absolute value of the minimum H_5 at a given time increases as time increases. The convective acceleration term always decreases head at any location and time. Figure 4.40 shows that the effect of H_5 does not become close to zero as time increases. The overall effect of H_5 on the

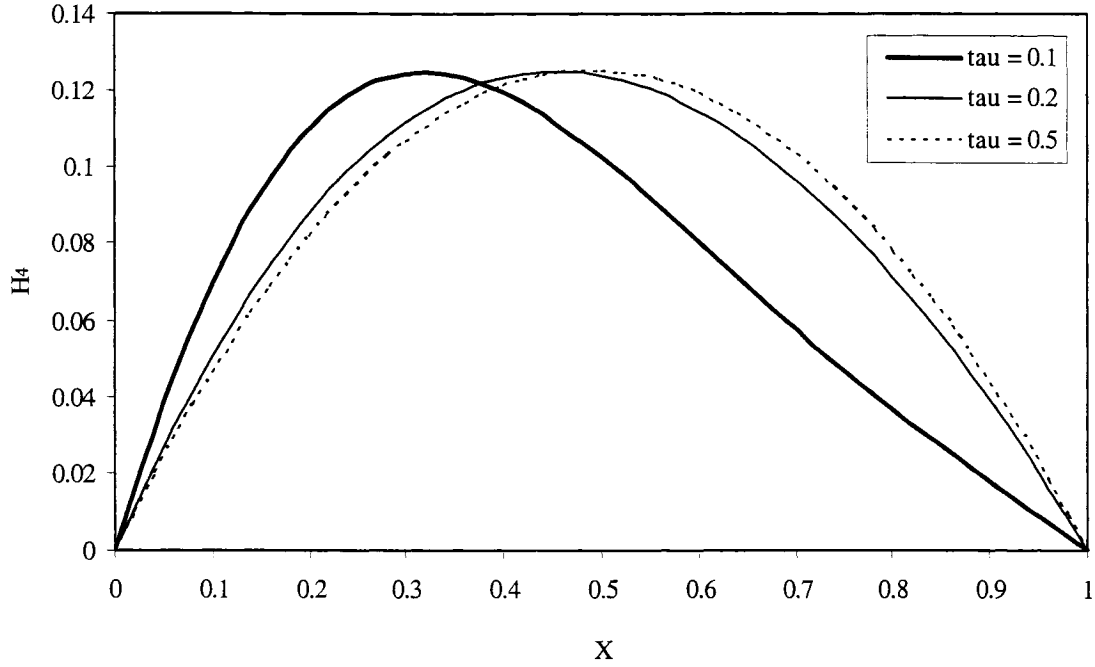

Figure 4.35 Spatial variation of H_4 (advective acceleration effect, i = 0.1).

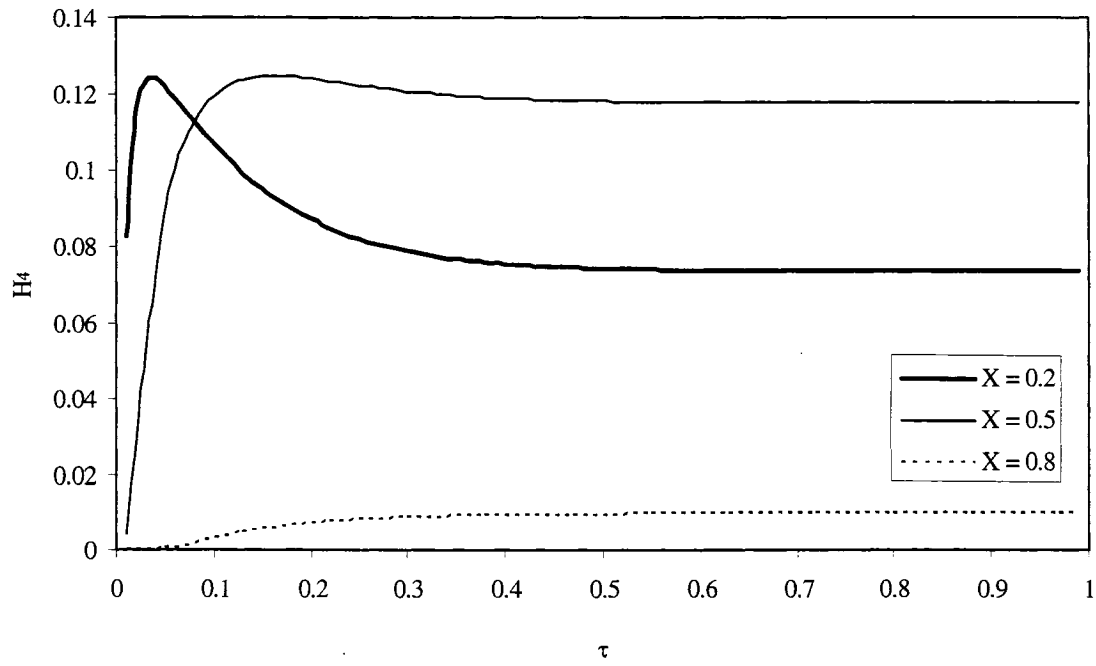

Figure 4.36 Temporal variation of H_4 (advective acceleration effect, i = 0.1).

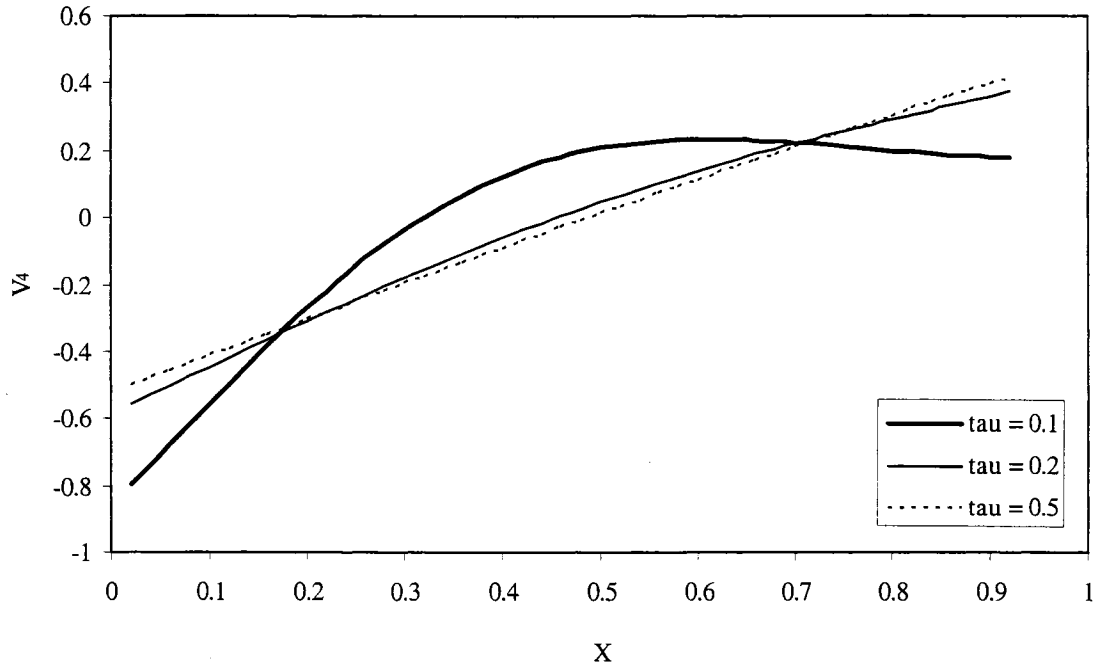

Figure 4.37 Spatial variation of V_4 (advective acceleration effect, i = 0.1).

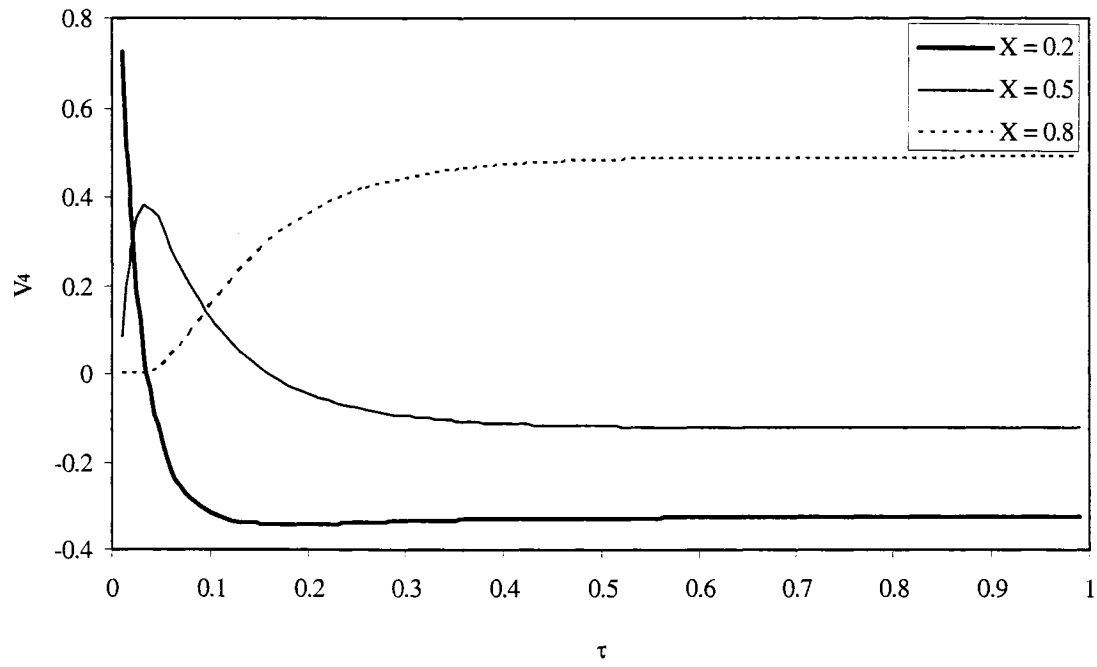

Figure 4.38 Temporal variation of V_4 (advective acceleration effect, i = 0.1).

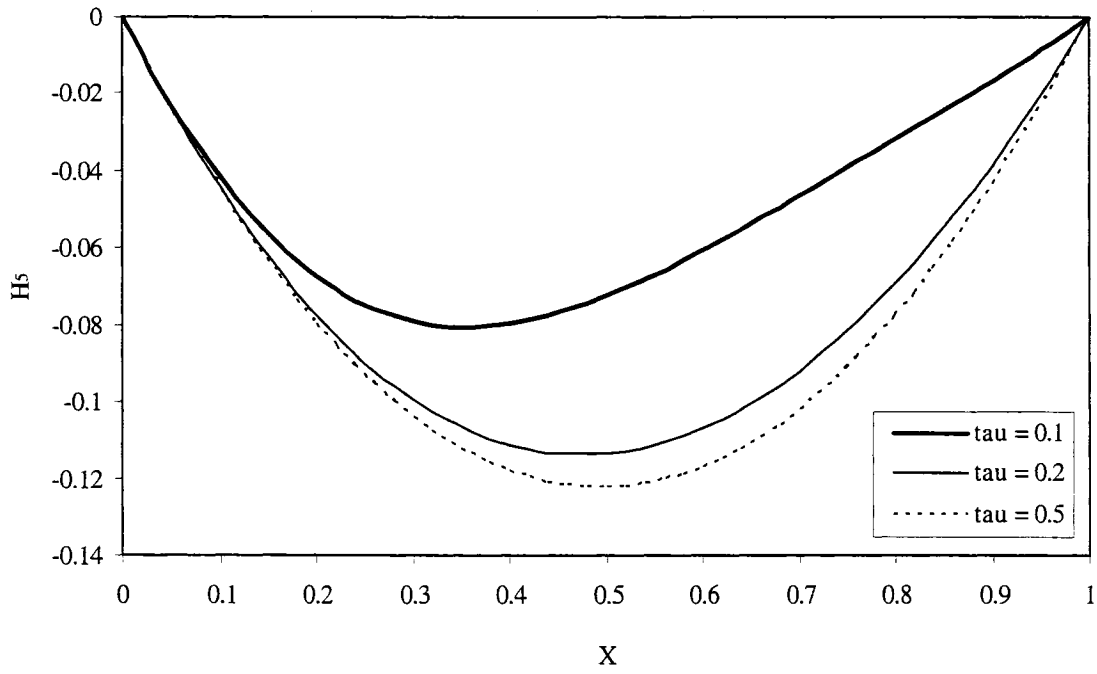

Figure 4.39 Spatial variation of H_5 (elevation head effect, i = 0.1).

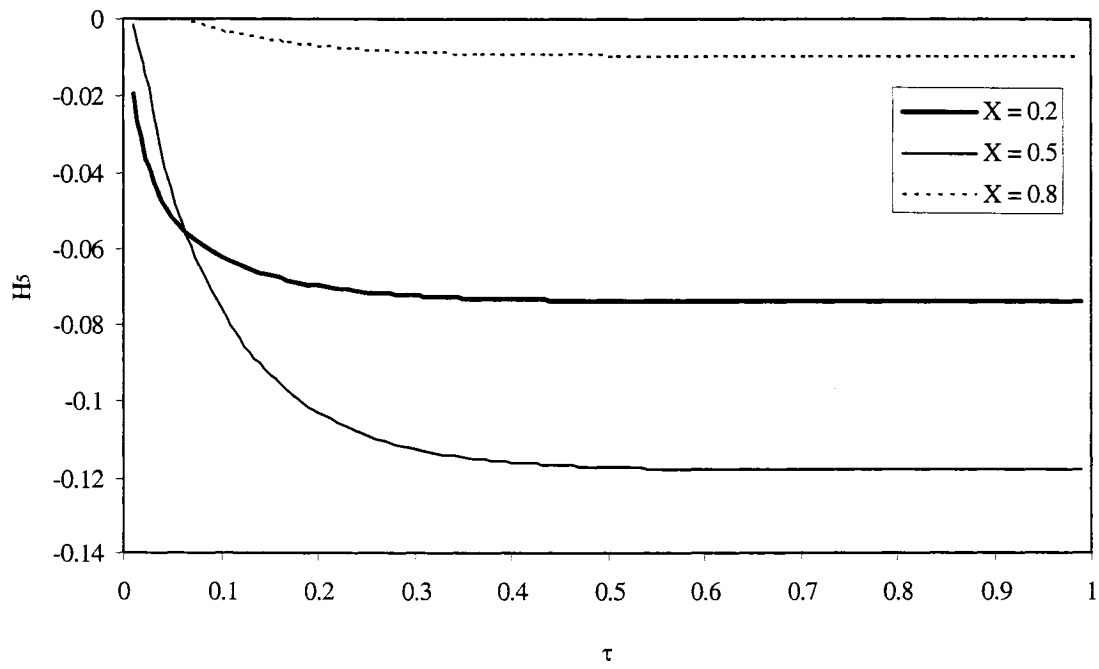

Figure 4.40 Temporal variation of H_5 (elevation head effect, i = 0.1).

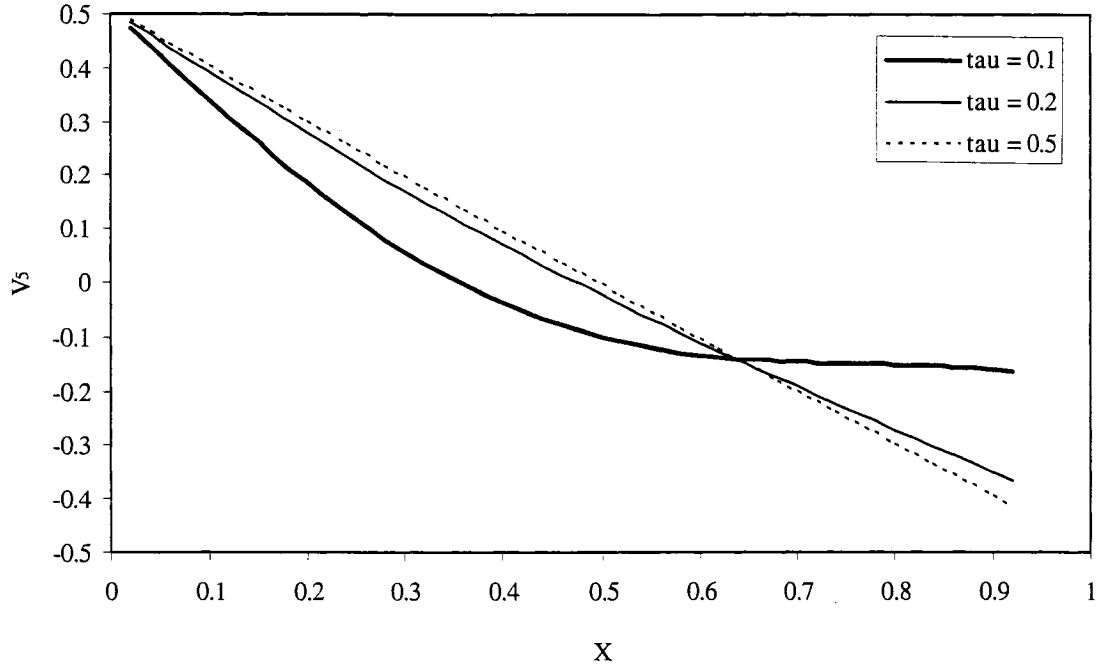

Figure 4.41 Spatial variation of V_5 (elevation head effect, i = 0.1).

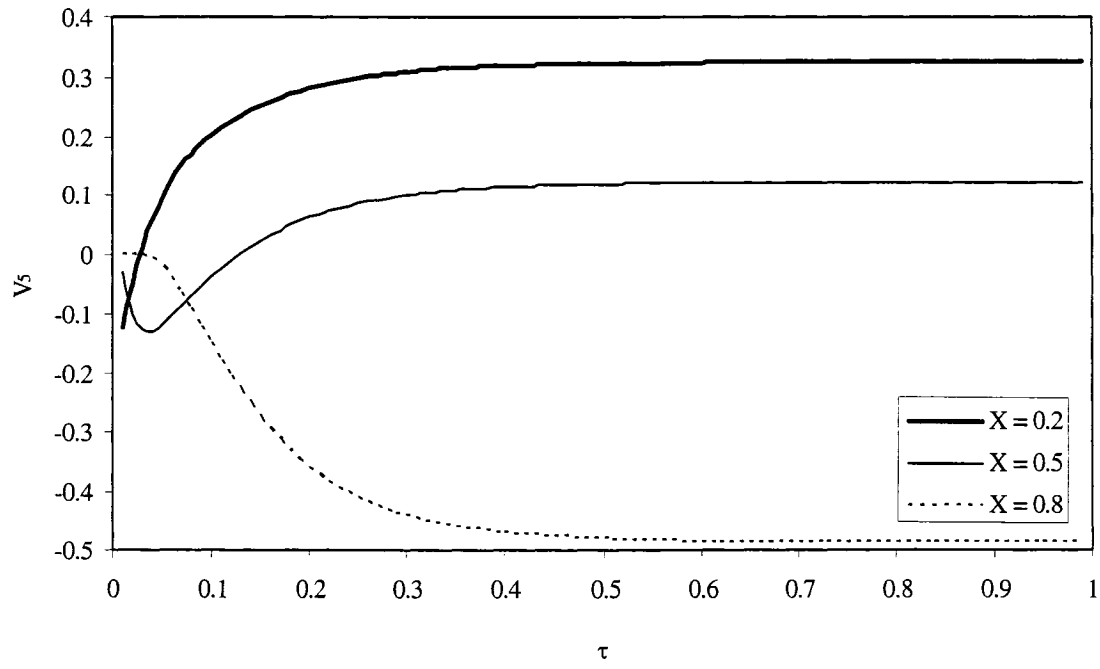

Figure 4.42 Temporal variation of V_5 (elevation head effect, i = 0.1).

propagation of H can be obtained by multiplying ω and H_5. Figures 4.41 and 4.42 show the spatial and temporal variation in V_5. Figure 4.41 shows that V_5 almost linearly decreases as X increases when $\tau = 0.2$ and 0.5. Figure 4.42 shows that V_5 approaches to some positive values as time increases at X = 0.2 and 0.5. On the other hand, at X = 0.8, V_5 decreases as time increases and converges to a negative value. We may summarize the effect of H_5 on the propagation of H as follows:

(1) the elevation head term decreases H for all stated times and locations (depending on the slope of the pipe, whether positive or negative).

(2) the elevation head term can increase or decrease V depending on the stated time and location (also depending on the slope of the pipe).

(3) the magnitude of H_5 is relatively small compared with H_1, H_2 and H_3, and V_5 also shows small magnitude compared with V_1, V_2, and V_3

4.2.3. Solutions in PDT and FDT Regime

Boundary and initial conditions are same as those in laminar flow regime. Using the perturbation expansion of H, $H = H_0 + \varepsilon H_1 + \delta H_2 + \gamma H_3 + \xi H_4$ and the boundary condition can be written as follows:

$$H_0(0,\tau) + \varepsilon H_1(0,\tau) + \delta H_2(0,\tau) + \gamma H_3(0,\tau) + \xi H_4(0,\tau) = 1 \qquad [4\text{-}45a]$$

$$H_0(1,\tau) + \varepsilon H_1(1,\tau) + \delta H_2(1,\tau) + \gamma H_3(1,\tau) + \xi H_4(1,\tau) = 0 \qquad [4\text{-}46a]$$

$$H_0(X,0) + \varepsilon H_1(X,0) + \delta H_2(X,0) + \gamma H_3(X,0) + \xi H_4(X,0) = 0 \qquad [4\text{-}47a]$$

(i) Solutions of H_0 and V_0

The boundary and initial conditions applied to H_0 can be obtained from eqn [4-45a], [4-46a] and [4-47a] and they are:

$$H_0 = 1 \text{ at } X = 0 \qquad [4\text{-}45b]$$

$$H_0 = 0 \text{ at } X = 1 \qquad [4\text{-}46b]$$

$$H_0 = 0 \text{ at } \tau = 0 \qquad [4\text{-}47b]$$

If we recall equation of H_0:

$$H_{0xx} = -\frac{\sqrt{C_3^{\,2} - 4C_1C_4H_{0x}}}{C_1}H_{0\tau} \qquad [3\text{-}119d]$$

An explicit finite-difference form of eqn [3-119a], with a backward difference in time and a central difference in space, is:

$$\frac{\left(H_{0i+1}^{k-1} - 2H_{0i}^{k-1} + H_{0i-1}^{k-1}\right)}{\Delta X^2} = \frac{\sqrt{C_3^{\,2} - 4C_1C_4\dfrac{H_{0i+1}^{k-1} - H_{0i-1}^{k-1}}{2\Delta X}}}{C_1}\frac{H_{0i}^{k} - H_{0i}^{k-1}}{\Delta\tau} \qquad [4\text{-}48]$$

By re-arrangement:

$$H_{0i}^{k} = \frac{\Delta\tau C_1}{\sqrt{C_3^{\,2} - 4C_1C_4\dfrac{H_{0i+1}^{k-1} - H_{0i-1}^{k-1}}{2\Delta X}}}\frac{\left(H_{0i+1}^{k-1} - 2H_{0i}^{k-1} + H_{0i-1}^{k-1}\right)}{\Delta X^2} + H_{0i}^{k-1} \qquad [4\text{-}49]$$

The V_0 may then be obtained from the explicit finite-difference solution of Ergun equation:

$$V_{0i}^{k} = \frac{-C_3 + \sqrt{C_3^{\,2} - 4C_1C_4\dfrac{H_{0i+1}^{k} - H_{0i-1}^{k}}{2\Delta X}}}{2C_4} \qquad [4\text{-}50]$$

(ii) Solutions of H_1 and V_1

The boundary and initial conditions for H_1 can be obtained from eqn [4-45a], [4-46a] and [4-47a] and they are:

$$H_1 = 0 \text{ at } X = 0 \qquad [4\text{-}45c]$$

$$H_1 = 0 \text{ at } X = 1 \qquad [4\text{-}46c]$$

$$H_1 = 0 \text{ at } \tau = 0 \qquad [4\text{-}47c]$$

In order to get finite difference form of eqn [3-121], the equation is re-arranged for $H_{1\tau}$:

$$H_{1\tau} = \frac{C_1}{C_3 + 2C_4V_0}H_{1XX} + \frac{C_1}{C_3 + 2C_4V_0}V_{0\tau X}$$

$$-\frac{2C_4}{C_1}\left(\frac{C_1}{C_3+2C_4V_0}\right)^2(H_{1X}+V_{0\tau})V_{0X} \qquad [4\text{-}51]$$

An explicit finite-difference form of eqn [4-51], using a backward difference in time and a central difference in space, is:

$$H_{1i}^k = \frac{\Delta\tau C_1}{C_3+2C_4V_{0i}^k}\frac{\left(H_{1i+1}^{k-1}-2H_{1i}^{k-1}+H_{1i-1}^{k-1}\right)}{\Delta X^2}$$

$$+\frac{C_1}{C_3+2C_4V_{0i}^k}\frac{V_{0i+1}^k-V_{0i+1}^{k-1}-V_{0i-1}^k+V_{0i-1}^{k-1}}{2\Delta X}$$

$$-\frac{2\Delta\tau C_1C_4}{\left(C_3+2C_4V_{0i}^k\right)^2}\left(\frac{H_{1i+1}^{k-1}-H_{1i-1}^{k-1}}{2\Delta X}+\frac{V_{0i}^k-V_{0i}^{k-1}}{\Delta\tau}\right)\left(\frac{V_{0i+1}^k-V_{0i-1}^k}{2\Delta X}\right)+H_{1i}^{k-1} \qquad [4\text{-}52]$$

Using eqn [3-120d], the dimensionless velocity, V_{1i}^k, becomes:

$$V_{1i}^k = -\frac{C_1}{C_3+2C_4V_{0i}^k}\left(\frac{H_{1i+1}^k-H_{1i-1}^k}{2\Delta X}+\frac{V_{0i}^k-V_{0i}^{k-1}}{\Delta\tau}\right) \qquad [4\text{-}53]$$

(iii) Solutions of H_2 and V_2

The boundary and initial conditions for H_2 can be obtained from eqn [4-45a], [4-46a] and [4-47a] and they are:

$$H_2 = 0 \text{ at } X = 0 \qquad [4\text{-}45d]$$

$$H_2 = 0 \text{ at } X = 1 \qquad [4\text{-}46d]$$

$$H_2 = 0 \text{ at } \tau = 0 \qquad [4\text{-}47d]$$

Re-arrangement of eqn [3-122f] gives:

$$H_{2\tau} = \frac{C_1}{C_3+2C_4V_0}H_{2XX}+\frac{C_1}{C_3+2C_4V_0}\left((V_{0X})^2-V_0V_{0XX}\right)$$

$$-\frac{2C_4}{C_1}\left(\frac{C_1}{C_3+2C_4V_0}\right)^2(H_{2X}+V_0V_{0X})V_{0X} \qquad [4\text{-}54]$$

An explicit finite-difference form of eqn [4-54], using a backward difference in time and a central difference in space, is:

$$H_{2i}^{k} = \frac{\Delta\tau C_1}{C_3 + 2C_4 V_{0i}^{k}} \frac{\left(H_{2i+1}^{k-1} - 2H_{2i}^{k-1} + H_{2i-1}^{k-1}\right)}{\Delta X^2}$$

$$+ \frac{C_1 \Delta\tau}{C_3 + 2C_4 V_{0i}^{k}} \left(\left(\frac{H_{0i+1}^{k} - H_{0i-1}^{k-1}}{\Delta\tau} \right)^2 - V_{0i}^{k} \left(\frac{H_{0i+1}^{k} - H_{0i+1}^{k-1} - H_{0i-1}^{k} + H_{0i-1}^{k-1}}{2\Delta X \Delta\tau} \right) \right)$$

$$- \frac{2\Delta\tau C_1 C_4}{\left(C_3 + 2C_4 V_{0i}^{k}\right)^2} \left(\frac{H_{2i+1}^{k-1} - H_{2i-1}^{k-1}}{2\Delta X} + V_{0i}^{k} \frac{H_{0i}^{k} - H_{0i}^{k-1}}{\Delta\tau} \right) \left(\frac{H_{0i}^{k} - H_{0i}^{k-1}}{\Delta\tau} \right) + H_{2i}^{k-1} \qquad [4\text{-}55]$$

Using eqn [3-122d] and $V_{0X} = -H_{0\tau}$, the dimensionless velocity, V_{2i}^{k}, is then:

$$V_{2i}^{k} = -\frac{C_1}{C_3 + 2C_4 V_{0i}^{k}} \left(\frac{H_{2i+1}^{k} - H_{2i-1}^{k}}{2\Delta X} + V_{0i}^{k} \left(-\frac{H_{0i}^{k} - V_{0i}^{k-1}}{\Delta\tau} \right) \right) \qquad [4\text{-}56]$$

(iv) Solutions of H_3 and V_3

The boundary and initial conditions for H_3 can be obtained from eqn [4-45a], [4-46a] and [4-47a] and they are:

$$H_3 = 0 \text{ at } X = 0 \qquad [4\text{-}45e]$$

$$H_3 = 0 \text{ at } X = 1 \qquad [4\text{-}46e]$$

$$H_3 = 0 \text{ at } \tau = 0 \qquad [4\text{-}47e]$$

Re-arrangement of eqn [3-123f] gives:

$$H_{3\tau} = \frac{C_1}{C_3 + 2C_4 V_0} H_{3XX} - V_0 H_{0X} - \frac{2C_4}{C_1} \left(\frac{C_1}{C_3 + 2C_4 V_0} \right)^2 H_{3X} V_{0X} \qquad [4\text{-}57]$$

An explicit finite-difference form of eqn [4-57], using a backward difference in time and a central difference in space, is:

$$H_{3i}^{k} = \frac{\Delta\tau C_1}{C_3 + 2C_4 V_{0i}^{k}} \frac{\left(H_{3i+1}^{k-1} - 2H_{3i}^{k-1} + H_{3i-1}^{k-1}\right)}{\Delta X^2} - \Delta\tau V_{0i}^{k} \left(\frac{H_{0i+1}^{k} - H_{0i-1}^{k}}{2\Delta X} \right)$$

$$-\frac{2\Delta\tau C_1 C_4}{\left(C_3+2C_4V_{0i}^k\right)^2}\left(\frac{H_{3i+1}^{k-1}-H_{3i-1}^{k-1}}{2\Delta X}\right)\left(-\frac{H_{0i}^k-H_{0i}^{k-1}}{\Delta\tau}\right)+H_{3i}^{k-1} \qquad [4\text{-}58]$$

Using eqn [3-123d], the dimensionless velocity, V_{3i}^k, is then:

$$V_{3i}^k=-\frac{C_1}{C_3+2C_4V_{0i}^k}\left(\frac{H_{3i+1}^k-H_{3i-1}^k}{2\Delta X}\right) \qquad [4\text{-}59]$$

(v) Solutions of H_4 and V_4

The boundary and initial conditions for H_4 can be obtained from eqn [4-45a], [4-46a] and [4-47a] and they are:

$$H_4=0 \text{ at } X=0 \qquad [4\text{-}45f]$$

$$H_4=0 \text{ at } X=1 \qquad [4\text{-}46f]$$

$$H_4=0 \text{ at } \tau=0 \qquad [4\text{-}47f]$$

Re-arrangement of eqn [3-124e] gives:

$$H_{4\tau}=\frac{C_1}{C_3+2C_4V_0}H_{4XX}-V_0-\frac{2C_4}{C_1}\left(\frac{C_1}{C_3+2C_4V_0}\right)^2H_{4X}V_{0X} \qquad [4\text{-}60]$$

An explicit finite-difference form of eqn [4-60], using a backward difference in time and a central difference in space, is:

$$H_{4i}^k=\frac{\Delta\tau C_1}{C_3+2C_4V_{0i}^k}\frac{\left(H_{4i+1}^{k-1}-2H_{4i}^{k-1}+H_{4i-1}^{k-1}\right)}{\Delta X^2}-\Delta\tau V_{0i}^k$$

$$-\frac{2\Delta\tau C_1 C_4}{\left(C_3+2C_4V_{0i}^k\right)^2}\left(\frac{H_{4i+1}^{k-1}-H_{4i-1}^{k-1}}{2\Delta X}\right)\left(-\frac{H_{0i}^k-H_{0i}^{k-1}}{\Delta\tau}\right)+H_{4i}^{k-1} \qquad [4\text{-}61]$$

The quantity V_{4i}^k may then be found using:

$$V_{4i}^k=-\frac{C_1}{C_3+2C_4V_{0i}^k}\left(\frac{H_{4i+1}^k-H_{4i-1}^k}{2\Delta X}\right) \qquad [4\text{-}62]$$

4.2.4. Effects of Each Term in PDT and FDT Case

The various modelled profiles of H and V in which viscous and/or inertial effects are built-in are similar to those obtained for the simple laminar regime case. The strength of each effect was found to depend on the applied hydraulic gradient, and the point in time and space.

(i) Local Acceleration Effect

The local acceleration effect was investigated using H_1 and V_1. The regular perturbation solutions for H and V that included viscous, inertial and local acceleration term, were obtained using $H = H_0 + \varepsilon H_1$ and $V = V_0 + \varepsilon V_1$. Figure4.43 and 4.44 show the spatial and temporal variation in H_1. From Figure 4.43 shows that H_1 takes on negative values for small τ. As shown for the case of the laminar regime, the effect of local acceleration on H can be positive or negative. The Figure 4.44 shows that H_1 becomes close to zero as time increases. The absolute value of the minimum H_1 is larger than that of the maximum H_1 at any given location. The overall effect of H_1 on H can be obtained by multiplying ε and H_1. Figures 4.45 and 4.46 show the spatial and temporal variation of V_1. The profiles of V_1 are similar to those in laminar regime case. Figure 4.45 shows that V_1 takes on some positive and some negative values at any given time depending on X. Figure 4.46 shows that the magnitude of V_1 is large at small times and becomes close to zero as time increases. Positive values of V_1 at small time and space can be related to the characteristics of the evolving-wave equation.

(ii) Convective Acceleration Effect

The convective acceleration effect was investigated using H_2 and V_2. The regular perturbation solutions for H and V that included viscous, inertial, local acceleration, and convective acceleration term, was obtained using $H = H_0 + \varepsilon H_1 + \delta H_2$ and $V = V_0 + \varepsilon V_1 + \delta V_2$. Figures 4.47 and 4.48 show the spatial and temporal variation of H_2. Figure 4.47 shows all positive values of H_3 at any stated times. Figure 4.48 shows that H_2 is large at small time and space and it approaches to zero as time increases. The overall effect of H_2 on H can be obtained by multiplying δ and H_2. Figures 4.49 and 4.50 show the spatial and temporal variation of V_2. V_2 shows some positive and some negative values at all

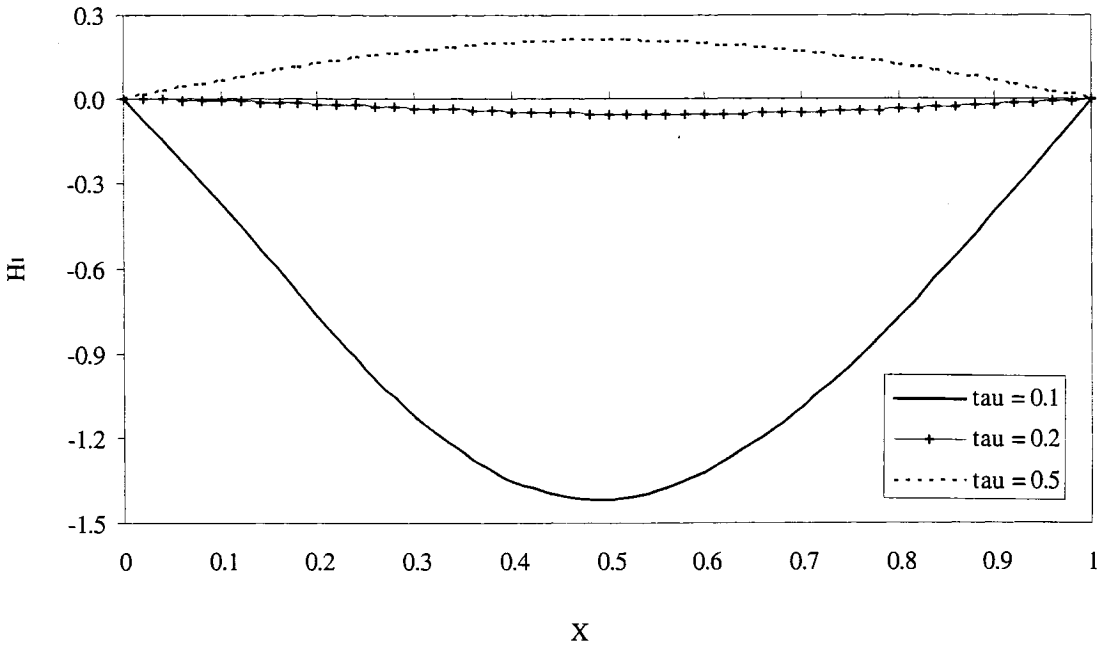

Figure 4.43 Spatial variation of H_1 (local acceleration effect, i = 10).

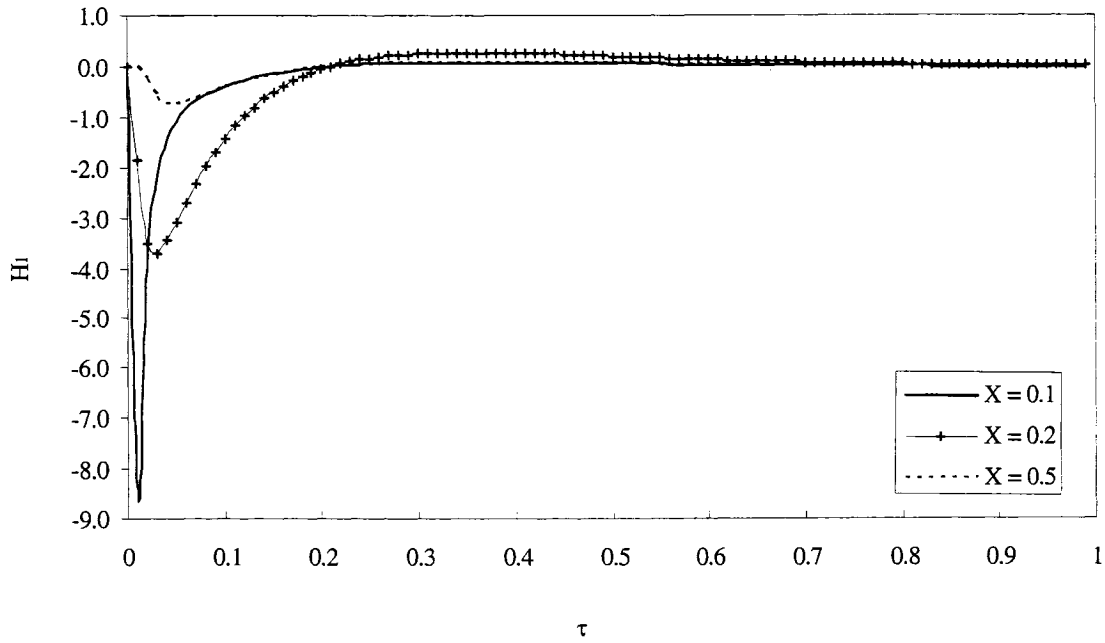

Figure 4.44 Temporal variation of H_1 (local acceleration effect, i = 10).

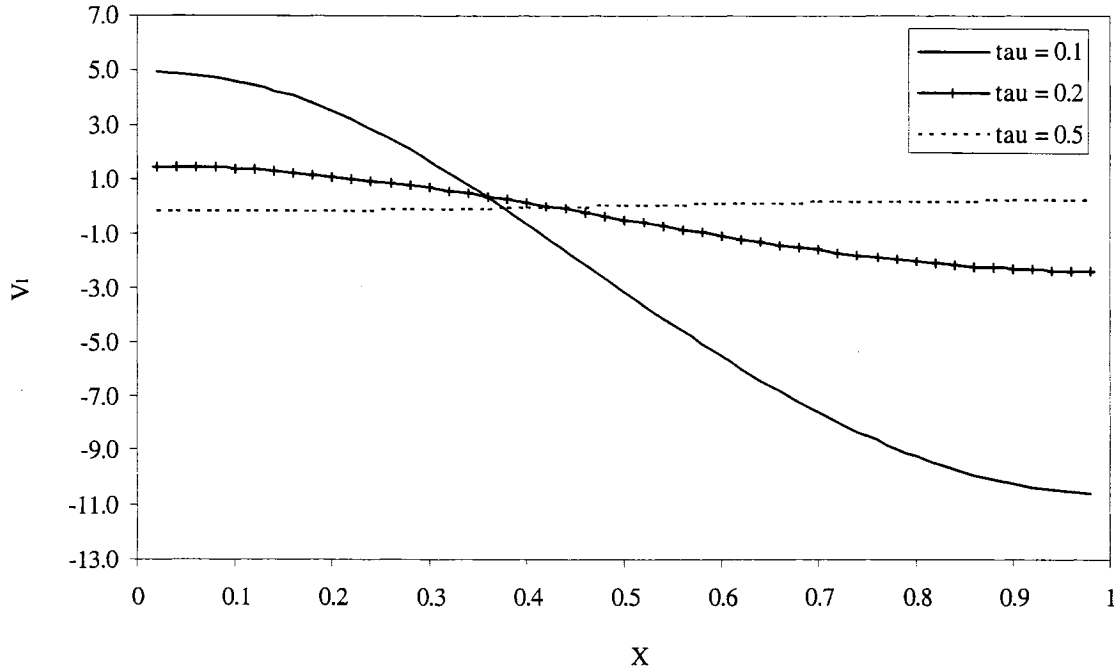

Figure 4.45 Spatial variation of V_1 (local acceleration effect, i = 10).

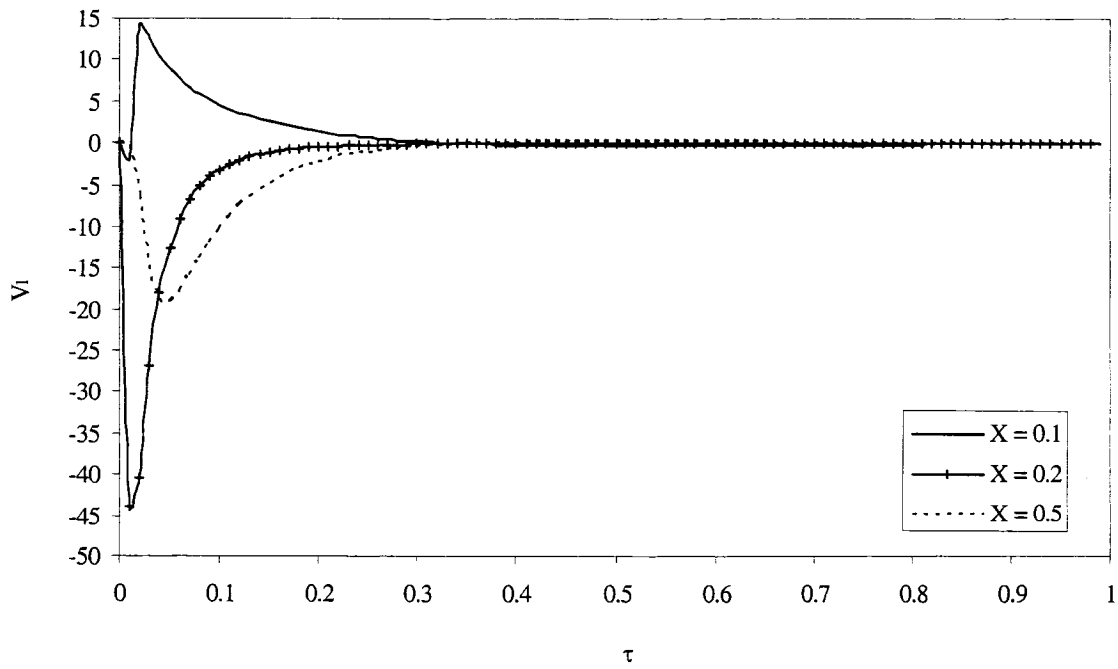

Figure 4.46 Temporal variation of V_1 (local acceleration effect, i = 10).

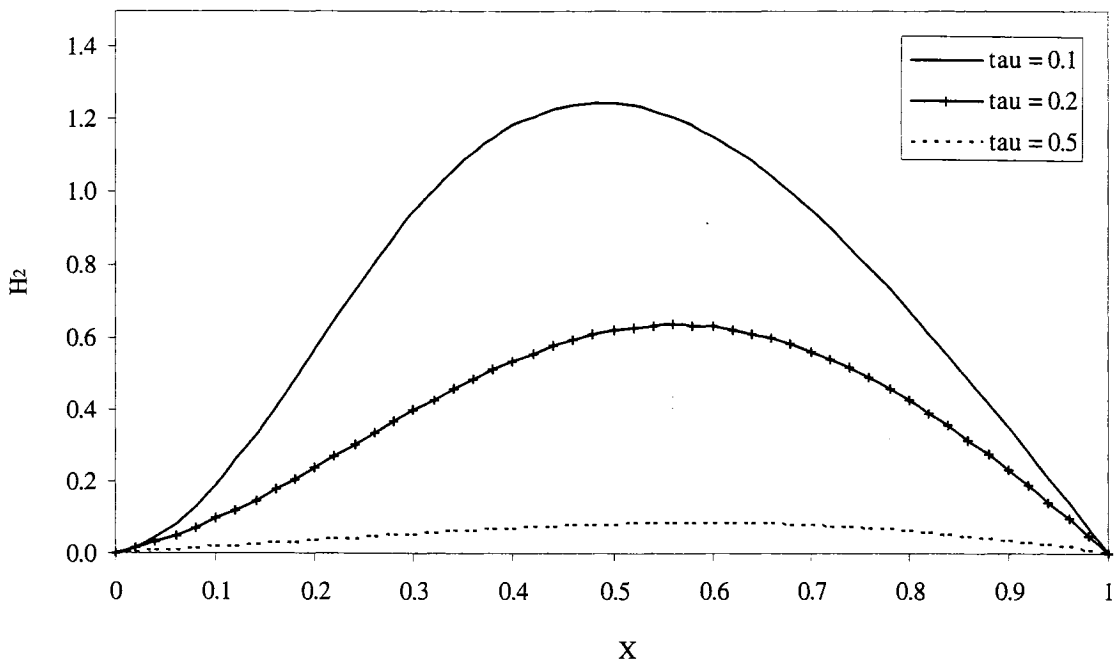

Figure 4.47 Spatial variation of H_2 (convective acceleration effect, i = 10).

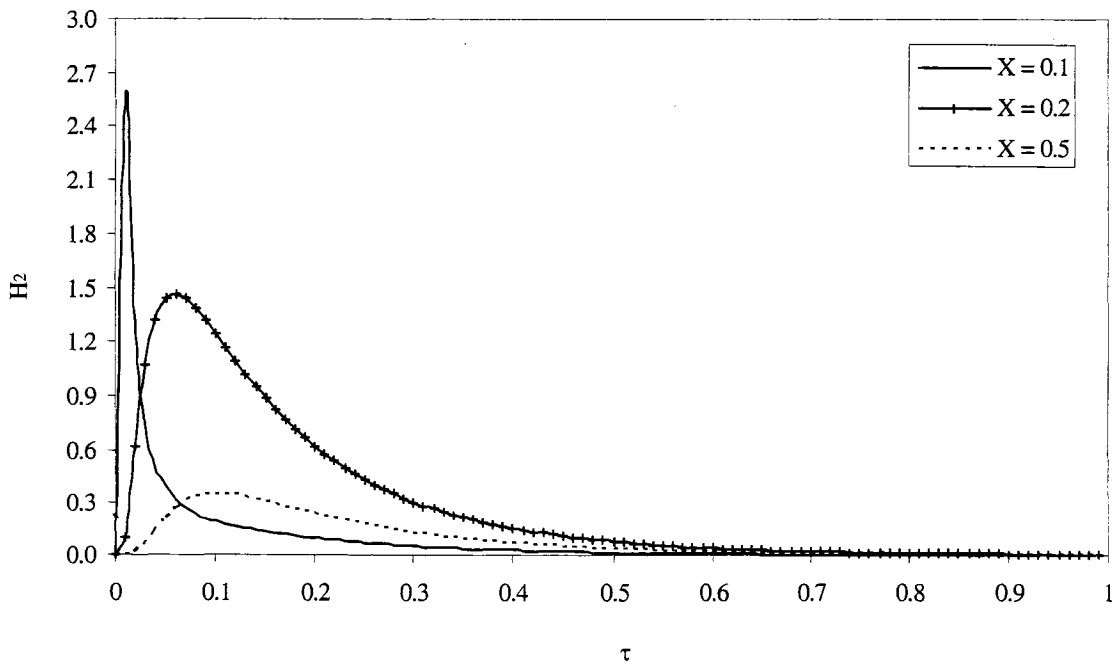

Figure 4.48 Temporal variation of H_2 (convective acceleration effect, i = 10).

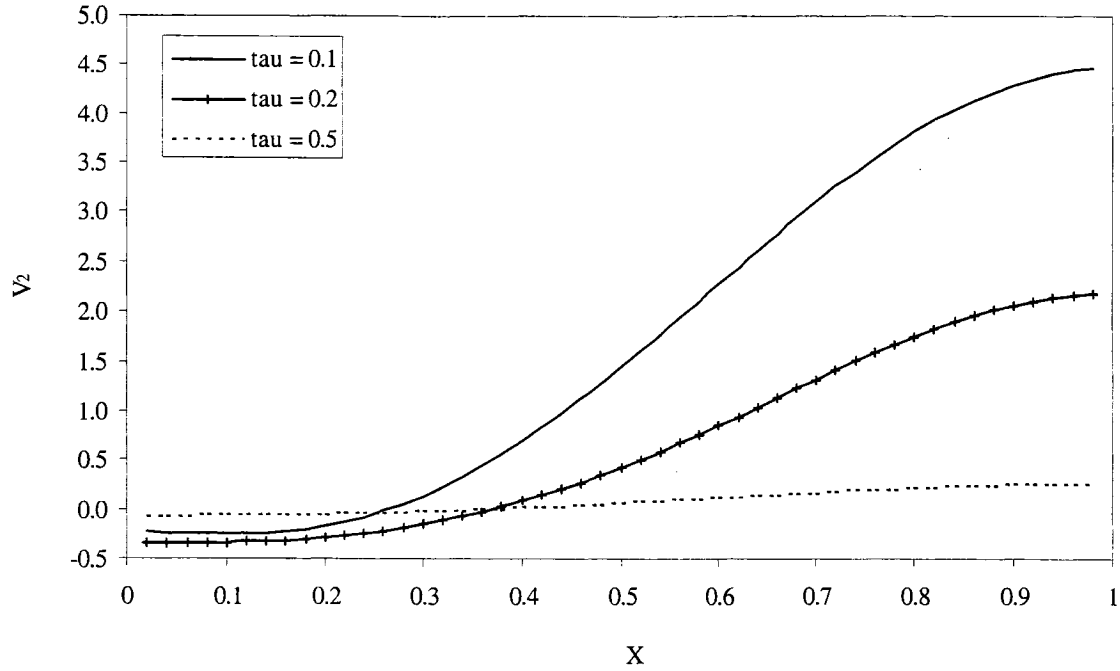

Figure 4.49 Spatial variation of V_2 (convective acceleration effect, i = 10).

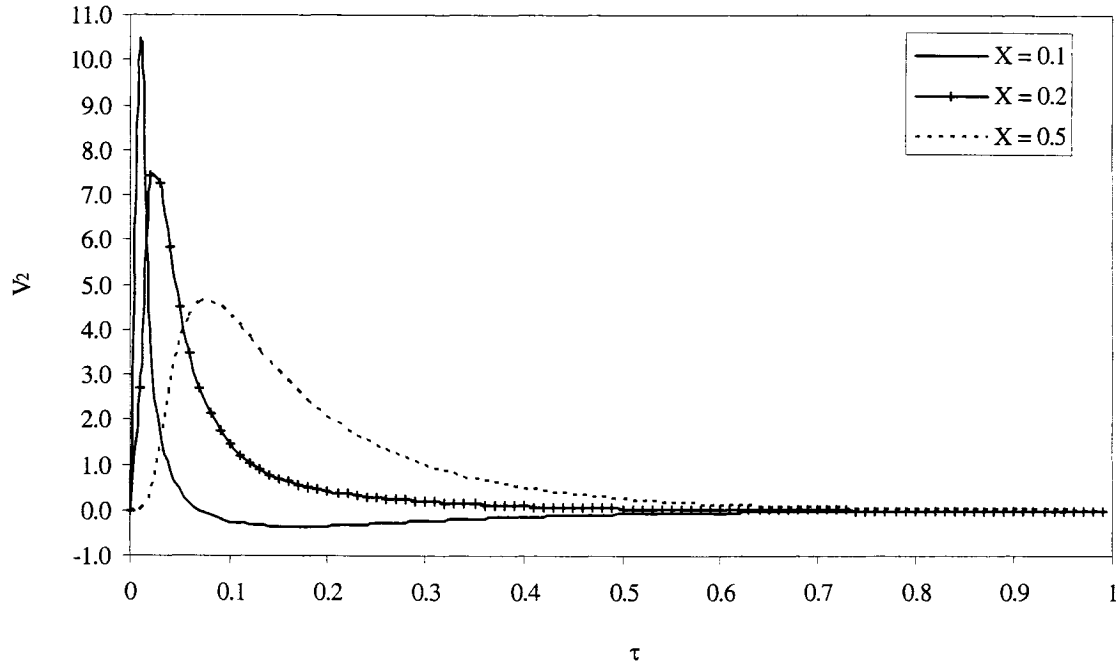

Figure 4.50 Temporal variation of V_2 (convective acceleration effect, i = 10).

three stated times. V_2 increases with respect to X but the maximum value of V_2 decreases as time increases. Figure 4.50 shows that V_2 is maximized at small τ and becomes close to zero as time increases.

(iii) Advective Acceleration Effect

The effects of the advective acceleration was investigated using H_3 and V_3. The regular perturbation solutions for H and V that included viscous, inertial, local acceleration, convective acceleration and advective acceleration term, were obtained using $H = H_0 + \varepsilon H_1 + \delta H_2 + \gamma H_3$ and $V = V_0 + \varepsilon V_1 + \delta V_2 + \gamma V_3$. 4.43 Figures 4.51 and 4.52 show spatial and temporal variation in H_3. The results are similar to those obtained for the laminar regime. The overall effect of H_4 on H can be obtained by multiplying γ and H_3. Figures 4.53 and 4.54 show spatial and temporal variation in V_3. These results are similar to those obtained for the laminar regime case. However, the time and space required to reach a given shape of curve is different from that of laminar regime case. This shows that the general effect of each term is similar but that the time and space needed to achieve a given pattern depends on the applied hydraulic gradient.

(iv) Elevation Head Effect

The effects of elevation head were investigated using the terms H_4 and V_4. The regular perturbation solutions for H and V that included viscous, inertial, local acceleration, convective acceleration, advective acceleration and elevation head effects were obtained using $H = H_0 + \varepsilon H_1 + \delta H_2 + \gamma H_3 + \xi H_4$ and $V = V_0 + \varepsilon V_1 + \delta V_2 + \gamma V_3 + \xi V_4$. Figures 4.55 and 4.56 show the spatial and temporal variation in H_4. The spatial and temporal profile in H_4 show results that are similar to those obtained for the laminar regime case. The overall effect of H_4 on H was obtained by multiplying ξ and H_4. Figures 4.57 and 4.58 show the spatial and temporal variation in V_4. The results are also similar to those obtained for the laminar regime.

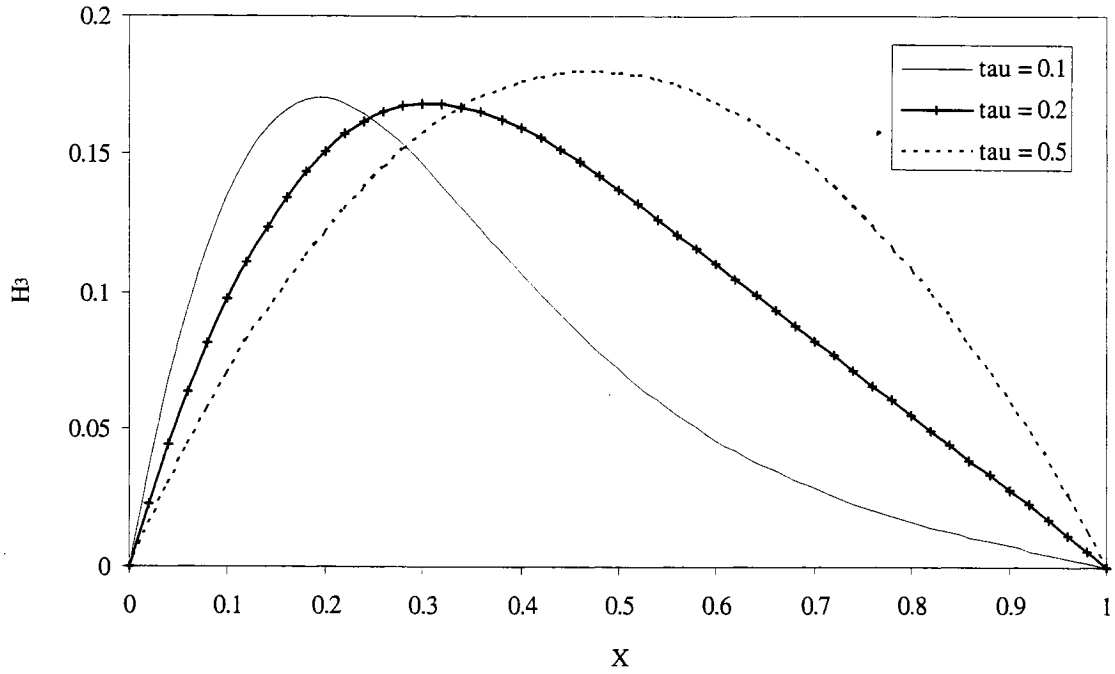

Figure 4.51 Spatial variation of H_3 (advective acceleration effect, i = 10).

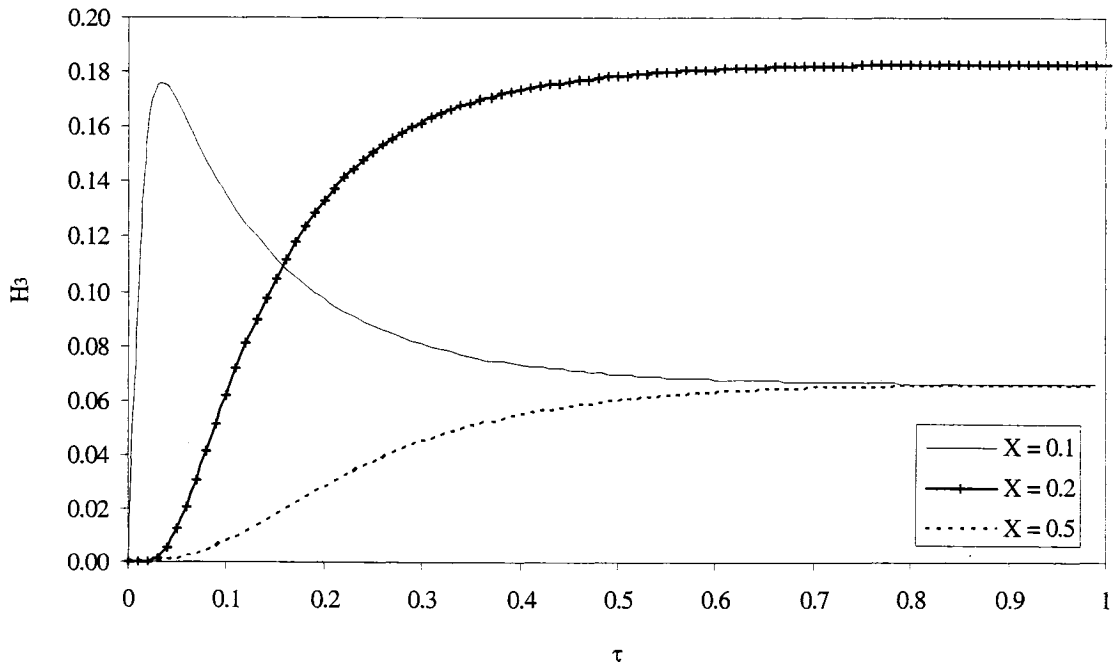

Figure 4.52 Temporal variation of H_3 (advective acceleration effect, i = 10).

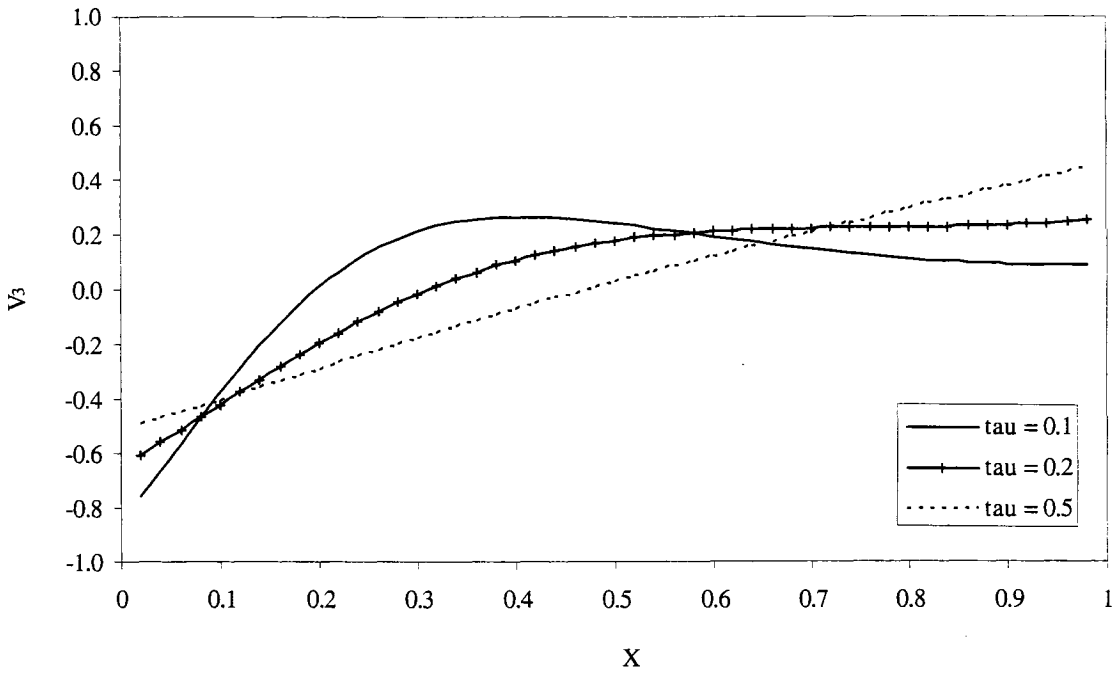

Figure 4.53 Spatial variation of V_3 (advective acceleration effect, i = 10).

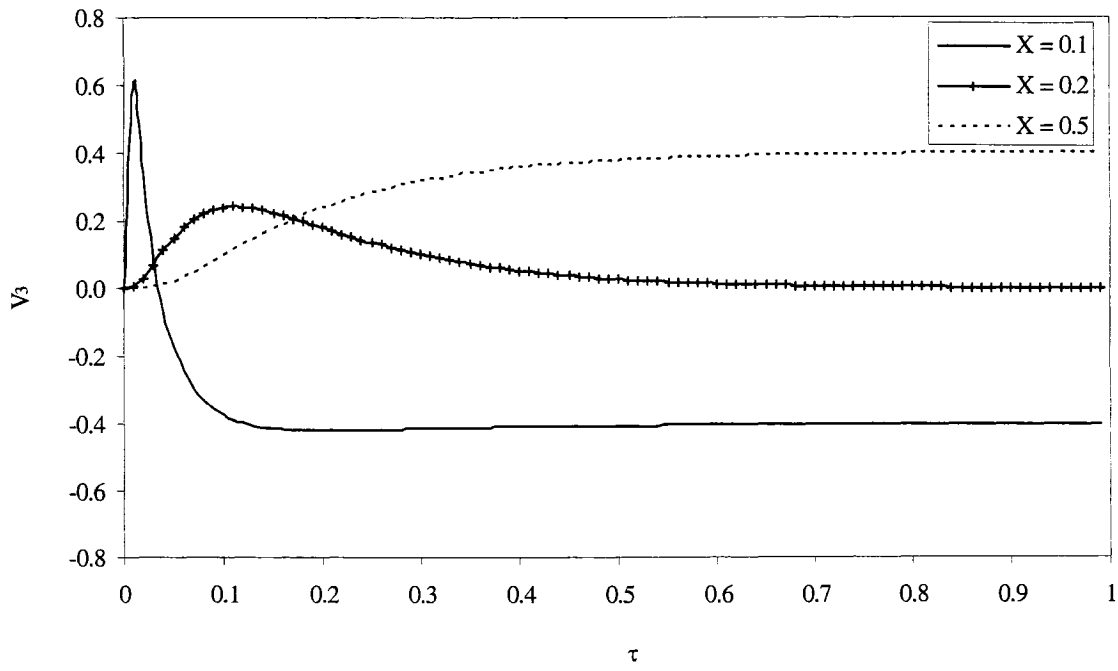

Figure 4.54 Temporal variation of V_3 (advective acceleration effect, i = 10).

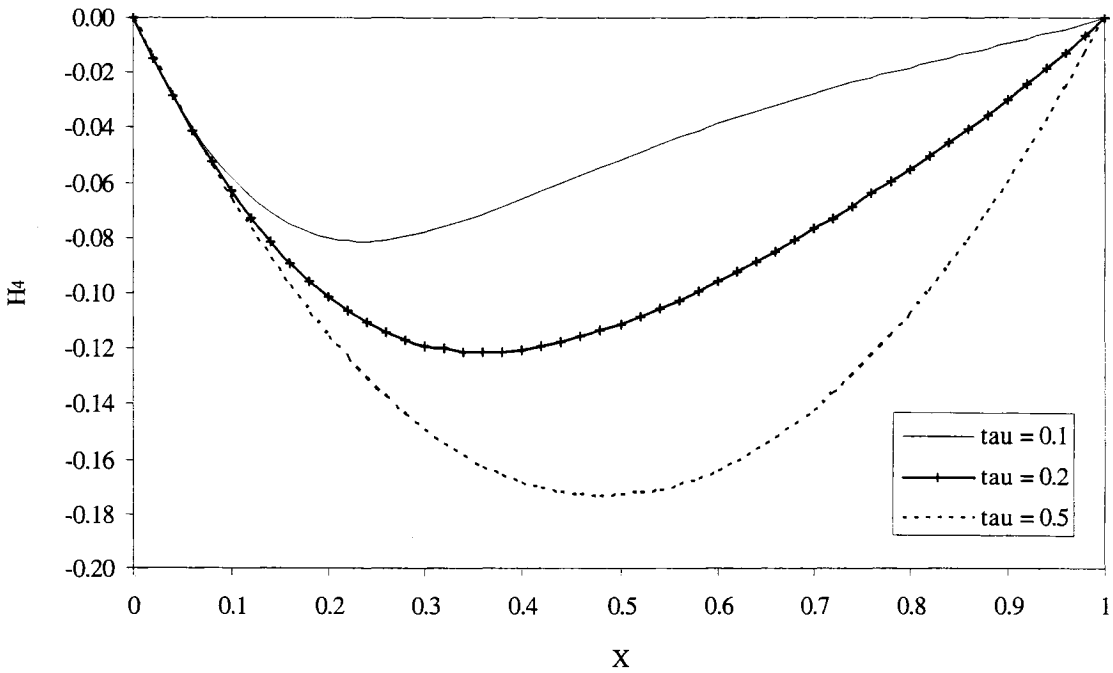

Figure 4.55 Spatial variation of H_4 (elevation head effect, i = 10).

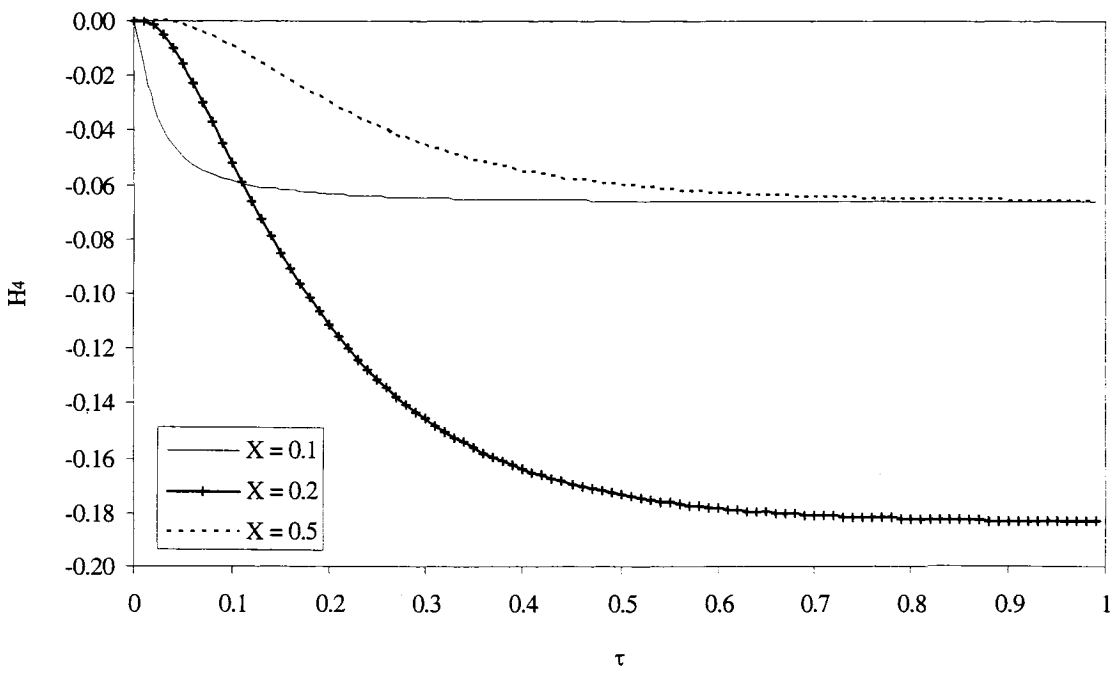

Figure 4.56 Temporal variation of H_4 (elevation head effect, i = 10).

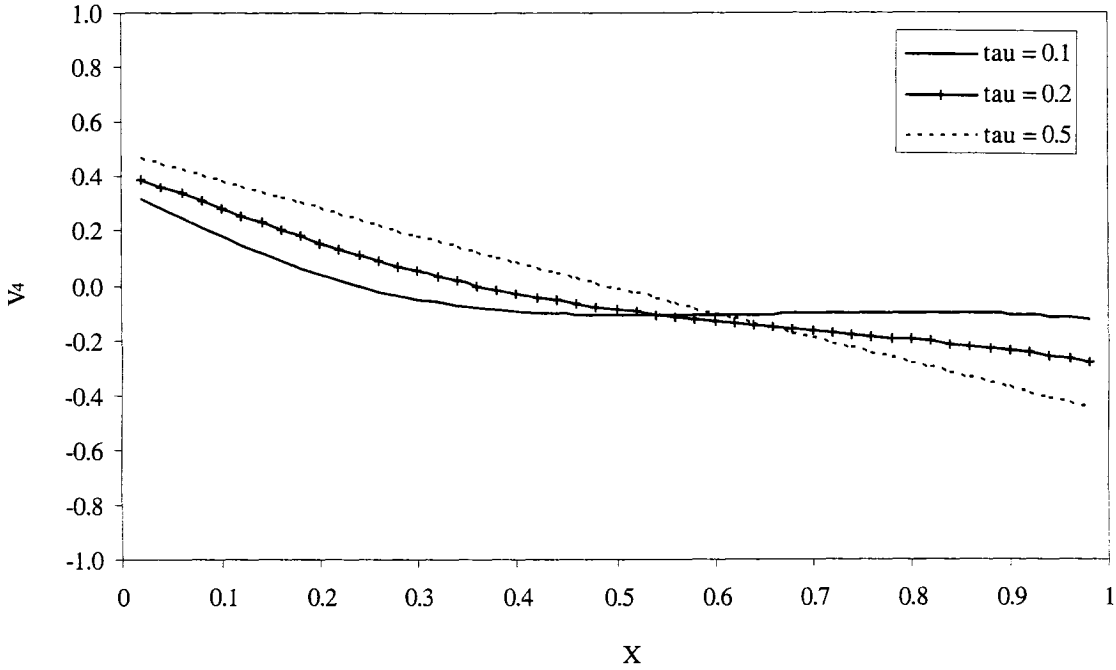

Figure 4.57 Spatial variation of V_4 (elevation head effect, i = 10).

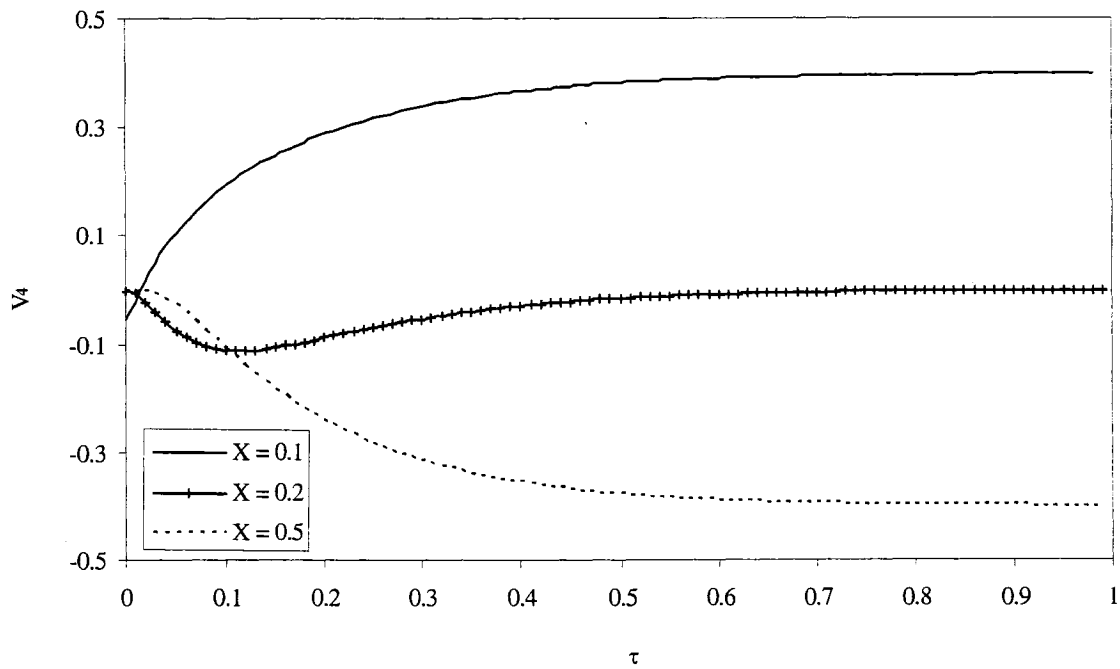

Figure 4.58 Temporal variation of V_4 (elevation head effect, i = 10).

4.3. Application of Matched Asymptotic Expansions

4.3.1. Inner and Outer Expansions

In this chapter, inner and outer expansions of the momentum and continuity equation are mathematically developed for the laminar, PDT, and FDT regimes. For the inner expansion of each regime, various forms of evolving-wave equations were investigated. The upper limit of the applicability of the inner-zone solution, both in time and in space, was determined using numerical solutions and compared for all three regimes.

4.3.1.1. Laminar Regime

The laminar regime is considered to be in effect if $Re_\infty < 1$, where Re_∞ is the Reynold number associated with equilibrium conditions ($t = \infty$). As shown in the previous chapters, for the laminar regime, it may be expected that viscous effects will dominate, being larger than inertial, local acceleration and convective acceleration effects.

(i) Outer Expansion

The original momentum and continuity equation were stated as:

$$H_x + \frac{C_2}{C_1} V V_x + \frac{C_3}{C_1} V + \frac{C_4}{C_1} V^2 + \frac{C_6}{C_1} V_\tau = 0 \qquad [3\text{-}62]$$

$$H_\tau + V_x + \frac{C_5}{C_6} V H_x + \frac{C_7}{C_6} V = 0 \qquad [3\text{-}63]$$

The outer forms of these equations can be obtained by investigating the magnitudes of the dimensionless groups in the above equations. Table 4.3 shows the magnitudes of these various groups at specified hydraulic gradients.

Table 4.3 Magnitudes of dimensionless groups for outer laminar case.

i [m/m]	C_2/C_1	C_3/C_1	C_4/C_1	C_6/C_1	C_5/C_6	C_7/C_6
0.01	2.1E-08	1.00	0.0016	0.003	6.7E-06	-6.7E-04
0.1	2.1E-07	1.00	0.016	0.003	6.7E-05	-6.7E-04

It can be seen that all the sets of parameters are much smaller than unity except C_3 / C_1, which is of order 1, O(1). The momentum equation can therefore be reduced to Darcy's Law, and the continuity equation can be reduced to its simplest form, having only elastic effects and no convective acceleration effect and no elevation head effect. The outer form of the momentum equation therefore becomes:

$$H_x + \frac{C_3}{C_1} V = 0 \qquad [4\text{-}63]$$

and the outer form of the continuity equation becomes:

$$H_\tau + V_x = 0 \qquad [4\text{-}64]$$

The outer expansions for H and V can be readily obtained by combining eqns [4-63] and [4-64]. The outer expansion of H is:

$$H_{XX} = \frac{C_3}{C_1} H_\tau \qquad [4\text{-}65]$$

and for V is:

$$V_{XX} = \frac{C_3}{C_1} V_\tau \qquad [4\text{-}66]$$

(ii) Inner Expansion

In order to be able to see velocity and head variation in the sharp change region, compound scaling is needed. This can be accomplished by rescaling to small space and time in order to magnify this small region. Rescaling X, τ and V as:

$$\tilde{X} = \frac{X}{a} \qquad [4\text{-}67a]$$

$$\tilde{\tau} = \frac{\tau}{b} \qquad [4\text{-}67b]$$

$$\tilde{V} = \frac{V}{c} \qquad [4\text{-}67c]$$

where a << 1, b << 1, and c >> 1 or c = O(1). In the inner zone, the inner variables, $\tilde{X}$, $\tilde{\tau}$, and $\tilde{V}$ will be used in the governing PDE's. Substituting rescaled X, τ and V (eqn [4-67]) into eqn [3-63] yields:

$$\frac{1}{b}H_{\tilde{\tau}} + \frac{c}{a}\tilde{V}_{\tilde{X}} + \frac{C_5}{C_6}\frac{c}{a}\tilde{V}H_{\tilde{X}} + \frac{C_7}{C_6}c\tilde{V} = 0 \qquad [4\text{-}68]$$

If we assume that the continuity equation is invariant in the inner zone, we can get an identical form of continuity equation for an outer zone by defining:

$$a = bc \qquad [4\text{-}69]$$

Since a << 1, b << 1, and c>>1 or c = O(1), bc << 1. If we divide all the terms in eqn [4-68] by 1/b (= c/a):

$$H_{\tilde{\tau}} + \tilde{V}_{\tilde{X}} + \frac{C_5}{C_6}\tilde{V}H_{\tilde{X}} + \frac{C_7}{C_6}a\tilde{V} = 0 \qquad [4\text{-}70]$$

Similarly, if we substitute the rescaled X, τ and V variables into eqn [3-62]:

$$\frac{1}{a}H_{\tilde{X}} + \frac{C_2}{C_1}\frac{c^2}{a}\tilde{V}\tilde{V}_{\tilde{X}} + \frac{C_3}{C_1}c\tilde{V} + \frac{C_4}{C_1}c^2\tilde{V}^2 + \frac{C_6}{C_1}\frac{c}{b}\tilde{V}_{\tilde{\tau}} = 0 \qquad [4\text{-}71]$$

In order to better investigate the sharp-change region, the unsteady acceleration part may be emphasized by defining:

$$\frac{1}{a} = \frac{C_6}{C_1}\frac{c^2}{a} \qquad [4\text{-}72]$$

The scaling parameter c is then:

$$c = \sqrt{\frac{C_1}{C_6}} \qquad [4\text{-}73]$$

where c>>1.

In order to better investigate viscous effects, we may define:

$$\frac{1}{a} = c \qquad [4\text{-}74]$$

Using eqns [4-69] and [4-74], expressions for the scaling parameters a and b can also be obtained:

$$a = \sqrt{\frac{C_6}{C_1}} \qquad [4\text{-}75]$$

and

$$b = \frac{C_6}{C_1} \qquad [4\text{-}76]$$

Using the above definitions for a, b and c, the new variables of interest for the inner zone became:

$$\tilde{X} = \frac{X}{\sqrt{\frac{C_6}{C_1}}} \qquad [4\text{-}77a]$$

$$\tilde{\tau} = \frac{\tau}{\frac{C_6}{C_1}} \qquad [4\text{-}77b]$$

$$\tilde{V} = \frac{V}{\sqrt{\frac{C_1}{C_6}}} \qquad [4\text{-}77c]$$

Table 4.4 shows the magnitude of the scaling factors at two hydraulic gradients.

Table 4.4 Magnitude of scaling factors.

i [m/m]	a	b	c
0.01	0.056	0.0032	17.73
0.1	0.056	0.0032	17.73

Equations [4-70] and [4-71] can be re-arranged using the relationships between a, b and c:

$$H_{\tilde{\tau}} + \tilde{V}_{\tilde{X}} + \frac{C_5}{C_6}\tilde{V}H_{\tilde{X}} + \frac{C_7}{\sqrt{C_1 C_6}}\tilde{V} = 0 \qquad [4\text{-}78]$$

$$H_{\tilde{X}} + \frac{C_2}{C_6}\tilde{V}\tilde{V}_{\tilde{X}} + \frac{C_3}{C_1}\tilde{V} + \frac{C_4}{\sqrt{C_1 C_6}}\tilde{V}^2 + \tilde{V}_{\tilde{\tau}} = 0 \qquad [4\text{-}79]$$

A comparison of the magnitude of various parameter-sets from eqns [4-78] and [4-79] are shown in the Table 4.5.

Table 4.5 Comparison of rescaled parameter-sets for laminar case.

i [m/m]	C_5/C_6	$C_7/\sqrt{C_1C_6}$	C_3/C_1	$C_4/\sqrt{C_1C_6}$	C_2/C_6
0.01	6.66E-06	-3.76E-05	1.00	0.029	6.66E-06
0.1	6.66E-05	-3.76E-05	1.00	0.29	6.66E-05

In light of the above relative magnitude parameter-sets, the following first-order equations can be obtained:

$$H_{\tilde{X}} + \frac{C_3}{C_1}\tilde{V} + \tilde{V}_{\tilde{\tau}} = 0 \qquad [4\text{-}80]$$

$$H_{\tilde{\tau}} + \tilde{V}_{\tilde{X}} = 0 \qquad [4\text{-}81]$$

An inner expansion of H can be obtained by combining the momentum and continuity equations:

$$H_{\tilde{X}\tilde{X}} = \frac{C_3}{C_1}H_{\tilde{\tau}} + H_{\tilde{\tau}\tilde{\tau}} \qquad [4\text{-}82]$$

If eqns [4-80] and [4-81] are combined for V,

$$\tilde{V}_{\tilde{X}\tilde{X}} = \frac{C_3}{C_1}\tilde{V}_{\tilde{\tau}} + \tilde{V}_{\tilde{\tau}\tilde{\tau}} \qquad [4\text{-}83]$$

then in the laminar regime with $\frac{C_3}{C_1} = 1$, the equations become:

$$H_{\tilde{X}\tilde{X}} = H_{\tilde{\tau}} + H_{\tilde{\tau}\tilde{\tau}} \qquad [4\text{-}84]$$

$$\tilde{V}_{\tilde{X}\tilde{X}} = \tilde{V}_{\tilde{\tau}} + \tilde{V}_{\tilde{\tau}\tilde{\tau}} \qquad [4\text{-}85]$$

The inner expansions of H and V have the form of an evolving wave. The behaviour of these waves will be presented in the section 4.3.2.

(iii) Inner Expression of Outer Expansion

In order to show the difference in behaviour between inner and outer, inner expression of outer is compared with inner in the inner coordinate. If we substitute inner variables in outer expansion, eqn [4-65] becomes:

$$H_{\tilde{X}\tilde{X}} = \frac{C_3}{C_1}H_{\tilde{\tau}} \qquad [4\text{-}86]$$

and for V eqn [4-66] becomes:

$$\tilde{V}_{\tilde{X}\tilde{X}} = \frac{C_3}{C_1}\tilde{V}_{\tilde{\tau}} \qquad [4\text{-}87]$$

4.3.1.2. PDT Regime

The PDT regime was obtained by applying intermediate hydraulic gradients, such that $1 < Re_{\infty} < 100$. As seen for the PDT outcomes presented in previous chapters, it was expected that the viscous and the inertial effects would be large compared to both the local and convective acceleration terms.

(i) Outer Expansion

The outer form for the PDT case can be obtained by comparing the magnitude of the various dimensionless groups present within eqns [3-62] and [3-63]. Table 4.6 states the relative magnitudes of these groups at two different hydraulic gradients.

Table 4.6 Magnitude of dimensionless groups for outer PDT case.

i [m/m]	C_2/C_1	C_3/C_1	C_4/C_1	C_6/C_1	C_5/C_6	C_7/C_6
1.0	1.6E-06	0.87	0.13	0.002	6.7E-04	-6.7E-04
10.0	6.0E-06	0.53	0.47	0.0009	6.7E-03	-6.7E-04

All the stated ratios are much smaller than 1 except the coefficients of C_3/C_1 and C_4/C_1. This means that the momentum equation can be reduced to the Ergun form and the continuity equation can be reduced to its basic form, but with the elastic effect retained. The outer form of the momentum is then:

$$H_x + \frac{C_3}{C_1}V + \frac{C_4}{C_1}V^2 = 0 \qquad [4\text{-}88]$$

and the outer continuity equation becomes:

$$H_\tau + V_x = 0 \qquad [4\text{-}89]$$

Because H_X is negative, $-|H_X| = H_X$. Therefore:

$$\frac{C_3}{C_1}V + \frac{C_4}{C_1}V^2 - |H_x| = 0 \qquad [4\text{-}90]$$

or

$$C_4V^2 + C_3V - C_1|H_x| = 0 \qquad [4\text{-}91]$$

Neglecting roots involving negative V, it can be shown that:

$$V = \frac{-C_3 + \sqrt{C_3^2 + 4C_1C_4|H_x|}}{2C_4} \qquad [4\text{-}92]$$

Differentiating eqn [4-88] with respect to X gives:

$$H_{XX} + \frac{C_3}{C_1} V_X + \frac{C_4}{C_1} 2VV_X = 0 \qquad [4\text{-}93]$$

By substituting eqns [4-89] and [4-92] in eqn [4-93]:

$$H_{XX} = \frac{C_3}{C_1} H_\tau + \left[-\frac{C_3}{C_1} + \frac{1}{C_1} \sqrt{C_3{}^2 + 4C_1C_4|H_x|} \right] H_\tau \qquad [4\text{-}94]$$

or

$$H_{XX} = \frac{C_3}{C_1} \sqrt{1 + \frac{4C_1C_4}{C_3{}^2}|H_X|} H_\tau \qquad [4\text{-}95a]$$

By re-arrangement:

$$H_{XX} = \frac{1}{C_1} \sqrt{C_3{}^2 + 4C_1C_4|H_x|} H_\tau \qquad [4\text{-}95b]$$

Equation [4-95b] can be re-arranged into the fast diffusion equation form:

$$\frac{H_{XX}}{\sqrt{1 + \frac{4C_1C_4|H_x|}{C_3{}^2}}} = \frac{C_3}{C_1} H_\tau \qquad [4\text{-}96]$$

If we define $\phi = 1 + \frac{4C_1C_4|H_x|}{C_3{}^2}$, ϕ_X is:

$$\phi_X = -\frac{4C_1C_4H_{XX}}{C_3{}^2} \qquad [4\text{-}97]$$

and ϕ_τ is:

$$\phi_\tau = -\frac{4C_1C_4H_{X\tau}}{C_3{}^2} \qquad [4\text{-}98]$$

By substituting H_{XX} and H_τ in eqns [4-97] and [4-98] into eqn [4-96]:

$$\left(-\frac{C_3^{\,2}}{4C_1C_4}\frac{\phi_X}{\sqrt{\phi}}\right)_X = \frac{C_3}{C_1}\left(-\frac{C_3^{\,2}}{4C_1C_4}\right)\phi_\tau \qquad [4\text{-}99]$$

After re-arrangement:

$$\left(\frac{1}{\sqrt{\phi}}\phi_X\right)_X = \frac{C_3}{C_1}\phi_\tau \qquad [4\text{-}100]$$

General fast diffusion problem can be defined with eqn [4-101]:

$$u_t = \nabla\cdot\left(mu^{m-1}\nabla u\right) \qquad [4\text{-}101]$$

where m <1.

If m = 0.5, eqn [4-101] becomes an identical form of eqn [4-100]. The problem has become a fast diffusion problem in ϕ.

(ii) Inner Expansion

Using the same scaling factors a, b and c as were used to handle the laminar regime, the values of these factors for the PDT regime are shown in Table 4.7.

Table 4.7 Magnitude of scaling factors.

i [m/m]	a	B	c
1	0.049	0.0024	20.284
10	0.03	0.0009	33.289

Table 7.5 shows that higher hydraulic gradients cause space and time scale factors to decrease. The magnitude of the various dimensionless groups and scaling parameters can be compared by substituting a, b and c into eqns [4-70] and [4-71]. The resulting numerical magnitudes of these groups are presented in the Table 4.8.

Table 4.8 Comparison of magnitude of rescaled sets of parameters for PDT regime.

i [m/m]	C_5/C_6	$C_7/\sqrt{C_1C_6}$	C_3/C_1	$C_4/\sqrt{C_1C_6}$	C_2/C_6
1	6.66E-04	-3.28E-05	0.874	2.554	6.66E-04
10	6.66E-03	-2.00E-05	0.533	15.559	6.66E-03

In light of these magnitudes, the first-order momentum and continuity equation can be re-stated:

$$H_{\tilde{x}} + \frac{C_3}{C_1}\tilde{V} + \frac{C_4}{C_1}c\tilde{V}^2 + \tilde{V}_{\tilde{\tau}} = 0 \qquad [4\text{-}102]$$

$$H_{\tilde{\tau}} + \tilde{V}_{\tilde{x}} = 0 \qquad [4\text{-}103]$$

The equation for H can be obtained by combining eqns [4-102] and [4-103]:

$$H_{\tilde{x}\tilde{x}} = \left(\frac{C_3}{C_1} + \frac{2C_4}{C_1}c\tilde{V}\right)H_{\tilde{\tau}} + H_{\tilde{\tau}\tilde{\tau}} = 0 \qquad [4\text{-}104]$$

The eqn for V is then:

$$\tilde{V}_{\tilde{x}\tilde{x}} = \frac{C_3}{C_1}\tilde{V}_{\tilde{\tau}} + \frac{2C_4}{C_1}c\tilde{V}_{\tilde{\tau}} + \tilde{V}_{\tilde{\tau}\tilde{\tau}} = 0 \qquad [4\text{-}105]$$

(iii) Inner Expression of Outer Zone

By substituting inner variables into eqn [4-95a], inner expression of outer zone can be expressed with:

$$H_{\tilde{x}\tilde{x}} = \frac{C_3}{C_1}\sqrt{1 + \frac{4C_1C_4}{C_3{}^2a}\left|H_{\tilde{x}}\right|}H_{\tilde{\tau}} \qquad [4\text{-}106]$$

4.3.1.3. FDT Regime

Physically, the FDT regime can be obtained by applying very high hydraulic gradients, resulting in $Re_\infty > 100$. As shown in the previous chapters, for the FDT

regime, it may be also expected that the inertial effect will be dominant in this regime, as compared to viscous, local accelerative and convective accelerative effects.

(i) Outer Expansion

In a manner similar way to the laminar case, the outer form may be obtained by comparing the relative magnitudes of the dimensionless groups implied by eqns [3-62] and [3-63]. Table 4.9 states these relative magnitudes:

Table 4.9 Magnitude of dimensionless groups for outer FDT case.

i [m/m]	C_2/C_1	C_3/C_1	C_4/C_1	C_6/C_1	C_5/C_6	C_7/C_6
350	1.13E-05	0.123	0.877	4.84E-05	0.233	-6.7E-04
400	1.14E-05	0.116	0.884	4.27E-05	0.266	-6.7E-04

All the ratios are much smaller than 1 except the coefficient C_4/C_1. Considering these relative magnitudes, the momentum equation may be reduced to eqn [4-107], with only the inertial term retained. The outer-zone momentum equation is then:

$$H_x + \frac{C_4}{C_1} V^2 = 0 \qquad [4\text{-}107]$$

Correspondingly, the continuity equation may be reduced to its basic form, but with the elastic effect term retained. The outer continuity equation is then:

$$H_\tau + V_x = 0 \qquad [4\text{-}108]$$

Because H_X is negative, $-|H_X| = H_X$. Outer momentum equation becomes:

$$V = \sqrt{\frac{C_1}{C_4}|H_x|} \qquad [4\text{-}109]$$

Differentiating eqn [4-107] with respect to X gives:

$$H_{XX} + \frac{C_4}{C_1} 2VV_X = 0 \qquad [4\text{-}110]$$

Using eqn [4-108] and [4-109] in eqn [4-110], it becomes:

$$H_{XX} = \frac{2C_4}{C_1}\sqrt{\frac{C_1|H_x|}{C_4}}H_\tau \qquad [4\text{-}111]$$

or

$$H_{XX} = 2\sqrt{\frac{C_4|H_x|}{C_1}}H_\tau \qquad [4\text{-}112]$$

If we define $\phi = |H_x| = -H_x$, $\phi_X = -H_{XX}$ and $\phi_\tau = -H_{X\tau}$, Another fast-diffusion equation is obtained:

$$\left(\frac{1}{\sqrt{\phi}}\phi_X\right)_X = 2\sqrt{\frac{C_4}{C_1}}\phi_\tau \qquad [4\text{-}113]$$

(ii) Inner Expansion

If it is assumed that the continuity equation (eqn [4-78]) is invariant in the inner coordinate system, we can get an identical form of continuity equation for the outer zone by defining:

$$a = bc \qquad [4\text{-}114]$$

In order to better investigate the sharp-change region, the unsteady acceleration part can be emphasized by defining:

$$\frac{1}{a} = \frac{C_6}{C_1}\frac{c^2}{a} \qquad [4\text{-}115]$$

Then we can get 'c':

$$c = \sqrt{\frac{C_1}{C_6}} \qquad [4\text{-}116]$$

where c>>1.

In order to investigate inertial effects, we may define:

$$\frac{1}{a} = c^2 \qquad [4\text{-}117]$$

Using eqns [4-114] and [4-115], 'a' and 'b' can be obtained:

$$a = \frac{C_6}{C_1} \qquad [4\text{-}118]$$

and

$$b = \left(\frac{C_6}{C_1}\right)^{\frac{3}{2}} \qquad [4\text{-}119]$$

Using 'a', 'b' and 'c', the inner variables can be re-defined with:

$$\tilde{X} = \frac{X}{\frac{C_6}{C_1}} \qquad [4\text{-}120a]$$

$$\tilde{\tau} = \frac{\tau}{\left(\frac{C_6}{C_1}\right)^{\frac{3}{2}}} \qquad [4\text{-}120b]$$

$$\tilde{V} = \frac{V}{\sqrt{\frac{C_1}{C_6}}} \qquad [4\text{-}120c]$$

Table 4.10 gives the magnitude of scaling factors 'a', 'b', and 'c' at two hydraulic gradients.

Table 4.10 Magnitude of scaling factors.

i [m/m]	a	b	c
350	0.000048	3.36E-07	143.8
400	0.000043	2.79E-07	153.1

Using the new inner variables, eqn [3-62] and [3-63] become:

$$H_{\tilde{X}} + \frac{C_2}{C_1} c^2 \tilde{V} \tilde{V}_{\tilde{X}} + \frac{C_3}{C_1} \frac{1}{c} \tilde{V} + \frac{C_4}{C_1} \tilde{V}^2 + \tilde{V}_{\tilde{\tau}} = 0 \qquad [4\text{-}121]$$

$$H_{\tilde{\tau}} + \tilde{V}_{\tilde{x}} + \frac{C_5}{C_6}\tilde{V}H_{\tilde{x}} + \frac{C_7}{C_6}a\tilde{V} = 0 \qquad [4\text{-}122]$$

Table 4.11 gives magnitudes of the various dimensionless parameter ratios.

Table 4.11 Comparison of magnitude of re-scaled sets of parameters for FDT case.

i [m/m]	C_5/C_6	C_7/C_1*a	C_3/C_1/c	C_4/C_1	C_2/C_6
350	0.233	-1.56E-12	0.00086	0.877	0.233
400	0.266	-1.21E-12	0.00076	0.884	0.266

The governing equations can be reduced to

$$H_{\tilde{x}} + \frac{C_4}{C_1}\tilde{V}^2 + \tilde{V}_{\tilde{\tau}} = 0 \qquad [4\text{-}123]$$

$$H_{\tilde{\tau}} + \tilde{V}_{\tilde{x}} = 0 \qquad [4\text{-}124]$$

in light of the relative numeric magnitudes in Table 7.9.

Combining the momentum and continuity equation gives:

$$H_{\tilde{x}\tilde{x}} + \frac{2C_4}{C_1}\tilde{V}H_{\tilde{\tau}} + H_{\tilde{\tau}\tilde{\tau}} = 0 \qquad [4\text{-}125]$$

and

$$V_{\tilde{x}\tilde{x}} + \frac{2C_4}{C_1}\tilde{V}\tilde{V}_{\tilde{\tau}} + \tilde{V}_{\tilde{\tau}\tilde{\tau}} = 0 \qquad [4\text{-}126]$$

(iii) Inner Expression for Outer Zone

If we substitute the inner variables into the expression for the outer expansion, eqn [4-112] becomes:

$$H_{\tilde{x}\tilde{x}} = 2\sqrt{\frac{C_4|H_{\tilde{x}}|}{C_1}}H_{\tilde{\tau}} \qquad [4\text{-}127]$$

4.3.2. Numerical Solutions

The inner and outer expansion expressions were solved using various numerical methods. The method of characteristics was used to solve the inner expansion (evolving-wave equation) and the implicit FDM used to solve the outer expansion expression (diffusion equation). The method of characteristics has advantages in solving evolving-wave equations in terms of stability, compared with most explicit finite difference methods. A disadvantage of this method is that it cannot solve diffusion equation that has no V_τ term in it. Thus, the outer expansion was solved using an implicit finite difference method.

4.3.2.1. Laminar Regime

(i) Outer Solutions

'Outer' equations are diffusion equations. Outer solutions were obtained using an implicit finite difference method (FDM) together with successive over-relaxation (SOR) scheme. The implicit finite difference form used herein for solving the outer expansion for the laminar regime case can be written:

$$\frac{H_i^{k+1} - H_i^k}{\Delta\tau} = \frac{C_1}{C_3}\left(\frac{H_{i+1}^{k+1} - 2H_i^{k+1} + H_{i-1}^{k+1}}{\Delta X^2}\right) \qquad [4\text{-}128]$$

Setting $A = \frac{C_1}{C_3}\frac{\Delta\tau}{\Delta X^2}$,

$$H_i^{k+1} = \frac{A}{1+2A}\left(H_{i+1}^{k+1} + H_{i-1}^{k+1}\right) + \frac{1}{1+2A}H_i^k \qquad [4\text{-}129]$$

For the implicit scheme, each time step was iterated until there was no change in the results. To accelerate the convergence SOR was used. SOR can be defined with eqn [4-130], with the over-relaxation factor w_0 being lies generally in the range from 1 to 2:

$$H_i^{(n'+1)} = w_0(\text{iteration equation}) + (1 - w_0)H_i^{(n')} \qquad [4\text{-}130]$$

$H_i^{(n)}$ is the n^{th} iteration of the relaxation calculation. After the H's for one time step were obtained, the V's for the same time step were obtained from the outer momentum equation. The finite difference form is of the outer momentum equation is:

$$V_i^{k+1} = -\frac{C_1}{C_3}\left(\frac{H_{i+1}^{k+1} - H_{i-1}^{k+1}}{2\Delta X}\right) \qquad [4\text{-}131]$$

(ii) Inner Solutions

The procedure used to get H and V was similar to the numerical solution described in Appendix III. First, the following zeroed coefficients are put into the full problem.

$$C_2 = C_4 = C_7 = 0 \qquad [4\text{-}132]$$

Second, the characteristic must be re-defined using the inner coordinate. The integration should follow the new inner characteristic:

$$\Delta\tau = \frac{\Delta X}{\sqrt{\frac{C_1}{C_6}}} \rightarrow \Delta\tilde{\tau} = \Delta\tilde{X} \qquad [4\text{-}133]$$

H_{P_i} can then be calculated using:

$$H_{P_i} = 0.5\left[H_{i-1} + H_{i+1} + \left(\tilde{V}_{i-1} - \tilde{V}_{i+1}\right) - \Delta\tilde{X}\left(\tilde{V}_{i-1} - \tilde{V}_{i+1}\right)\right] \qquad [4\text{-}134]$$

After calculating H_{P_i}, the value of V_{P_i} can be obtained using:

$$\tilde{V}_{P_i} = \left[-H_{P_i} + H_{i-1} - \Delta\tilde{X}\tilde{V}_{i-1}\right] + \tilde{V}_{i-1} \qquad [4\text{-}135]$$

or using:

$$\tilde{V}_{P_i} = \left[H_{P_i} - H_{i+1} - \Delta\tilde{X}\tilde{V}_{i+1}\right] + \tilde{V}_{i+1} \qquad [4\text{-}136]$$

The value of $\tilde{V}$ at the upstream end of the problem can be calculated using eqn [4-136], and its value at its downstream end can be calculated using eqn [4-135].

(iii) Solutions for Inner Expression of Outer Zone

We can get the solution to inner expression of the outer-zone expression following the same method used for the outer solution. If we set $A_2' = \frac{C_1}{C_3}\frac{\Delta\tilde{\tau}}{\Delta\tilde{X}^2}$, then:

$$H_i^{k+1} = \frac{A_2'}{1+2A_2'}\left(H_{i+1}^{k+1} + H_{i-1}^{k+1}\right) + \frac{1}{1+2A_2'}H_i^k \qquad [4\text{-}137]$$

The value of $\tilde{V}$ may then be obtained from the momentum equation:

$$\tilde{V}_i^{k+1} = -\frac{C_1}{C_3}\left(\frac{H_{i+1}^{k+1} - H_{i-1}^{k+1}}{2\Delta\tilde{X}}\right) \qquad [4\text{-}138]$$

(iv) Comparison of Results: Inner Coordinate Zone

In order to limit the flow to the laminar regime, a hydraulic gradient of 0.1 was applied[9]. The solutions for the inner case were obtained using the method of characteristics; the solutions for the outer-zone case were obtained using an implicit finite difference method with SOR. The spatial and temporal development of head are presented in Figures 4.59 and 4.60. Solutions to both the inner and outer expansions are compared in Figure 4.59. Because of the evolving wave property, the inner expansion shows a sudden drop of head at around $\tilde{X} = \tilde{\tau}$. On the other hand, the solution to the outer expansion shows a gradual decrease of head, i.e. following a diffusive behaviour. As time and space increase, the magnitude of the drop using the inner-expansion solution decreases. In Figure 4.60, temporal development of head using both inner and outer-expansion solutions is compared, at various locations. It is observed that at very small time-space positions, the head development is governed not by diffusion but by a shock wave. Figure 4.61 shows a spatial profile of $\tilde{V}$ at various times, which is similar to the trend of H. If the outer-expansion solution is used in the inner zone, the profile of $\tilde{V}$ is smooth compared to the profile obtained using inner-expansion solution. The maximum difference between the inner and outer solutions occurs at around $\tilde{X} = \tilde{\tau}$. It can also be seen that the $\tilde{V}$'s based

[9] only realized through the sample at $t = \infty$.

on the inner expansion are larger than the $\tilde{V}$'s based on the outer expansion if $\tilde{X}$ is smaller than $\tilde{\tau}$. After passing this location ($\tilde{X} = \tilde{\tau}$), $\tilde{V}$'s from the inner expansion are smaller than the $\tilde{V}$'s of outer expansion. In other words, if the outer expansion is used to estimate the velocities near the boundary at the very beginning of the experiment, $\tilde{V}$ will be underestimated until $\tilde{X}$ becomes equal to $\tilde{\tau}$. After that location is passed, $\tilde{V}$ may be overestimated. As can be seen in the very small time-and-space region, both the order of the error can be close to 1. In Figure 4.62, the temporal profile of $\tilde{V}$ using both inner and outer expansions solutions are compared. The outer expansion overestimates $\tilde{V}$ when $\tilde{\tau}$ is smaller than $\tilde{X}$, but can underestimate $\tilde{V}$ when $\tilde{\tau}$ becomes larger than $\tilde{X}$.

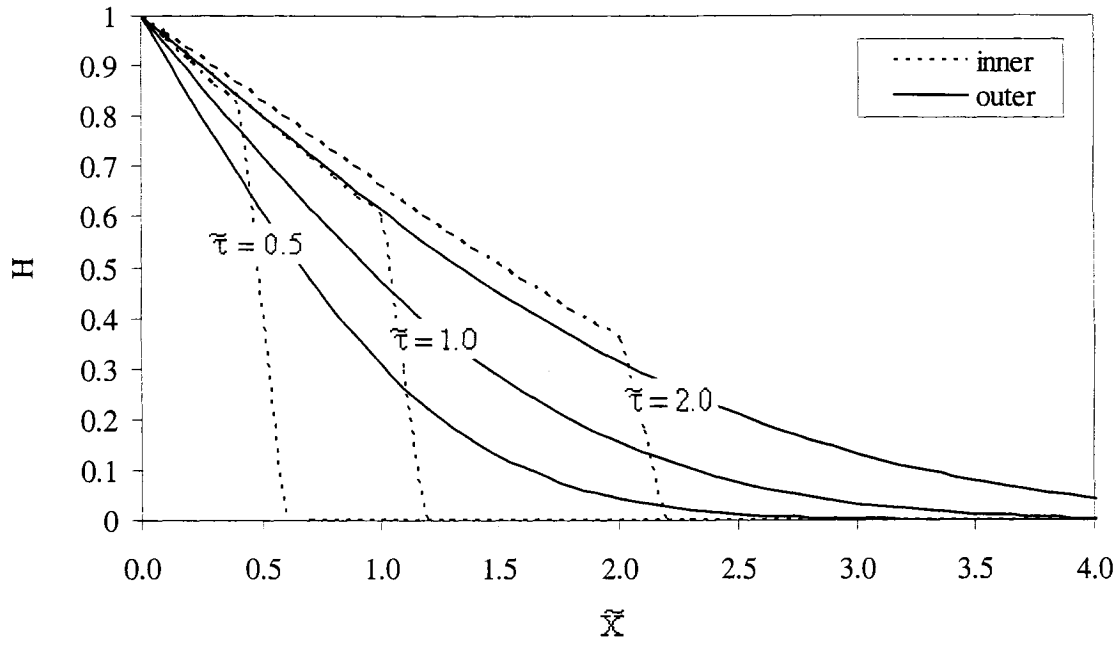

Figure 4.59 Comparison of spatial head development using inner and outer expansions, at various times.

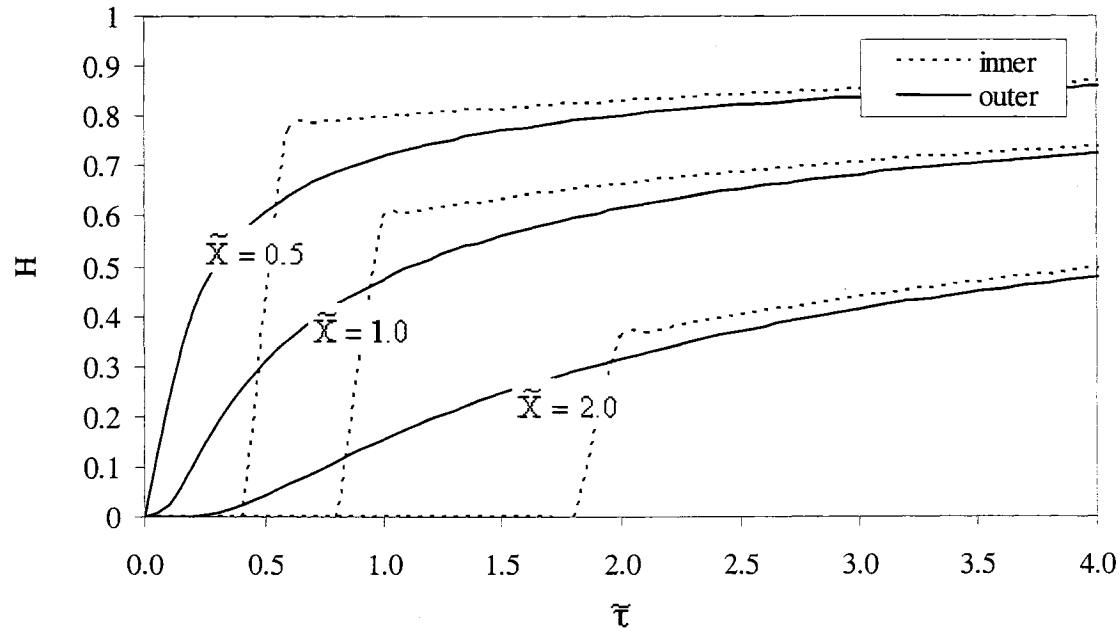

Figure 4.60 Comparison of temporal head development using inner and outer expansions, at various distances.

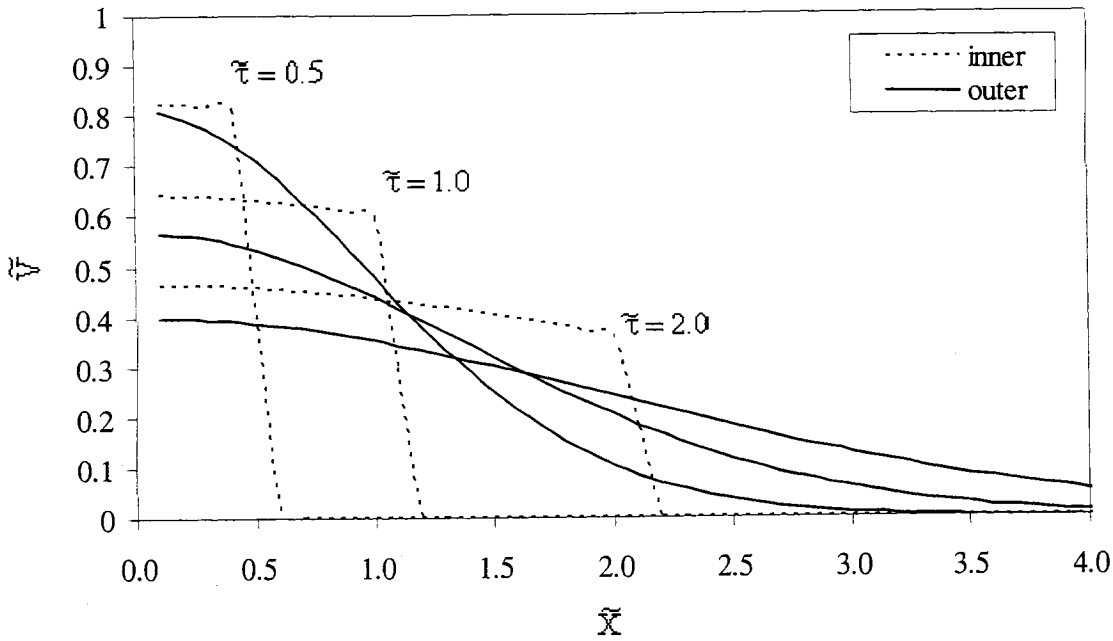

Figure 4.61 Comparison of spatial velocity development using inner and outer expansions, at various times.

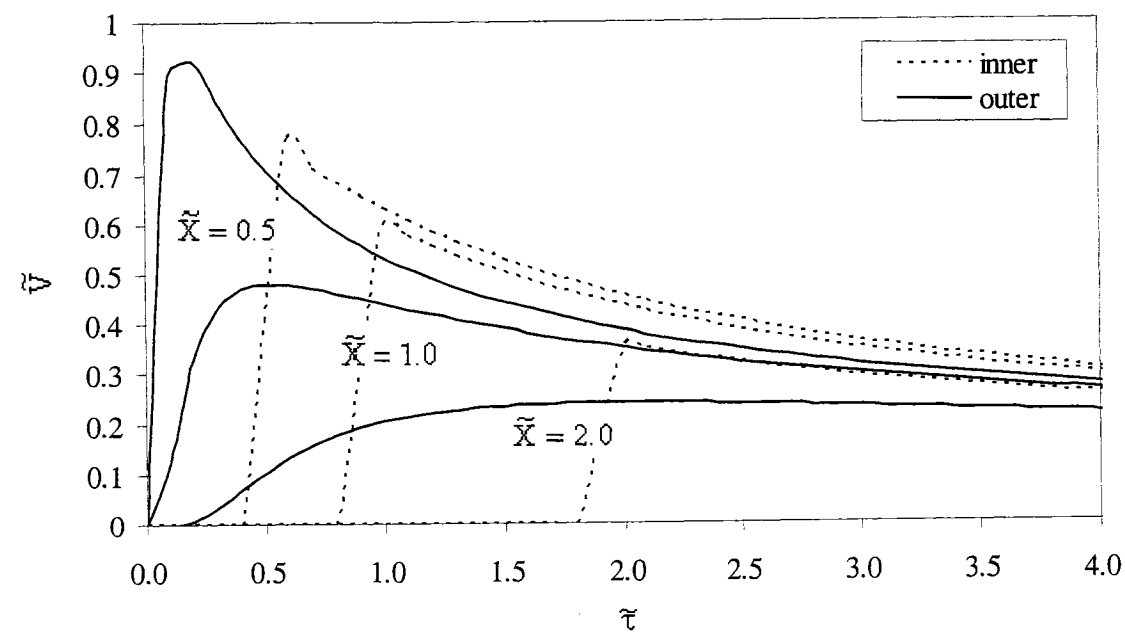

Figure 4.62 Comparison of temporal velocity development using inner and outer expansions, at various distances.

4.3.2.2. PDT Regime

(i) Outer Solutions

The implicit finite difference form used herein for solving the outer expansion for the PDT regime case can be written:

$$\frac{H_i^{k+1} - H_i^k}{\Delta\tau} = \frac{C_1}{C_3} \frac{1}{\sqrt{1 + \frac{4C_1C_4}{C_3^2} \frac{H_{i+1}^{k+1} - H_{i-1}^{k+1}}{2\Delta X}}} \frac{H_{i+1}^{k+1} - 2H_i^{k+1} + H_{i-1}^{k+1}}{\Delta X^2} \qquad [4\text{-}139]$$

Re-arrangement gives:

$$H_i^{k+1} = \frac{1}{1 + \frac{C_1}{C_3} \frac{2\Delta\tau}{\Delta X^2} \frac{1}{A}} \frac{C_1}{C_3} \frac{1}{A_3'} \frac{\Delta\tau}{\Delta X^2} (H_{i+1}^{k+1} + H_{i-1}^{k+1}) + H_i^k \qquad [4\text{-}140]$$

where

$$A_3' = \sqrt{1 + \frac{4C_1C_4}{C_3^2} \frac{H_{i+1}^{k+1} - H_{i-1}^{k+1}}{2\Delta X}} \quad . \qquad [4\text{-}141]$$

The term V can simply be calculated using H_X.

$$V_i^{k+1} = \frac{-C_3 + \sqrt{C_3^{\,2} + 4C_1C_4 \frac{H_{i+1}^{k+1} - H_{i-1}^{k+1}}{2\Delta X}}}{2C_4} \qquad [4\text{-}142]$$

(ii) Inner Solutions

The procedure used to get H and V was similar to the numerical solution described in Appendix III. First, the following zeroed coefficients are put into the full problem:

$$C_2 = C_7 = 0 \qquad [4\text{-}143]$$

and the ratio cC_4/C_1 is substituted for C_4/C_1.

Second, the characteristic must be re-defined using inner coordinate. The integration should follow the inner characteristic:

$$\Delta\tau = \frac{\Delta X}{\sqrt{\frac{C_1}{C_6}}} \rightarrow \Delta\tilde{\tau} = \Delta\tilde{X} \qquad [4\text{-}144]$$

H_{P_i} can then be calculated using:

$$H_{P_i} = 0.5\left[H_{i-1} + H_{i+1} + \left(\tilde{V}_{i-1} - \tilde{V}_{i+1}\right) - \frac{C_3}{C_1}\Delta\tilde{X}\left(\tilde{V}_{i-1} - \tilde{V}_{i+1}\right)\right.$$
$$\left. - \frac{C_4}{C_1}c\Delta\tilde{X}\left(\tilde{V}_{i-1}\left|\tilde{V}_{i-1}\right| - \tilde{V}_{i+1}\left|\tilde{V}_{i+1}\right|\right)\right] \qquad [4\text{-}145]$$

After calculating H_{P_i}, the value of V_{P_i} can be obtained using:

$$\tilde{V}_{P_i} = \left[-H_{P_i} + H_{i-1} - \frac{C_3}{C_1}\Delta X\tilde{V}_{i-1} - \frac{C_4}{C_1}c\Delta\tilde{X}\tilde{V}_{i-1}\left|\tilde{V}_{i-1}\right|\right] + \tilde{V}_{i-1} \qquad [4\text{-}146]$$

or using:

$$\tilde{V}_{P_i} = \left[H_{P_i} - H_{i+1} - \frac{C_3}{C_1}\Delta\tilde{X}\tilde{V}_{i+1} - \frac{C_4}{C_1}c\Delta\tilde{X}\tilde{V}_{i+1}\left|\tilde{V}_{i+1}\right|\right] + \tilde{V}_{i+1} \qquad [4\text{-}147]$$

The value of $\tilde{V}$ at the upstream end of the problem can be calculated using eqn [4-147], and its value at its downstream end can be calculated using eqn [4-146].

(iii) Solutions for Inner Expression of Outer Zone

We can get the solution to inner expression of the outer-zone expression following the same method used for the outer solution.

$$H_i^{k+1} = \frac{1}{1 + \frac{C_1}{C_3}\frac{2\Delta\tilde{\tau}}{\Delta\tilde{X}^2}\frac{1}{A_4'}}\frac{C_1}{C_3}\frac{1}{A_4'}\frac{\Delta\tilde{\tau}}{\Delta\tilde{X}^2}\left(H_{i+1}^{k+1} + H_{i-1}^{k+1}\right) + H_i^k \qquad [4\text{-}148]$$

where $A_4' = \sqrt{1 + \frac{4C_1C_4}{C_3^2 a}\frac{H_{i+1}^{k+1} - H_{i-1}^{k+1}}{2\Delta\tilde{X}}}$.

The value of $\tilde{V}$ may then be obtained from momentum equation:

$$\tilde{V}_i^{k+1} = \frac{-C_3 + \sqrt{C_3^{\,2} + 4C_1C_4c\dfrac{H_{i+1}^{k+1} - H_{i-1}^{k+1}}{2\Delta\tilde{X}}}}{2C_4c} \qquad [4\text{-}149]$$

(iv) Comparison of Results: Inner Coordinate Zone

In order to achieve PDT flow in the regime, a hydraulic gradient of 10 was applied. The same numerical methods used for the laminar regime were applied to obtain the solutions for this regime. The spatial and temporal profiles of head are presented for the PDT case in Figures 4.63 and 4.64,. The spatial development of head using the various numerical solutions to the inner and outer expansion is compared in Figure 4.63 (for various times). The results are similar to those obtained for the laminar regime. However, if scaling factors of time and space are considered, the evolving wave properties disappear in smaller time-space than those of the laminar regime. The relative size of the space scaling-factor, 'a' is:

$$a_{i=10_{PDT}} = 0.61a_{i=0.1_{LAM}}$$

and for time scaling factor 'b' this is:

$$b_{i=10_{PDT}} = 0.37b_{i=0.1_{LAM}}$$

In Figure 4.64 temporal profiles of head, using solutions to the inner and outer expansions, are compared at various locations. It is observed that in very small time-space, the head approaches any given point of interest in the form of a shock wave. Figure 4.65 is a spatial profile of $\tilde{V}$ at various times, for the PDT case. Trend similar to that of the laminar case are evident, and again the maximum difference between the inner and outer solutions occurs at around $\tilde{X} = \tilde{\tau}$. It is also shown that the $\tilde{V}$'s based on the inner expansion are smaller than the $\tilde{V}$'s using the outer expansion at most locations,

except a small zone up to but near $\tilde{X} = \tilde{\tau}$. As time increases, this small region increases. It is expected that in large time and space, we get the same results as laminar regime where $\tilde{V}$ of inner expansion was larger than $\tilde{V}$ of outer expansion when $\tilde{X}$ is smaller than $\tilde{\tau}$. As can be seen for the small time-space zone, the order of the error (the difference in $\tilde{V}$ between the inner and outer expansions) is close to 1. In Figure 4.66 the temporal profile of $\tilde{V}$ based on solutions of the inner and outer expansions is compared. The $\tilde{V}$ from outer expansion starts to increase from $\tilde{\tau} = +0$, onward, but the $\tilde{V}$ from inner solution starts to increase near $\tilde{X} = \tilde{\tau}$.

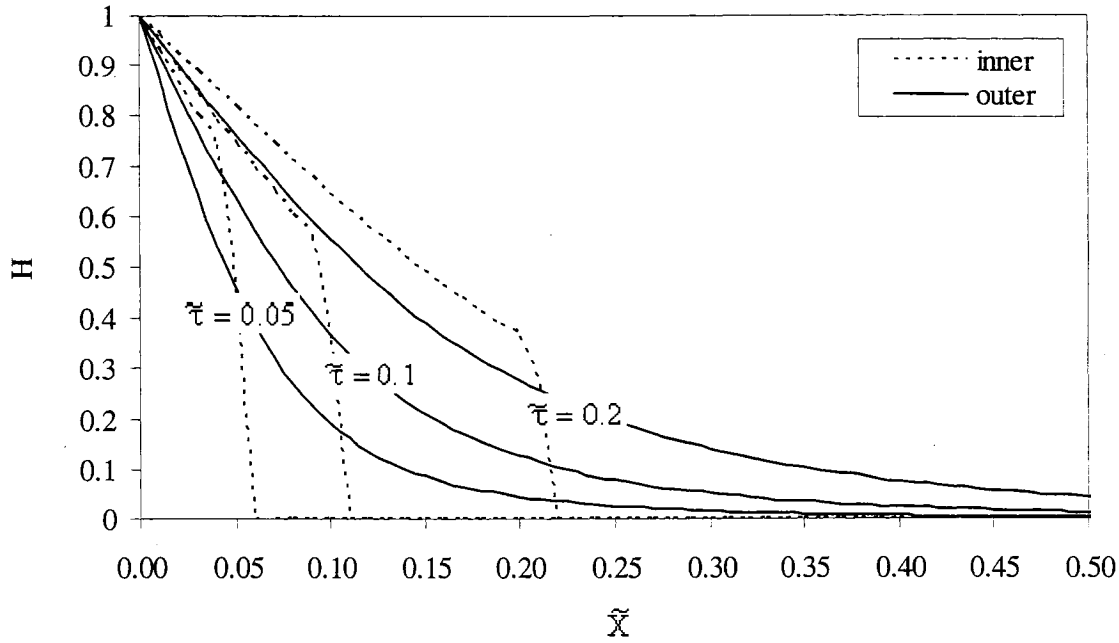

Figure 4.63 Comparison of spatial head development using inner and outer expansions, at various times.

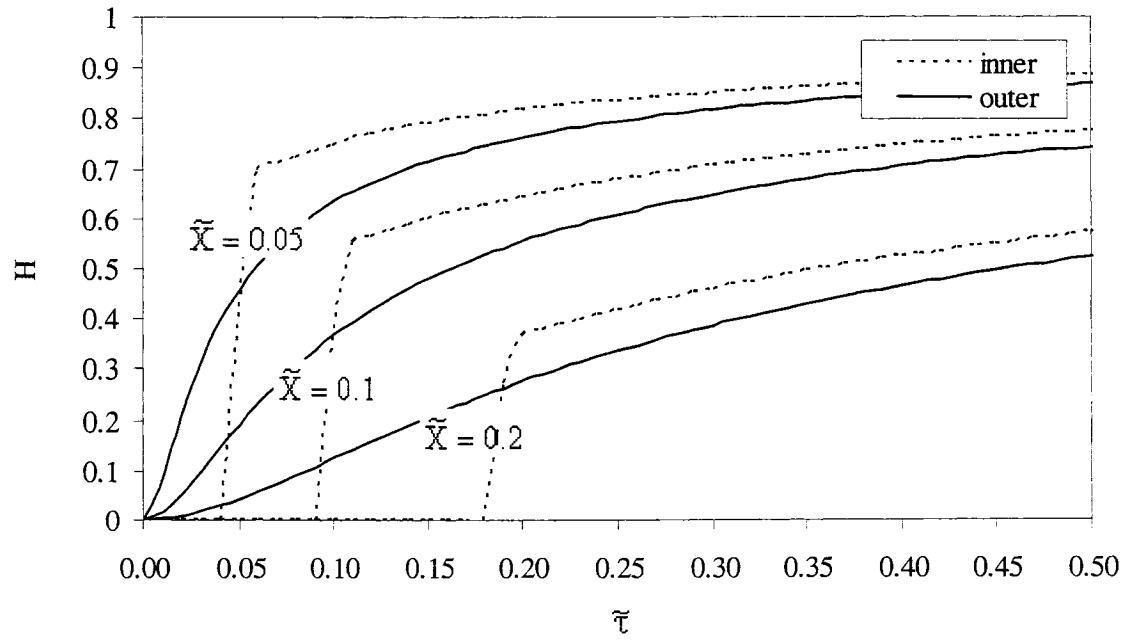

Figure 4.64 Comparison of temporal head development using inner and outer expansions, at various distances.

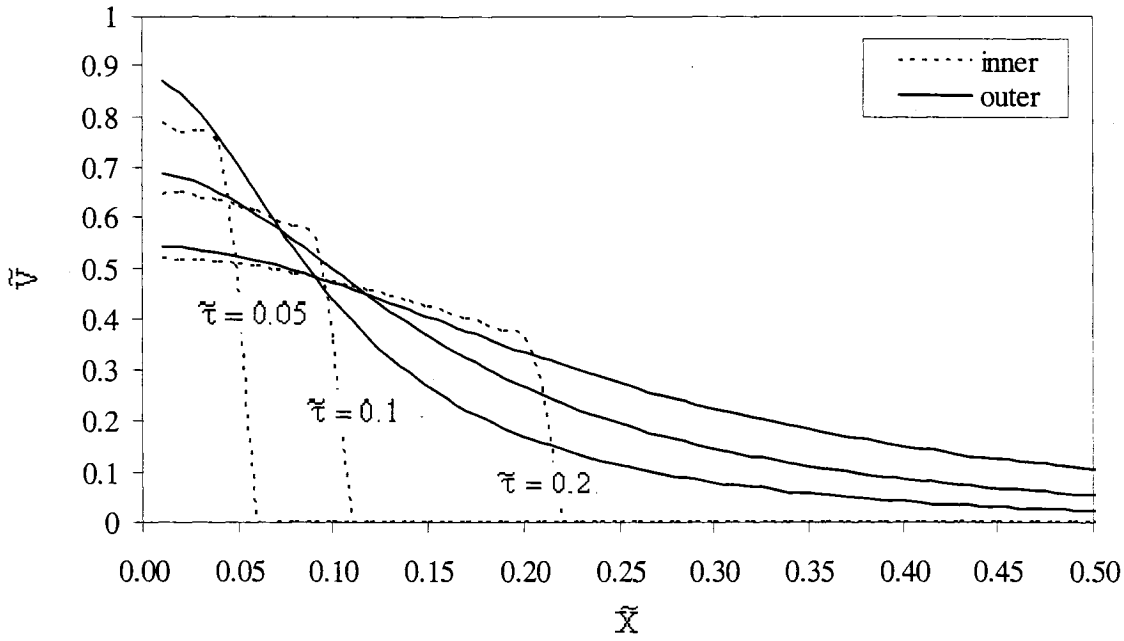

Figure 4.65 Comparison of spatial velocity development using inner and outer expansions, at various times.

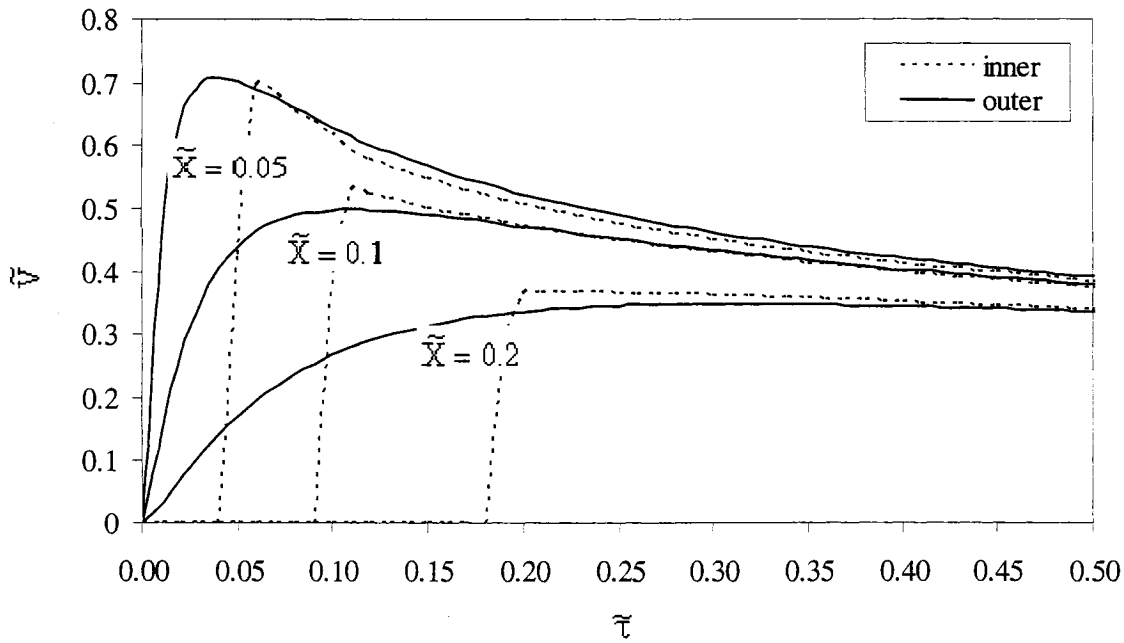

Figure 4.66 Comparison of temporal velocity development using inner and outer expansions, at various distances.

4.3.2.3. FDT Regime

(i) Outer Solutions

The implicit finite difference form used herein for solving the outer expansion for the FDT regime case can be written:

$$\frac{H_i^{k+1} - H_i^k}{\Delta\tau} = \frac{1}{\sqrt{\frac{C_4}{C_1}\frac{H_{i+1}^{k+1} - H_{i-1}^{k+1}}{2\Delta X}}} \frac{H_{i+1}^{k+1} - 2H_i^{k+1} + H_{i-1}^{k+1}}{\Delta X^2} \qquad [4\text{-}150]$$

In case $H_X = 0$, the denominator becomes zero. In order to eliminate this problem, the objective function was defined to find out the optimum value of H_i^{k+1} instead of rearranging the equation for H_i^{k+1}. The objective function can be expressed as:

$$\sqrt{\frac{C_4}{C_1}\frac{H_{i+1}^{k+1} - H_{i-1}^{k+1}}{2\Delta X}}\left(\frac{H_i^{k+1} - H_i^k}{\Delta\tau}\right) - \frac{H_{i+1}^{k+1} - 2H_i^{k+1} + H_{i-1}^{k+1}}{\Delta X^2} = 0 \qquad [4\text{-}151]$$

To solve the above objective function for H_i^{k+1}, MATLAB function 'fzero' was used. The V can be obtained using:

$$V_i^{k+1} = \sqrt{\frac{C_1}{C_4}\frac{H_{i+1}^{k+1} - H_{i-1}^{k+1}}{2\Delta X}} \qquad [4\text{-}152]$$

(ii) Inner Solutions

The procedure used to get H and V was similar to the numerical solution described in laminar and PDT cases. First, the following zeroed coefficients are put into the full problem.

$$C_2 = C_3 = C_7 = 0 \qquad [4\text{-}153]$$

Second, the characteristic must be re-defined using inner coordinate. The integration should follow the new inner characteristic:

$$\Delta\tau = \frac{\Delta X}{\sqrt{\frac{C_1}{C_6}}} \rightarrow \Delta\tilde{\tau} = \Delta\tilde{X} \qquad [4\text{-}154]$$

H_{P_i} can then be expressed as:

$$H_{P_i} = 0.5\left[H_{i-1} + H_{i+1} + \sqrt{\frac{C_6}{C_1}}\left(\tilde{V}_{i-1} - \tilde{V}_{i+1}\right) - \frac{C_4}{C_1}\Delta\tilde{X}\left(\tilde{V}_{i-1}\left|\tilde{V}_{i-1}\right| - \tilde{V}_{i+1}\left|\tilde{V}_{i+1}\right|\right)\right] \qquad [4\text{-}155]$$

After calculating H_{P_i}, the value of V_{P_i} can be obtained using:

$$\tilde{V}_{P_i} = \sqrt{\frac{C_1}{C_6}}\left[-H_{P_i} + H_{i-1} - \frac{C_4}{C_1}\Delta\tilde{X}\tilde{V}_{i-1}\left|\tilde{V}_{i-1}\right|\right] + \tilde{V}_{i-1} \qquad [4\text{-}156]$$

or using:

$$\tilde{V}_{P_i} = \sqrt{\frac{C_1}{C_6}}\left[H_{P_i} - H_{i+1} - \frac{C_4}{C_1}\Delta\tilde{X}\tilde{V}_{i+1}\left|\tilde{V}_{i+1}\right|\right] + \tilde{V}_{i+1} \qquad [4\text{-}157]$$

The value of $\tilde{V}$ at the upstream end of the problem can be calculated using eqn [4-157] and its value at its downstream end can be calculated using eqn [4-156].

(iii) Solutions for Inner Expression of Outer Zone

The implicit finite difference form for inner expression of the outer zone can be expressed as:

$$\frac{H_i^{k+1} - H_i^k}{\Delta\tilde{\tau}} = \frac{1}{\sqrt{\frac{C_4}{C_1}\frac{H_{i+1}^{k+1} - H_{i-1}^{k+1}}{2\Delta\tilde{X}}}} \frac{H_{i+1}^{k+1} - 2H_i^{k+1} + H_{i-1}^{k+1}}{\Delta\tilde{X}^2} \qquad [4\text{-}158]$$

In case $H_X = 0$, the denominator becomes zero. In order to eliminate this problem, the objective function was defined to find out the optimum value of H_i^{k+1} instead of rearranging the equation for H_i^{k+1}. The objective function can be expressed as:

$$\sqrt{\frac{C_4}{C_1}\frac{H_{i+1}^{k+1}-H_{i-1}^{k+1}}{2\Delta\tilde{X}}}\left(\frac{H_i^{k+1}-H_i^k}{\Delta\tilde{\tau}}\right)-\frac{H_{i+1}^{k+1}-2H_i^{k+1}+H_{i-1}^{k+1}}{\Delta\tilde{X}^2}=0 \qquad [4\text{-}159]$$

The V can then be calculated using:

$$\tilde{V}_i^{k+1}=\sqrt{\frac{C_1}{C_4}\frac{H_{i+1}^{k+1}-H_{i-1}^{k+1}}{2\Delta\tilde{X}}} \qquad [4\text{-}160]$$

(iv) Comparison of Results: Inner Coordinate Zone

In order to achieve the FDT regime a hydraulic gradient of 400 was applied. The same numerical methods were used that were applied for laminar and PDT cases. In Figures 4.67 and 4.68 the spatial and temporal profiles of head are presented. The spatial development of head using the inner and outer expansion is depicted in Figure 4.67, at various snapshots in time. The results show profiles that are similar to those for the laminar and PDT regimes. Because the definition of scaling factors for the FDT regime was different from those of the laminar and PDT regimes, the evolving wave properties disappear in much smaller time-space than those of the laminar and PDT regimes. The relative size of the space scaling-factor 'a' is:

$$a_{i=400_{FDT}}=0.0014a_{i=10_{PDT}}$$

and for the time scaling factor 'b' this is:

$$b_{i=400_{FDT}}=0.0003b_{i=10_{PDT}}$$

In Figure 4.68 temporal development of head using the inner and outer-expansion solutions is compared at various locations. It is observed that in very small time and space, the head development of the inner expansion shows a sharper rate of increase than the outer expression solution. Figure 4.69 shows the spatial profile of $\tilde{V}$ at various times. It can be seen that H and $\tilde{V}$ behave in a similar manner. The maximum difference between inner and outer solutions again occurs at around $\tilde{X}=\tilde{\tau}$. As was observed for the PDT case, the $\tilde{V}$'s using the inner expansion are smaller than $\tilde{V}$'s using

the outer expansion when $\tilde{\tau} = 0.5$. When $\tilde{\tau} = 1.0$ and $\tilde{\tau} = 2.0$, the $\tilde{V}$'s for the inner solution case are smaller than those of the outer case except for a small range near $\tilde{X} \rightarrow \tilde{\tau}$. In the small time-space region, the order of error can be close to 1. The temporal profile of $\tilde{V}$ using both the inner and outer-expansion solutions are presented in Figure 4.70. The outer expansion overestimates $\tilde{V}$ when $\tilde{\tau}$ is smaller than $\tilde{X}$.

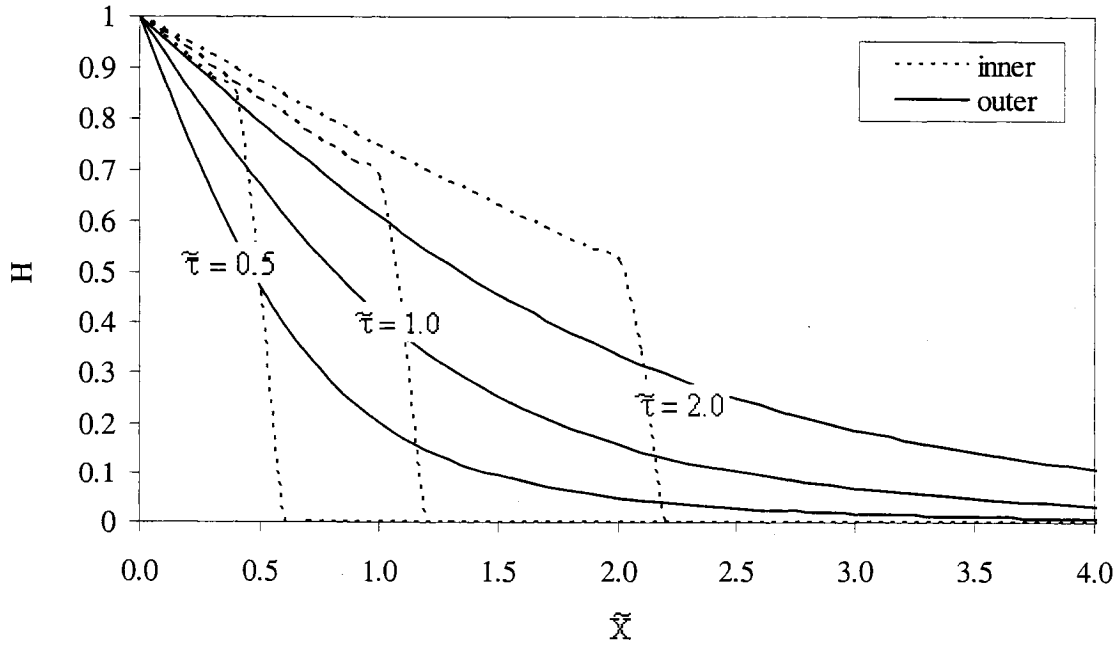

Figure 4.67 Comparison of spatial head development using inner and outer expansions, at various times.

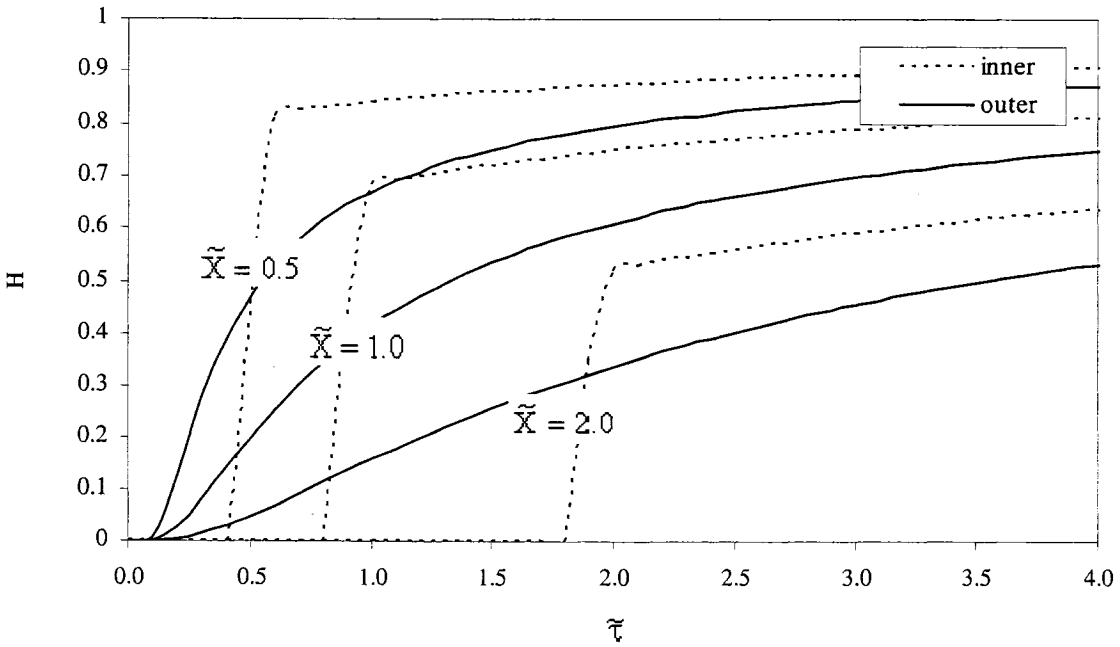

Figure 4.68 Comparison of temporal head development using inner and outer expansions, at various distances.

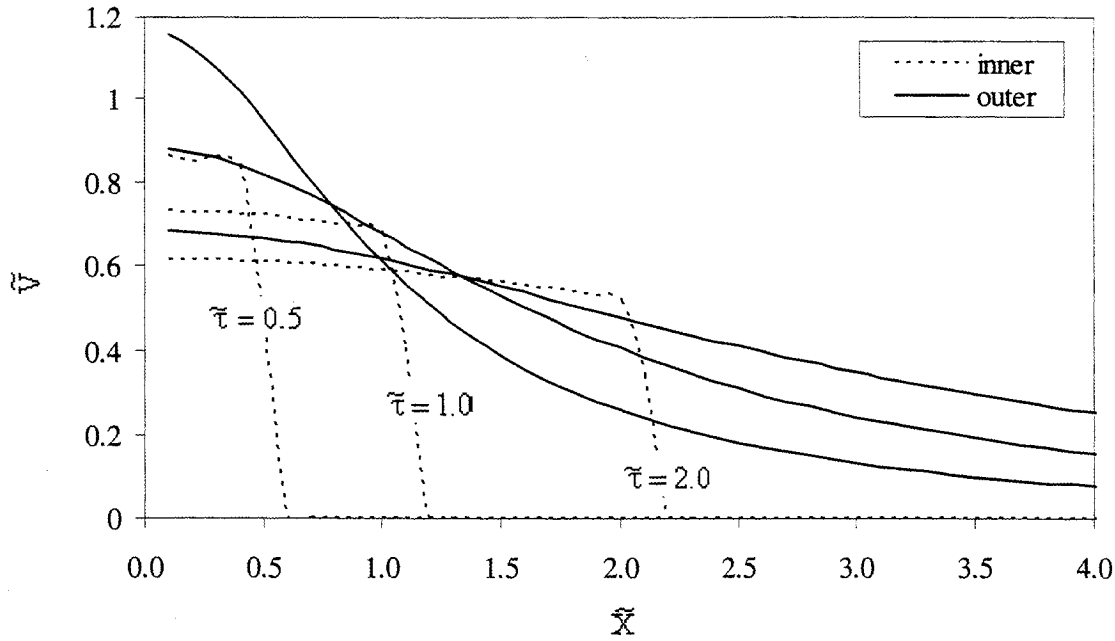

Figure 4.69 Comparison of spatial velocity development using inner and outer expansions, at various times.

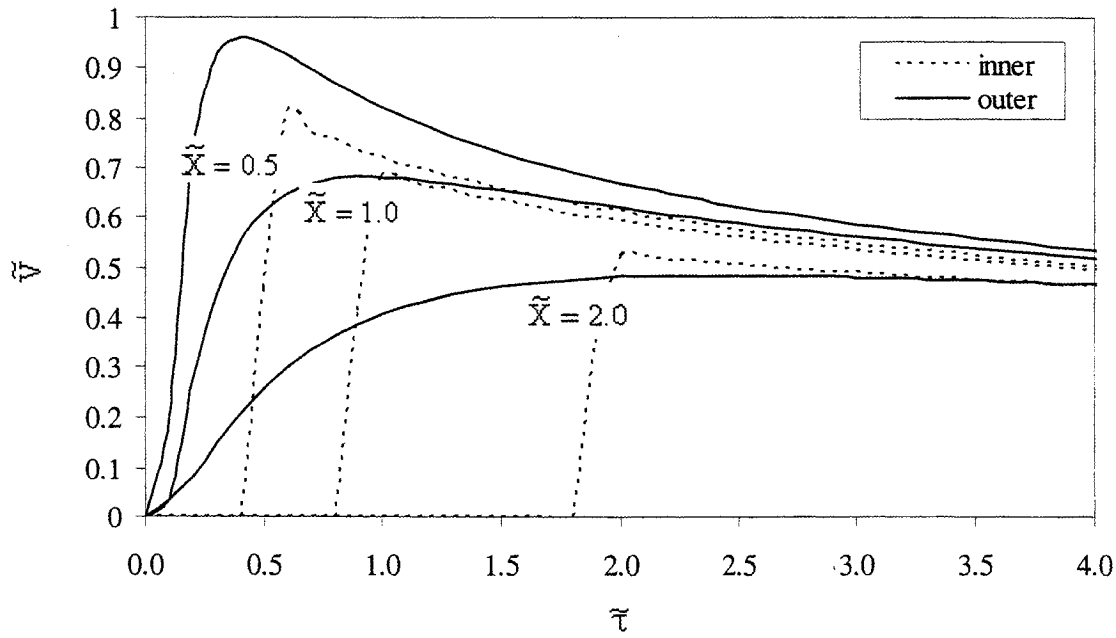

Figure 4.70 Comparison of temporal velocity development using inner and outer expansions, at various distances.

4.3.3. Matching

The outcomes for H and V using inner and outer expansions were matched using numerical methods. Large differences in the inner, intermediate differences in an overlap zone, and small differences in the outer zone were expected between the results of inner and outer expansions. The results for the inner expansion versus the inner expression of the outer case/zone were compared using contour maps. The H and V solutions from the inner expansion versus the solutions via the inner expression of outer expansion and the inner expression of the complete momentum and continuity equation were also compared by following $\tau = \sqrt{\frac{C_6}{C_1}}X$ characteristic. The solutions for inner expansion were obtained using method of characteristics, and the solutions of outer expansion were obtained using implicit finite difference numerical solutions, and for all three regimes.

4.3.3.1. Laminar Regime

Inner and outer-expansion solutions were compared using a relatively wide range of time-space positions. Figures 4.71 and 4.72 are contour maps of the differences in H between inner and outer expansion in the laminar regime for an applied hydraulic gradient of 0.1. As shown in section 4.3.2 on numerical solutions, the differences are large in the inner region but become small close to outer region. Figure 4.71 shows large differences in the inner region. Because the differences in the inner and outer regions have different order, the differences in the outside of the inner region are presented separately (Figure 4.72). From the momentum equations for the inner and the outer expansions, it is evident the differences between inner and outer must be caused by the local acceleration term, $(C_6 / C_1)V_\tau$. Thus, in the outer region we may predict the order of error to be O(C6/C1). For an applied hydraulic gradient of 0.1, the order of the error is O(0.003). Figure 4.72 shows that the error is distributed homogeneously, with the order of the error being O(0.003) in the outer region.

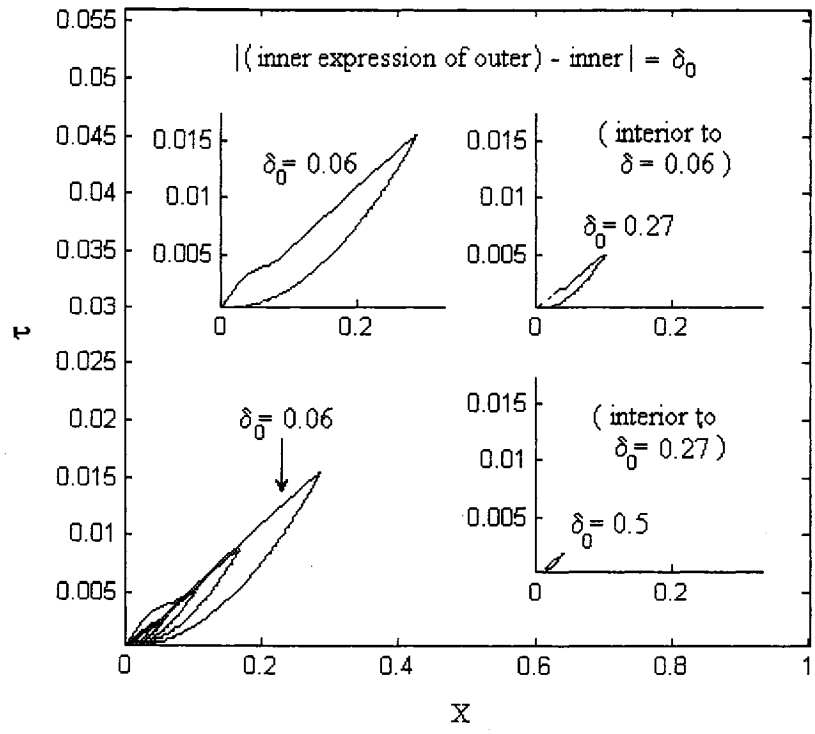

Figure 4.71 Differences of H between inner and outer expansions.

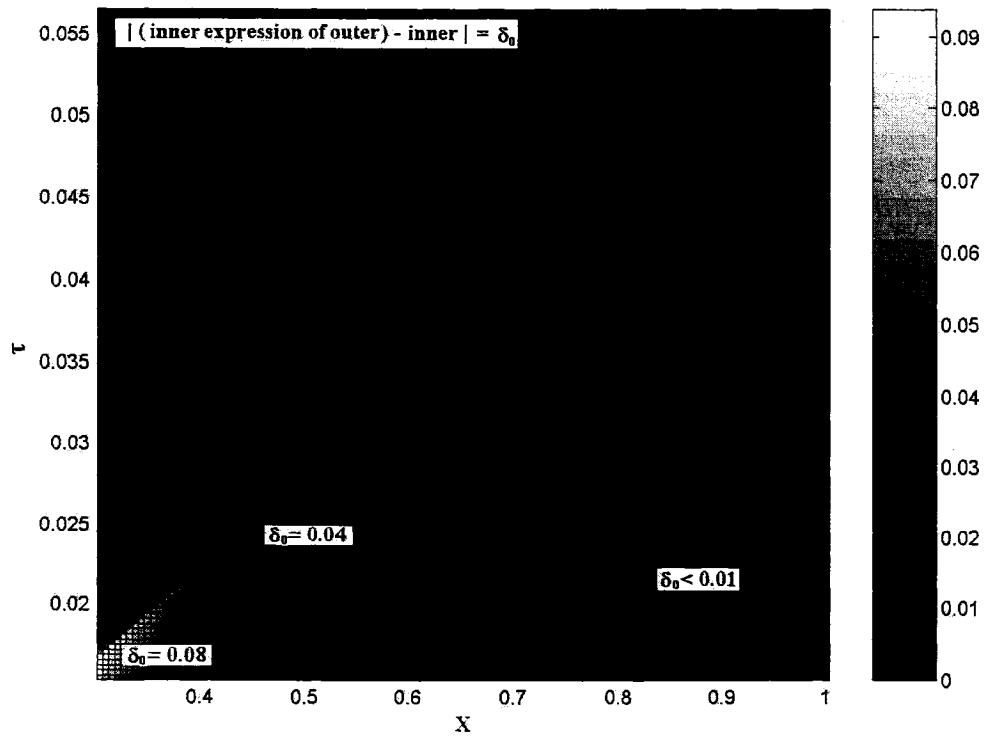

Figure 4.72 Differences of H between inner and outer expansions in outside inner.

Similar results were obtained for velocity, as compared to head. Figure 4.73 7.15 and 4.74 are contour maps showing the differences in V between the inner and outer expansions. Figure 4.73 shows large differences in the inner zone. Considering the magnitude of X and τ on the horizontal and vertical axes, it is observed that contour lines exist, and follow $\tau = \sqrt{\frac{C_6}{C_1}}X$, or $\tau = \sqrt{0.03}X$. Figure 4.74 shows differences in V between the inner and outer expansion on the outside of the inner region. A homogeneous error distribution is evident in this region.

As shown in the comparison of the spatial and temporal development of H and V, the inner expansion produces sudden changes in H and V when $\tau = \sqrt{\frac{C_6}{C_1}}X$. Because of the evolving wave characteristics, large differences are expected along the $\tau = \sqrt{\frac{C_6}{C_1}}X$ characteristic or $\tilde{\tau} = \tilde{X}$ in the inner. In Figure 4.75, the H from inner-expansion solution, the inner expression of the outer expansion, and the inner expression of the complete momentum and continuity equation were compared along the $\tau = \sqrt{\frac{C_6}{C_1}}X$ characteristic. The solutions for the inner expansion and the complete equation were obtained using the method of characteristics; the solutions for outer expansion were obtained using the implicit finite difference method. The results as a contour map are similar. For the inner expansion, the initial head of 1 around X = 0 decreases slowly compared with the outer expansion. This shows the wave property in the evolving wave equation. Figure 4.76 compares the velocity development for inner expansion only, the inner expression of the outer expansion, and the inner expression of the complete momentum and continuity equation along $\tau = \sqrt{\frac{C_6}{C_1}}X$. Because the momentum equation in the outer zone follows Darcy's Law, the hydraulic gradient becomes extremely large as X tends to zero. As a result, the velocity can increase to unrealistic values, i.e. $\tilde{V} > 1$.

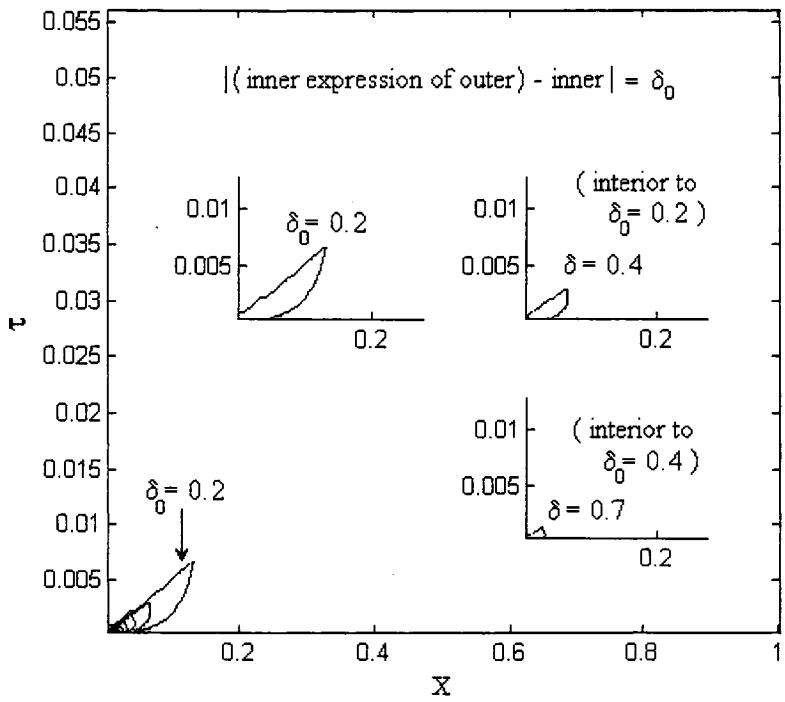

Figure 4.73 Differences of V between inner and outer expansions.

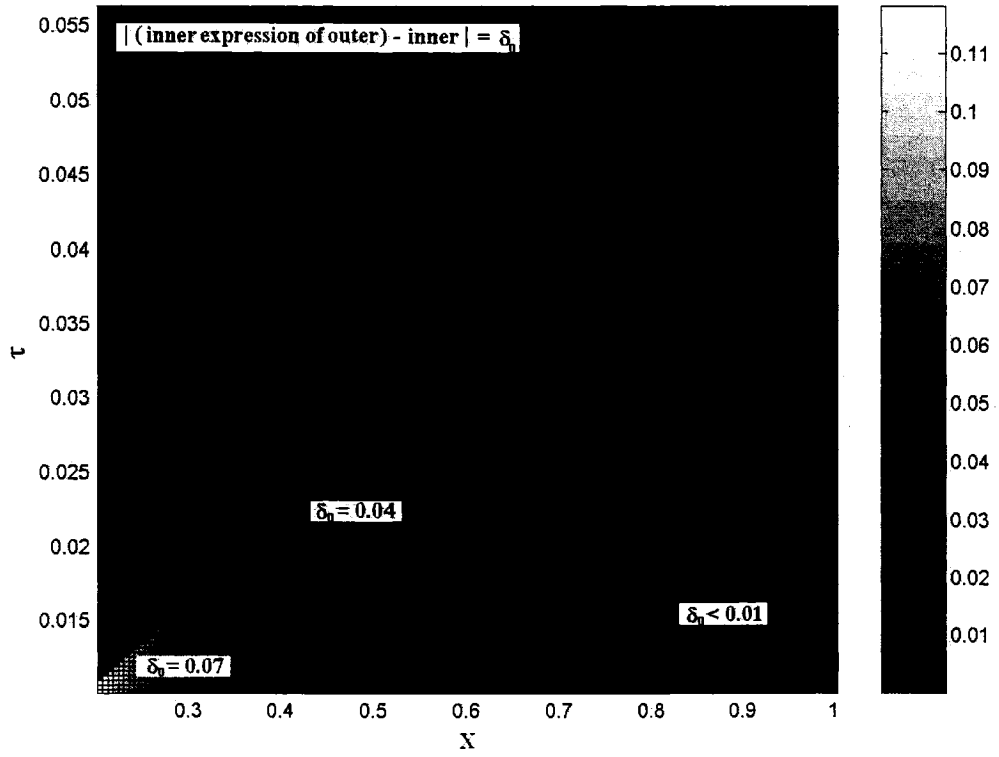

Figure 4.74 Differences of V between inner and outer expansions in outside inner.

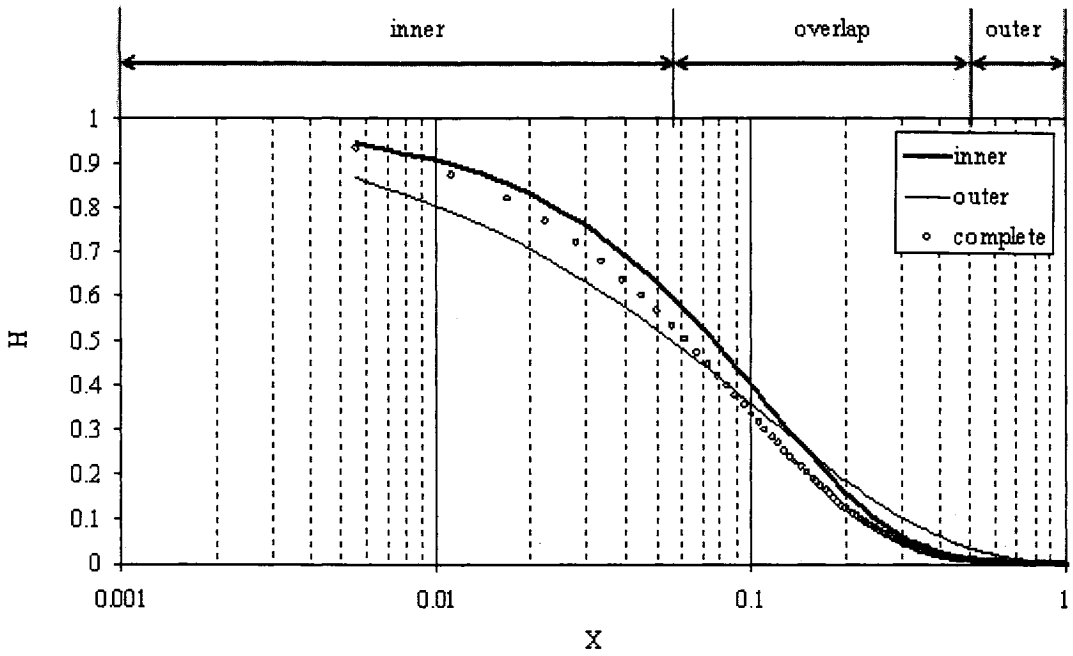

Figure 4.75 Head development along $\tau = \sqrt{\frac{C_6}{C_1}}X$.

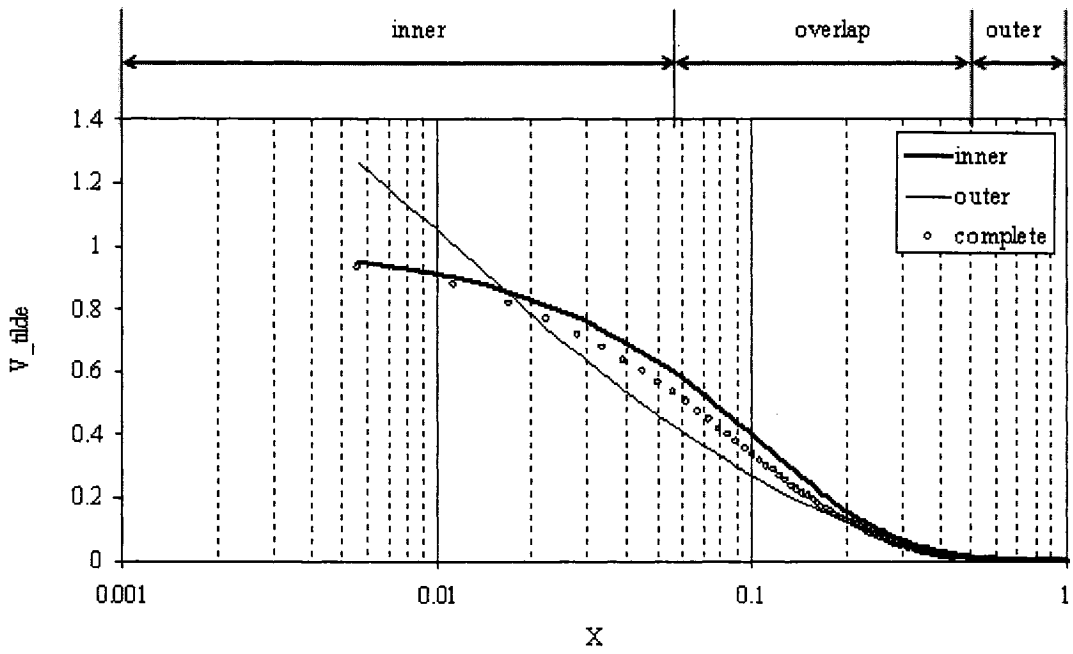

Figure 4.76 Velocity development along $\tau = \sqrt{\frac{C_6}{C_1}}X$.

4.3.3.2. PDT Regime

In order to investigate the PDT regime, a hydraulic gradient of 10 was applied. Figure 4.77 and 4.78 show the differences in H between the inner and outer expansions for this regime. As with the laminar regime, the differences are large in the inner region but become small close to the outer region. Figure 4.77 clearly shows the large differences of H in the inner region. In Figure 4.78, the differences in inner and outer-expansion solutions are seen at the outside of the inner region. As with the laminar regime, the differences between the inner and outer solutions are caused by the local acceleration term, $(C_6 / C_1)V_\tau$, in the momentum equation. Thus, the order of error in the outer region is O(C6/C1). For an applied hydraulic gradient of 10, the order of the error in the outer region is O(0.001). It can be seen in Figure 4.78 that the errors are distributed homogeneously, with the order of the error being O(0.001) in the outer region. When we compare the results for PDT regime with those of laminar regime, the relative scales of time and space must not be forgotten. The PDT figures cover X up to about 0.35 and τ up to 0.01. These are smaller than X up to 1 and τ up to 0.055 plotted for the laminar regime.

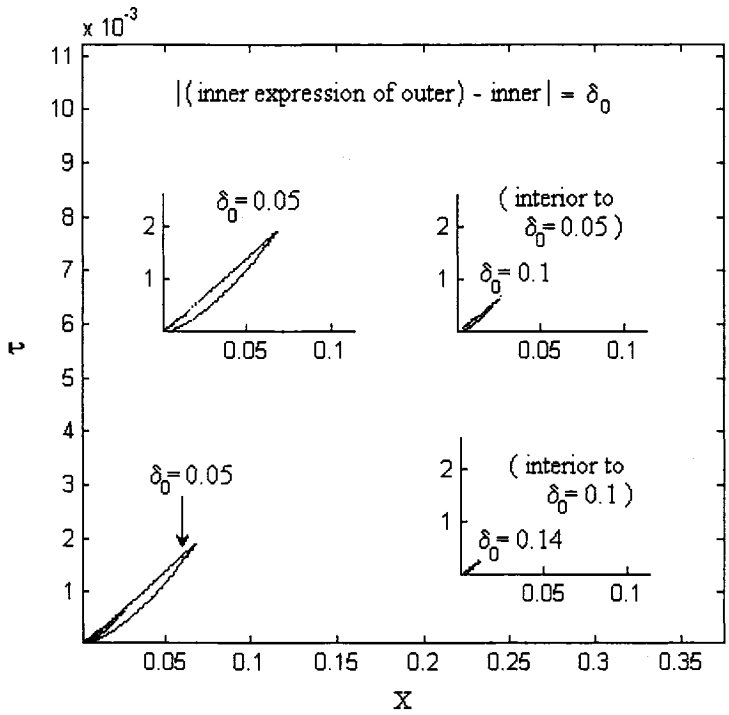

Figure 4.77 Differences of H between inner and outer expansions.

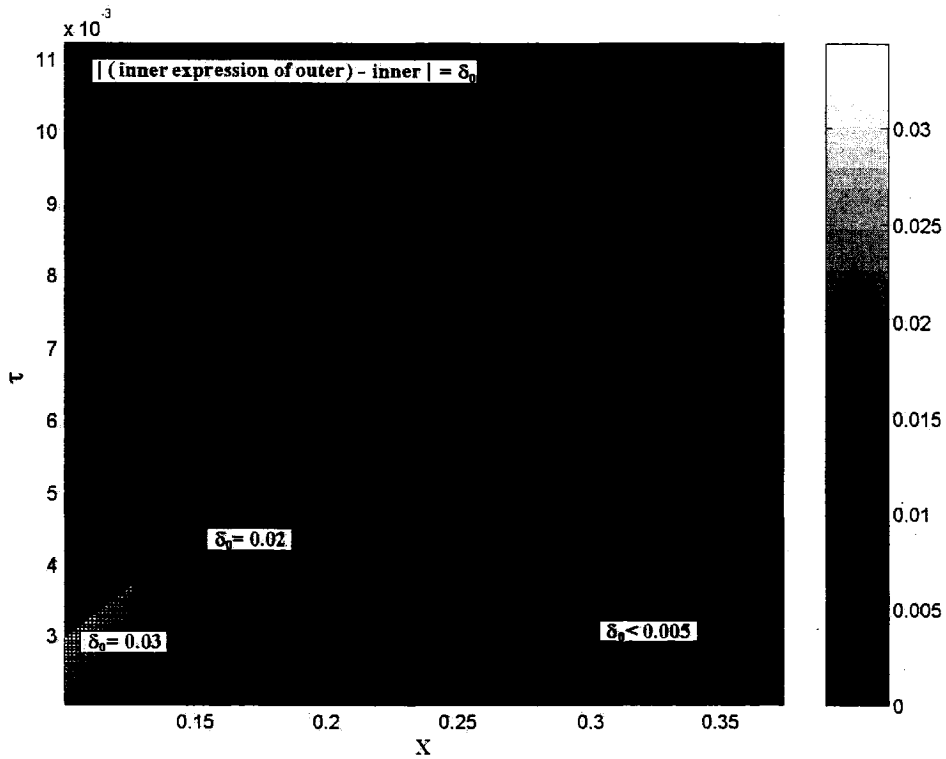

Figure 4.78 Differences of H between inner and outer expansions in outside inner.

For velocity, results to those seen for head are evident. Figure 4.79 and 4.80 are the contour maps showing differences in V between inner and outer-expansion solutions. In Figure 4.81, contour lines are present along $\tau = \sqrt{\frac{C_6}{C_1}}X$, or $\tau = \sqrt{0.001}X$. Figure 4.82 shows differences in V between inner and outer-expansion solutions at the outside of the inner region. A relatively uniform distribution of error is seen in the outer region. In Figure 4.81, the H from the inner expansion, from the inner expression of outer expansion, and from the inner expression of the complete solution of the momentum and continuity equations are compared along the $\tau = \sqrt{\frac{C_6}{C_1}}X$ characteristic. Similar results are evident on the contour map. Figure 4.82 compares the velocity from the same three solution methods. Because the momentum equation for the outer zone follows the Ergun equation with the inertial term retained, we can see as X tends to zero, the hydraulic gradient becomes extremely large and as a result, the velocity becomes unrealistic (i.e. $\tilde{V} > 1$). For both H and V the inner region and the overlap region are smaller in time and space than for the laminar regime. Also, even though the magnitude of maximum $\tilde{V}$ in the PDT regime is similar to the laminar regime, very different dimensionless V's result because of the scaling factor for V. For an applied hydraulic gradient of 10, the scaling factor for V is about twice as large than that of the laminar regime with an applied hydraulic gradient of 0.1.

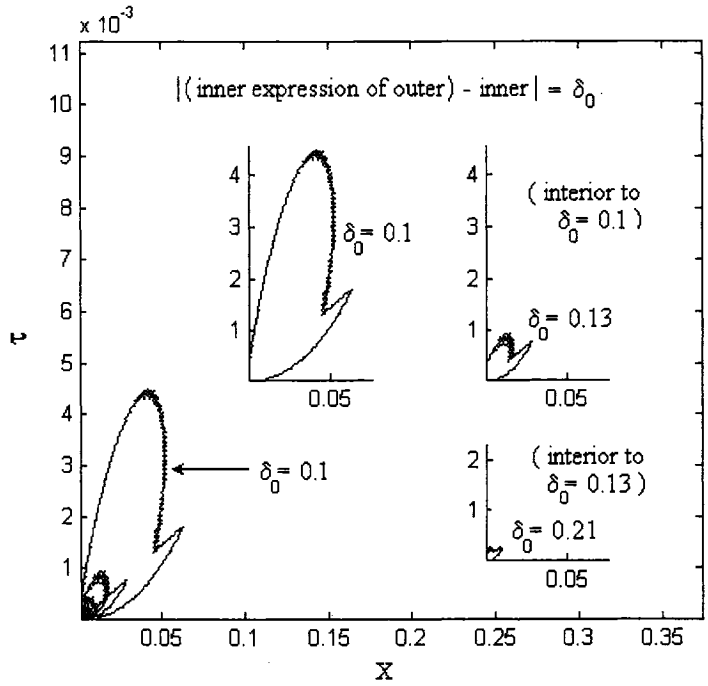

Figure 4.79 Differences of V between inner and outer expansions.

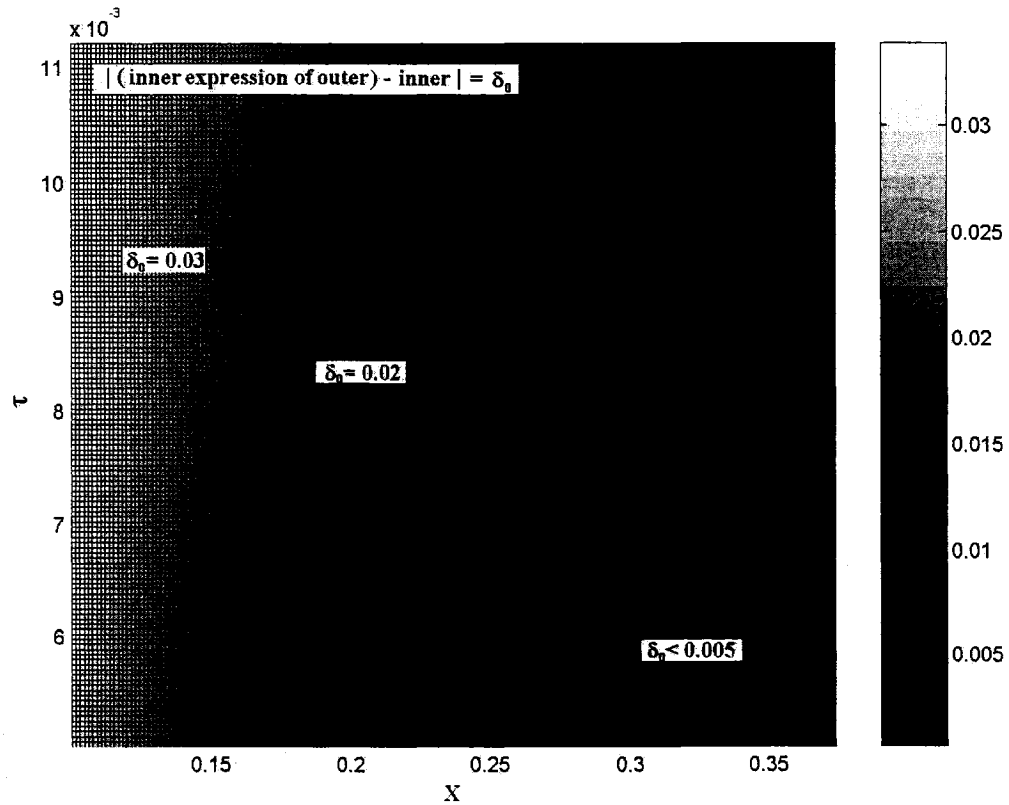

Figure 4.80 Differences of V between inner and outer expansions in outside inner.

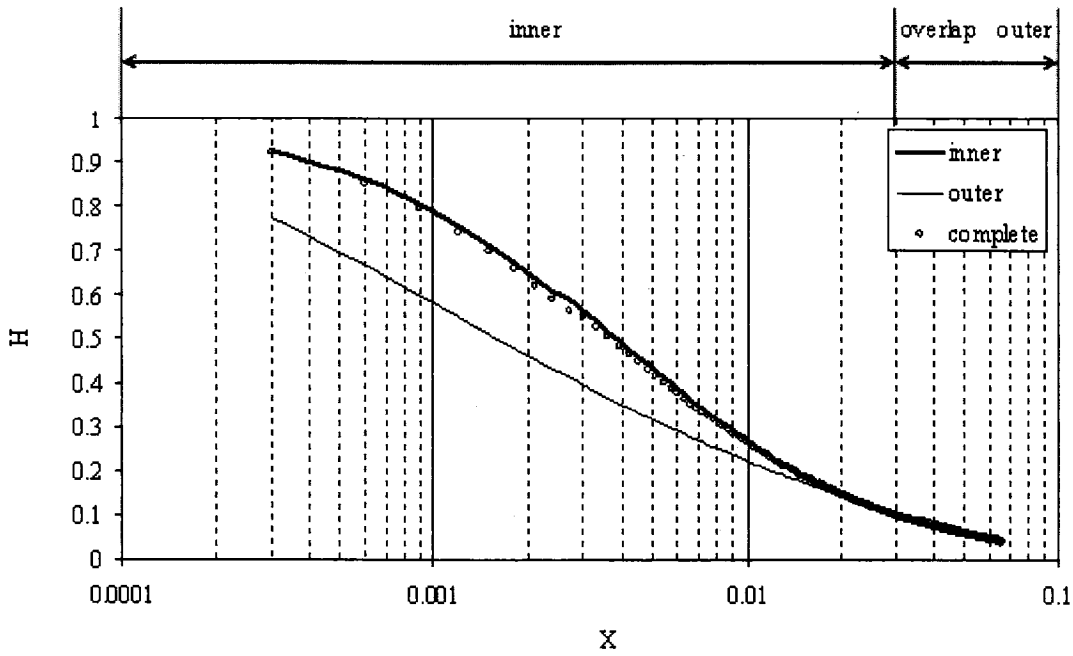

Figure 4.81 Head development along $\tau = \sqrt{\frac{C_6}{C_1}}X$.

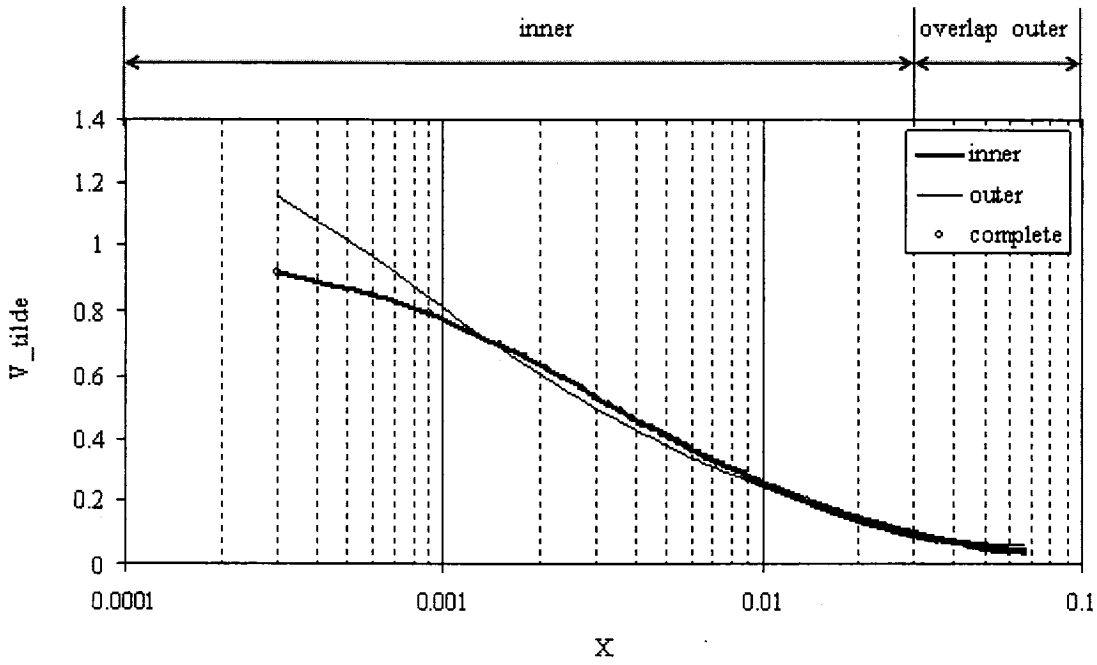

Figure 4.82 Velocity development along $\tau = \sqrt{\frac{C_6}{C_1}}X$.

4.3.3.3. FDT Regime

For FDT regime, a hydraulic gradient of 400 was applied. Figures 4.83 and 4.84 show the differences in H between the inner and outer expansions for the FDT regime. As shown for the laminar and PDT regimes, the differences are large in the inner region but become small close to the outer region. Figure 4.83 clearly shows the large differences in H in the inner region. Differences between inner and outer-expansion solutions are shown in the outside of the inner region in Figure 4.84. As with the, laminar and PDT regime cases, the differences between the inner and outer were caused by the local acceleration term, $(C_6 / C_1)V_\tau$, in the momentum equation. Thus, the order of error will be O(C6/C1) in the outer region. For an applied hydraulic gradient of 400, the order of the error is O(0.0004). The figures for FDT contours cover X up to about 0.005 and τ up to 0.00003, which are much smaller than X and τ in the laminar and PDT regimes.

Velocity results are similar to those for head. Figures 4.85 and 4.86 are contour maps showing differences in V between inner and outer expansions. In Figure 4.85, the contour lines develop along $\tau = \sqrt{\frac{C_6}{C_1}}X$, or $\tau = \sqrt{0.0004}X$. Figure 4.86 shows differences in V between inner and outer expansion in the outside of the inner region. A relatively uniform distribution of error can be seen in the outer region. In Figure 4.87, the H from the inner expansion, from the inner expression of outer expansion, and from the inner expression of the complete solution of the momentum and continuity equations are compared along $\tau = \sqrt{\frac{C_6}{C_1}}X$ characteristic. Similar results are evident in the contour map. Figure 4.88 compares the velocity from the same three solution methods. For both H and V, it can be seen that the inner region and the overlap region are smaller in time and space than for the laminar and PDT regimes.

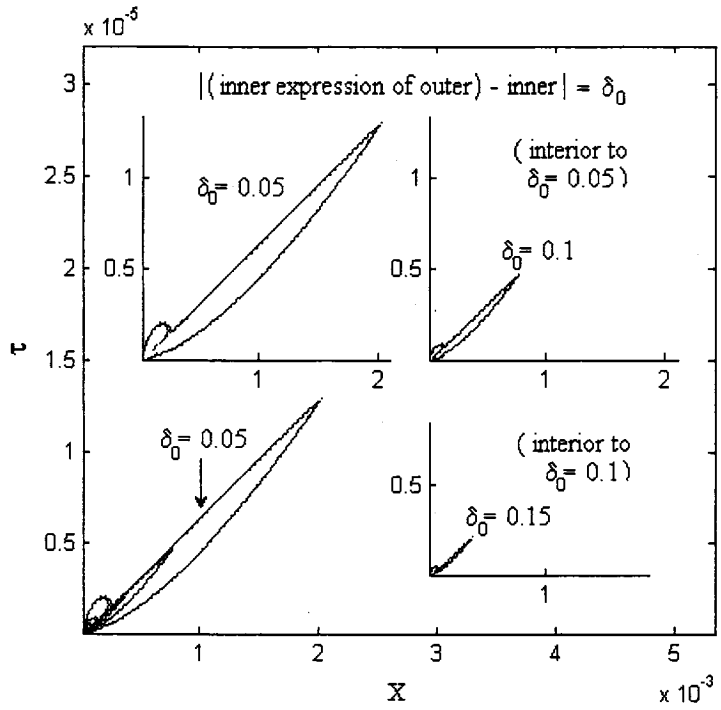

Figure 4.83 Differences of H between inner and outer expansions.

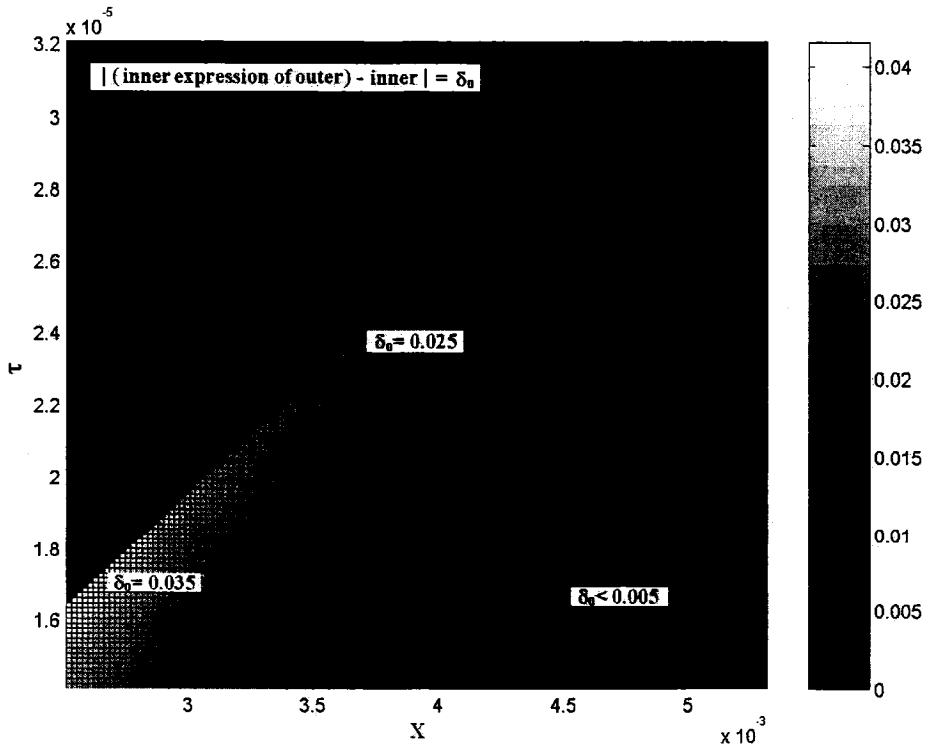

Figure 4.84 Differences of H between inner and outer expansions in outside inner.

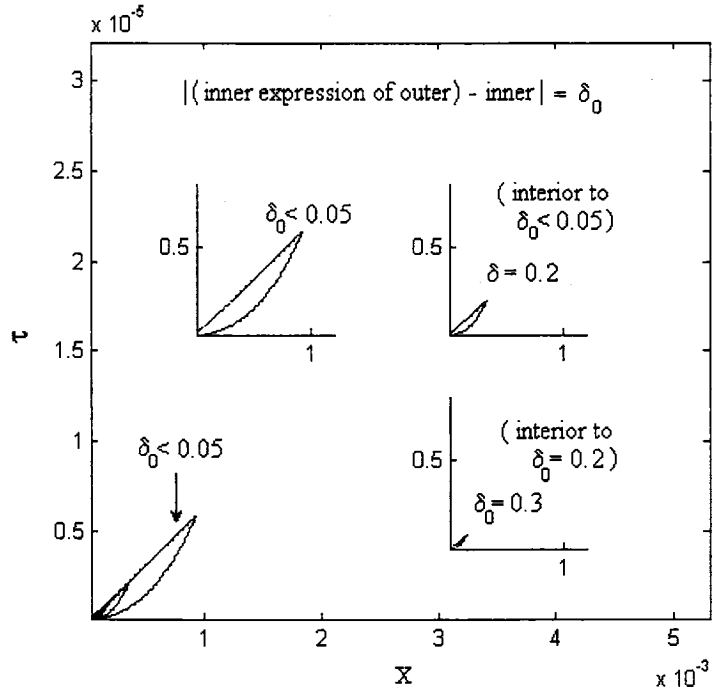

Figure 4.85 Differences of V between inner and outer expansions.

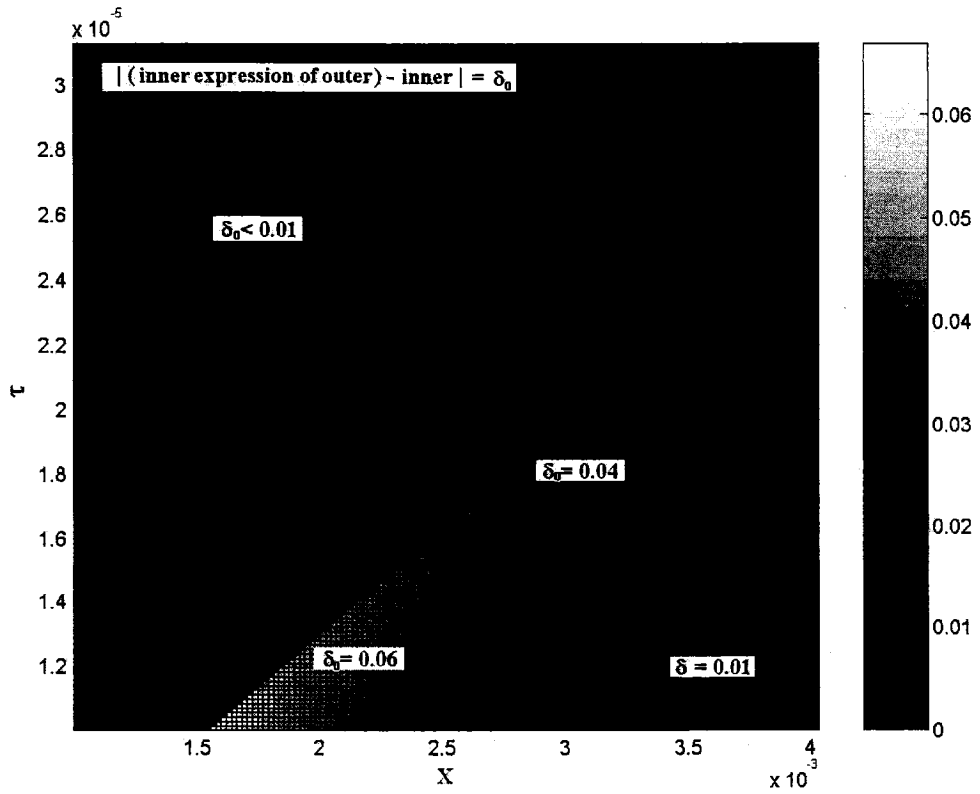

Figure 4.86 Differences of V between inner and outer expansions in outside inner.

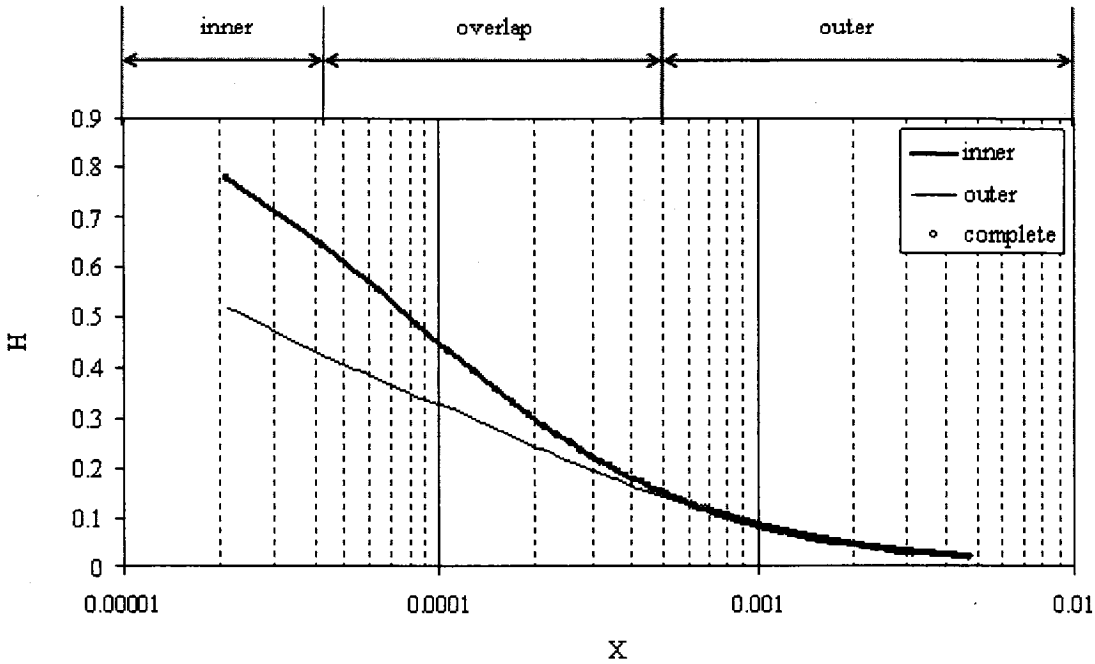

Figure 4.87 Head development along $\tau = \sqrt{\frac{C_6}{C_1}}X$.

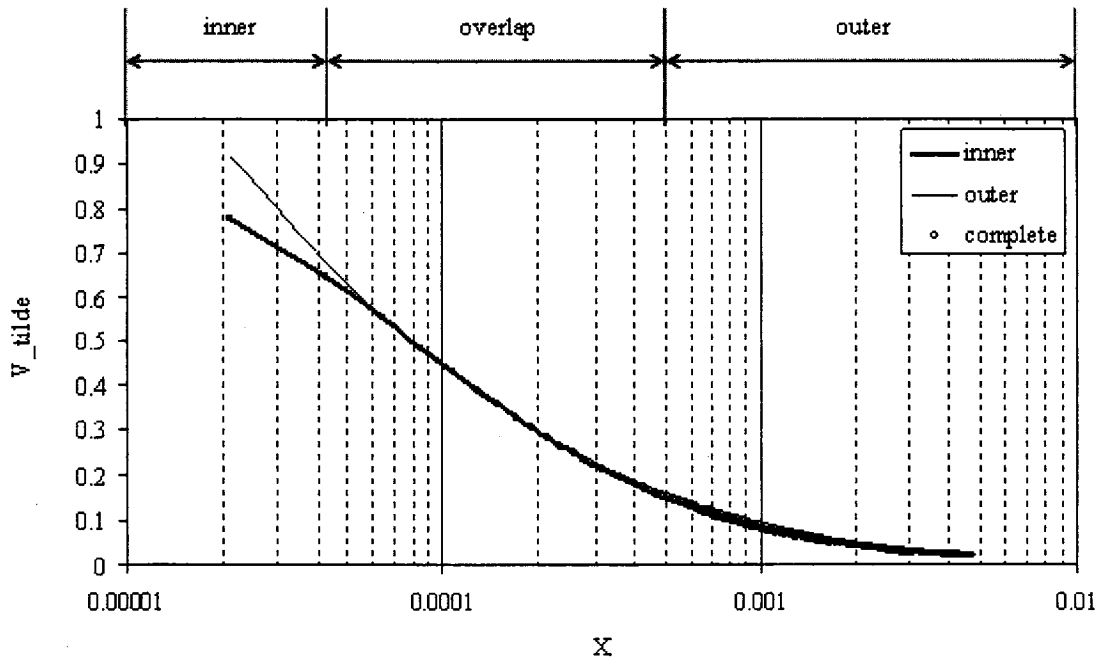

Figure 4.88 Head development along $\tau = \sqrt{\frac{C_6}{C_1}}X$.

Also, even though the magnitude of maximum inner velocity, $\tilde{V}$, in the FDT regime is similar to that of the laminar and PDT regimes, we may get very different dimensionless outer V's because of the inner variable scaling-factor for V. For an applied hydraulic gradient of 400, the scaling factor for V is about 4.6 times larger than that of the PDT regime with an applied hydraulic gradient of 10, and about 8.6 times larger than that of laminar regime with an applied hydraulic gradient of 0.1.

4.3.4. Summary

4.3.4.1. Inner and Outer Expansions in LAM, PDT and FDT Regime

A simple diffusion equation governs laminar flow in the outer zone. Within this zone, describable by this outer expansion, it is evident that H can be obtained using only its boundary and initial conditions, without even considering V. It is also evident that a fast diffusion equation governs PDT and FDT flows in the outer zone. In the zone describable by the inner expansion, the governing equation is an evolving-wave for all three regimes. However, each such evolving wave equation has its own form. In the laminar regime, H can be obtained without considering $\tilde{V}$. Further, $\tilde{V}$ can be calculated without considering H, as long as proper boundary and initial conditions can be defined for $\tilde{V}$. In the PDT and FDT regimes, $\tilde{V}$ is involved in the equation for H. Because H cannot be obtained without considering $\tilde{V}$ simultaneous calculation of H and $\tilde{V}$ is required. The momentum equation for the PDT regime includes both viscous and inertial terms. However, the inner and outer expansions describing unsteady PDT flow can be changed to forms identical to those of either the laminar or the FDT regimes if the conditions for these regimes are carefully defined. From the inner expansion expression for the PDT case, if the inertial term, $2cC_4 / C_1$, is negligible, the expression reduces to the inner expansion of the laminar case because $C_3 / C_1 = 1$ in the laminar regime. Similarly, if the viscous term, C_3 / C_1, is negligible, the expression reduces to the inner expansion for FDT flow. Whether the factor 'c' should be included in the inertial term or not depends on the scaling factors. For the outer expansion, if the inertial term, C_4 / C_1,

is negligible, the expression for the PDT regime reverts to the outer expansion of the laminar regime. Similarly, if the C_3 / C_1, viscous term is negligible, the expression for the PDT regime reverts to the outer expansion for the FDT regime.

4.3.4.2. Compound Scale

Figure 4.89 presents the scaling that were used for the laminar, PDT and FDT regimes. The size or extent of the inner zone in time and space decreased as the equilibrium flow became more turbulent (laminar to PDT and FDT). In other words, if a larger hydraulic gradient was applied, the equilibrium velocity increased and the extent of inner zone decreased. Notably, the dimensionless groups which defined or limited the extent of the inner zone were C_1 and C_6, and for all three regimes.

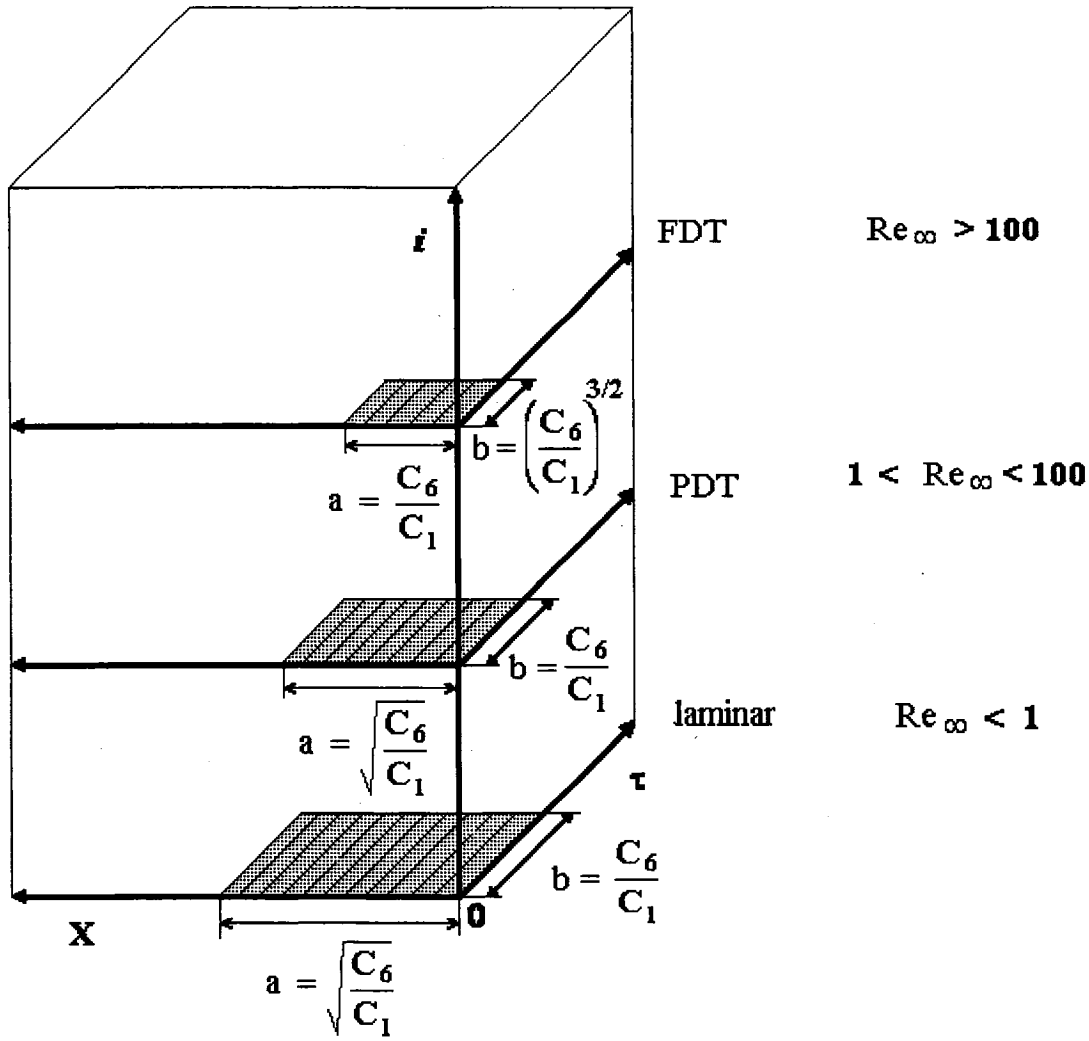

Figure 4.89 Illustration of how inner zone (hatched area) decreased with higher applied hydraulic gradient (not to scale).

Figure 4.90 shows space-scaling factor 'a' for various applied hydraulic gradients. As shown in Figure 4.90, 'a' decreased with increasing applied hydraulic gradient. Because of the linear relationship between velocity and hydraulic gradient, 'a' is in general, constant in laminar regime. Because the definition of scaling factors for the FDT regime were different from those of the laminar and PDT regimes, very small 'a' can be seen in the FDT regime. Similar results are shown for time-scaling factor 'b' in Figure 4.91. If we compare the magnitude of 'a' and 'b', it can be seen that the time-scaling factor, is much smaller than the space-scaling factor, which is due to the fact that

$\tau = \sqrt{C_6 / C_1} X$. Figure 4.92 shows the velocity-scaling factor 'c' as a function of the applied hydraulic gradients. The range of 'c' is from about 18 to about 170. This does not mean that the inner velocity for the FDT regime is 10 times larger than that of the laminar regime. Rather, it implies that the ratio of inner and outer velocity for the FDT is 10 times larger than the associated ratio for the laminar regime.

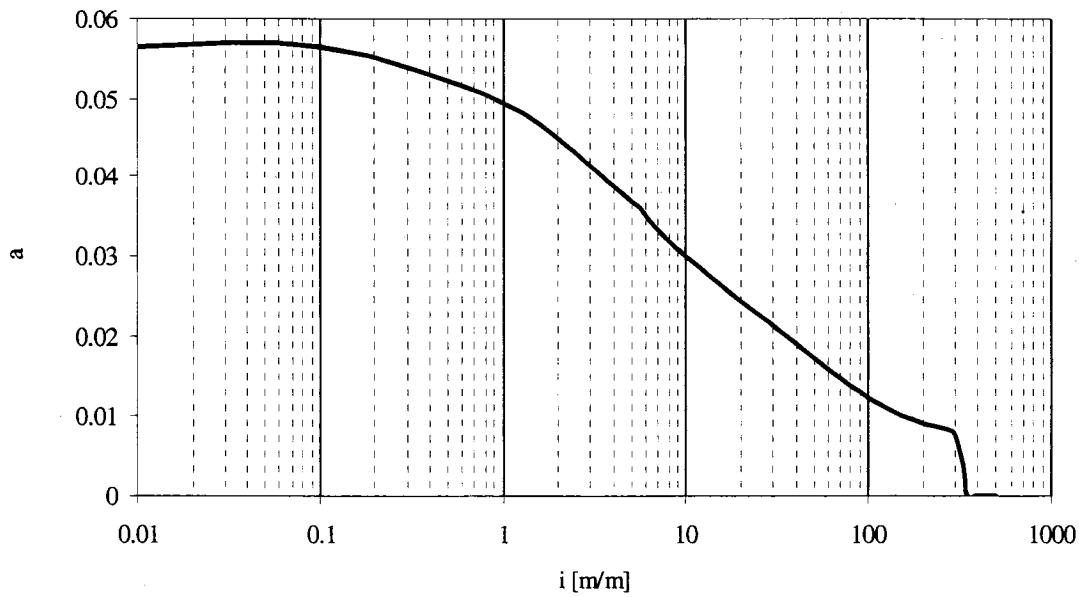

Figure 4.90 Space-scaling factor 'a' as a function of applied hydraulic gradient.

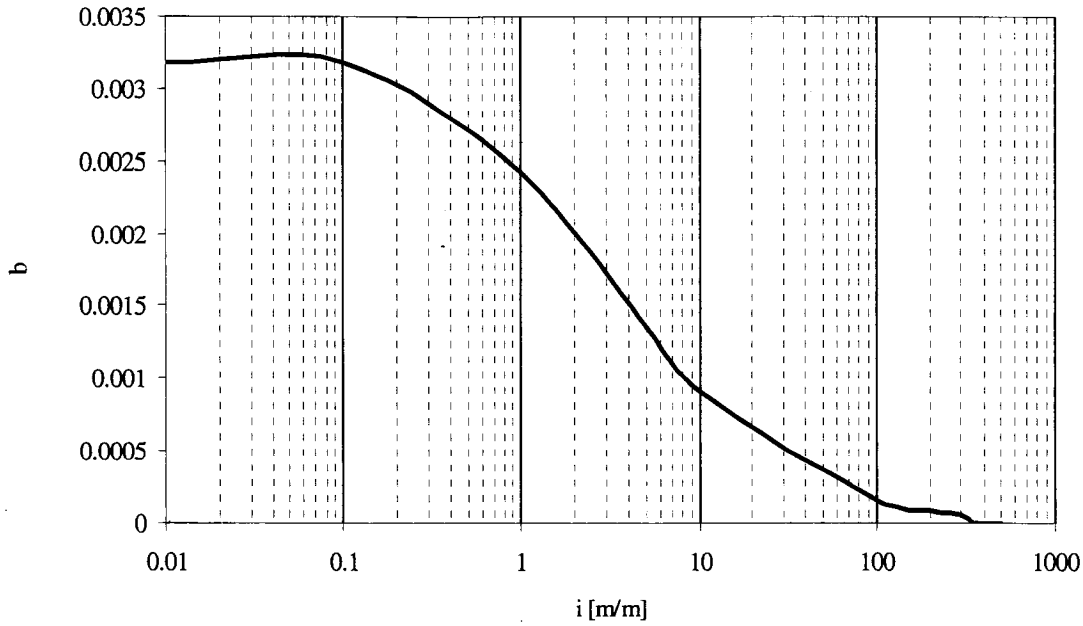

Figure 4.91 Time-scaling factor 'b' as a function of applied hydraulic gradient.

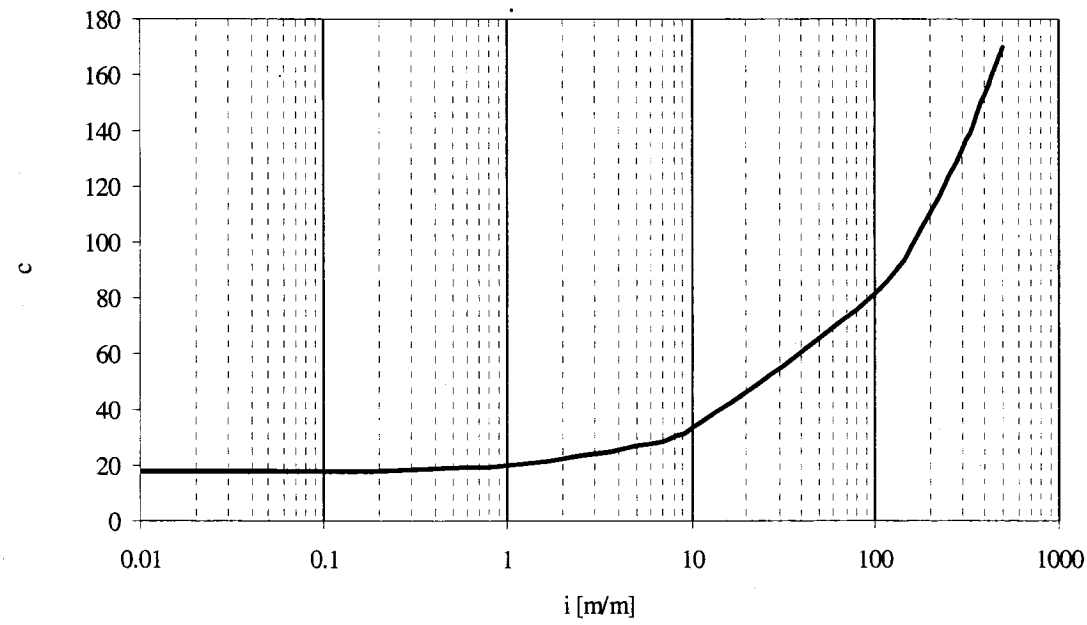

Figure 4.92 Velocity-scaling factor 'c' as a function of applied hydraulic gradient.

4.4. Dimensional Analysis

Many dimensionless numbers exist in fluid mechanics. However, only a limited number of them can be applicable for the porous media flow. For example, the Froude number plays a dominant role in free-surface flows but is usually negligible for unconfined flow through saturated porous media. Another example is the Weber number, which is the ratio of the effects of pressure to the effects of surface tension.

$$We = \frac{\rho L V^2}{\gamma} \qquad [4\text{-}161]$$

where:

ρ = density of fluid,

Υ = weight density of fluid,

L = sample length,

V = velocity of flow.

The Weber number is important only when the amount of curvature in the free surface is comparable to the depth. A typical boundary-value problem governing fluid transients in a rigid pipe involves two dimensionless numbers, the Reynolds number (Re) and the Mach number (Ma). Especially, the Reynolds number is one of the most important parameters in the study of flow through porous media (Ergun 1953, Mccourqudals 1978). For ordinary flow conditions, Re is large and Ma is small. For high-speed flow, if the speed of flow is comparable to the speed of sound in the fluid in question, density changes can become significant and the Mach number becomes relevant. If the pressure drops low enough to cause vapour formation (cavitation) in the liquid, the Euler number (Eu) should be considered. Euler number is a measure of the relative effects of pressure and inertia. For oscillatory flow conditions, Keulegan-Carpenter (KC) number can also be considered.

$$KC = \frac{V_m T_l}{d} \qquad [4\text{-}162]$$

where V_m is the maximum velocity, T_l is the period of the oscillatory flow and d is the diameter of media. The Peclet number (Pe) is an index of the relative importance of

diffusive effects compared to advective effects. It is normally used to address questions involving heat or chemical transfer. However, the concept of the Peclet number might be applied for head or pressure propagation in porous media flow study. In this chapter, various dimensionless ratios are investigated. The magnitude of each such ratio and the ratio of groups (ratios) are considered. Relationships between existing dimensionless numbers and ratios of dimensionless numbers are presented. These relationships can be used to show how the ratio of dimensionless groups can be used as criteria to indicate regime change, the relative importance of inertial effects, the state of the flow (compressible or incompressible), and the dominant mechanism governing the changes in head and velocity (diffusion or advection).

4.4.1. Dimensionless Groups

The momentum equation and continuity equations can be re-arranged to a form that is similar to the standard groundwater flow equation. The momentum equation becomes:

$$H_x = -\frac{C_3}{C_1}V - \frac{C_4}{C_1}V^2 - \frac{C_6}{C_1}V_\tau - \frac{C_2}{C_1}VV_X \qquad [3\text{-}62]$$

The continuity equation becomes:

$$V_X = -H_\tau - \frac{C_5}{C_6}VH_x - \frac{C_7}{C_6}V \qquad [3\text{-}63]$$

Seven dimensionless groups (C_1 through C_7) were defined. These dimensionless groups show the relative importance of each term in the momentum and continuity equation. The C_1 group is related to the relative importance of head gradient in porous media flow:

$$C_1 = \frac{gnh_aSL}{V_\infty T} \qquad [4\text{-}163]$$

The C_2 and C_5 groups are identical. Therefore, C_2 shows the contribution of convection in the momentum equation and of advection in the continuity equation. The C_2 group is proportional to the equilibrium velocity:

$$C_2 = \frac{V_\infty SL}{T} \qquad [4\text{-}164]$$

The C_3 group is related to viscous effects and, when coupled with head gradient, can be used to obtain Darcy's Law:

$$C_3 = \frac{gnSLr}{T} \qquad [4\text{-}165]$$

The C_4 group is related with inertial effect on flow through porous media. When this term combined with head gradient and viscous term, the Ergun equation can be obtained.

$$C_4 = \frac{gnSLsV_\infty}{T} \qquad [4\text{-}166]$$

The C_6 group shows the relative importance of local acceleration:

$$C_6 = \frac{c_p{}^2 V_\infty SL}{gnh_a T} \qquad [4\text{-}167]$$

The C_7 group is related with the effect of elevation head:

$$C_7 = \frac{V_\infty SL^2 \sin\theta}{h_a T} \qquad [4\text{-}168]$$

The ratios of dimensionless groups can represent the relative effects of each term. The ratio between C_3 and C_1 is:

$$\frac{C_3}{C_1} = \frac{V_\infty}{h_a} r \qquad [4\text{-}169]$$

For the laminar case, using $h_a = rV_\infty$ and $C_3 / C_1 = 1$, the ratio between C_4 and C_1 is:

$$\frac{C_4}{C_1} = \frac{V_\infty{}^2}{h_a} s \qquad [4\text{-}170]$$

For the FDT case, using $h_a = sV_\infty{}^2$ and $C_4 / C_1 = 1$, the ratio between C_6 and C_1 is:

$$\frac{C_6}{C_1} = \left(\frac{c_p V_\infty}{g n h_a} \right)^2 \qquad [4\text{-}171]$$

If the physical experimental set-up is fixed, changing boundary conditions i.e. applying various hydraulic gradients, does not make any difference to c_p. The ratio C_6 / C_1 can show the changes in V_∞ with various applied hydraulic gradients. The ratio between C_2 and C_1 is:

$$\frac{C_2}{C_1} = \frac{V_\infty{}^2}{g n h_a} \qquad [4\text{-}172a]$$

We may re-write eqn [4-182a] using potential and kinetic energy forms:

$$\frac{C_2}{C_1} = 2 \left(\frac{\frac{1}{2} m V_{\infty p}{}^2}{m g h_a} \right) \qquad [4\text{-}172b]$$

The ratio C_2 / C_1 can be considered as the ratio of kinetic energy remaining at the downstream end to the potential energy applied at the upstream end. For porous media flow, this ratio will be very small number because most of the energy used up by friction loss. The ratio between C_5 and C_6 is:

$$\frac{C_5}{C_6} = \frac{g n h_a}{c_p{}^2} \qquad [4\text{-}173]$$

The ratio between C_7 and C_6 is:

$$\frac{C_7}{C_6} = \frac{g n L \sin\theta}{c_p{}^2} \qquad [4\text{-}174a]$$

If we use $L\sin\theta = z$ (elevation head), we can get:

$$\frac{C_7}{C_6} = \frac{gnz}{c_p^{\,2}} \qquad [4\text{-}174b]$$

4.4.2. Relevant Dimensionless Numbers

Some well-known dimensionless numbers in fluid mechanics are directly applicable to the momentum and continuity equation and can be related to combinations of defined dimensionless groups. Even though some of them are not directly relevant to this study, their underlying concepts might be used to give a physical explanation of each dimensionless group or a combination of groups.

(i) Reynolds Number

Reynolds number is the ratio of the effects of inertia and viscosity.

$$\mathrm{Re} = \frac{\text{inertia}}{\text{viscosity}} = \frac{Vm}{\nu} \qquad [4\text{-}175]$$

where m is the characteristic length.

Using the momentum equation, relative effects of inertia and viscosity can be studied. If r is substituted to eqn [4-165]:

$$C_3 = \frac{S}{T}\frac{1}{c_1}\frac{L^2\nu}{m^2} \qquad [4\text{-}176]$$

If s is substituted to eqn [4-166]:

$$C_4 = \frac{S}{T}\frac{1}{c_2}\frac{L^2}{mn}\frac{V_\infty}{2} \qquad [4\text{-}177]$$

If we calculate the ratio of dimensionless groups related with inertia term (V^2) and viscous term (V):

$$\frac{C_4}{C_3} = \frac{c_1}{2c_2}\frac{mV_\infty}{n\nu} \qquad [4\text{-}178]$$

If pore velocity is used instead of bulk velocity:

$$\frac{C_4}{C_3} = \frac{c_1}{2c_2}\frac{mV_{p\infty}}{\nu} \qquad [4\text{-}179]$$

We may define the equilibrium Reynolds number which can be obtained from the terminal velocity with given applied hydraulic gradient:

$$Re_\infty = \frac{mV_{p\infty}}{\nu} \qquad [4\text{-}180]$$

The ratio between C_4 and C_3 becomes:

$$\frac{C_4}{C_3} = \frac{c_1}{2c_2}Re_\infty \qquad [4\text{-}181]$$

If Forchheimer type equation (including viscous and inertial term) is used, dimensionless number, Be, can be used to show the ratio of inertial effect and viscous effect. Forchheimer equation for 1-D horizontal case is:

$$\frac{\partial p}{\partial x} = -\frac{\mu}{K}v - \rho\beta_0' v^2 + \rho g \qquad [4\text{-}182]$$

Belhaj (2003) shoed *Be* number as:

$$Be = \frac{\rho\beta_0' Kv}{\mu} \qquad [4\text{-}183]$$

Joseph (1966) had shown that using Forchheimer equation when the deviation from the Darcian flow becomes 5 %, Be was 0.0526. Belhaj (2003) estimated Be as 0.0756, using his numerical simulations. These values of Be, like Re, indicate departure from laminar flow behaviour. If we use Re = 1, we may get similar values of Be by simply using the ratio, C_4/C_3. In order to get C_4/C_3 from eqn [4-181], we need to use proper values for

c_1 and c_2. From Carman (1937, 1939), $c_1 = 0.24$ and from Burke-Plummer, $c_2 = 0.174$ can be used. Using c_1, c_2 and $Re_\infty = 1$ in eqn [4-181]:

$$\frac{C_4}{C_3} = 0.070 \quad \text{(laminar to PDT)} \qquad [4\text{-}184]$$

The calculated value is in between the values predicted by Joseph (1966) and Belhaj (2003). We can also see that this ratio is independent of applied boundary condition if Re is given. As a result, this ratio can therefore also be used to indicate the transition in regime, for flow through porous media. It must be pointed out however, that unlike ordinary flow in pipes, a sharp and clear transition from the laminar regime to the partially-developed turbulent regime simply does not exist - the change is gradual, progressive, and without discontinuities. Another mathematical significance of the ratio given by eqn [4-181] is that if we consider the orders-of-magnitude for the parameters in the momentum equation: C_4 has a different order when C_3 is around $Re_\infty = 1$. In such cases C_4 cannot be negligible at around $Re_\infty = 1$. If we extend this ratio to the case when $Re_\infty = 100$ (transition from PDT to FDT) we can get:

$$\frac{C_4}{C_3} = 7.0012 \quad \text{(PDT to FDT)} \qquad [4\text{-}185]$$

It is observed that C_4 starts to dominate the effect on flow through porous media and the order of C_4 starts to be different from C_3. Figure 4.93 shows the variation of Re_∞ for various applied hydraulic heads. If we are using the length of pipe = 10m, about 4000m of head is needed to get fully developed turbulent flow.

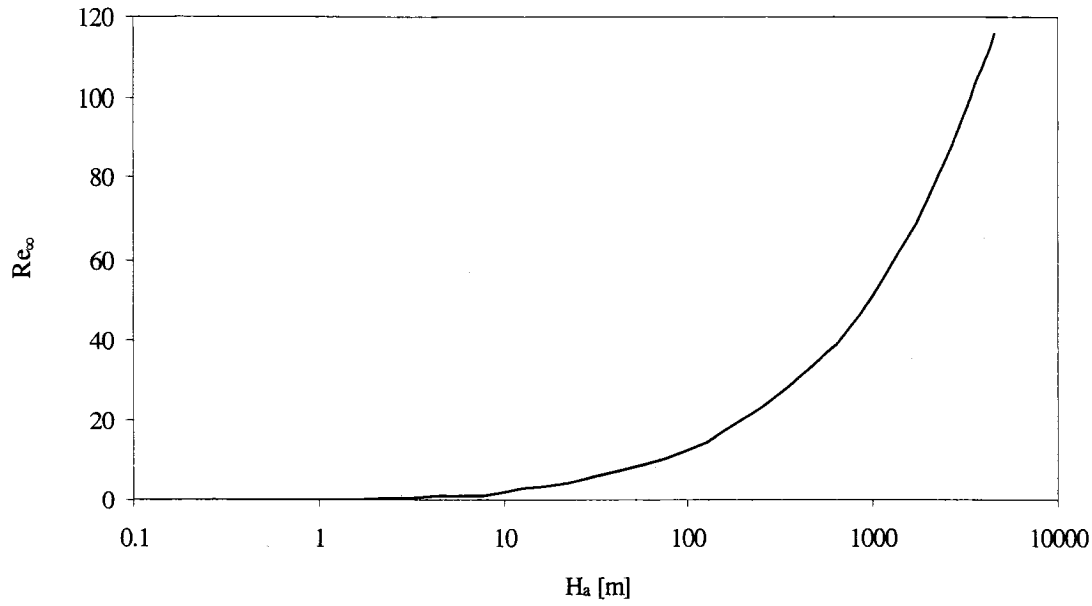

Figure 4.93 Re_∞ as a function of applied hydraulic head (L = 10 m).

(ii) Mach Number Analogy

Mach number is applied for compressible flow. Even for pipe flow, it is difficult to obtain such flow in liquids because pressure needed to generate sonic velocities is very high (about 1000 atm). However, using dimensionless groups in the momentum equation and continuity equation, Ma can be expressed using combinations of other dimensionless groups. Even though the magnitude of Ma is very small in the general of study on flow through porous media, it is possible to check whether we need more equations than just the momentum and continuity equations to explain the flow. If Ma is larger than 0.3 the flow is no longer incompressible and the density change cannot be ignored. If the density change is not negligible, it is necessary to use an equation of state, or an equation of state and the energy equation. In the most complicated cases, it is necessary to solve four equations simultaneously with four different variables, pressure, density, temperature, and velocity of flow. Using the computed Ma, the validity of using two equations (the momentum and continuity equation) can be proved. The Mach number is defined as:

$$Ma = \frac{V_{flow}}{V_{sound}} \qquad [4\text{-}186]$$

If we use equilibrium pore velocity for V_{flow} and c_p for V_{sound} in eqn [4-196], Ma_∞ can be defined by:

$$Ma_\infty = \frac{V_{p\infty}}{c_p} \qquad [4\text{-}187]$$

From the ratio of dimensionless groups (C_1 and C_6) of hydraulic gradient and local acceleration term:

$$\frac{C_6}{C_1} = \left(\frac{c_p V_0}{gnH_0}\right)^2 = \frac{\left(\frac{V_{p\infty}^{\ 2}}{gH_0}\right)}{\left(\frac{V_{p\infty}}{c_p}\right)}^2 \qquad [4\text{-}188]$$

As shown in the above ratio of dimensionless groups, the numerator is the ratio C_2 / C_1, and the denominator is the Mach number (Ma_∞).

Using eqns [4-172a] and [4-187], eqn [4-188] becomes:

$$\frac{C_6}{C_1} = \frac{\left(\frac{C_2}{C_1}\right)^2}{Ma_\infty^{\ 2}} \qquad [4\text{-}189]$$

If we re-arrange for Ma_∞:

$$Ma_\infty = \frac{C_2}{\sqrt{C_1 C_6}} \qquad [4\text{-}190]$$

The Mach number can be obtained using the combination of dimensionless groups. Figure 4.94 shows the Ma_∞ variation with applied hydraulic head. It is shown that Ma_∞ is less than 0.002, even for the FDT regime.

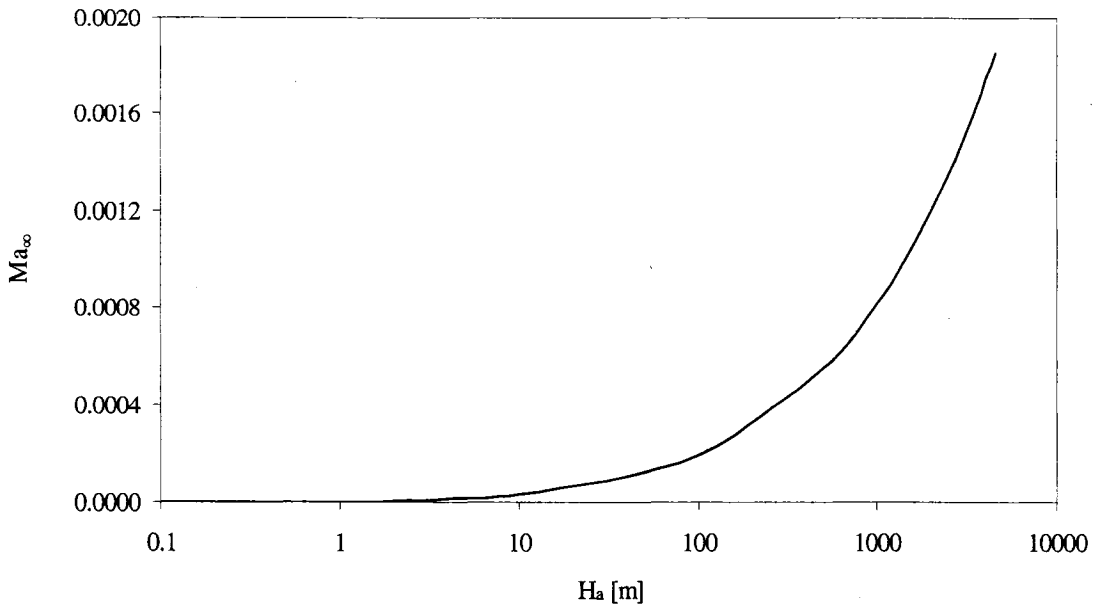

Figure 4.94 Ma_∞ as a function of applied hydraulic head (L = 10 m).

(iii) Euler Number Analogy

The Euler number is a measure of the relative effects of pressure and inertia.

$$Eu = \frac{\Delta p}{\rho V^2} \qquad [4\text{-}191]$$

where Δp = pressure difference.

In the momentum equation, there is a term for hydraulic gradient and a term for inertial effects. If we consider the effect of hydraulic head instead of pressure difference, we can get a dimensionless number that is similar to the Euler number. We may define an Eu_∞ using the ratio of previously-defined dimensionless groups as:

$$\frac{\text{head gradient}}{\text{inertial effect}} = \frac{C_1}{C_4} = \frac{1}{s}\frac{h_a}{V_\infty^2} \qquad [4\text{-}192]$$

Figure 4.95 shows how this Eu_∞ depends on the applied hydraulic head. As hydraulic head increases, C_1 and C_4 increase. In the laminar regime, the inertial effect is negligible compared to the applied hydraulic head but it becomes significant in the PDT and FDT regimes.

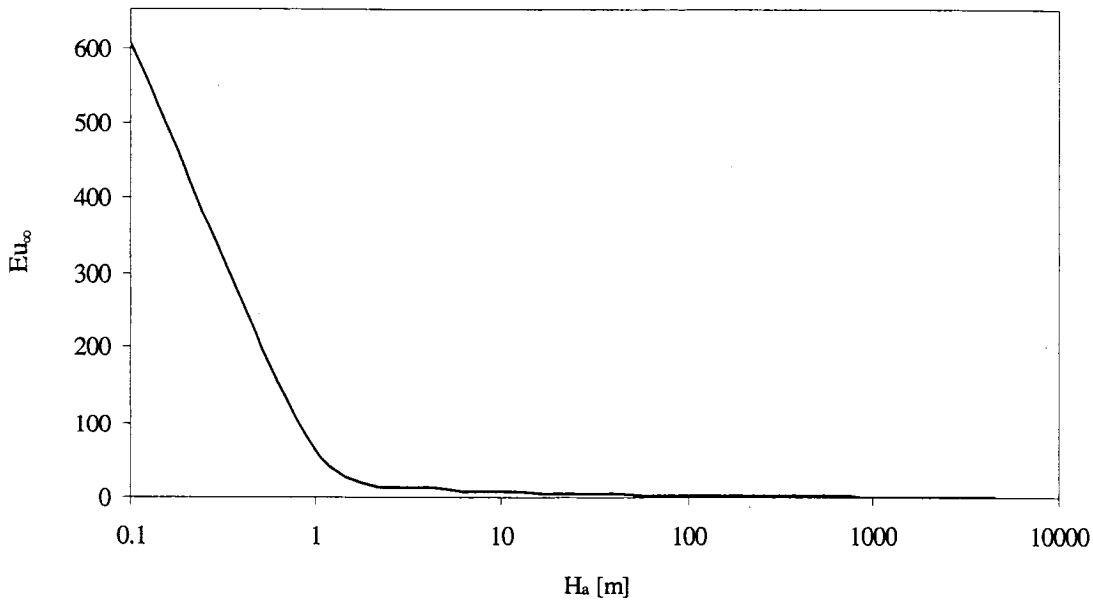

Figure 4.95 Eu_∞ as a function of applied hydraulic head (L = 10 m).

(iv) Peclet Number Analogy

The concept behind of the Peclet Number can be used to show the relative effects of the diffusion of hydraulic head versus the advection of that head. In general, the advection of head is neglected in studies of flow through porous media. Advection-dominated flow disappears at short times and very near the upstream boundary. For the physical layout (hypothetical experiment) considered herein, when the gate is suddenly opened, head can simply be 'pushed out' at the beginning, but is soon governed by a diffusion phenomena. How far and how long this advection propagates depend on the characteristics of porous media, the fluid and the boundary conditions. Using matched asymptotic expansions, it was found that the length of the closed conduit should be divided into two regions, an 'inner' and an 'outer' region or zone. The inner zone is governed by an evolving-wave equation and the outer zone is governed by diffusion

equation. For the laminar regime, if we consider only the viscous and local acceleration terms (which are negligible in the outer zone), the momentum equation becomes:

$$H_x + \frac{C_3}{C_1} V + \frac{C_6}{C_1} V_\tau = 0 \qquad [4\text{-}193]$$

If eqn [4-193] is combined with the continuity equation:

$$H_{XX} = \underbrace{\frac{C_3}{C_1} H_\tau}_{(i)} + \underbrace{\frac{C_6}{C_1} H_{\tau\tau}}_{(ii)} \qquad [4\text{-}194]$$

If we neglect part (i), eqn [4-194] becomes a wave equation. On the other hand, if we neglect part (ii), it becomes a diffusion equation. It may therefore be said that C_3 / C_1 is a diffusion coefficient and that C_6 / C_1 is a wave or advection coefficient. A Peclet Number analogy can then be used to indicate the relative effects or importance of diffusion versus advection. In the outer coordinate zone, the Peclet Number for the laminar regime may be defined as:

$$Pe_{Lam} = \frac{\text{advection coeff.}}{\text{diffusion coeff.}} = \frac{\frac{C_6}{C_1}}{\frac{C_3}{C_1}} \qquad [4\text{-}195]$$

In laminar regime, $C_3 = C_1$, so:

$$Pe_{Lam} = \frac{C_6}{C_1} \qquad [4\text{-}196]$$

If we apply a hydraulic gradient of 0.1, $Pe_{Lam} = 0.003$. The advection effect is therefore only about 0.3 % of the size of the diffusion effect. Because of this small effect, head advection can be neglected for ordinary groundwater flow. However, different results may arise if the inner variables, defined in the matched asymptotic expansion, are used. The momentum equation for the inner zone is:

$$H_{\tilde{x}} + \tilde{V} + \tilde{V}_{\tilde{\tau}} = 0 \qquad [4\text{-}197a]$$

Equation [4-197a] can be expressed with a general form:

$$H_{\tilde{x}} + C_{dv}\tilde{V} + C_a\tilde{V}_{\tilde{\tau}} = 0 \qquad [4\text{-}197b]$$

where:

C_{dv} = the inner diffusion coefficient due to viscous effect.

C_a = the inner advection coefficient.

The Peclet number for the inner zone can then be defined as:

$$Pe_{Lam}^{(i)} = \frac{C_a}{C_{dv}} \qquad [4\text{-}198]$$

In light of eqn [4-197a], it can bee seen that the ratio, $Pe^{(i)}$, of the coefficient on the diffusion term to that on the advection term is 1. Therefore, the advection effect cannot be ignored within the inner zone. Large $Pe^{(i)}$ may be expected to be associated with more advection-dominated cases.

If only the inertial and local acceleration terms are considered in the FDT regime, the momentum equation becomes:

$$H_x + \frac{C_4}{C_1}V^2 + \frac{C_6}{C_1}V_\tau = 0 \qquad [4\text{-}199]$$

Using the ratio of the diffusion effect to the advection effect in the outer coordinate system, the Peclet Number for FDT regime may be defined as:

$$Pe_{FDT} = \frac{\text{advection coeff.}}{\text{diffusion coeff.}} = \frac{\frac{C_6}{C_1}}{\frac{C_4}{C_1}} \qquad [4\text{-}200]$$

In the FDT regime, $C_4 = C_1$, so:

$$Pe_{FDT} = \frac{C_6}{C_1} \qquad [4\text{-}201]$$

If we apply a hydraulic gradient of 400, Pe_{FDT} becomes 0.00005, in which case the advection effect is about 0.005 % of the diffusion effect. The relative effect of advection

in the FDT regime is therefore much smaller than in the laminar regime. If we use the inner variables in eqn [4-199], the momentum equation for the inner expansion becomes:

$$H_{\tilde{x}} + \tilde{V}^2 + \tilde{V}_{\tilde{\tau}} = 0 \qquad [4\text{-}202a]$$

Equation [4-202a] can be expressed with a general form:

$$H_{\tilde{x}} + C_{di}\tilde{V}^2 + C_a\tilde{V}_{\tilde{\tau}} = 0 \qquad [4\text{-}202b]$$

where:

C_{di} = the inner diffusion coefficient due to inertial effect.

The Peclet number for the inner zone can then be defined as:

$$Pe_{FDT}^{(i)} = \frac{C_a}{C_{di}} \qquad [4\text{-}203]$$

Again, in light of eqn [4-202a], the ratio of advection and diffusion effect becomes 1. As with the laminar regime, advection effect now cannot be ignored.

For the PDT regime, neither viscous nor inertial effects can be ignored. The momentum equation, including the local acceleration term, becomes:

$$H_x + \frac{C_3}{C_1}V + \frac{C_4}{C_1}V^2 + \frac{C_6}{C_1}V_\tau = 0 \qquad [4\text{-}204]$$

It may be expected that Pe_{PDT} is in between Pe_{Lam} and Pe_{FDT}. By adding the coefficient of viscous term and inertial term, we may get the total effect of diffusion. For the PDT regime, it is suggested that a head-based Pe_{PDT} be defined by:

$$Pe_{PDT} = \frac{\text{advection coeff.}}{\text{diffusion coeff.}} = \frac{\frac{C_6}{C_1}}{\frac{C_3 + C_4}{C_1}} \qquad [4\text{-}205]$$

but because in the PDT regime $\frac{C_3 + C_4}{C_1} \approx 1$, this Pe_{PDT} becomes:

$$Pe_{PDT} = \frac{C_6}{C_1} \qquad [4\text{-}206]$$

For an applied hydraulic gradient of 10, Pe_{PDT} is 0.001, so the advection effect is about 0.1 % of the diffusion effect. The range of Pe_{PDT} is observed in between Pe_{Lam} and Pe_{FDT}. If we substitute the inner variables into eqn [4-204], we can get the momentum equation for the inner expansion:

$$H_{\tilde{x}} + \frac{C_3}{C_1}\tilde{V} + \frac{C_4}{C_1}c\tilde{V}^2 + \tilde{V}_{\tilde{\tau}} = 0 \qquad [4\text{-}207a]$$

Equation [4-207a] can be expressed with a general form:

$$H_{\tilde{x}} + C_{dv}\tilde{V} + C_{di}\tilde{V}^2 + C_a\tilde{V}_{\tilde{\tau}} = 0 \qquad [4\text{-}207b]$$

The Peclet number for the inner zone can then be defined as:

$$Pe_{PDT}^{(i)} = \frac{C_a}{C_{dv} + C_{di}} \qquad [4\text{-}208]$$

In light of eqn [4-207a], the Pe for the inner may not become 1 rather, it depends on the velocity scaling factor c. For example, based on the scaling-factors used herein, $Pe_{PDT}^{(i)}$ is about 0.06 for an applied hydraulic gradient of 10, thus, the advection effect is about 6 % of the diffusion effect.

Even though Pe_∞ was always small compared with $Pe_\infty^{(i)}$, Pe_∞ can be used to the variations of the advective effect under various hydraulic gradients. Figure 4.96 shows Pe_∞ as a function of the applied hydraulic gradient. In laminar regime, Pe_∞ is relatively constant but in the PDT regime, Pe_∞ declines dramatically. This dramatic decrease in Pe_∞ in the PDT regime is supported by the results obtained using the matched asymptotic expansion. Using these expansions, it was shown that increased hydraulic gradient made the inner region smaller in time and space. In the FDT regime the Pe_∞ becomes very small and almost constant.

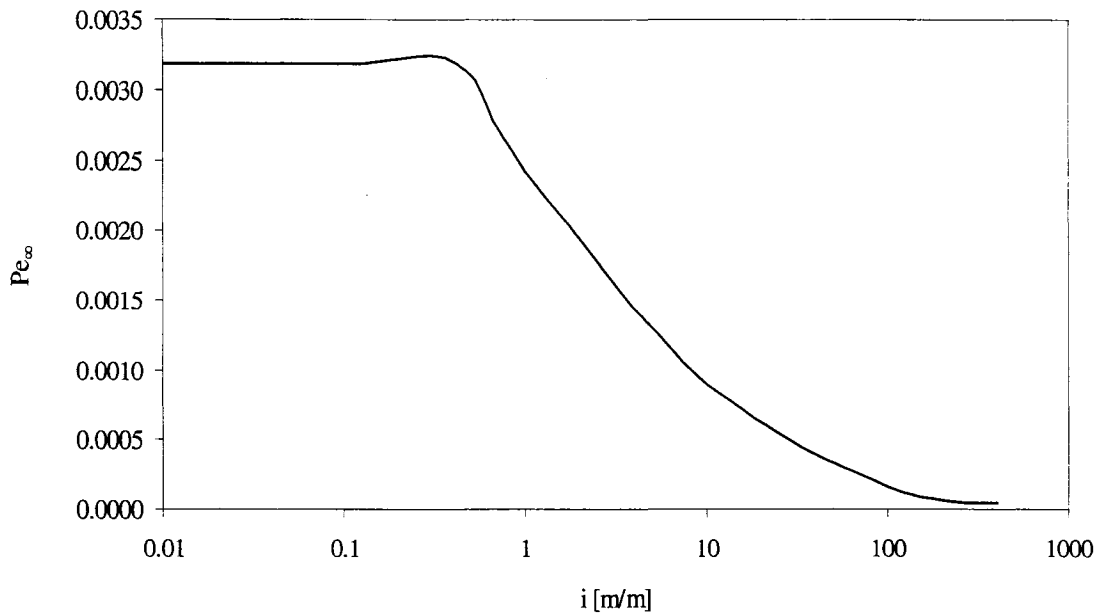

Figure 4.96 Pe_∞ as a function of applied hydraulic gradient.

In the outer coordinate realm, Pe_∞ in laminar, PDT and FDT regimes are all much smaller than unity. However, in the inner coordinate realm (inner zone), $Pe^{(i)}$ can readily be made 1 by choosing proper scaling factors. When $Pe^{(i)} = O(1)$ the contributions from diffusion and advection are equal. As $Pe^{(i)}$ decreases below 1, diffusion becomes dominant, and as $Pe^{(i)}$ exceeds unity, advection becomes dominant. Table 4.12 shows ranges $Pe^{(i)}$ and the effect of the mechanism.

Table 4.12 Ranges of inner Peclet number and the associated mechanism.

	$Pe^{(i)} = 0$	$0 < Pe^{(i)} < 1$	$Pe^{(i)} = 1$	$1 < Pe^{(i)}$	$Pe^{(i)} \to \infty$
diffusion (%)	100	larger than 50	50	less than 50	0
advection (%)	0	less than 50	50	larger than 50	100
governing equation	diffusion	evolving-wave			wave
region	outer	inner			origin

(v) Viscous Resistance and Inertial Resistance

If the flow reaches equilibrium, the pressure driving flow is equals to the sum of viscous resistance and inertial resistance. Barr (2001) used the Pouiseuille equation and the length adjustment from Carman's observations (1937) to state the following eqn:

$$F_p = F_v + F_i \qquad [4\text{-}209]$$

where F_p is the pressure force, F_v is the viscous resistant force, and F_i is the inertial resistant force.

If we divide both sides by F_p:

$$1 = B + E \qquad [4\text{-}210]$$

where B and E are dimensionless numbers. B represents the ratio of viscous force to pressure force and E represents the inertial-force to pressure-force ratio.

Similarly, from the momentum equation and using the coefficients of head gradient, viscous effect, and inertial effect, it can be shown that:

$$C_1 = C_3 + C_4 \qquad [4\text{-}211]$$

or:

$$1 = \frac{C_3}{C_1} + \frac{C_4}{C_1} \qquad [4\text{-}212]$$

Using the definitions of dimensionless groups in section 4.4.1:

$$1 = \frac{V_\infty}{h_a} r + \frac{V_\infty^{\,2}}{h_a} s \qquad [4\text{-}213]$$

Using the definitions of r and s:

$$1 = \frac{V_\infty}{h_a}\frac{1}{c_1}\frac{L\nu}{m^2 n}\frac{1}{g} + \frac{V_\infty^{\,2}}{h_a}\frac{1}{c_2}\frac{L}{mn^2}\frac{1}{2g} \qquad [4\text{-}214]$$

In all three regimes, the total of C_3/C_1 and C_4/C_1 is always close or equal to unity (see Tables 4.3, 4.6 and 4.9). In the laminar regime, C_3/C_1 is much larger than C_4/C_1. In the PDT regime, as an applied hydraulic gradient increases, C_3/C_1 decreases but C_4/C_1

increases. In the FDT regime, C_3 / C_1 becomes very small compared with C_4 / C_1.

4.4.3. Effects of Dimensional Parameters on Dimensionless Groups

The relative importance of the various components of the physical problem was investigated using dimensionless groups. Table 4.13 shows the ranges of the parameters, appearing in the literature. The largest numeric ranges for physical quantities are for hydraulic conductivity and transmissivity. The range for the compressibility of porous media and porosity was also not small. Changes in compressibility result in changes in celerity, which was found to be an important parameter in investigating the evolving-wave property. Figure 4.97 shows celerity as a function of the compressibility of porous media. As the compressibility of the porous media increases, celerity decreases. If sand is the media, the celerity will be in the range of 60 to 600 m/s. Figure 4.98 shows celerity as a function of the porosity. It can be seen that the celerity increases linearly as porosity increases. Table 4.14 shows the ranges in the magnitudes of the dimensionless groups used herein, with various sets of dimensional parameters, for an applied hydraulic gradient of 0.1. This table does not cover all possible cases but does give useful information about the effects of each dimensional parameter on the various dimensionless groups.

Table 4.13 Ranges of values for physical parameters, appearing in the literature.

No.	Symbols	Parameters/constants	Typical units	Max.	Min.	Max/Min
1	K	hydraulic conductivity[1]	m/s	0.01	1.00E-06	10000.0
2	n	porosity[1]	-	0.5	0.25	2.0
3	α	compressibility[1]	1/Pa	1.00E-07	1.0E-09	100.0
4	β	compressibility of water	1/Pa	4.40E-10	4.4E-10	1.0
5	E	Young's modulus for steel	Pa	2.10E+11	1.9E+11	1.1
6	S_s	specific storage[2]	1/m	9.83E-04	1.1E-05	90.3
7	T	transmissivity[1]	m^2/s	0.001	1E-07	10000.0
8	S	storativity[2]	-	9.83E-05	1.09E-06	90.3

[1] for porous media consisting of cohesionless granular material, such as a sand.

[2] $S_s = \gamma(\alpha + n\beta)$ [1/L],
confined $S = DS_s$ [dimensionless], D = pipe diameter in this case.

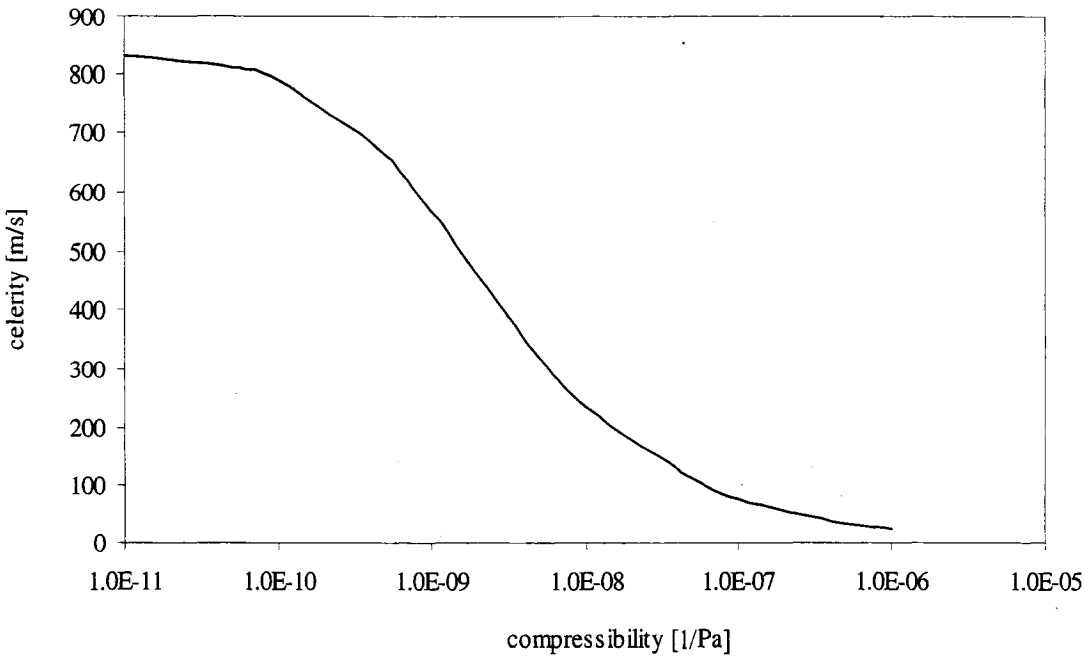

Figure 4.97 Variation in celerity with compressibility (L = 10 m).

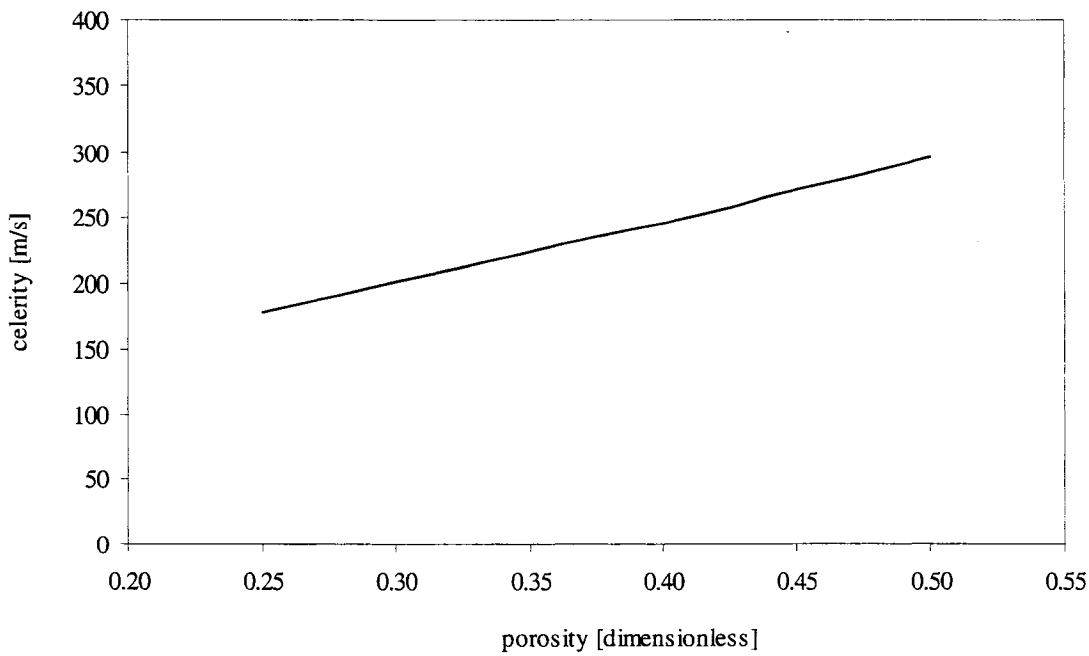

Figure 4.98 Variation of celerity with porosity (L = 10 m).

Table 4.14 Ranges of dimensionless groups with various parameters.

	Case 1	Case 2	Case 3	Case 4	Case 5	Case 6	Case 7	Case 8
α	1.0E-07	1.0E-07	1.0E-07	1.0E-09	1.0E-09	1.0E-09	1.0E-09	1.0E-09
β	4.4E-10	4.4E-10	4.4E-10	4.4E-10	4.4E-10	4.4E-10	4.4E-10	4.4E-10
E	2.1E+11	1.9E+11	2.1E+11	1.9E+11	2.1E+11	1.9E+11	2.1E+11	2.1E+11
n	0.250	0.375	0.500	0.250	0.375	0.500	0.250	0.500
e	0.333	0.600	1.000	0.333	0.600	1.000	0.333	1.000
m	5.6E-05	1.0E-04	1.7E-04	5.6E-05	1.0E-04	1.7E-04	5.6E-05	1.7E-04
r	5.5E+03	1.1E+03	3.1E+02	5.5E+03	1.1E+03	3.1E+02	5.5E+03	3.1E+02
s	85676.1	21174.9	7139.7	85676.1	21174.9	7139.7	85676.1	7139.7
v_∞	1.8E-04	8.7E-04	3.1E-03	1.8E-04	8.7E-04	3.1E-03	1.8E-04	3.1E-03
S	9.8E-05	9.8E-05	9.8E-05	1.1E-06	1.1E-06	1.2E-06	1.1E-06	1.2E-06
T	1.8E-04	8.8E-04	3.3E-03	1.8E-04	8.8E-04	3.3E-03	1.8E-04	3.3E-03
θ^*	7.9E-01	7.9E-01	7.9E-01	7.9E-01	7.9E-01	7.9E-01	7.9E-01	7.9E-01
c_p	5.8E+01	7.7E+01	9.9E+01	4.7E+02	5.7E+02	6.3E+02	4.8E+02	6.5E+02
C_1	73185.8	4721.7	483.1	811.5	54.9	5.9	811.5	5.9
C_2	9.8E-04	9.7E-04	9.2E-04	1.1E-05	1.1E-05	1.1E-05	1.1E-05	1.1E-05
C_3	72980.2	4646.4	451.0	809.2	54.0	5.5	809.2	5.5
C_4	205.6	75.2	32.1	2.3	0.9	0.4	2.3	0.4
C_6	1.32	1.56	1.85	0.99	1.00	0.91	1.01	0.95
C_7	6.9E-03	6.8E-03	6.5E-03	7.7E-05	7.9E-05	7.9E-05	7.7E-05	7.9E-05

* 45° upslope

The largest variations are in C_1 and C_3. These large variations show that these groups are sensitive to the magnitude of various sets of dimensional parameters. Even though the variations in magnitude of most of the dimensionless groups were not small, and thus they are sensitive to the relevant dimensional parameters, this did not necessarily result in behaviours high sensitive to the viscous, inertial, local accelerative or convective accelerative terms. Rather, the sensitivity of these terms depends on the ratios of these dimensionless groups. Table 4.15 shows the variation in the ratios of the dimensionless groups for the stated cases.

Table 4.15 Ranges of ratios of dimensionless groups.

	Case 1	Case 2	Case 3	Case 4	Case 5	Case 6	Case 7	Case 8
C_2/C_1	1.3E-08	2E-07	1.9E-06	1.3E-08	2.0E-07	1.9E-06	1.3E-08	1.9E-06
C_3/C_1	0.997	0.984	0.934	0.997	0.984	0.934	0.997	0.934
C_4/C_1	0.003	0.016	0.066	0.003	0.016	0.066	0.003	0.066
C_6/C_1	0.00002	0.0003	0.004	0.001	0.018	0.155	0.001	0.162
C_5/C_6	7.4E-04	6E-04	5.0E-04	1.1E-05	1.1E-05	1.2E-05	1.1E-05	1.2E-05
C_7/C_6	5.2E-03	4E-03	3.5E-03	7.8E-05	8.0E-05	8.6E-05	7.6E-05	8.3E-05

It may be noted that the local acceleration term is not necessarily negligible if the minimum α and the maximum porosity are used, as in Case 8.

In order to see the elevation-head effect, the dimensionless group C_7 was varied using various slopes in Table 4.17. The parameters used in this investigation are listed in Table 4.16. A slope of 90° and a slope of 270° correspond to a vertical upslope and a vertical downslope, respectively. The magnitude of the absolute value of C_7 did not show significant changes for these extreme slopes.

Table 4.16 Applied values of parameters.

	α	β	E	N	d	m	L
unit	[1/Pa]	[1/Pa]	[Pa]	[ ]	[m]	[m]	[m]
values	1.0E-08	4.4E-10	2E+11	0.375	1.0E-03	1.0E-04	10

For a slope of 90°, C_7 has a positive value; for a slope of 270°, C_7 is negative but has the same magnitude as that of the slope of 90°. The same amount of effect is therefore expected, but with an opposite direction, depending on whether an upslope or a downslope is in effect.

Table 4.17 Effects of slope on dimensionless group C_7.

	slope 1	slope 2	slope 3	slope 4	slope 5	slope 6
θ [degree]*	0	30	45	60	90	270
C_7	0.0E+00	4.9E-04	6.9E-04	8.5E-04	9.8E-04	-9.8E-04

* angle from horizontal line to upslope, see Figure 1.1.

Table 4.18 shows the effect of the length of the pipe on the dimensionless group C_7, for a 45° upslope. As can be seen in the definition of C_7, the total length has a significant effect on C_7. The magnitude of C_7 can be 1 around L = 380 m. From the C_7 values for length 4, 5, and 6 in Table 4.18, it is evident that we may not neglect the elevation-head effect if we use a pipe length of longer than 1 km.

Table 4.18 Effects of length on dimensionless group C_7.

	length 1	length 2	length 3	length 4	length 5	length 6
L	1	10	100	1000	10000	100000
C_7	6.9E-06	6.9E-04	6.9E-02	6.9E+00	6.9E+02	6.9E+04

5. Conclusions and Recommendations

5.1 Conclusions

This body of mathematical and numerical work described herein was performed under the constraints implied by a relatively simple hypothetical experiment, i.e. the sudden introduction of a fixed head (a Dirichlet boundary condition) at the upstream end of an elastic conduit filled with a saturated porous medium. With respect to its elastic and hydraulic behaviour, the latter was treated as if it were a homogeneous medium or substance, as is commonly assumed, the primary interest being the temporal and spatial variation in hydraulic head and bulk velocity. Said applied head was given a range of temporally-invariant possible values, values which would result (in a physical experiment) in the equilibrium flow condition at $t = \infty$ being either laminar, partially-developed turbulent (PDT), or fully-developed turbulent (FDT) flow.

It was found that the resulting highly unsteady flow exhibited fundamentally different behaviours, some of which departed dramatically from behaviours predicted by widely-accepted and commonly-presented PDE's. For example, for unsteady laminar flow 'far' away[10] from the source of the unsteadiness, a de-dimensionalized form of the *communis opinio* can be expressed by (cf. Laminar-Outer-Diffusion upper entry in Table 5.1):

$$\frac{\partial^2 H}{\partial X^2} = \frac{C_3}{C_1}\frac{\partial H}{\partial \tau} \qquad [3\text{-}67]$$

the solution to which allows bulk velocities to be determined via Darcy's Law.

It was found that the PDE (eqn [3-67]) would not adequately describe the variation in bulk velocity near the face of the suddenly-opened valve (Figure 1-1) at very small times. Also, using the regular perturbation method, it was found that the complete problem can depend on the small parameters in a "singular" way. The matched asymptotic expansion was used to solve these singular problems near the upstream

[10] It is not necessary to be very far away, see results of analyses presented in chapters 3.5.7, 4.3.2.

boundary at very small times. The development of a very complete form of the momentum equation and a doubly-rescaled continuity equation gave rise to an evolving-wave behaviour near the face of the valve or gate at very small times. The PDE for this laminar but evolving-wave condition was successfully solved both analytically[11] and numerically, with the numerical efforts including a comparison of the Method of Characteristic and finite difference methods.

Further systematic consideration of PDT and FDT regimes resulted in the confirmation that evolving-waves also existed in a 'inner' zone (near the valve face), but that fast diffusion occurred in an 'outer' zone at longer times (greater distances from the valve face). Thus, a new taxonomy for highly unsteady one-dimensional multi-regime flow through porous media was discovered (see Table 5.1). The application of regular perturbation and matched asymptotic theory provided a systematic way to assess the relative importance of sub-phenomenon and quantitatively establish regions (validity for the PDE's and their associated solutions. The 'combined forms' in Table 5.1 represent the combinations of the momentum and continuity equations. In laminar regime, if the boundary and initial conditions of H are known, equation of H can be solved regardless of V, similarly, equation of V can be solved regardless of H if the boundary and initial conditions of V are given. However, in PDT and FDT regimes, H and V cannot be independent on each other thus H and V interact in the solutions.

The single-most general equations in Table 5.1 are perhaps[12] those for the evolving wave PDT case, which may also be written:

$$\frac{\partial^2 H}{\partial \tilde{X}^2} = \left[\frac{C_3}{C_1} + 2\frac{C_4}{C_1} c\tilde{V}\right]\frac{\partial H}{\partial \tilde{\tau}} + \frac{\partial^2 H}{\partial \tilde{\tau}^2} \qquad [4\text{-}104]$$

From the above equation, it was found that H cannot be obtained without considering V. However, in the outer expansions, H was found to be independent of V.
Further conclusions and findings are as follows:

---

[11] apparently.
[12] "perhaps" because the low-gradient low-velocity (low Re) end of steady PDT eqn's only give fair estimates of laminar behaviour, just as the high Re end of such eqn's only give fair approximations of steady FDT behaviour.

(1) Using the momentum and continuity equations, it has been shown that the functional dependence in the problem with respect to the various dimensional parameters is not unique. Dimensional analysis was therefore used to reduce the complexity of the problem. Dimensionless forms of the momentum and continuity equations were derived and seven dimensionless groups resulted. These groups gave direct indication of the relative significance or contribution of each effect whether viscosity, inertia, local acceleration, convective acceleration or elevation.

(2) The comparison of the solutions of various models could not give information about the individual effect of terms consisting the momentum and continuity equations, i.e. viscosity, inertia, local acceleration, convective acceleration, and elevation. The regular perturbation method gave information whether these terms can be safely neglected, how small these terms are, and the variations of these terms in time and space.

(3) Using the regular perturbation method, even though some of the terms were multiplied by parameters having very small magnitudes, it was found that the presence of these terms cannot be simply neglected because the problem can depend on these small parameters in a "singular" way. The matched asymptotic expansion was used to solve these singular problems near the upstream boundary at very small times. The inner and outer expansions were developed for the laminar, PDT and FDT flow regimes. It was presented that the extent of the inner zone varied depending on the applied hydraulic gradient. It was also shown that the local acceleration which is negligibly small in the outer expansion plays an important role in the inner expansion.

Table 5.1 Inner and outer formula for Laminar, PDT, and FDT regimes.

Regime	Equation	Inner	Outer
Laminar	Momentum equation	$H_{\tilde{X}} + \frac{C_3}{C_1}\tilde{V} + \tilde{V}_{\tilde{\tau}} = 0$	$H_X + \frac{C_3}{C_1}V = 0$
	Continuity equation	$H_{\tilde{\tau}} + \tilde{V}_{\tilde{X}} = 0$	$V_X + H_\tau = 0$
	Combined form	$H_{\tilde{X}\tilde{X}} = H_{\tilde{\tau}} + H_{\tilde{\tau}\tilde{\tau}}$ $\tilde{V}_{\tilde{X}\tilde{X}} = \tilde{V}_{\tilde{\tau}} + \tilde{V}_{\tilde{\tau}\tilde{\tau}}$	$H_{XX} = \frac{C_3}{C_1}H_\tau$ $V_{XX} = \frac{C_3}{C_1}V_\tau$
	Type	Evolving-wave	Diffusion
PDT	Momentum equation	$H_{\tilde{X}} + \frac{C_3}{C_1}\tilde{V} + \frac{C_4}{C_1}c\tilde{V}^2 + \tilde{V}_{\tilde{\tau}} = 0$	$H_X + \frac{C_3}{C_1}V + \frac{C_4}{C_1}V^2 = 0$
	Continuity equation	$H_{\tilde{\tau}} + \tilde{V}_{\tilde{X}} = 0$	$V_X + H_\tau = 0$
	Combined form	$H_{\tilde{X}\tilde{X}} = \left(\frac{C_3}{C_1} + \frac{2C_4}{C_1}c\tilde{V}\right)H_{\tilde{\tau}} + H_{\tilde{\tau}\tilde{\tau}}$ $\tilde{V}_{\tilde{X}\tilde{X}} = \frac{C_3}{C_1}\tilde{V}_{\tilde{\tau}} + \frac{2C_4}{C_1}c\tilde{V}_{\tilde{\tau}} + \tilde{V}_{\tilde{\tau}\tilde{\tau}}$	$H_{XX} = \frac{1}{C_1}\sqrt{C_3^{\,2} + 4C_1C_4\lvert H_x\rvert}H_\tau$
	Type	Evolving-wave	Fast Diffusion
FDT	Momentum equation	$H_{\tilde{X}} + \frac{C_4}{C_1}\tilde{V} + \tilde{V}_{\tilde{\tau}} = 0$	$H_X + \frac{C_4}{C_1}V^2 = 0$
	Continuity equation	$H_{\tilde{\tau}} + \tilde{V}_{\tilde{X}} = 0$	$V_X + H_\tau = 0$
	Combined form	$H_{\tilde{X}\tilde{X}} + \frac{2C_4}{C_1}\tilde{V}H_{\tilde{\tau}} + H_{\tilde{\tau}\tilde{\tau}} = 0$ $V_{\tilde{X}\tilde{X}} + \frac{2C_4}{C_1}\tilde{V}\tilde{V}_{\tilde{\tau}} + \tilde{V}_{\tilde{\tau}\tilde{\tau}} = 0$	$H_{XX} = 2\sqrt{\frac{C_4\lvert H_x\rvert}{C_1}}H_\tau$
	Type	Evolving-wave	Fast Diffusion

5.2 Recommendations

The question of how to design an experiment which might be used to verify (or negate) the theoretical outcomes might be raised. An apparatus not unlike that shown in Figure 1.1 could be fabricated. A very high head at the source would be needed (many $10^{'s}$ of meters), perhaps using a steel conduit that extends to the top of a tall building. The valve at the upstream end would need to be opened as instantly as possible, perhaps using a powerful solenoid (electromagnetically-operated actuator). A series of wall-mounted highly sensitive pressure-transducers would be needed, closely spaced near the upstream valve, and less closely-spaced further away from the valve. A data-acquisition system, connected to the valve-actuator and to all the transducers, would be needed and would require the use of an extremely high rate of data acquisition ($\Delta t \approx 10^{-9}$ seconds). An alternative source of upstream head might be a pressure vessel that contains a gas which has been compressed to an extreme level.

It would be of interest to use the mathematical and numerical methods described herein with more general and/or more complicated energy-loss equations[13], such as those expressed with a form using power law, a polynomial, or combined forms. Such a study might lead not only to the new solutions to the problem but also yield new information about the solutions which could help reveal the mechanisms behind the phenomena of highly unsteady non-Darcy flow through porous media.

The approaches described herein could be readily applied to fracture flow. Using a suitable energy-loss equation for a fracture network, similar numerical methods and mathematical theories could be applied to solve and analyze fracture flow problems.

The approaches described herein could also be applied to problems with other, very different boundary conditions. For example if a pump is introduced somewhere in the problem, the temporal and spatial variations in head and velocity very near the pump could be obtained using matched asymptotic methods.

[13] most of these are not yet well accepted.

6. REFERENCES

Anandakrishnan M. and Varadalajulu G.H.: 1963. Laminar and turbulent flow of water through sand. *ASCE J. of Soil Mechanics and Foundations Div.*, 89(SM5):1-15.

Andrade, J.S. Jr., Costa, U.M.S., Almeida M.P., Makse H.A. and Stanley H.E.: 1999. Inertial Effects on Fluid Flow through Disordered Porous Media. Physical Review Letters. 82(26): 5249-5252.

Arbhabhirama A. and Dinoy A.A.: 1973. Friction factor and Reynolds number in porous media flow. ASCE Journal of the Hydraulics Division, 99(HY6): 901-911.

Arfaie, M., Suwan K. and Anderson A.: 1993. Stability and accuracy of pipe friction approxmations in method of characteristics solutions for waterhammer. Math. Engne. Ind., 4(1): 265-281.

Aronson, D.G.: 1985. The Porous Medium Equation, in Nonlinear Diffusion Problems, A. Fasano & M. Primicerio (eds.), Lecture Notes in Mathematics 1224, Springer Verlag, Berlin, 1-46.

ASTM: 2002a. Standard test method for permeability of granular soils (constant head) (D2434). *In ASTM Annual Standards Book*, Amer. Soc. Testing & Materials, Philadelphia, PA.

ASTM: 2002b. Standard test method for measurement of hydraulic conductivity of porous materials using a rigid-wall, compaction-mold permeameter (D5856). *In* ASTM *Annual Standards Book*, Amer. Soc. Testing & Materials, Philadelphia, PA.

Auriault, J.-L., Borne, L. and Chambon, R.: 1985. Dynamics of porous saturated media, checking of the generalized law of Darcy. J. Acoust. Soc. Am. 77(5): 1641-1650.

Barr, D.W.: 2001. Turbulent Flow Through Porous Media. Ground Water. 39(5): 646-650

Barree, R.D. and Conway, M.W.: 2004. Beyond Beta Factors: A Complete Model for Darcy, Forchhiemer, and Trans-Forchheimer Flow in Porous Media. Paper SPE 89325 presented at the SPE Annual Technical Conference and Exhibition in Houston, 26-29.

Barree, R.D. and Conway, M.W.: 2005. Beyond Beta Factors: A Model for Darcy, Forchhiemer, and Trans-Forchheimer Flow in Porous Media. JPT. Mar.: 43-45.

Bear, J.: 1972. Dynamics of fluids in porous media. American Elsevier Publishing Co., Inc., New York, N.Y.

Bear, J.: 1979. Hydraulics of Groundwater. McGraw-Hill, New York.

Belhaj H.A., Agha K.R., Butt S.D. and Islam M.R.: 2003. A Comprehensive Numerical Simulation Model for Non-Darcy Flow including Viscous, Inertial and Convective Contributions. Annual SPE International Technical Conference and Exhibition in Abuja. SPE 85678:1-11

Belhaj H.A.: 2004. Numerical Simulation and Experimental Modeling of Matrix/Fracture Flow in Porous Media. PhD Thesis. Dalhousie University.

Benilov, M.S.: 2004. Method of matched asymptotic expansions versus intuitive approaches: Calculation of arc cathode spots. Transactions on Plasma Science. 32(1) III: 249-255.

Biot, M.A.: 1955. Theory of Elasticity and Consolidation for a Porous Anisotropic Solid. J. of Applied Physics. 26(2): 182-185.

Blasius, H.: 1908. Grenzschichten in Flussigkeiten mit kleiner Reibung, Z. Math. Phys. vol 56, p. 1-37.

Blick, E. F. and Civan, F.: 1987. Porous Media Momentum Equation for Highly Accelerated Flow. Society of Petroleum Engineers of AIME, (Paper) SPE, 169-177.

Blick, E.F. and Civan, F.: 1988. Porous-media momentum equation for highly accelerated flow. SPE Reservoir Engineering (Society of Petroleum Engineers), 3(3): 1048-1052.

Brinkman, H.C: 1947. A calculation of the viscous force exerted by a flowing fluid on a dense swarm of particles. Appl. Sci. Res. A(1): 27-34.

Brownell L.E. and Katz D.L.: 1947. Flow of fluids through porous media. AICE Chemical Engineering Progress. vol.43, Oct., p.537-548.

Brownell L.E., Dombrowski H.S., and Dickey C.A.: 1950. Pressure drop through porous media. AICE Chemical Engineering Progress. vol.46, Aug., p.ÿ415-422.

Burcharth, H.F., Andersen, O.H.: 1995. On the one-dimensional steady and unsteady porous flow equations. Coastal Engineering. 24(3-4): 233-257.

Bush, A.W. and Schmidt, R.: 1993. Perturbation methods for engineers and scientists. Applied Mechanics Reviews. 46(3): B34.

Carman P.C.: 1937. Fluid flow through granular beds. *Transactions of the Institution of Chemical Engineers*, London, 15: 150-166.

Carrier, G.G.: 1970. Singular perturbation theory and geophysics. SIAM review. 12: 175-193.

Carslaw, H.S and Jaeger, J.C.: 1959. Conduction of heat in solids. Oxford University Press. New York.

Cedergren, H.R.: 1997. Seepage, drainage, and flow nets. 3rd Ed. John Wiley & Sons.

Chauveteau, G. and Thirriot, C.: 1967. Régimes d'écoulement en milieu poreux et limite de la loi de Darcy. La Houille Blanche (2):141-148.

Cole, J.D.: 1994. The development of perturbation theory at galcit. SIAM Review. 36(3): 425-430.

Dagan, G: 1968. A derivation of Dupuit solution of steady flow toward wells by matched asymptotic expansions, Water Resources Res. 2(4): 403-412.

Dake L.P.: 2001. the practive of reservoir engineering. Developments in petroleum science 36.

de Boer, R., Ehlers, W., Liu, Z.: 1993. One-dimensional transient wave propagation in fluid-saturated incompressible porous media, Archive of Applied Mechanics. 63(1): 59-72.

Dettman, J.W.: 1965. Applied Complex Variables. The Macmillan Company. New York.

Duan, N.: 1983. Smearing estimate: a nonparametric retransformation method. Journal American Stat. Assoc. 78(383):605-610.

Dullien, F.A.L.: 1975. Invited Review; Single Phase Flow through Porous Media and Pore Structure. The Chemical Engineering J. 10: 1-34.

Du Plessis, J.P. and Masliyah, J.H.: 1988. Mathematical Modelling of Flow Through Consolidated Isotropic Porous Media. Transport in Porous Media. 3(2): 145-161.

Du Plessis, J.P.: 1994. Analytical quantification of coefficients in the ergun equation for fluid friction in a packed bed. Transport in Porous Media, 16(2): 189-207.

Eckhaus, W.: 1994. Fundamental concepts of matching. SIAM Review. 36(3): 431-439.

Edelman, Inna Ya.: 1997. Asymptotic research of nonlinear wave processes in saturated porous media, Nonlinear Dynamics. 13(1): 83-98.

Edelman, Inna Ya.: 1999. Wave dynamics of saturated porous media and evolutionary equations, Transport in Porous Media. 34(1-3): 117-128.

Engelund, F.: 1953. On the Laminar and turbulent flows of ground water through homogeneous sand. *Transactions of the Danish Academy of Technical Sciences*, 3(4): 7-105.

Erdelyi, A., Magnus, W. Oberhettinger, F., Tricomi, F.G.: 1954. Tables of Integral Transforms Volume I. McGraw-Hill Book Company, Inc.

Ergun, S.: 1952. Fluid flow through packed columns. *Chem. Eng. Progress*, 48(2): 89-94.

Falade, G. K.: 1979. Generalised Solution to the Problems of Transient Flow of Fluid in Porous Media. International Journal of Engineering Science. 17(7): 869-878.

Fand, R.M., Kim, B.Y.K., and Lam, A.C.C.: 1987. Resistance to the Flow of Fluids Through Simple and Complex Porous Media Whose Matrices Are Composed of Randomly Packed Spheres. Transactions of the ASME. 109. Sep: 268-274.

Fand, R.M. and Thinakaran, R.: 1990. The influence of the wall on flow through pipes packed with spheres. *ASME J. of Fluid Engineering*, 112: 84-88.

Fetter, C.W.: 1994. Applied Hydrogeology. 4th ed. Prentice-Hall, Englewood Cliffs, NJ.

Forchheimer, P.: 1901. Wasserbewegung durch Boden. ZVDI. 45: 1781.

Forchheimer, P.: 1924. Hydraulik, 2nd ed. Verlag und Druck von B.G. Teubner, Leipzig, Berlin, 566 pp.

Foster, W.R., McMillen, J.M., and Odeh, A.S.: 1967. The Equations of Motion of Fluids in Porous Media: I. Propagation Velocity of Pressure Pulses. Society of Petroleum Engineers Journal. 7(4): 333-341.

Freeze, R.A. and Cherry, J.A.: 1979. Groundwater, Prentice-Hall, Englewood Cliffs, NJ.

Furman, A., Neuman, S.P.: 2003. Laplace-transform analytic element solution of transient flow in porous media. Advances in Water Resources. 26(12): 1229-1237.

Gambolati, G.: 1973. Equation for One-Dimensional Vertical Flow of Groundwater 2. Validity Range of the Diffusion Equation. Water Resources Research. 9(5): 1385-1395.

Gambolati, G.: 1974. Second-Order Theory of Flow in Three-Dimensional Deforming Media. Water Resources Research. 10(6): 1217-1228.

George, G. and Hansen, D.: 1992. Conversion between quadratic and power law for non-Darcy flow. *ASCE Journal of Hydraulic Eng.*, 118(5): 792-797.

Ghidaoui, M.S. and Karney, B.W.: 1995. Modified Transformation and Integration of 1D Wave Equations. J. of Hydraulic Engineering. Oct.: 758-760.

Ghidaoui, M.S., Karney, B.W. and McInnis D.A.: 1998. Energy Estimates for Discretization Errors in Water Hammer Problems. J. of Hydraulic Engineering. Apr:384-393.

Golan, M. and Whitson, C. H.: 1991. Well Performance. 2nd Ed. P T R Prentice Hall. New Jersey.

Greenkorn, R.A.: 1964. Flow models and scaling laws for flow through porous media. Industrial and Engineering Chemistry. 56(3): 32-37.

Hansen, D.: 2003. A review of terminology pertaining to Darcy's Law and flow through porous media. *Journal of Porous Media*, Begell House Publishing, 6(2): 83-97.

Hansen, D.: 2004. Discussion of "On the use of the Kozeny-Carmen equation to predict the hydraulic conductivity of soils" by Chapuis R. and Aubertin M., *Canadian Geotechnical J.*, accepted in 2003 and in press for fall 2004.

Hansen, D., Garga, V.K., and Townsend D.R.: 1995. Selection and application of one-dimensional non-Darcy flow equation for two-dimensional flow through rockfill embankments. *Canadian Geotechnical J.*, 32(2): 223-232.

Hansen, D. and George, G.H.: 1993. Errors in the application of Ergun-type non-Darcy flow equations. 11th *CSCE Canadian Hydrotechnical Conference*, Fredericton, N.B., June 8-11, vol.1, p.417-426.

Happel, J. and Brenner, H.: 1965. Low Reynolds Number Hydrodynamics, with Special Application to Particulate Media. Prentice-Hall, Englewood Cliffs, N.J.

Hayes, R.E., Afacan, A. and Boulanger, B.: 1995. An Equation of Motion for an Incompressible Newtonian Fluid in a Packed Bed. Transport in Porous Media. 18: 185-198.

Hellfferich, F. and Plesset, M.S.: 1958. Ion exchange kinetics: A nonlinear diffusion problem. J. Chem. Phys. 28(3): 418-424.

Hooman, K. and Ranjbar-Kani, A.A.: 2004. A perturbation based analysis to investigate forced convection in a porous saturated tube. J. of Computational and Applied Mathematics. 162(2): 411-419.

Ipsen, D.C.: 1960. Units, Dimensions, and Dimensionless Numbers. McGrauw-Hill Book Company, Inc., New York, Toronto, London.

Jayasinghe, D.A.P., and Leutheusser, H.J.: 1972. Pulsatile waterhammer subject to laminar friction. J. of Basic Engr., Trans. ASME, Series D. 94(2): 467-473.

Kaper, H.G. and Leaf, G.K.: 1980. Initial value problems for the Carleman equation. Nonlear Anal. 4(2): 343-362.

Kaplun, S.: 1954. The role of coordinate systems in boundary layer theory. PhD Thesis. California Institute of Technology. Pasadena.

Kolodziej, J.A.: 1988. Influence of the Porosity of a Porous Medium on the Effective Viscosity in Brinkman's Filtration Equation. ACTA Mechanica. 75: 241-254.

Kolodziej, J.A.: 1992. Motion Equations of the Dynamic Theory of Consolidation from the Point of View of the Theory of Transient Pipe Flows. Transport in Porous Media 8: 227-241.

Kozeny J.: 1927. Uber kapillare leitung des wassers im boden. Sitzungsber Acad. Wiss. Wienner, 136(2a):271-306. ("About capillaries conducting water in the earth. Committee Report of the Viennese Academy.")

Kresnik, P.: 1906. Einfache Formeln fur die Zeitdauer des Fu llens und Entleerens von Kammerschleusen. Zeitschrift des Oesterreichischen Ingenieur- und Architekten Vereines. Feb 9.

Lacher, H.: 1976. Solutions for unconfined non-Darcy seepage. J. of the Irrigation and Drainage Division (ASCE). 102: 169-171.

Lagerstrom, P.A.: 1957. Note on the preceding two papers. J. Math. Mech. 6:605-606.

Lax, P.D. and Wendroff, B.: 1960. Systems of Conservation Laws. Comm. Pure and Appl. Math., 13: 217-237.

Levin, M.P.: 1996. On the Propagation of Pressure Waves in Saturated Porous Media. Fluid Dynamics. 31(6): 865-867.

Levy, A., Sorek, S., Ben-Dor, G., Skews, B.: 1996. Waves propagation in saturated rigid porous media: analytical model and comparison with experimental results. Fluid Dynamics Research. 17(2): 49-65.

Lonngren, K.E. and Hirose, A.: 1976. Expansion of an electron cloud. Physics Lett. A. 59(4): 285-286.

MacDonald, I. F., El-Sayed, M. S., Mow, K. and Dullien, F. A. L.: 1979. Flow through porous media-the Ergun equation revisited. Ind. Eng. Chem. Fundam. 18(3): 199-208.

Macedo, H.H., Costa U.M.S. and Almeida M.P.: 2001. Turbulent effects on fluid flow through disordered porous media. Physica A. 299: 371-377.

Mahdaviani, M.A.: 1967. Steady and unsteady flow towards gravity wells. J. of the Hydraulics Division. Proc. of the ASCE. Nov. (HY6): 135-146

McCorquodale J.A., Hannoura A.A., and Nasser M.S.: 1978. Hydraulic conductivity of rockfill. Journal of Hydraulic Research. 16(2): 123-137.

McInnis, D. and Karney, B.W.: 1990. Application of energy equations in unsteady closed conduit flow. Proceedings - Annual Conference and 1st Biennial Environmental Speciality Conference. 5: 147.

Mei, C.C. and Auriault, J.-L.: 1991. The effect of weak inertia on flow through a porous medium. J. Fluid Mech. 222: 647-663

Moutsopoulos, K.N., Tsihrintzis, V.A.: 2005. Approximate analytical solutions of the Forchheimer equation. Journal of Hydrology. 309(1-4): 93-103.

Naidu, D. S., Price, D.B. and Hibey, J.L.: 1987. Singular Perturbations and Time Scales (SPaTS) in Discrete Control Systems – an Overview. Proceedings of the IEEE Conference on Decision and Control Including The Symposium on Adaptive Pro. 2096-2103.

Nayfeh, A.H., and Hassan S.D.: 1971. The method of multiple scales and nonlinear dispersive waves. J. Fluid Mech. 48, 463-475.

Nield, D.A.: 1994. Modelling high speed flow of a compressible fluid in a saturated porous medium. Transport in Porous Media. 14(1): 85-88.

Nilson, R.H.: 1981. Transient Fluid Flow in Porous Media: Inertia-Dominated to Viscous-Dominated Transition. J. of Fluids Engineering. 103. June: 339-343.

O'Malley, R.E. Jr.: 1994. On singular perturbations, especially matching. SIAM Review. 36(3): 413-414

Peletier, L.A.: 1971. Asymptotic Behavior of Solutions of the Porous Media Equation. SIAM Journal on Applied Mathematics. 21(4): 542-551.

Peletier, M.A. and Zhang H.: 1994. Self-similar solutions of a fast diffusion equation that do not conserver mass. Delft University of Technology, Faculty of Technical Mathematics and Informatics. Report 94-40: 1-24.

Pigott, R.J.S.: 1944. Discussion of "Friction factors for pipe flow". *Trans. Amer. Soc. Mech. Eng.*, 66(Nov):680.

Polubarinova-Kochina, P.Ya.: 1962. Theory of ground water movement. Princeton University Press.

Prandtl, L.: in Verhandlungen des dritten internationalen Mathematiker-Kongresses in Heidelberg 1904, A. Krazer, ed., Teubner, Leipzig, Germany (1905), p. 484. English trans. in Early Developments of Modern Aerodynamics, J. A. K. Ackroyd, B. P. Axcell, A. I. Ruban, eds., Butterworth-Heinemann, Oxford, UK (2001), p. 77.

Pruess, K., Narasimhan, T. N.: 1985. Practical Method for Modeling Fluid and Heat Flow in Fractured Porous Media. SPEJ, Society of Petroleum Engineers Journal. 25(1): 14-26.

Rahman, M.: 1992. Applied complex variables. D and R Texts Publications.

Reichelt, W.: 1972. ZUR BERECHNUNG DES DRUCKVERLUSTES EINPHASIG DURCHSTROEMTER KUGEL- UND ZYLINDERSCHUETTUNGEN. left bracket Calculation of Pressure Drop in Spherical and Cylindrical Packings for Single-Phase Flow right bracket . Chemie-Ingenieur-Technik. 44(18): 1068-1071.

Richtmyer, R. D.: 1963. A Survey of Difference Methods for Nonsteady Fluid Dynamics. NCAR Technical Note 63-2, National Center for Atmospheric Research, Boulder, Colorado.

Rose H.E.: 1945. The isothermal flow of gases through beds of granular materials. Proceedings of the Institute of Mechanical Engineers, War Emergency Issues 1-12, p.148-153.

Rosenau, P.: 1995. Fast and superfast diffusion processes. Physical Review Letters. 74(7): 1056-1059.

Rumpf H. and Gupte A.R.: 1971. Chemical Eng. Tech. 43: 367.

Sabin G.C.W. and Hansen D.: 1994. The effects of particle shape and surface roughness on the hydraulic mean radius of a porous medium consisting of quarried rock. *ASTM Geotechnical Testing Journal*, 17(1):43-49, March.

Scheidegger, A.E.: 1960. Flow through porous media. Applied Mechanics Reviews 13(5): 313.

Schlichting, H.: 1960. Boundary-Layer Theory. McGraw-Hill. New York.

Seneviratne, A.; Karney, B.W.: 1990. Energy concepts in porous media. Application to transient groundwater flow. Proceedings - Annual Conference and 1st Biennial Environmental Speciality Conference. 1-2: 778.

Sissom, L.E. and Pitts D.R.: 1972. Elements of Transport Phenomenon. McGraw-Hill, NY, 814 pp.

Skjetne, E. and Auriault J.-L.: 1999. High-Velocity Laminar and Turbulent Flow in Porous Media. Transport in Porous Media. 36:131-147.

Stephen, W.: 1996. Forchheimer equation: a theoretical development. Transport in Porous Media, 25(1): 27-61

Streeter, V.L. and Wylie E.B.: 1968. Two and Three-dimensional Fluid Transients. J. of Basic Engineering. Series D. 90(4). Dec.:501-510.

Streeter, V.L. and Wylie E.B.: 1975. Fluid Mechanics. 6th Ed. McGaw-Hill Book Company.

Sturm, T.W.: 2001. Open Channel Hydraulics. McGraw-Hill, New York.

van Duyn, C.J. and Peletier, L.A.: 1977. Asymptotic Behavior of Solutions of a Nonlinear Diffusion Equation. Archive for Rational Mechanics and Analysis, 65(4): 363-377.

van Dyke, M.: 1994. Nineteenth-century roots of the boundary-layer idea. SIAM Review. 36(3): 415-424.

Vazquez, J.L.: 1983. Asymptotic Behaviour and Propagation Properties of the One-Dimensional Flow of Gas in a Porous Medium. American Mathematical Society. 277(2): 507-527.

Vazquez J.L.: 1992. An Introduction to the Mathematical Theory of the Porous Medium Equation: Shape Optimization and Free Boundaries. edited by Delfour M.C. and Sabidussi G. Kluwer Academic Publishers. Dordrecht/Boston/London. 347-389.

Vazquez, J.L.: 2003. Asymptotic behaviour for the porous medium equation posed in the whole space. Journal of Evolution Equations. 3(1): 67-118.

Veldman, A.E.P.: 2001. Matched asymptotic expansions and the numerical treatment of viscous-inviscid interaction. Journal of Engineering Mathematics. 39(1-4), Practical Asymptotics: 189-206.

Venkataraman, P. and Rao, P.R.M.: 1998. Darcian, transitional, and turbulent flow through porous media. J. of Hydraulic Engineering. 124(8): 840-846.

Volker, R.: 1975. Solutions for unconfined non-Darcy seepage. J. of the Irrigation and Drainage Division (ASCE). 101: 53-65.

Wahyudi I., Montillet A., and Abderahmane O.A.K.: 2002. Darcy and post-Darcy flows within different sands. *IAHR Journal of Hydraulic Research* 40(4):519-525.

Walker, J.S.: 1975. Perturbation Solutions for Steady One-Dimensional Waterhammer Waves. J. of Fluids Engineering. Transactions of the ASME. 97(1-2): 260-262.

Wang, J.G., Leung, C.F., Chow, Y.K.: 2003, Numerical solutions for flow in porous media, International Journal for Numerical and Analytical Methods in Geomechanics, v 27, n 7, June, 2003, p 565-583.

Ward, J.C.: 1964. Turbulent flow in porous media. Journal of the Hydraulics Division, ASCE, vol.92, HY4, Sept., p.1-12.

White, F.M.: 1999. Fluid Mechanics. 4th ed. WCB/McGraw-Hill.

Wiggert, D.C. and Wylie E.B.: 1976. Numerical Predictions of Two-Dimensional Transient Groundwater Flow by the Method of Characteristics. Water Resources Research. 12(5):971-977.

Wilkins, J. K.: 1956. Flow of water through rockfill and its application to the design of dams. Proc. of 2nd Australia-New Zealand Conf. on Soil Mechanics and Foundation Engineering, Canterbury University, Christchurch, New Zealand, p.141-149.

Whitaker, S.: 1996. The Forchheimer Equation: A Theoretical Development. Transport in Porous Media. 25: 27-61.

Wright, D.E.: 1968. Non-linear flow through granular materials. J. of the Hydraulics Division, 94(HY4): 851-872.

Wu, Y.S.: 2002. An approximate analytical solution for non-Darcy flow toward a well in fractured media. Water Resources Research. 38(3): 5-1, 5-7.

Wylie, E.B.: 1975. Seismic Response of Reservoir-Dam Systems. J. of the Hydraulics Divison. March (HY3)403-419.

Wylie, E.B.: 1976. Transient aquifer flows by characteristics method. J. of the Hydraulics Divison. March (HY3) 293-305.

Wylie, E.B.: 1983. The microcomputer and pipeline transients. J of Hydraulic Engineering, ASCE. 109:1723-1739.

Wylie, E.B., Streeter V.L.: 1978. Fluid Transient. McGraw-Hill Inc. New York.

Yamamoto, K.: 1973. Flow of Viscous Fluid at Small Reynolds Numbers past a Porous Body. J. of the Physical Society of Japan. 34(3): 814-820.

Yan, B., Liu, Z, and Zhang, X: 1999. Finite element analysis of wave propagation in fluid-saturated porous media. Applied Mathematics and Mechanics (English Edition), 20(12): 1331-1341.

Zeng, Z., Grigg, R.: 2006. A criterion for non-darcy flow in porous media. Transport in Porous Media. 63(1): 57-69.

Zhang, W.: 2005. A numerical method for wave propagation in viscoelastic stratified porous media. Transport in Porous Media. 61(1): 15-24.

7. APPENDIX

I. Analytical Solution of Groundwater Flow Model

Combining Darcy's law and the reduced form of the continuity equation results in typical groundwater flow equation for Laminar flow condition.

$$H_\tau = JH_{XX} \qquad [I\text{-}1]$$

where $J = \frac{C_1}{C_3}$.

Boundary conditions are:

$$H = 1 \text{ at } X = 0 \qquad [I\text{-}2a]$$

$$H = 0 \text{ at } X = 1 \qquad [I\text{-}2b]$$

Initial condition can be given as a general function of X:

$$H = f(X) \text{ when } \tau = 0 \qquad [I\text{-}2c]$$

The analytical solution can be obtained by separating the problem into a problem of steady head with stated boundary conditions (H_1) and an unsteady diffusion problem with fixed zero boundary head (H_2).

$$H = H_1 + H_2 \qquad [I\text{-}3]$$

H_1 is a function of X and H_2 is a function of X and τ. H_1 satisfies:

$$\frac{\partial^2 H_1}{\partial X^2} = 0 \qquad (0 < X < 1) \qquad [I\text{-}4]$$

Boundary conditions of H_1 can be:

$$H_1 = 1 \text{ at } X = 0 \qquad [I\text{-}5a]$$

$$H_1 = 0 \text{ at } X = 1 \qquad [I\text{-}5b]$$

H_2 satisfies:

$$\frac{\partial H_2}{\partial \tau} = J\frac{\partial^2 H_2}{\partial X^2} \qquad (0 < X < 1) \qquad \text{[I-6]}$$

Boundary conditions and initial condition of H_2 can be:

$$H_2 = 0 \text{ at } X = 0 \qquad \text{[I-7a]}$$

$$H_2 = 0 \text{ at } X = 1 \qquad \text{[I-7b]}$$

$$H_2 = f(X) - H_1 \text{ when } \tau = 0 \qquad \text{[I-7c]}$$

From eqn [I-4], H_1 is a linear function of X and using boundary condition, H_1 can be expressed with eqn [I-5].

$$H_1 = 1 + (0-1)X = 1 - X \qquad \text{[I-8]}$$

In order to get H_2, we need to separate variables.

$$H_2(X,\tau) = \Theta(X)\Xi(\tau) \qquad \text{[I-9]}$$

If H_2 is substituted in eqn [I-4]:

$$J\Theta_{XX}\Xi = \Theta\Xi_\tau \qquad \text{[I-10]}$$

Re-arrangement gives:

$$J\frac{\Theta_{XX}}{\Theta} = \frac{\Xi_\tau}{\Xi} \qquad \text{[I-11]}$$

Θ is a function of X and Ξ is a function of τ. In order to get equality for both sides they should be constant. If the constant is larger than or equal to zero the only solution is $H_2(X,\tau) = 0$. For the negative constant we get:

$$\frac{\Theta_{XX}}{\Theta} = \frac{\Xi_\tau}{J\Xi} = -\lambda_2^2 \qquad \text{[I-12]}$$

We can re-write eqn [I-9] with two differential equations.

$$\Theta_{xx} + \lambda_2^2 \Theta = 0 \qquad \text{[I-10]}$$

$$\Xi_\tau + J\lambda_2^2 \Xi = 0 \qquad \text{[I-11]}$$

The general solutions for Θ and Ξ can be expressed with eqns [I-12] and [I-13], respectively.

$$\Theta = A_1 \cos\lambda_2 X + B_1 \sin\lambda_2 X \qquad \text{[I-12]}$$

$$\Xi = C_1' e^{-J\lambda_2^2 \tau} \qquad \text{[I-13]}$$

By substitution of eqns [I-12] and [I-13] into eqn [I-6],

$$H_2 = C_1' e^{-J\lambda^2 \tau}\left(A_1 \cos\lambda_2 X + B_1 \sin\lambda_2 X\right) \qquad \text{[I-14]}$$

The unknown constants, A_1, B_1, and C_1' can be decided from boundary conditions and initial condition. Using $H_2 = 0$ at $X = 0$,

$$H_2 = A_1 C_1' e^{-J\lambda_2^2 \tau} = 0 \qquad \text{[I-15]}$$

If $C_1' = 0$, Ξ becomes zero thus $A_1 = 0$. Using $H_2 = 0$ at $X = 1$,

$$H_2 = B_1 C_1' e^{-J\lambda_2^2 \tau} \sin\lambda_2 = 0 \qquad \text{[I-16]}$$

Because B_1 and C_1' cannot be zero, $\lambda_2 = n'\pi$. Considering particular solutions of H_2

$$H_{2n'} = B_{n'} C_{n'} e^{-J\lambda_{2n'}^2 \tau} \sin\lambda_{2n'} X = 0 \qquad \text{[I-17]}$$

If we set $B_{1n'} C_{1n'}' = D_{n'}$,

$$H_{2n'} = D_{n'} e^{-J\lambda_{2n'}^2 \tau} \sin\lambda_{2n'} X = 0 \qquad \text{[I-18]}$$

The general solution is the sum of the particular solutions,

$$H_2 = \sum_{n'=1}^{\infty} H_{2n'}(X,\tau) = \sum_{n'=1}^{\infty} D_{n'} e^{-Jn'^2\pi^2\tau} \sin(n'\pi X) = 0 \qquad \text{[I-19]}$$

From initial condition, we can get $D_{n'}$.

$$H_2(X,0) = \sum_{n'=1}^{\infty} D_{n'} \sin(n'\pi X) = f(X) - H_1 \qquad \text{[I-20]}$$

Using Fourier sine series and f(X) = 0,

$$D_{n'} = 2\int_0^1 -H_1 \sin(n'\pi X)dX \qquad \text{[I-21]}$$

Substitution of $D_{n'}$ into eqn [I-20] gives:

$$H_2 = 2\sum_{n'=1}^{\infty} e^{-Jn'^2\pi^2\tau} \sin(n'\pi X)\int_0^1 -H_1 \sin(n'\pi X)dX = 0 \qquad \text{[I-22]}$$

Summation of H_1 and H_2 gives:

$$H = 1 - X - 2\sum_{n'=1}^{\infty} e^{-Jn'^2\pi^2\tau} \sin(n'\pi X)\int_0^1 (1-X)\sin(n'\pi X)dX = 0 \qquad \text{[I-23]}$$

The integral part in eqn [I-23] becomes:

$$\int_0^1 (1-X)\sin(n'\pi X)dX = \frac{1}{n'\pi} \qquad \text{[I-24]}$$

Substitution of eqn [I-24] into eqn [I-23] gives:

$$H = 1 - X - \frac{2}{\pi}\sum_{n'=1}^{\infty} e^{-Jn'^2\pi^2\tau} \frac{\sin(n'\pi X)}{n'} = 0 \qquad \text{[I-25]}$$

II. Solution Using Lax-Wendroff Scheme

The Lax-Wendroff scheme (Lax and Wendroff 1960) for the continuity and momentum equations can be directly obtained from a Taylor series expansion in time. The expansion of H in time can be expressed as:

$$H_i^{k+1} = H_i^k + \left(\frac{\partial H}{\partial \tau}\right)_i^k \Delta\tau + \left(\frac{\partial^2 H}{\partial \tau^2}\right)_i^k \frac{(\Delta\tau)^2}{2} \qquad \text{[II-1]}$$

The expansion of V in time can be expressed as:

$$V_i^{k+1} = V_i^k + \left(\frac{\partial V}{\partial \tau}\right)_i^k \Delta\tau + \left(\frac{\partial^2 V}{\partial \tau^2}\right)_i^k \frac{(\Delta\tau)^2}{2} \qquad \text{[II-2]}$$

Finite difference approximations are then substituted for the derivatives of H and V with respect to X. The resulting scheme can be simplified and is equivalent to a two-step method in which the Lax diffusive scheme is used in the first half of the time step ((k+1/2)$\Delta\tau$) and then the leapfrog method is applied in the second half of the time step (k$\Delta\tau$) (Richtmyer 1963 and Sturm 2001). V can be obtained from the momentum equation and H from the continuity equation. For the first step, V and H are found using:

$$V_{i+\frac{1}{2}}^{k+\frac{1}{2}} = \frac{1}{2}\left(V_{i+1}^k + V_i^k\right) - \frac{C_1}{C_6}\frac{\Delta\tau}{2}\left(\frac{H_{i+1}^k - H_i^k}{\Delta X}\right) - \frac{C_2}{C_6}\frac{\Delta\tau}{2}\left(\frac{V_{i+1}^k + V_i^k}{2}\right)\left(\frac{V_{i+1}^k - V_i^k}{\Delta X}\right)$$
$$- \frac{C_3}{C_6}\frac{\Delta\tau}{2}\left(\frac{V_{i+1}^k + V_i^k}{2}\right) - \frac{C_4}{C_6}\frac{\Delta\tau}{2}\left(\frac{V_{i+1}^k + V_i^k}{2}\right)^2 \qquad \text{[II-3]}$$

$$V_{i-\frac{1}{2}}^{k+\frac{1}{2}} = \frac{1}{2}\left(V_i^k + V_{i-1}^k\right) - \frac{C_1}{C_6}\frac{\Delta\tau}{2}\left(\frac{H_i^k - H_{i-1}^k}{\Delta X}\right) - \frac{C_2}{C_6}\frac{\Delta\tau}{2}\left(\frac{V_i^k + V_{i-1}^k}{2}\right)\left(\frac{V_i^k - V_{i-1}^k}{\Delta X}\right)$$
$$- \frac{C_3}{C_6}\frac{\Delta\tau}{2}\left(\frac{V_i^k + V_{i-1}^k}{2}\right) - \frac{C_4}{C_6}\frac{\Delta\tau}{2}\left(\frac{V_i^k + V_{i-1}^k}{2}\right)^2 \qquad \text{[II-4]}$$

$$H_{i+\frac{1}{2}}^{k+\frac{1}{2}} = \frac{1}{2}\left(H_{i+1}^{k} + H_{i}^{k}\right) - \frac{C_5}{C_6}\frac{\Delta\tau}{2}\left(\frac{V_{i+1}^{k} + V_{i}^{k}}{2}\right)\left(\frac{H_{i+1}^{k} + H_{i}^{k}}{\Delta X}\right) - \frac{\Delta\tau}{2}\left(\frac{V_{i+1}^{k} - V_{i}^{k}}{\Delta X}\right)$$
$$- \frac{C_7}{C_6}\frac{\Delta\tau}{2}\left(\frac{V_{i+1}^{k} + V_{i}^{k}}{2}\right) \qquad \text{[II-5]}$$

$$H_{i-\frac{1}{2}}^{k+\frac{1}{2}} = \frac{1}{2}\left(H_{i}^{k} + H_{i-1}^{k}\right) - \frac{C_5}{C_6}\frac{\Delta\tau}{2}\left(\frac{V_{i}^{k} + V_{i-1}^{k}}{2}\right)\left(\frac{H_{i}^{k} + H_{i-1}^{k}}{\Delta X}\right) - \frac{\Delta\tau}{2}\left(\frac{V_{i}^{k} - V_{i-1}^{k}}{\Delta X}\right)$$
$$- \frac{C_7}{C_6}\frac{\Delta\tau}{2}\left(\frac{V_{i}^{k} + V_{i-1}^{k}}{2}\right) \qquad \text{[II-6]}$$

For the second step, V and H are obtained using leapfrog scheme:

$$V_i^{k+1} = V_i^{k} - \frac{C_1}{C_6}\Delta\tau\frac{\left(H_{i+\frac{1}{2}}^{k+\frac{1}{2}} - H_{i-\frac{1}{2}}^{k+\frac{1}{2}}\right)}{\Delta X} - \frac{C_2}{C_6}\Delta\tau\frac{\left(V_{i+\frac{1}{2}}^{k+\frac{1}{2}} + V_{i-\frac{1}{2}}^{k+\frac{1}{2}}\right)}{2}\frac{\left(V_{i+\frac{1}{2}}^{k+\frac{1}{2}} - V_{i-\frac{1}{2}}^{k+\frac{1}{2}}\right)}{\Delta X}$$
$$- \frac{C_3}{C_6}\Delta\tau\frac{\left(V_{i+\frac{1}{2}}^{k+\frac{1}{2}} + V_{i-\frac{1}{2}}^{k+\frac{1}{2}}\right)}{2} - \frac{C_4}{C_6}\Delta\tau\frac{\left(V_{i+\frac{1}{2}}^{k+\frac{1}{2}} + V_{i-\frac{1}{2}}^{k+\frac{1}{2}}\right)^2}{4} \qquad \text{[II-7]}$$

$$H_i^{k+1} = H_i^{k} - \frac{C_5}{C_6}\Delta\tau\frac{\left(V_{i+\frac{1}{2}}^{k+\frac{1}{2}} + V_{i-\frac{1}{2}}^{k+\frac{1}{2}}\right)}{2}\frac{\left(H_{i+\frac{1}{2}}^{k+\frac{1}{2}} - H_{i-\frac{1}{2}}^{k+\frac{1}{2}}\right)}{\Delta X} - \Delta\tau\frac{\left(V_{i+\frac{1}{2}}^{k+\frac{1}{2}} - V_{i-\frac{1}{2}}^{k+\frac{1}{2}}\right)}{\Delta X}$$
$$- \frac{C_7}{C_6}\Delta\tau\frac{\left(V_{i+\frac{1}{2}}^{k+\frac{1}{2}} + V_{i-\frac{1}{2}}^{k+\frac{1}{2}}\right)}{2} \qquad \text{[II-8]}$$

Figure 4.5 illustrates the two steps of the Lax-Wendroff scheme:

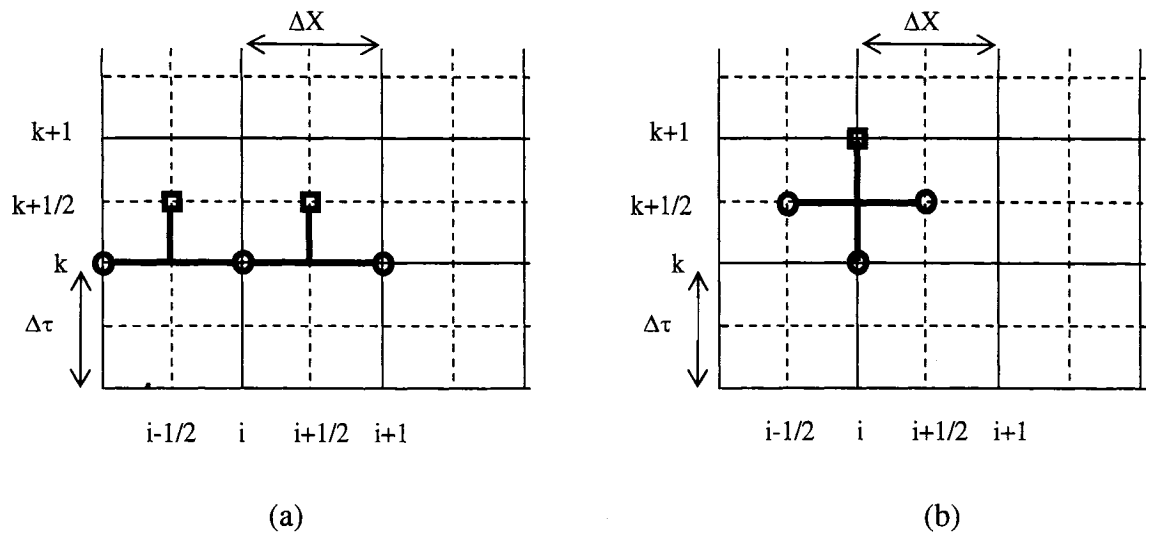

Figure 7.1 (a) first step (Lax diffusive scheme) (b) second step (leapfrog scheme).

III. Solution Using Method of Characteristics

In order to use method of characteristics, the momentum equation is set to L_2 and continuity equation is set to L_1:

$$L_2 = V_\tau + \frac{C_1}{C_6} H_x + \frac{C_2}{C_6} V V_X + \frac{C_3}{C_6} V + \frac{C_4}{C_6} V^2 = 0 \qquad \text{[III-1]}$$

$$L_1 = H_\tau + \frac{C_5}{C_6} V H_x + V_X + \frac{C_7}{C_6} V = 0 \qquad \text{[III-2]}$$

The equations for L_1 and L_2 can be combined using an unknown multiplier as $L = L_1 + \lambda L_2$:

$$L = \left[\frac{\partial H}{\partial X}\left(\frac{C_2}{C_6} V + \frac{C_1}{C_6}\lambda'\right) + \frac{\partial H}{\partial \tau}\right] + \lambda'\left[\frac{\partial V}{\partial X}\left(\frac{C_2}{C_6} V + \frac{1}{\lambda'}\right) + \frac{\partial V}{\partial \tau}\right]$$
$$+ \lambda'\left(\frac{C_3}{C_6} V + \frac{C_4}{C_6} V^2\right) + \frac{C_7}{C_6} V = 0 \qquad \text{[III-3]}$$

If $\frac{dX}{d\tau} = \frac{C_2}{C_6} V + \frac{C_1}{C_6}\lambda'$ and $\frac{dX}{d\tau} = \frac{C_2}{C_6} V + \frac{1}{\lambda'}$, the terms in the first brackets become total derivatives, $dH/d\tau$. The terms in the second brackets also become total derivatives, $dV/d\tau$. From the relationships for $dX/d\tau$ with V and λ':

$$\frac{C_2}{C_6} V + \frac{C_1}{C_6}\lambda' = \frac{C_2}{C_6} V + \frac{1}{\lambda'} \qquad \text{[III-4]}$$

The unknown λ' can be found as:

$$\lambda' = \pm\sqrt{\frac{C_6}{C_1}} \qquad \text{[III-5]}$$

If λ' is substituted,

$$\left.\frac{dH}{d\tau} + \sqrt{\frac{C_6}{C_1}}\frac{dV}{d\tau} + \left(\frac{C_3}{\sqrt{C_1 C_6}} + \frac{C_7}{C_6}\right) V + \frac{C_4}{\sqrt{C_1 C_6}} V^2 = 0 \qquad \text{[III-6a]}\right\} C^+$$

$$\frac{dX}{d\tau} = \frac{C_2}{C_6}V + \sqrt{\frac{C_1}{C_6}} \qquad \text{[III-6b]}$$

$$\left.\begin{aligned} &\frac{dH}{d\tau} - \sqrt{\frac{C_6}{C_1}}\frac{dV}{d\tau} + \left(-\frac{C_3}{\sqrt{C_1C_6}} + \frac{C_7}{C_6}\right)V - \frac{C_4}{\sqrt{C_1C_6}}V^2 = 0 \quad \text{[III-6c]} \\ &\frac{dX}{d\tau} = \frac{C_2}{C_6}V - \sqrt{\frac{C_1}{C_6}} \qquad \text{[III-6d]} \end{aligned}\right\} \; C^-$$

Because $\frac{C_2}{C_6}V << \sqrt{\frac{C_1}{C_6}}$, $\frac{dX}{d\tau} = \pm\sqrt{\frac{C_1}{C_6}}$. From the grid, $\Delta\tau = \frac{\Delta X}{\sqrt{\frac{C_1}{C_6}}}$.

Multiplying eqn [III-6a] by $d\tau$ and integrating along the C^+ characteristic yields:

$$H_{P_i} - H_{i-1} + \sqrt{\frac{C_6}{C_1}}\left(V_{P_i} - V_{i-1}\right) + \left(\frac{C_3}{C_1} + \frac{C_7}{\sqrt{C_1C_6}}\right)\Delta X V_{i-1} + \frac{C_4}{C_1}\Delta X V_{i-1}|V_{i-1}| = 0 \qquad \text{[III-7]}$$

Multiplying eqn [III-6c] by $d\tau$ and integrating along the C^- characteristic yields:

$$H_{P_i} - H_{i+1} - \sqrt{\frac{C_6}{C_1}}\left(V_{P_i} - V_{i+1}\right) + \left(-\frac{C_3}{C_1} + \frac{C_7}{\sqrt{C_1C_6}}\right)\Delta X V_{i+1} - \frac{C_4}{C_1}\Delta X V_{i+1}|V_{i+1}| = 0 \qquad \text{[III-8]}$$

Adding eqn [III-7] and [III-8] results in:

$$H_{P_i} = 0.5\left[H_{i-1} + H_{i+1} + \sqrt{\frac{C_6}{C_1}}\left(V_{i-1} - V_{i+1}\right) - \frac{C_3}{C_1}\Delta X\left(V_{i-1} - V_{i+1}\right)\right.$$
$$\left. - \frac{C_7}{\sqrt{C_1C_6}}\Delta X\left(V_{i-1} + V_{i+1}\right) - \frac{C_4}{C_1}\Delta X\left(V_{i-1}|V_{i-1}| - V_{i+1}|V_{i+1}|\right)\right] \qquad \text{[III-9]}$$

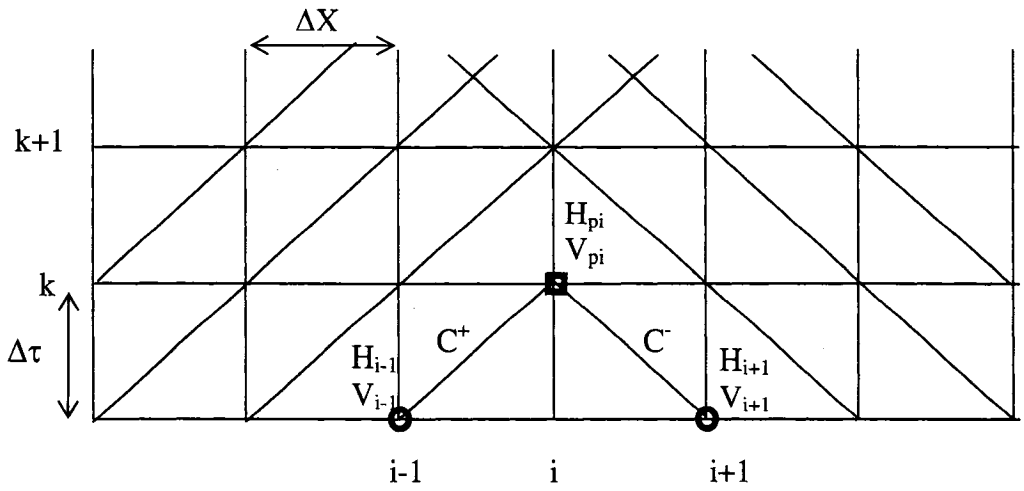

Figure 7.2 Nodal definitions and characteristic lines for MoC calculations.

After obtaining H_{Pi}, V_{Pi} can be calculated using eqn [III-7] or [III-8] as:

$$V_{P_i} = \sqrt{\frac{C_1}{C_6}}\left[-H_{P_i} + H_{i-1} - \left(\frac{C_3}{C_1} + \frac{C_7}{\sqrt{C_1 C_6}}\right)\Delta X V_{i-1} - \frac{C_4}{C_1}\Delta X V_{i-1}\left|V_{i-1}\right|\right] + V_{i-1} \quad \text{[III-10]}$$

$$V_{P_i} = \sqrt{\frac{C_1}{C_6}}\left[H_{P_i} - H_{i+1} + \left(-\frac{C_3}{C_1} + \frac{C_7}{\sqrt{C_1 C_6}}\right)\Delta X V_{i+1} - \frac{C_4}{C_1}\Delta X V_{i+1}\left|V_{i+1}\right|\right] + V_{i+1} \quad \text{[III-11]}$$

The boundary conditions of H are given at the upstream and downstream ends. At the upstream end, the C^+ characteristic can give an equation for V at the boundary and the C^- characteristic provides an equation for V at the downstream end.

IV. Analytical Solution of Evolving-wave Equation

The evolving-wave equation for V can be expressed as:

$$V_{XX} = V_{\tau\tau} + V_{\tau} \qquad \text{[IV-1]}$$

The initial condition and the boundary conditions are:

$$V = V_{\tau} = 0 \qquad \text{at } \tau = 0 \qquad \text{[IV-2a]}$$

$$V_X = -\delta(\tau) \qquad \text{at } X = 0 \qquad \text{[IV-2b]}$$

$$V_X = 0 \qquad \text{at } X = 1 \qquad \text{[IV-2c]}$$

V can be transformed to:

$$V = e^{\frac{-\tau}{2}} G(X, \tau) \qquad \text{[IV-3]}$$

If we differentiate with τ:

$$V_{\tau} = e^{\frac{-\tau}{2}} \left[-\frac{G}{2} + G_{\tau} \right] \qquad \text{[IV-4]}$$

The second-order differential equation of V becomes:

$$V_{\tau\tau} = e^{\frac{-\tau}{2}} \left[\frac{G}{4} - \frac{G_{\tau}}{2} - \frac{G_{\tau}}{2} + G_{\tau\tau} \right] \qquad \text{[IV-5]}$$

Using eqns [IV-4] and [IV-5]:

$$V_{\tau\tau} + V_{\tau} = e^{\frac{-\tau}{2}} \left[-\frac{G}{4} + G_{\tau\tau} \right] \qquad \text{[IV-6]}$$

Substituting eqns [IV-3] and [IV-6] into eqn [IV-1] gives:

$$G_{XX} = G_{\tau\tau} - \frac{G}{4} \qquad \text{[IV-7]}$$

The initial condition and the boundary conditions for G are:

$$G = G_\tau = 0 \qquad \text{at } \tau = 0 \qquad \text{[IV-8a]}$$

$$G_X = -\delta(\tau) \qquad \text{at } X = 0 \qquad \text{[IV-8b]}$$

$$G_X = 0 \qquad \text{at } X = 1 \qquad \text{[IV-8c]}$$

Laplace transform of eqn [IV-7] is:

$$\overline{G}_{XX} = (s_L^2 - \frac{1}{4})\overline{G} \qquad \text{[IV-9]}$$

The boundary conditions for $\overline{G}$ are:

$$\overline{G}_X = -1 \qquad \text{at } X = 0 \qquad \text{[IV-10a]}$$

$$\overline{G}_X = 0 \qquad \text{at } X = 1 \qquad \text{[IV-10b]}$$

If we define:

$$\tilde{s}^2 = s_L^2 - \frac{1}{4} \qquad \text{[IV-11]}$$

The term $\tilde{s}$ becomes:

$$\tilde{s} = \sqrt{s_L^2 - \frac{1}{4}} \qquad \text{[IV-12]}$$

Using the boundary conditions:

$$\overline{G} = \frac{e^{-\tilde{s}X} + e^{(X-2)\tilde{s}}}{\tilde{s}(1 - e^{-2\tilde{s}})} \qquad \text{[IV-13]}$$

If we define pole set 1 from $1 - e^{-2\tilde{s}} = 0$:

$$1 - e^{-2\tilde{s}} = 0 \qquad \text{[IV-14]}$$

Re-arrangement gives:

$$e^{-2\tilde{s}} = e^{2n'\pi i} \qquad \text{[IV-15]}$$

$\tilde{s}$ can be obtained from eqn [IV-15]:

$$\tilde{s}_{n'} = -n'\pi i \qquad n' \geq 1 \qquad \text{[IV-16]}$$

Using eqn [IV-12], $\tilde{s}_{n'}$ becomes:

$$\tilde{s}_n = -n'\pi i = \sqrt{s_{n'}{}^2 - \frac{1}{4}} \qquad \text{[IV-17]}$$

$$s_{n'}{}^2 - \frac{1}{4} = -n'^2\,\pi^2 \qquad \text{[IV-18]}$$

The term $s_{n'}$ can be obtained:

$$s_{n'} = \pm\sqrt{\frac{1}{4} - n'^2\,\pi^2} \qquad \text{[IV-19]}$$

Because $n' \geq 1$:

$$s_{n'} = \pm i\sqrt{n'^2\,\pi^2 - \frac{1}{4}} \qquad \text{[IV-20]}$$

In order to calculate residue from pole set 1, we will define P(s):

$$P(s_L) = \frac{e^{-\tilde{s}X} + e^{(X-2)\tilde{s}}}{\tilde{s}} \qquad \text{[IV-21]}$$

We will define $Q(s_L)$:

$$Q(s_L) = 1 - e^{-2\tilde{s}} \qquad \text{[IV-22]}$$

Then we get $\overline{G}$ using $P(s_L)$ and $Q(s_L)$:

$$\overline{G} = \frac{P(s_L)}{Q(s_L)} \qquad \text{[IV-23]}$$

The residue is:

$$R_{\overline{G}} = \frac{P(s_{Ln'})}{Q'(s_{Ln'})} \qquad \text{[IV-24]}$$

The derivative of $Q(s_L)$ is:

$$Q(s_L)' = \frac{e^{-2\sqrt{s_L^2 - \frac{1}{4}}}}{\sqrt{s_L^2 - \frac{1}{4}}}(2s_L) \qquad \text{[IV-25]}$$

Substituting $Q(s_L)'$ in eqn [IV-24] gives:

$$R_{\bar{G}} = \frac{e^{\tilde{s}X} + e^{(2-X)\tilde{s}}}{2s_L} \qquad \text{[IV-26]}$$

Evaluating $R_{\bar{G}}$ at s_L and $\tilde{s}$ gives:

$$R_{\bar{G}} = \frac{\left(e^{-n'\pi iX} + e^{-(2-X)n'\pi i}\right)}{2i\sqrt{n'^2\pi^2 - \frac{1}{4}}} e^{i\sqrt{n'^2\pi^2 - \frac{1}{4}}\tau} + \frac{\left(e^{-n'\pi iX} + e^{-(2-X)n'\pi i}\right)}{-2i\sqrt{n'^2\pi^2 - \frac{1}{4}}} e^{-i\sqrt{n'^2\pi^2 - \frac{1}{4}}\tau} \qquad \text{[IV-27]}$$

$$R_{\bar{G}} = \frac{\left(e^{-n'\pi iX} + e^{-(2-X)n'\pi i}\right)}{2i\sqrt{n'^2\pi^2 - \frac{1}{4}}} e^{i\sqrt{n'^2\pi^2 - \frac{1}{4}}\tau} + \frac{\left(e^{-n'\pi iX} + e^{-(2-X)n'\pi i}\right)}{-2i\sqrt{n'^2\pi^2 - \frac{1}{4}}} e^{-i\sqrt{n'^2\pi^2 - \frac{1}{4}}\tau} \qquad \text{[IV-28]}$$

Re-arrangement gives:

$$R_{\bar{G}} = \frac{\left(e^{-n'\pi iX} + e^{-(2-X)n'\pi i}\right)}{\sqrt{n'^2\pi^2 - \frac{1}{4}}} \sin\left(\sqrt{n'^2\pi^2 - \frac{1}{4}}\tau\right) \qquad \text{[IV-29]}$$

$$R_{\bar{G}} = \frac{2\cos(n'\pi X)}{\sqrt{n'^2\pi^2 - \frac{1}{4}}} \sin\left(\sqrt{n'^2\pi^2 - \frac{1}{4}}\tau\right) \qquad \text{[IV-30]}$$

If we define pole set 2 from $\tilde{s} = 0$:

$$\sqrt{s_2' - \frac{1}{4}} = 0 \qquad \text{[IV-31]}$$

$$s_{L1} = \frac{1}{2} \text{ and } s_{L2} = -\frac{1}{2} \qquad \text{[IV-32]}$$

In order to calculate residue from pole set 2, we will define P(s):

$$P(s_L) = e^{-\tilde{s}X} + e^{(X-2)\tilde{s}} \qquad \text{[IV-33]}$$

We will define $Q(s_L)$:

$$Q(s_L) = \tilde{s}\left(1 - e^{-2\tilde{s}}\right) \qquad \text{[IV-34]}$$

Then we get $\overline{G}$ using $P(s_L)$ and $Q(s_L)$:

$$\overline{G} = \frac{P(s_L)}{Q(s_L)} \qquad \text{[IV-35]}$$

The residue is:

$$R_{\overline{G}} = \frac{P(s_n)}{Q'(s_n)} \qquad \text{[IV-36]}$$

The derivative of $Q(s_L)$ is:

$$Q(s)' = \left(1 - e^{-2\tilde{s}} + 2\tilde{s}e^{-2\tilde{s}}\right)\frac{s_L}{\tilde{s}} \qquad \text{[IV-37]}$$

Substituting $Q(s_L)'$ in eqn [IV-36] gives:

$$R_{\overline{G}} = \frac{e^{\tilde{s}X} + e^{(2-X)\tilde{s}}}{\frac{\left(1 + (2\tilde{s} - 1)e^{-2\tilde{s}}\right)}{\tilde{s}}_{s_L}} \qquad \text{[IV-38]}$$

As $\tilde{s} \to 0$, the denominator becomes:

$$\lim_{\tilde{s}\to 0} \frac{\left(1 + (2\tilde{s} - 1)e^{-2\tilde{s}}\right)}{\tilde{s}} = \lim_{\tilde{s}\to 0} \frac{e^{-2\tilde{s}}\left(-(2\tilde{s} - 1) + 2\right)}{1} = 4 \qquad \text{[IV-39]}$$

In order to evaluate $R_{\bar{G}}$ at $s_L = \pm\frac{1}{2}$ and $\tilde{s} = 0$:

$$R_{\bar{G}} = 2\left[\frac{e^{\frac{\tau}{4}} - e^{-\frac{\tau}{4}}}{2}\right] \qquad \text{[IV-40]}$$

$$R_{\bar{G}} = 2\sinh\left(\frac{\tau}{2}\right) \qquad \text{[IV-41]}$$

Contour integral is:

$$\int_{\vartheta} +A_0 + B_0 + C_0 + D_0 = \sum \text{residue from poles} \qquad \text{[IV-42]}$$

Using two sets of poles:

$$\int_{\vartheta} +A_0 + B_0 + C_0 + D_0 = R_{\bar{G}\text{pole1}} + R_{\bar{G}\text{pole2}} \qquad \text{[IV-43]}$$

So we can get the integral of G from

$$\int_{\vartheta} = R_{\bar{G}\text{pole1}} + R_{\bar{G}\text{pole2}} - (A_0 + B_0 + C_0 + D_0) \qquad \text{[IV-44]}$$

To get the integral of B_0, z_0 can be expressed with:

$$s_L - \frac{1}{2} = z_0 e^{i\pi} \qquad \text{[IV--45]}$$

Using the definition of $\tilde{s}$:

$$\tilde{s} = \sqrt{\left(s_L - \frac{1}{2}\right)\left(s_L + \frac{1}{2}\right)} \qquad \text{[IV-46]}$$

or

$$\tilde{s} = \sqrt{z_0 e^{i\pi}}\sqrt{1 - z_0} \qquad \text{[IV-47]}$$

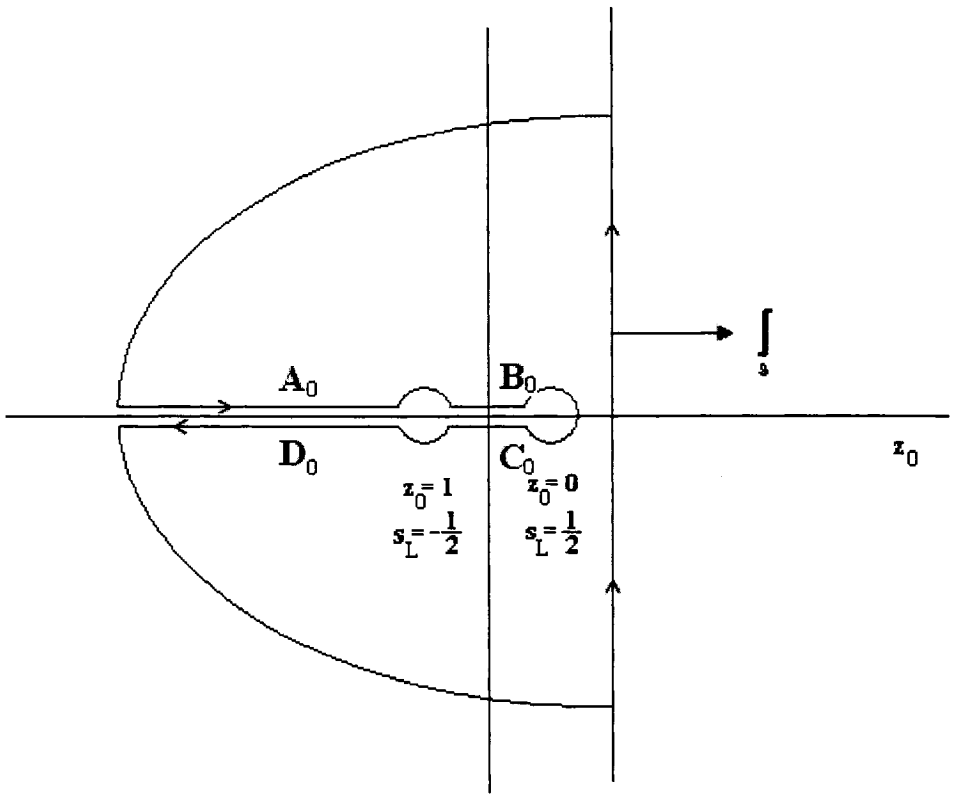

Figure 7.3 Residue theorem for inverse Laplace transform.

or

$$\tilde{s} = e^{\frac{i\pi}{2}} \sqrt{z_0} \sqrt{1 - z_0} \qquad \text{[IV-48]}$$

or

$$\tilde{s} = \sqrt{z_0 (1 - z_0)}\, i \qquad \text{[IV-49]}$$

For the integral of C_0:

$$s_L - \frac{1}{2} = z_0 e^{-i\pi} \qquad \text{[IV-50]}$$

Using the definition of $\tilde{s}$:

$$\tilde{s} = \sqrt{z_0 e^{-i\pi}} \sqrt{1 - z_0} \qquad \text{[IV-51]}$$

or

$$\tilde{s} = -\sqrt{z_0(1-z_0)}i \qquad \text{[IV-52]}$$

For the integral of A_0:

$$s_L - \frac{1}{2} = z_0 e^{i\pi} \qquad \text{[IV-53]}$$

Following the same procedure for getting integral of B_0:

$$\tilde{s} = \sqrt{z_0(1-z_0)}i \qquad \text{[IV-53]}$$

For the integral of D_0:

$$s_L - \frac{1}{2} = z_0 e^{-i\pi} \qquad \text{[IV-54]}$$

Following the same procedure used to get the integral of C_0:

$$\tilde{s} = -\sqrt{z_0(1-z_0)}i \qquad \text{[IV-55]}$$

The sum of integrals of B_0 and C_0 can be expressed with:

$$\int_{B_0+C_0} \frac{e^{-\tilde{s}X} + e^{(X-2)\tilde{s}}}{\tilde{s}(1-e^{-2\tilde{s}})} e^{s\tau} ds_L \qquad \text{[IV-56]}$$

Substituting s_L and $\tilde{s}$ gives integral of B_0 as:

$$B_0 = \int_0 \frac{e^{-i\sqrt{z_0(1-z_0)}X} + e^{i(X-2)\sqrt{z_0(1-z_0)}}}{i\sqrt{z_0(1-z_0)}(1-e^{-2i\sqrt{z_0(1-z_0)}})} e^{(\frac{1}{2}-z_0)\tau}(-dz_0) \qquad \text{[IV-57]}$$

Substituting s_L and $\tilde{s}$ gives integral of C_0 as:

$$C_0 = \int_0 \frac{e^{-i\sqrt{z_0(1-z_0)}X} + e^{i(X-2)\sqrt{z_0(1-z_0)}}}{-i\sqrt{z_0(1-z_0)}(1-e^{-2i\sqrt{z_0(1-z_0)}})} e^{(\frac{1}{2}-z_0)\tau}(-dz_0) \qquad \text{[IV-58]}$$

Defining:

$$a_1' = i\sqrt{z(1-z)} \qquad \text{[IV-59]}$$

Using B_0, C_0, and a_1':

$$\int_{B_0+C_0} \frac{e^{-\tilde{s}X} + e^{(X-2)\tilde{s}}}{\tilde{s}(1-e^{-2\tilde{s}})} e^{s_L\tau} ds_L = \int_0^1 \frac{e^{-a_1'X} + e^{(X-2)a_1'}}{a_1'(1-e^{-2a_1'})} e^{(\frac{1}{2}-z_0)\tau} dz_0 + \int_0^1 \frac{e^{a_1'X} + e^{-(X-2)a_1'}}{a_1'(1-e^{-2a_1'})} e^{(\frac{1}{2}-z_0)\tau} dz_0$$

[IV-60]

Re-arrangement gives:

$$\int_{B_0+C_0} \frac{e^{-\tilde{s}X} + e^{(X-2)\tilde{s}}}{\tilde{s}(1-e^{-2\tilde{s}})} e^{s_L\tau} ds_L = \int_0^1 \frac{e^{-a_1'X}}{a_1'} \left(\frac{1}{1-e^{-2a_1'}} - \frac{e^{2a_1'X}}{1-e^{2a_1'}} \right) e^{(\frac{1}{2}-z_0)\tau} dz_0 +$$

$$\int_0^1 \frac{e^{a_1'X}}{a_1'} \left(\frac{1}{1-e^{2a_1'}} - \frac{e^{-2a_1'X}}{1-e^{-2a_1'}} \right) e^{(\frac{1}{2}-z_0)\tau} dz_0 \qquad \text{[IV-61]}$$

It can be simplified as:

$$\int_{B_0+C_0} \frac{e^{-\tilde{s}X} + e^{(X-2)\tilde{s}}}{\tilde{s}(1-e^{-2\tilde{s}})} e^{s_L\tau} ds_L = \int_0^1 \frac{e^{(\frac{1}{2}-z_0)\tau}}{a_1'} \left(\frac{e^{-a_1'X}}{1-e^{-2a_1'}} - \frac{e^{a_1'X}}{1-e^{2a_1'}} + \frac{e^{a_1'X}}{1-e^{2a_1'}} - \frac{e^{-a_1'X}}{1-e^{-2a_1'}} \right) dz_0 \qquad \text{[IV-62]}$$

The sum of integrals of A_0 and D_0 can be expressed as:

$$\int_{A_0+D_0} \frac{e^{-\tilde{s}X} + e^{(X-2)\tilde{s}}}{\tilde{s}(1-e^{-2\tilde{s}})} e^{s_L\tau} ds_L \qquad \text{[IV-63]}$$

Substituting s_L and $\tilde{s}$ gives integral of A_0:

$$A_0 = \int_\infty^0 \frac{e^{-i\sqrt{z_0(1-z_0)}X} + e^{i(X-2)\sqrt{z_0(1-z_0)}}}{i\sqrt{z_0(1-z_0)}(1-e^{-2i\sqrt{z_0(1-z_0)}})} e^{(\frac{1}{2}-z_0)\tau} (-dz_0) \qquad \text{[IV-64]}$$

Substituting s_L and $\tilde{s}$ gives integral of C_0 as:

$$D_0 = \int_{\infty}^{} \frac{e^{-i\sqrt{z_0(1-z_0)}X} + e^{i(X-2)\sqrt{z_0(1-z_0)}}}{-i\sqrt{z_0(1-z_0)}(1-e^{-2i\sqrt{z_0(1-z_0)}})} e^{(\frac{1}{2}-z_0)\tau}(-dz_0) \qquad \text{[IV-65]}$$

Following same procedure for $B_0 + C_0$:

$$\int_{A_0+D_0} \frac{e^{-\tilde{s}X} + e^{(X-2)\tilde{s}}}{\tilde{s}(1-e^{-2\tilde{s}})} e^{s\tau} ds_L = 0 \qquad \text{[IV-66]}$$

Using residues from the poles and $A_0+B_0+C_0+D_0$ we can get G:

$$G(X,\tau) = \frac{2\cos(n'\pi X)}{\sqrt{n'^2\pi^2 - \frac{1}{4}}} \sin\left(\sqrt{n'^2\pi^2 - \frac{1}{4}}\tau\right) + 2\sinh\left(\frac{\tau}{2}\right) \qquad \text{[IV-67]}$$

From the relationship between V and G:

$$V(X,\tau) = \left(\frac{2\cos(n'\pi X)}{\sqrt{n'^2\pi^2 - \frac{1}{4}}} \sin\left(\sqrt{n'^2\pi^2 - \frac{1}{4}}\tau\right) + 2\sinh\left(\frac{\tau}{2}\right) \right) e^{-\frac{\tau}{2}} \qquad \text{[IV-68]}$$